Design of Novel Octahedral Stereogenic-at-Metal Complexes for Applications in Asymmetric Catalysis

A DISSERTATION

In

Chemistry

Presented to the Faculties of Philipps-Universität Marburg in Partial Fulfillment

of the Requirements for the Degree of Doctor of Science

(Dr. rer. nat.)

Yu Zheng

Anhui, P. R. China

Marburg/Lahn 2018

Acknowledgements

Publications and Poster Presentation

Part of work has been already published

1. <u>Y. Zheng</u>, L. Zhang, E. Meggers, Catalytic Enantioselective Synthesis of Key Propargylic Alcohol Intermediates of the Anti-HIV Drug Efavirenz. *Org. Process Res. Dev.* **2018**, *22*, 103−107.

2. <u>Y. Zheng</u>, Y. Tan, K. Harms, M. Marsch, R. Riedel, L. Zhang, E. Meggers, Octahedral Ruthenium Complex with Exclusive Metal-Centered Chirality for Highly Effective Asymmetric Catalysis. *J. Am. Chem. Soc.* **2017**, *139*, 4322−4325. (Highlighted by *Synfacts* **2017**, 0625)

3. <u>Y. Zheng</u>, K. Harms, L. Zhang, E. Meggers, Enantioselective Alkynylation of 2-Trifluoroacetyl Imidazoles Catalyzed by Bis-Cyclometalated Rhodium(III) Complexes Containing Pinene-Derived Ligands. *Chem. Eur. J.* **2016**, *22*, 11977−11981. (Highlighted by *Synfacts* **2016**, 1156)

4. S. Luo, X. Zhang, <u>Y. Zheng</u>, K. Harms, L. Zhang, E. Meggers, Enantioselective Alkynylation of Aromatic Aldehydes Catalyzed by a Sterically Highly Demanding Chiral-at-Rhodium Lewis Acid. *J. Org. Chem.* **2017**, *82*, 8995−9005.

5. C. Wang, <u>Y. Zheng</u>, H. Huo, P. Röse, L. Zhang, K. Harms, E. Meggers, Merger of Visible Light Induced Oxidation and Enantioselective Alkylation with Chiral Iridium Catalyst. *Chem. Eur. J.* **2015**, *21*, 7355−7359.

Poster Presentation

1. "**20th EUROPEAN SYMPOSIUM ON ORGANIC CHEMISTRY**", Poster: Octahedral Ruthenium Complex with Exclusive Metal-Centered Chirality for Highly Effective Asymmetric Catalysis, 2th-6th July **2017**, Cologne, Germany.

Abstract (English)

This thesis details the synthesis of three classes of chiral octahedral metal complexes and their applications in asymmetric catalysis.

In the first section, two new octahedral chiral-at-metal iridium(III) and rhodium(III) Lewis acid complexes with modified ligands were synthesized to expand the family of previous complexes in our group. While the newly synthesized complexes Λ/Δ-**Ir/Rh**(**Se**) did not demonstrate higher catalytic activities than the existing ones, we believe that these Lewis acid catalysts might be applied to other enantioselective reactions such as visible-light driven photocatalysis in the future.

In the second section, four new bis-cyclometalated rhodium(III) and iridium(III) complexes were synthesized in a diastereomerically and enantiomerically pure fashion by employing chiral cyclometalating ligands. One of these complexes was identified to catalyze the enantioselective alkynylation of 2-trifluoroacetyl imidazoles with different substituted alkynes to provide the propargyl alcohols in good to excellent yields with excellent enantioselectivities (up to >99% *ee*). We found that the asymmetric induction in the course of creating a new stereogenic center is controlled by the metal-centered chirality not the chirality of the coordinating ligands. Moreover, the rhodium complexes display higher catalytic reactivity than our previous catalysts and thus our chiral catalyst library is further expanded. Importantly, the synthetic methodology provides a new strategy for the straightforward synthesis of enantiomerically pure octahedral complexes with metal-centered chirality.

Lastly, the first example of an octahedral chiral-at-ruthenium complex bearing two *N*-(2-pyridyl)-subsituted *N*-heterocyclic carbene (PyNHC) ligands was successfully developed. It was demonstrated that the helically chiral catalyst catalyzes the enantioselective alkynylation of simple trifluoromethyl ketones to provide the corresponding propargylic alcohols with high efficiency at catalyst loading down to 0.2% and with excellent enantioselectivities of up to > 99% *ee*. A significant application of our new catalyst is the enantioselective catalytic synthesis of two key chiral intermediates of the anti-AIDS drug efavirenz.

Zusammenfassung (Deutsch)

Die vorliegende Arbeit beschreibt die Synthese von drei Klassen von chiralen oktaedrischen Metallkomplexen und die Anwendung dieser Komplexe in asymmetrischer Katalyse.

Der erste Teil behandelt zwei neue oktaedrische Iridium(III)- und Rhodium(III)-Lewis-Säure-Komplexe, deren Strukturen durch Ligandmodifikationen von den existierenden Komplexen entwickelt wurden, um das von der Gruppe MEGGERS entwickelte Katalysatorsystems zu erweitern. Die Synthese und die Anwendung dieser neuen Komplexe in asymmetrischer Katalyse wurde entwickelt. Obwohl die neuen Komplexe Λ/Δ-**Ir/Rh**(**Se**) entgegen der Erwartungen keine höhere Reaktivität aufwiesen als die bereits vorhandenen Katalysatoren, glauben wir, dass diese künftig in anderen asymmetrischen Reaktionen wie z.B. in der Photokatalyse mit sichtbarem Licht Anwendung finden könnten.

Teil zwei behandelt vier neue Rhodium(III)- und Iridium(III)-Komplexe mit chiralen cyclometallierenden Liganden. Die Komplexe wurden diastereomeren- und enantiomerenrein synthetisiert und anschließend als chirale Katalysatoren eingesetzt. Einer dieser Komplexe ist in der Lage die enantioselektive Alkinylierung von 2-Trifluoroacetylimidazolen mit verschieden substituierten Alkinen zu den entsprechenden Propargylalkoholen mit exzellenten Ausbeuten sowie Enantioselektivitäten (bis >99% *ee*) zu katalysieren. Interessanterweise wird die asymmetrische Induktion bei der Erzeugung des neuen stereogenen Zentrums von der metallzentrierten Chiralität kontrolliert und nicht von der Chiralität der Liganden. Darüber hinaus zeigen die Rhodium-Komplexe eine höhere katalytische Reaktivität als vorhergehende Katalysatoren dieser Klasse, wodurch unsere Bibliothek an verschiedenen chiralen Katalysatoren weiter bereichert wird. Zudem konnte eine einfache Synthesestrategie für die Synthese von enantiomerenreinen chiralen oktaedrischen Komplexen mit metallzentrierter Chiralität entwickelt werden.

Der dritte Teil behandelt einen oktaedrischen Ruthenium(II)-Komplex mit metallzentrierter Chiralität. Die Einführung von zwei *N*-(2-Pyridyl)-substituierten *N*-hetereocyclischen Carben-Liganden (PyNHC) ist entscheidend für die erfolgreiche Synthese dieses Komplexes. Der Ruthenium(II)-Komplex katalysiert die enantioselektive Alkinylierung von einfachen Trifluoromethylketonen zu den entsprechenden Propargylalkohlen mit hoher Effizienz

(Katalysatorbeladung bis 0.2 mol%) und mit exzellenten Enantiomerenüberschüssen (bis zu >99% *ee*). Der neue Katalysator ermöglicht einen Zugang zur enantioselektiven katalytischen Synthese von zwei Schlüsselintermediaten des HIV-Medikamentes Efavirenz.

Table of Contents

Chapter 1: Theoretical Part

1.1 Introduction

Research on enantiomerically pure chiral compounds has attracted a lot of attention, because of their wide applications in pharmaceuticals, agrochemicals and the flavor industries.[1] The rapid growth of the market for enantiopure compounds is due to the fact that the different enantiomers or diastereomers of a molecule have quite different biological activities. Chemists have spent great efforts in developing methods to synthesize enantiopure chiral compounds. A variety of strategies are available to build enantiopure molecules, such as the classical resolution of racemates, however the drawback of affording desired molecules with a maximum of 50% yield makes this method apparently not attractive. Asymmetric synthesis by using stoichiometric amounts of chiral precursors from Nature's chiral pool is also limited by the availability of starting materials with a great resemblance to the desired molecule. Asymmetric catalysis is therefore considered to be the most elegant and atom economic strategy to introduce chirality into a molecule,[2] which is mainly realized by three kinds of catalysts: organocatalysts, enzymatic catalysts and chiral transition metal catalysts.

The development of chiral transition metal catalysts has been one of the most important and interesting research areas.[3] In 2001, the Nobel prize was awarded to Knowles and Noyori for their work on asymmetric catalytic hydrogenation,[4] and to Sharpless for his work on asymmetric catalytic oxidation.[5] In all their catalytic systems, chiral transition metal complexes were employed as chiral catalysts. For the most of chiral transition metal complexes, overall chirality originates from chiral ligands that coordinate to the metal center.[6] Transition metal complexes can also derive their chirality exclusively from stereogenic metal centers. The octahedral coordination geometry constitutes one of the most popular coordination modes. Chiral octahedral complexes which feature a stereogenic metal center can be mainly divided into two classes based on the types of coordinating ligands: one class are chiral octahedral metal complexes with chiral ligands, in which the chiral ligands induce a stereogenic metal center and also control the absolute configuration; another class are octahedral chiral-at-metal complexes. "Chiral-at-metal" refers to chiral metal complexes in which the chirality origainates only from a stereogenic metal center, all coordinating ligands being achiral.[7] Much less attention has been

devoted to such octahedral chiral-at-metal complexes.[8] In the following, the synthesis and applications of chiral octahedral metal complexes containing a stereogenic metal center for use in asymmetric catalysis will be discussed.

1.2 Chiral Octahedral Metal Complexes with Chiral Ligands

The asymmetric synthesis of a chiral octahedral complex by transferring the chirality from a stereogenic carbon to a metal center was first reported by Alexander P. Smirnoff in 1920.[9] From then on, numerous chiral ligands such as the CHIRAGEN ligands[10] and the chiral salen ligands[11] were empolyed to highly diastereoselective synthesis of chiral octahedral metal complexes which covered by several excellent reviews.[12] Some examples of chiral octahedral metal complexes were also successfully applied to asymmetric catalytic reactions. These complexes can be classified into two types: 1.) inert chiral octahedral metal complexes, in which the central metal serves as a structural center, while catalysis is mediated through the organic ligand sphere; 2.) reactive chiral octahedral metal complexes, in which the metal center activates a substrate to facilitate further transformation. In this section, some representative examples of synthesis and applications of chiral octahedral complexes with chiral ligands are discussed.

1.2.1 Inert chiral octahedral metal complexes bearing chiral ligands

The Belokon group reported a class of inert chiral octahedral metal complexes with two chiral tridentate ligands.[13,14] These chiral Co(III) complexes combine metal-centered chirality with stereogenic carbons in the coordinating ligands. A high diastereomeric purity for these complexes can be obtained from the reaction of $Na_3[Co(CO_3)_3]$ and two chiral Schiff base ligands, prepared from the condensation of salicylaldehyde and deprotonated chiral α-amino acids, followed by chromatographic separation and ion-exchange chromatography (Scheme 1).[13]
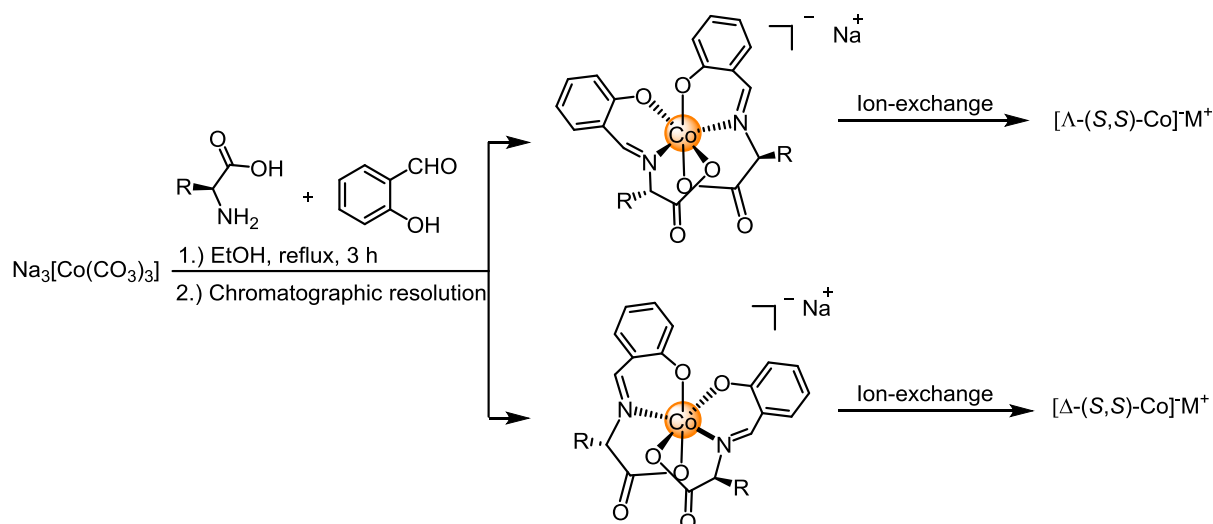
Scheme 1 Asymmetric synthesis of inert chiral octahedral cobalt complexes.

These chiral complexes are used as catalysts for a variety of asymmetric reactions. The catalytic properties of these complexes can be tuned by varying the amino acid side chain. For example, the authors found that the chiral potassium cobaltate salt Λ-(*S,S*)-Co-**1** can efficiently catalyze the enantioselective trimethylsilylcyanation of benzaldehyde. In the presence of PPh$_3$, the desired product was obtained in 89% yield with moderate enantioselectivity (77% *ee*) at room temperature (Figure 1). Interestingly, the diastereomer Δ-(*S,S*)-Co-**1**, did not provide any enantioselectivity under the same reaction conditions, which implied that the centrochirality was responsible for the asymmetric induction in this transformation. The authors proposed that the carboxylate moieties in the chiral ligand coordinate with a potassium ion, which itself serves as a Lewis acid to activate benzaldehyde and the activated benzaldehyde can form a hydrogen bond with an indole NH group in the chiral ligand. At the same time, trimethylsilylcyanide can be activated by the nucleophilic carboxylate groups in the cobaltate anion.

They later reported that the related lithium cobaltate complex Δ-(*S,S*)-Co-**2** can catalyze the asymmetric Michael addition of diethyl malonate to 2-cyclohexen-1-one in the presence of a strong base (PhOLi) in high yield and moderate enantioselectivity (69% *ee*).[14]
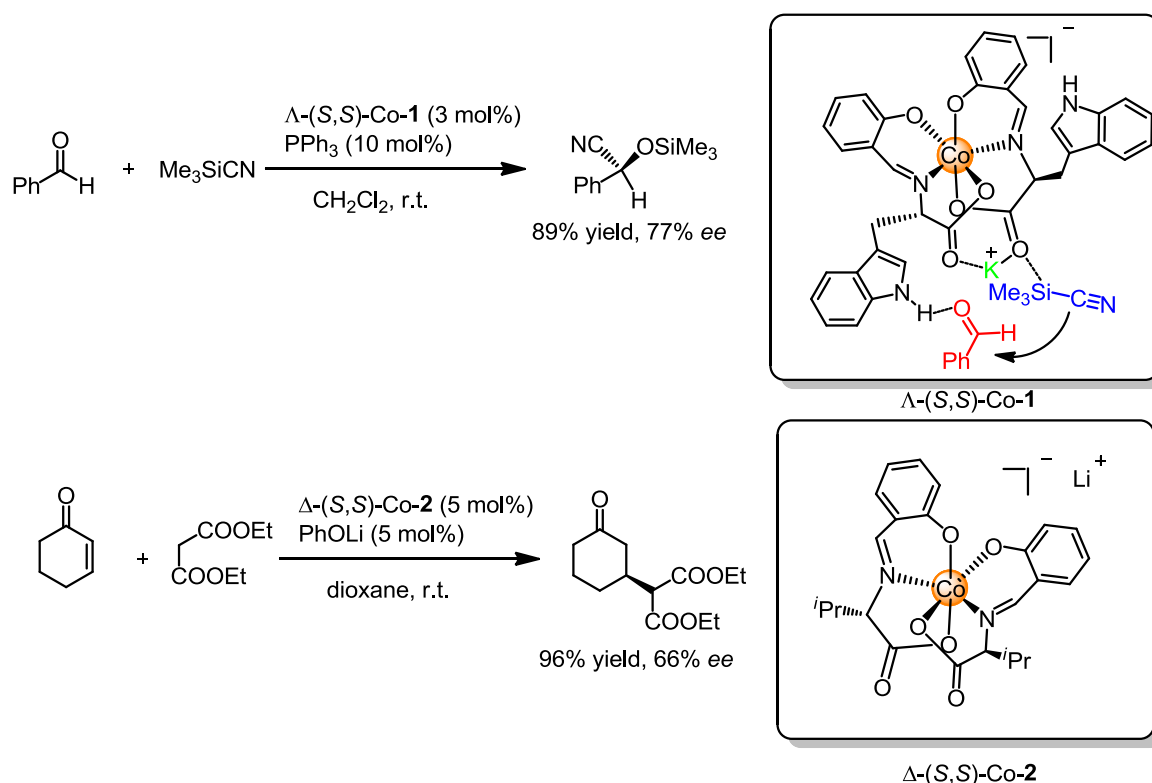
Figure 1 Asymmetric reactions catalyzed by inert chiral octahedral cobalt Schiff base complexes.

Ohkuma and co-workers introduced another class of inert chiral octahedral ruthenium complex in which the chirality at the metal center was combined with chirality in the ligand sphere.[15] In these ruthenium(II) complexes, in addition to chirality at the metal center, the axial chirality was provided from one (*S*)-2,2′-bis(diphenylphosphino)-1,1'-binaphthyl ligand and chirality arising from stereogenic carbons was provided by two α-amino acid ligands. In this unique system, the chiral ligands actually control the diastereoselective asymmetric implementation of the configuration of the metal center. Accordingly, the reaction of [RuCl₂{(*S*)-binap}(*N*,*N*-dimethylformamide)]ₙ (oligomeric form) with three equivalents of (*S*)-phenylglycine sodium salt in a mixture of DMF/CH₃OH afforded Δ-(*S*,*S*,*S*)-Ru in 74% yield as a single diastereoisomer. This complex can be purified by regular silica gel chromatography under an air atmosphere (Scheme 2). They also demonstrated that this new chiral complex could be easily modified by changing the chiral α-amino acid ligands.[16]
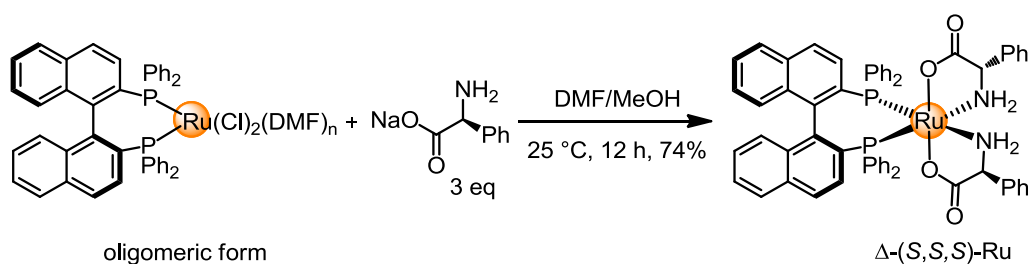
Scheme 2 Asymmetric synthesis of chiral octahedral ruthenium complex.

In the presence of Li$_2$CO$_3$, Δ-(*S,S,S*)-Ru can act as a highly active and enantioselective catalyst in the cyanosilylation of aldehydes (Figure 2). Mechanistic studies indicated that the bimetallic Ru-Li intermediate was the real catalyst, which acted as a chiral Lewis acid catalyst in the transformation. The combined catalytic system also showed high reactivity in the asymmetric hydrocyanation of α,β-unsaturated ketones.[17] Notably, the catalyst was so robust that it could be reused several times without any loss in the enantioselectivity of the reaction.
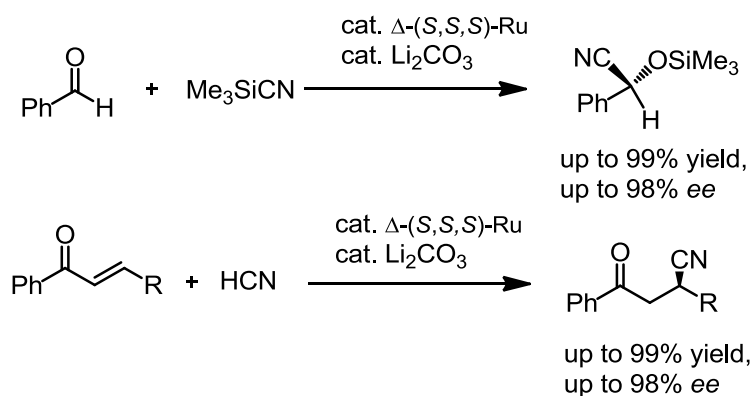
Figure 2 Asymmetric reactions catalyzed by an inert chiral octahedral ruthenium complex.

1.2.2 Reactive chiral octahedral metal complexes bearing a chiral ligand

Chiral tetradentate ligands are one of most explored motifs used in the diastereomeric synthesis of chiral octahedral metal complexes. A complex bearing one chiral tetradentate ligand in a *cis*-α-topology or a *cis*-β-topology possesses metal-centered chirality. The tetradentate ligand around the octahedral coordination sphere allows for two labile sites to be available for substrate coordination which then undergoes further transformation. Carefully tailored chiral tetradentate ligands have been vigorously investigated in the asymmetric synthesis of reactive chiral octahedral metal complexes by several research groups.

The "NOON" type of chiral tetradentate ligands have been explored in the asymmetric synthesis of reactive chiral octahedral metal complexes. In 1999, Belokon and North reported that the chiral (salen)TiCl$_2$ complex can induce the asymmetric addition of trimethylsilyl cyanide to aldehydes.[18a] Interestingly, in their catalytic system, water had a significant influence on this reaction since under rigorously anhydrous conditions a much lower *ee* was produced. During their studies, it was found that the dimeric titanium oxo complex *cis*-β-Δ-Ti could be easily obtained upon the reaction of the chiral (salen)TiCl$_2$ complex with water (Scheme 3). In the dimeric complex, the two bridging oxygen atoms adopt a *cis* conformation whereby the salen ligands cannot adopt a planar conformation around the

titanium center. Instead the salen ligands adopt a *cis*-β-Δ configuration around both titanium atoms.[18b]
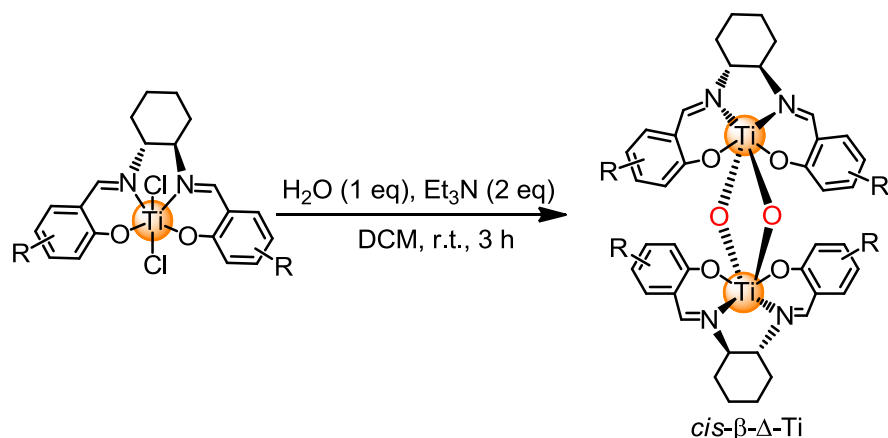
Scheme 3 Asymmetric synthesis of chiral dimeric titanium oxo complexes.

The authors demonstrated that the dimeric oxo complexes were the real catalyst precursors because of its higher reactivity than the corresponding dichloride complex. Using *cis*-β-Δ-Ti-**1** as a catalyst, the desired cyanohydrin trimethylsilyl ethers could be obtained with up to 92% *ee* after less than 1 hour at room temperature (Figure 3).

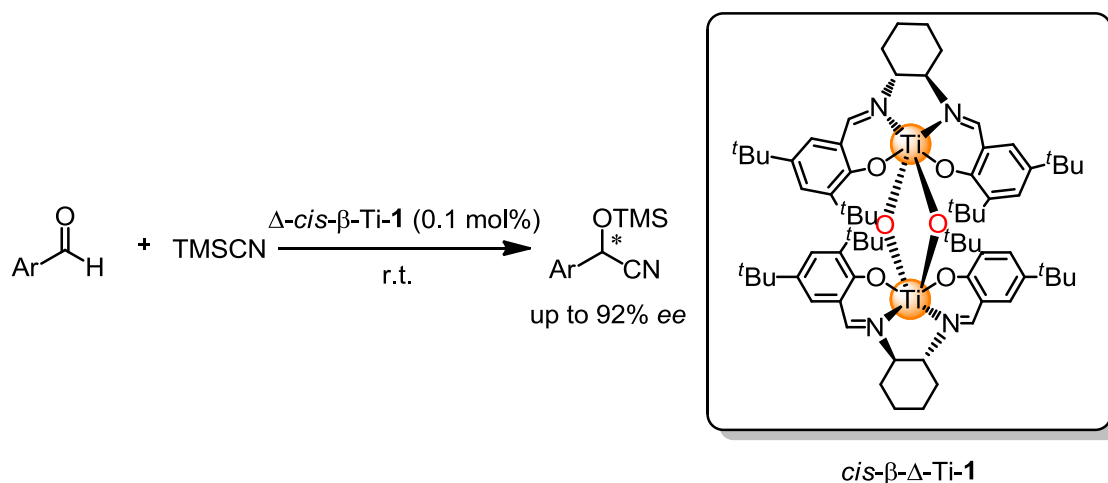**Figure 3** Asymmetric trimethylsilylcyanation of aldehydes catalyzed by *cis*-β-Δ-Ti-**1**.

The Yamamoto group used another chiral tetradentate ligand tethered bis(8-quinolinolato) to react with CrCl$_2$, followed by air oxidation, to give the *cis*-β-Λ-Cr complex in quantitative yield. The complex was isolated as a single stereoisomer due to the rotational restriction of the chiral ligand (Scheme 4).[19]
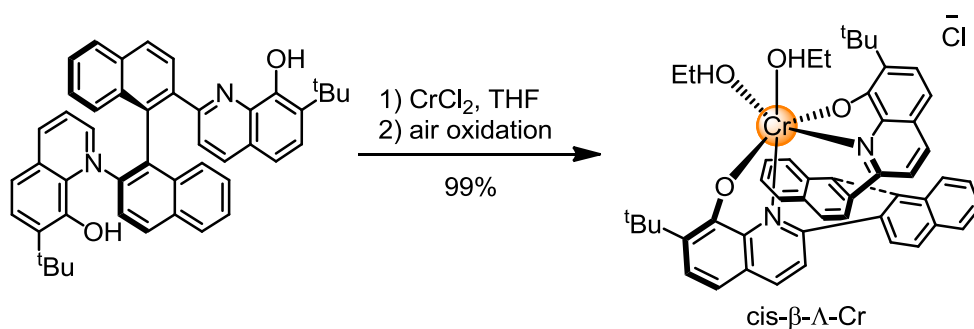
Scheme 4 "NOON" tetradentate ligand controls of synthesis of reactive chiral octahedral chromium complex.

The complex acted as an effective catalyst for a variety of asymmetric transformations including the pinacol coupling reaction, Nozaki-Hiyama allylation, Pudovik reaction and Stecker reaction.[20] Figure 4 shows one example in which the *cis-β-Λ-Cr* complex was used to catalyze the asymmetric pinacol coupling reaction with enantioselectivities observed up to 98% *ee*.
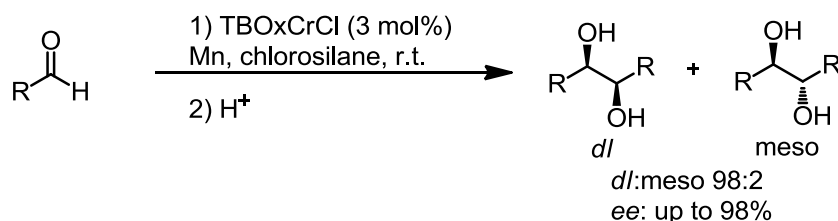
Figure 4 Asymmetric pinacol coupling catalyzed by a reactive chiral octahedral chromium complex.

A "NNNN" type tetradentate chiral ligand has also been applied to efficiently control the relative and absolute configurations upon metal complexation.[21] For example, Que Jr. et al. reported that the reaction of a bipyridinebipyrrolidine ligand with Fe(OTf)₂ 2MeCN provided exclusively the iron complex, *cis-α-Δ-Fe*, in 75% yield, in which the chiral ligand coordinated on the iron center adopts a *cis-α* topology (Scheme 5).[22]
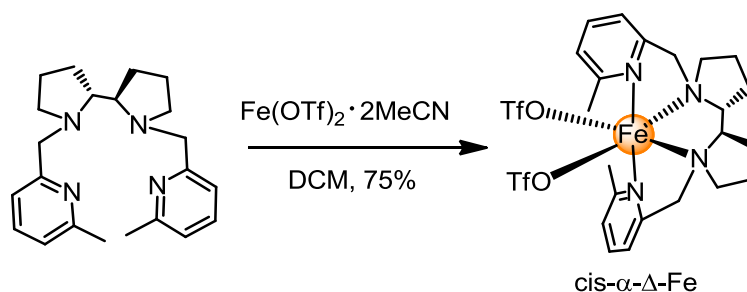
Scheme 5 "NNNN" tetradentate ligand controls of synthesis of chiral octahedral iron complex.

The authors then demonstrated that the complex could catalyze the dihydroxylation reaction of olefins using H₂O₂ to give the corresponding *cis*-diol products with high selectivity and high enantioselectivity (up to 97% *ee*) (Figure 5).

up to 97% *ee*
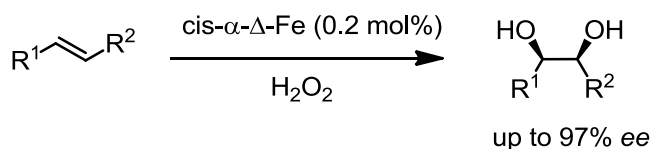
Figure 5 Oxidation of olefins with H_2O_2 catalyzed by chiral octahedral iron complex.

1.3 Octahedral Chiral-at-Metal Complexes

Octahedral chiral-at-metal complexes in which the chirality is solely a consequence of a stereogenic metal center are rare. These chiral complexes display structural simplicity because all the ligands are achiral, while the metal-centered chirality is only derived from the asymmetric coordination of the ligands around the metal center. These complexes have some attractive features, for example, without chiral ligands, there are more options regarding the tuning of the electronic and steric effects of the ligand sphere, and the metal-centered chirality is solely responsible for asymmetric induction without any other interference. Several methods have been developed for the enantioselective synthesis of chiral-at-metal complexes, including the resolution of racemic mixtures using chiral chromatography, the resolution of diastereomers using chiral counterions or the use of chiral auxiliaries. The applications of octahedral chiral-at-metal complexes are a very recent development. In this section, I will focus on the synthesis of octahedral chiral-at-metal complexes, including inert complexes and reactive complexes, and their applications in asymmetric synthesis.

1.3.1 Inert octahedral chiral-at-metal complexes

In 1911, the Nobel Prize winner Alfred Werner reported the resolution of the two enantiomers of $[Co(en)_2(NH_3)X]^{2+}$ (X = Cl and Br; en = ethylene diamine) using (+)-3-bromo-camphor-9-sulphonate as a chiral anion, which represented direct evidence of the existence of octahedral chiral-at-metal complexes (Figure 6).[23]
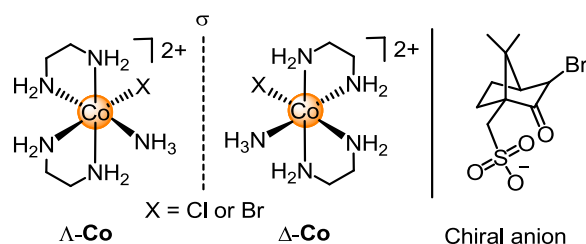

Figure 6 The resolution of octahedral chiral-at-cobalt complexes with a chiral anion.

Although the first example had already been reported for more than 100 years, the synthesis of

chiral-at-metal complexes is still challenging. Perhaps for this reason, their applications in asymmetric catalysis remain much less explored. In 2008, Gladysz et al. reported that the simple chiral-at-cobalt Werner complex, Δ-[Co(1,2-ethylenediamine)$_3$]$^{3+}$, can serve as asymmetric H-bonding catalyst.[24] This complex combined with the large tetrakis[3,5-bis(trifluoromethyl)phenyl]borate (BAr$_4$F$_{24}$) counter ion catalyzed the Michael addition of dimethyl malonate to 2-cyclopentene-1-one affording the Michael addition product in 78% yield and 33% *ee* in the presence of Et$_3$N (Figure 7).
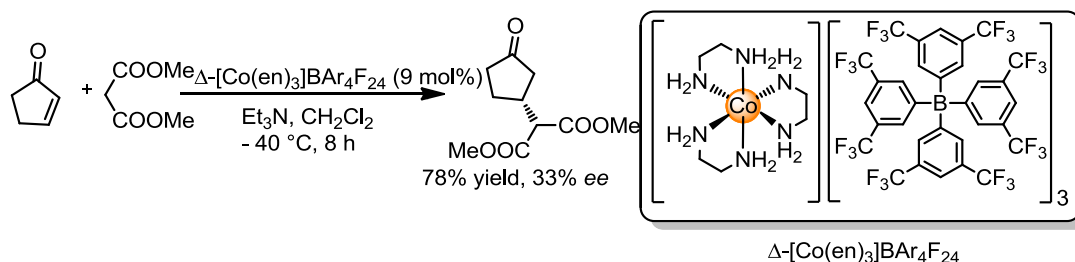
Figure 7 Enantioselective Michael addition catalyzed by an inert chiral-at-cobalt complex.

The Fontecave group reported a new dinuclear ruthenium complex, in which the chiral octahedral ruthenium complex served as a "metalloligand" for another reactive ruthenium center.[25] Accordingly, Λ-[(bpy)$_2$Ru(py)$_2$][R] (R = O,O′-dibenzoyl-L-tartrate), which was prepared according to procedures described in the literature,[26] was reacted with bipyrimidine in hot ethylene glycol solution to give Λ-[(bpy)$_2$Ru(bpym)][PF$_6$]$_2$ in 81% yield. The subsequent reaction of Λ-[(bpy)$_2$Ru(bpym)][PF$_6$]$_2$ with [RuCl$_2$(p-cymene)]$_2$ followed by anion metathesis during the chromatographic purification step provided Λ-[Ru(bpy)$_2$(bpym)RuCl(p-cymene)][NO$_3$]$_3$ (Λ-[Ru][Ru][NO$_3$]$_3$) in 78% yield (Scheme 6).
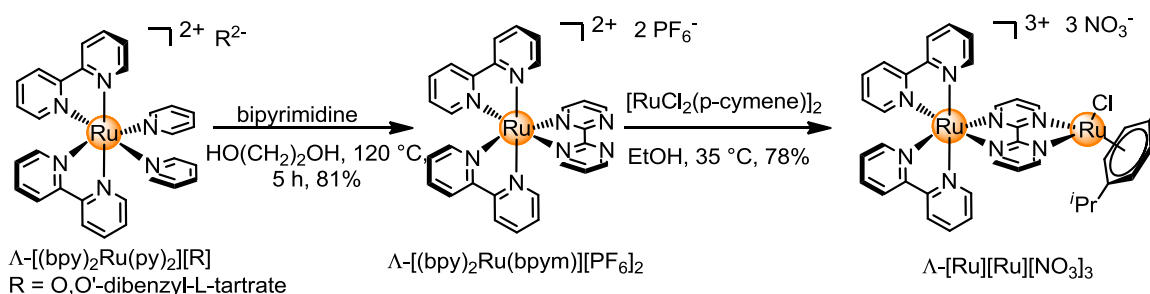
Scheme 6 The synthesis of octahedral "metalloligands" ruthenium complex.

This complex can catalyze the asymmetric transfer hydrogenation of arylketones giving the corresponding chiral alcohols with enantioselectivities up to 26% *ee*. It is worth noting that the inefficient asymmetric induction was attributed to the large distance between the chiral and catalytic metal centers (Figure 8).

78% conv., 26% *ee*
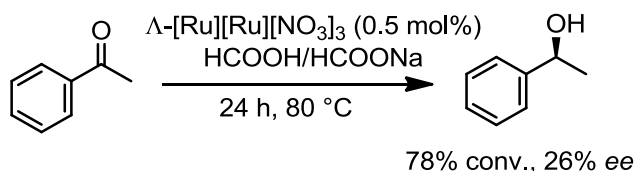
Figure 8 Asymmetric transfer hydrogenation catalyzed by octahedral "metalloligands" ruthenium complex.

The Meggers group has recently made great contributions towards the synthesis of inert octahedral chiral-at-metal complexes. These complexes can also be successfully applied for some asymmetric transformations. In 2013, the Meggers group reported the synthesis of a series of highly sophisticated octahedral chiral-at-metal iridium complexes.[27] The reaction of $IrCl_3$ trihydrate with a cyclometalating ligand affords the di-μ-chloro-bridged dimer. The dimer reacts with the chiral phenol thiazoline (*S*)-**2** as an auxiliary to provide two diastereomers, which can be separated using conventional silica gel column chromatography. Then, substitution of the chiral auxiliary with a pyridylpyrazole ligand upon protonation with NH_4PF_6 and the subsequent introduction of the BAr_4F_{24} counter ion gave the enantiopure octahedral chiral-at-metal iridium complex with the retention of its configuration (Scheme 7).
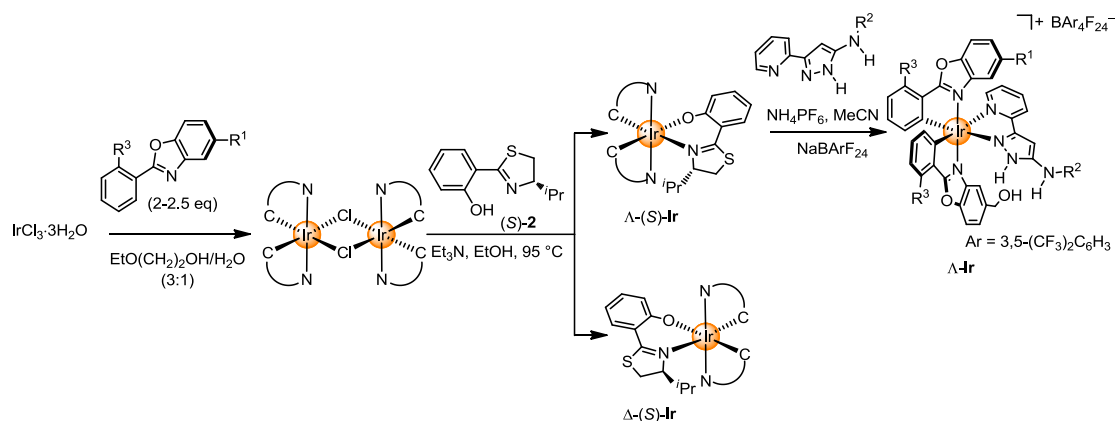
Scheme 7 Chiral auxiliary-mediated asymmetric synthesis of inert octahedral chiral-at-iridium complex.

Reactivity studies showed that these complexes were highly efficient catalysts for the asymmetric transfer hydrogenation of β,β-disubstituted nitroalkenes in the presence of a Hantzsch ester used as the reducing agent (Figure 9). It was demonstrated that Λ-**Ir1** was a superior catalyst and could catalyze the transformation delivering the reduced products in excellent yield (89%–96%) with excellent enantioselectivity (93%–99% *ee*).
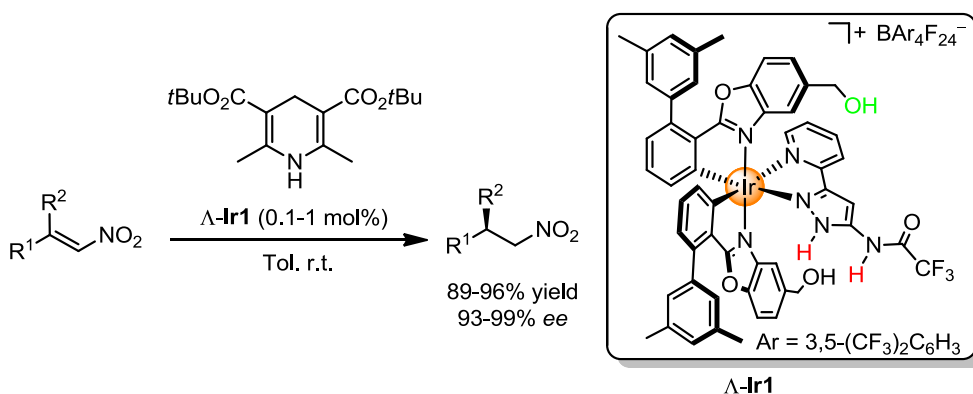
Figure 9 Asymmetric transfer hydrogenation catalyzed by an octahedral chiral-at-iridium complex.

Encouraged by these results, the Meggers group continued to design and synthesize a series of substitutionally inert octahedral chiral-at-metal complexes, which were applied as Brønsted base catalysts and enamine catalysts. These complexes can serve as highly effective chiral catalysts for the Friedel–Crafts reaction, sulfa-Michael addition reaction, α-amination of aldehydes and Henry reaction.[28]

1.3.2 Reactive octahedral chiral-at-metal complexes

In 2003, Fontecave and co-workers demonstrated that the reactive octahedral chiral-at-metal complexes, *cis*-[Δ-Ru(dmp)$_2$(CH$_3$CN)$_2$][Λ-trisphat]$_2$ or *cis*-[Λ-Ru(dmp)$_2$(CH$_3$CN)$_2$][Δ-trisphat]$_2$, could be selectively precipitated from the reaction of *cis*-[*rac*-Ru(dmp)$_2$(CH$_3$CN)$_2$] with [n-Bu$_3$NH][Λ-trisphat] or [n-Bu$_3$NH][Δ-trisphat], respectively (Scheme 8).[7b,29]
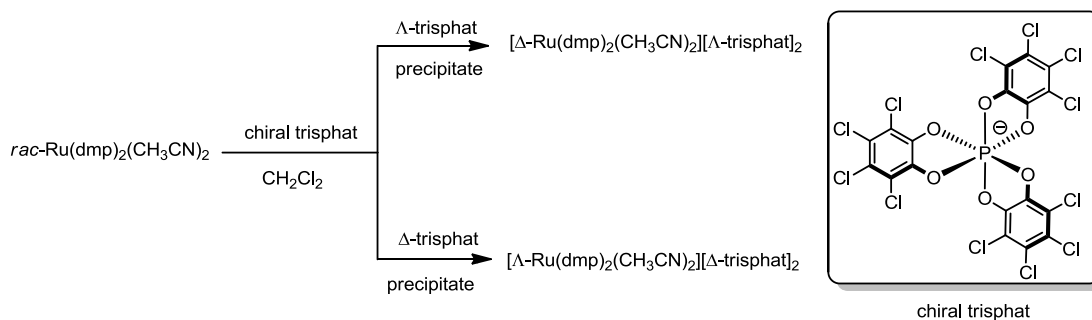
Scheme 8 The resolution of octahedral chiral-at-ruthenium complex with a chiral anion.

The octahedral chiral-at-metal complex *cis*-[Λ-Ru(dmp)$_2$(CH$_3$CN)$_2$] can catalyze the oxidation of organic sulfides to sulfoxides with a maximal 18% *ee*. Although the obtained enantioselectivity was disappointing, it was the first example in which chiral information could be transferred from an octahedral chiral-at-metal complex during a catalytic asymmetric reaction (Figure 10).
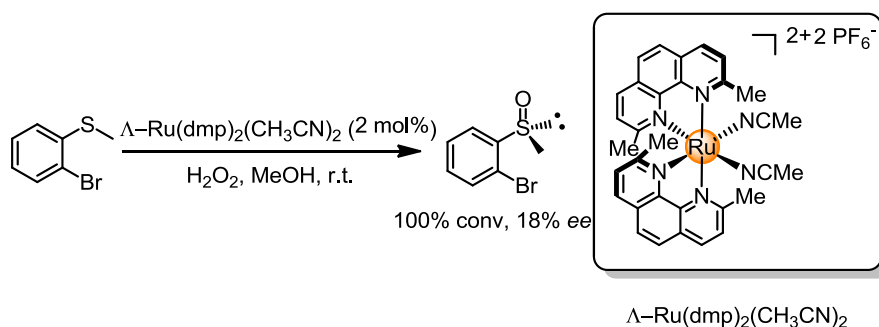
Figure 10 Asymmetric oxidation catalyzed by chiral-at-ruthenium complex.

In 2014, the Meggers group reported an example of a reactive octahedral chiral-at-metal complex.[30] This new chiral Lewis acid was structurally quite simple as all the coordinating ligands were achiral. A Λ-**Ir(O)** or Δ-**Ir(O)** metal center was cyclometalated using two achiral bidentate ligands and two labile acetonitrile ligands, which serve as the sole source of chirality. Accordingly, the reaction of IrCl$_3$ trihydrate with the 5-*tert*-butyl-2-phenylbenzoxazole ligand afforded the corresponding di-μ-chloro-bridged dimers, which exist as mixtures of the ΛΛ- and ΔΔ-isomers, respectively. Replacement of the two chlorides by introducing the chiral auxiliary (*S*)-**2** results in pairs of diastereomers, which can be separated using conventional silica gel column chromatography. The auxiliary was then substituted by two acetonitrile molecules via protonation under acidic conditions affording the Λ-isomer or Δ-isomer with a complete retention of configuration (Scheme 9).
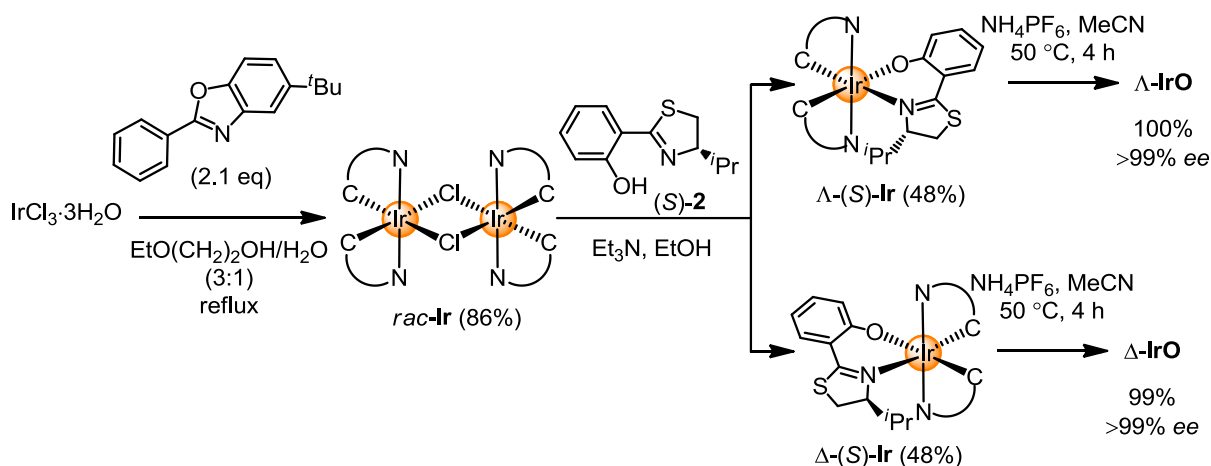
Scheme 9 Asymmetric synthesis of chiral-at-metal complexes Λ-**Ir(O)** and Δ-**Ir(O)**.

As shown in Figure 11, this newly developed enantiopure complex **Ir(O)** can serve as a highly effective Lewis acid catalyst. The enantioselective Friedel–Crafts reaction of a variety of indoles to α,β-unsaturated 2-acyl imidazoles was catalyzed using Λ- or Δ-**Ir(O)** to afford the desired products in high yield (up to 99% yield) and excellent enantioselectivity (up to 98% *ee*) at a low catalyst loading.
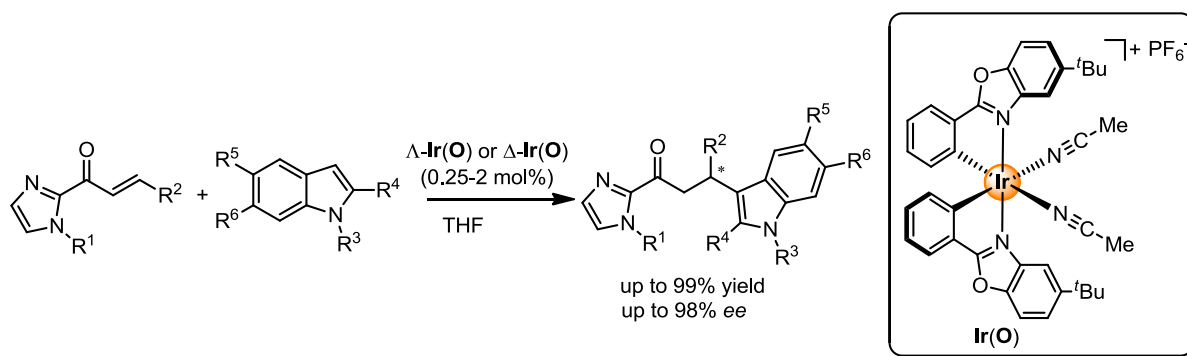
Figure 11 Asymmetric Friedel-Crafts reaction catalyzed by chiral-at-metal Lewis acid catalyst **Ir(O)**.

The Meggers group later reported another related complex, **Ir(S)**, which was also synthesized using the auxiliary-mediated strategy upon replacement of the cyclometalated 2-phenylbenzoxazole with 2-phenylbenzothiazole.[31] They then tested this complex as the catalyst for a variety of asymmetric reactions including the Friedel–Crafts alkylation reaction, Michael addition reaction using CH-acidic compounds and a variety of cycloaddition reactions, and compared the catalytic properties of Λ-**Ir(S)** with Λ-**Ir(O)**.

Ir(S) turned out to be a more effective catalyst than **Ir(O)** in several asymmetric transformations (Figure 12). Crystallographic studies show that the distance between the quaternary carbon atoms in the *tert*-butyl group and the plane though the iridium center and two acetonitrile molecules in **Ir(S)** was shorter than that in **Ir(O)**, which may explains why **Ir(S)** gave higher asymmetric induction (see Xiaodong Shen's PhD thesis for details).
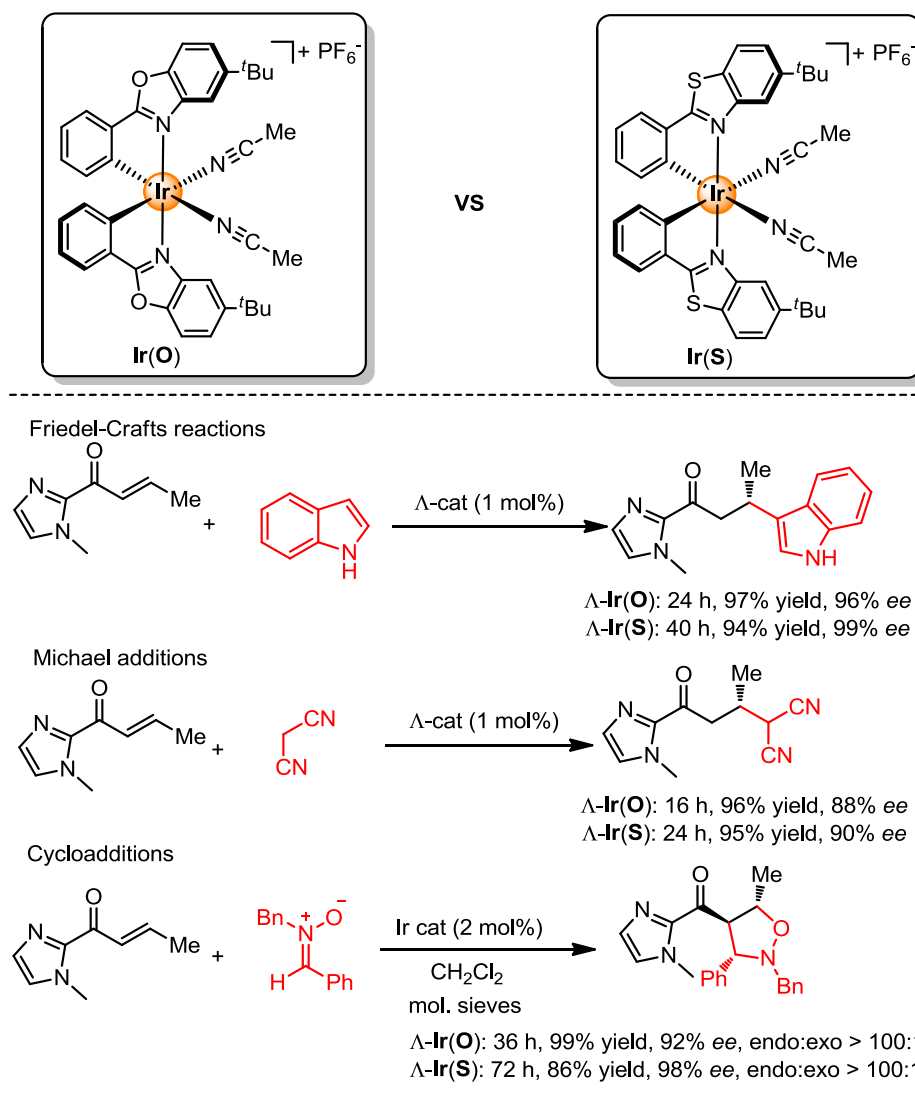
Figure 12 Asymmetric reactions catalyzed by octahedral chiral-at-metal Lewis acid complexes Λ-**Ir(O)** and Λ-**Ir(S)**.

In 2015, the Meggers group developed an example of an octahedral chiral-at-rhodium complex, which could be synthesized in an enantiopure fashion using proline-mediated synthesis and diastereoselective precipitation (Scheme 10).[32]
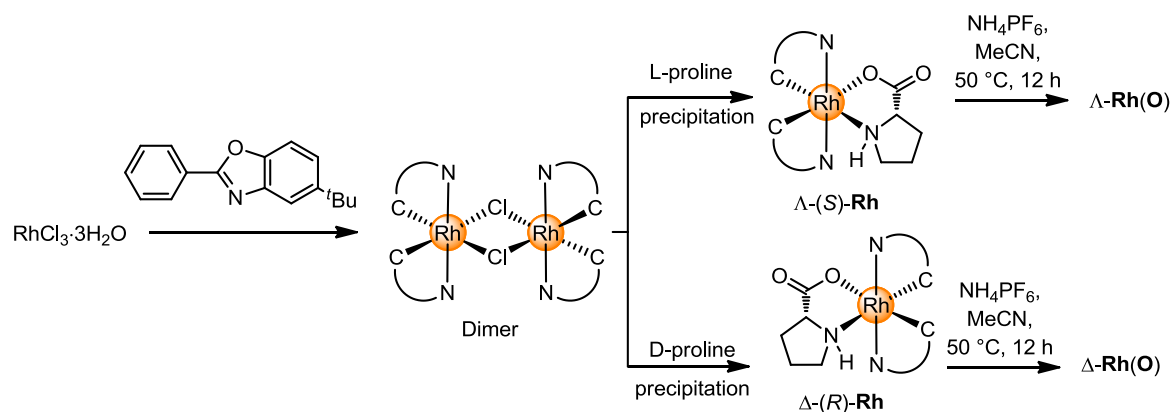
Scheme 10 Asymmetric synthesis of the enantiopure Lewis acid complexes Λ- and Δ-**Rh(O)**.

Catalytic reactivity studies indicated that the **Rh(O)** was often a better choice of catalyst than its iridium congener in the Michael addition reaction and cascade reactions (Figure 13). The higher reactivity of **Rh(O)** was mainly attributed to the higher lability of the two acetonitrile ligands, which was confirmed using acetonitrile exchange experiments (see Chuanyong Wang's PhD thesis for details).

Δ-**Ir(O)** (1 mol%), 20 h, 97% yield, 96% *ee*
Δ-**Rh(O)** (1 mol%), 40 h, 94% yield, 95% *ee*

Δ-**Ir(O)** (1 mol%), 16 h, 96% yield, 89% *ee*
Δ-**Rh(O)** (1 mol%), 16 h, 96% yield, 92% *ee*

Δ-**Ir(O)** (1 mol%), 16 h, 99% yield, 68% *ee*
Δ-**Rh(O)** (1 mol%), 16 h, 99% yield, 85% *ee*

Δ-**Ir(O)** (2 mol%), 16 h, 0% yield
Δ-**Rh(O)** (2 mol%), 16 h, 82% yield, 92% *ee*, 4:1 *dr*

Δ-**Ir(O)** (1 mol%), 96 h, 41% yield, 97% *ee*, 3:1 *dr*
Δ-**Rh(O)** (1 mol%), 48 h, 83% yield, 99% *ee*, 4:1 *dr*

Δ-**Ir(O)** (1 mol%), 72 h, 89% yield, 97% *ee*, 10:1 *dr*
Δ-**Rh(O)** (1 mol%), 20 h, 92% yield, 96% *ee*, 14:1 *dr*
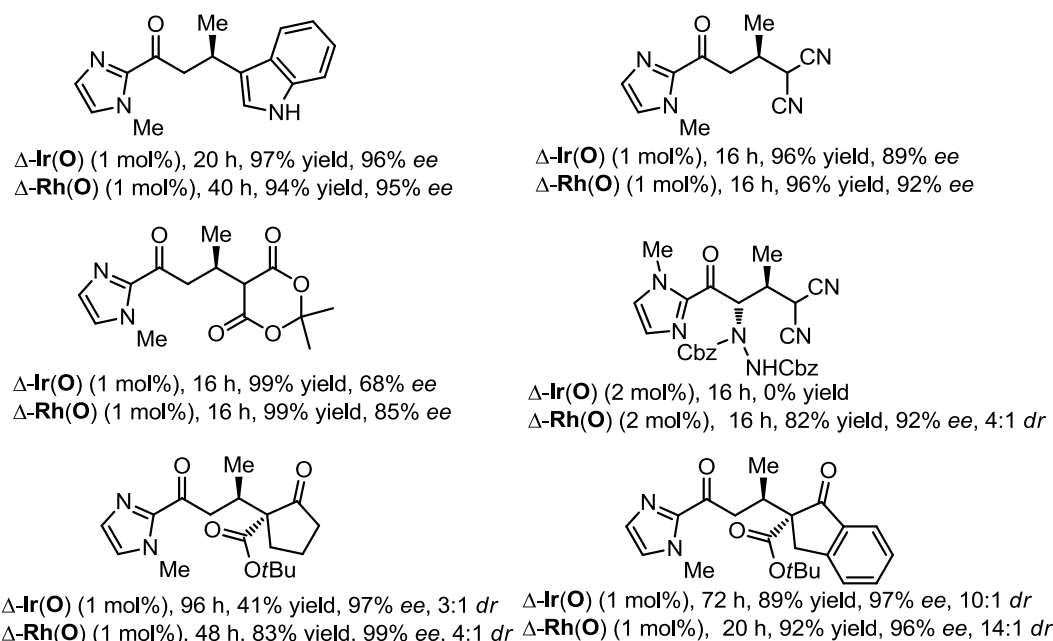
Figure 13 Asymmetric reactions catalyzed by chiral-at-metal Lewis acid complexes Δ-**Ir(O)** and Δ-**Rh(O)**.

The Meggers group was then intrigued to develop the **Rh(O)** derivative, **Rh(S)**, with the hope that it would display stronger Lewis acidity and better asymmetric induction.[33] After several chiral auxiliaries were screened, fluorinated phenol oxazoline was employed in the resolution of the Λ- and Δ-isomers giving the configurationally stable and highly enantiomerically pure catalysts. The improved properties of the **Rh(S)** catalyst were confirmed by the results obtained from two asymmetric reactions. In both the enantioselective Michael addition reaction and photo-excited enantioselective radical reaction,[34] the observed enantioselectivities were higher for the benzothiazole (**Rh(S)**) catalyst than the benzoxazole (**Rh(O)**) catalyst (Figure 14).

Michael addition

Δ-**Rh**(**O**) (1 mol%), 99% yield, 85% *ee*
Λ-**Rh**(**S**) (1 mol%), 99% yield, 93% *ee*

Photoredox reaction

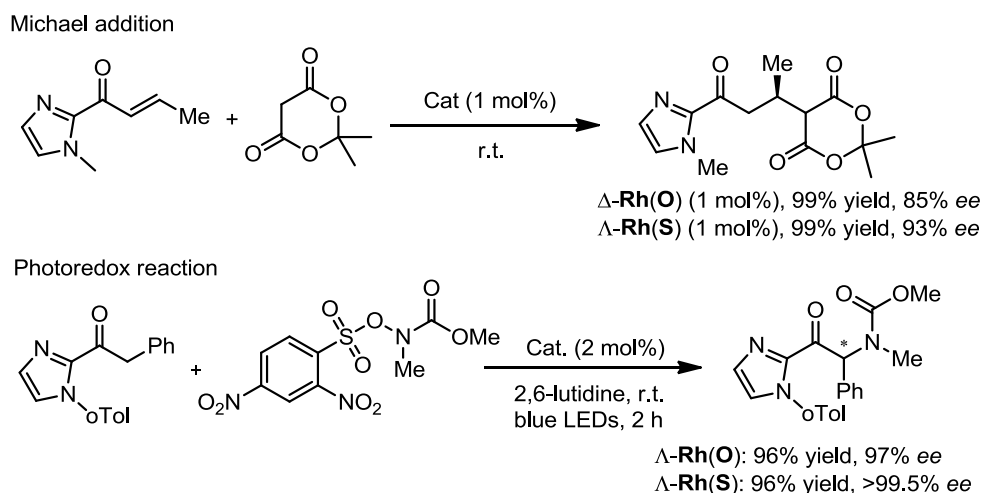Λ-**Rh**(**O**): 96% yield, 97% *ee*
Λ-**Rh**(**S**): 96% yield, >99.5% *ee*

Figure 14 Comparison of catalytic performances of chiral-at-metal Lewis acid complexes **Rh**(**O**) and **Rh**(**S**).

Recently, visible-light induced organic reactions have received a great deal of attention because they use an inexpensive and abundant form of energy.[35] Bis-cyclometalated iridium complexes are well known for their photophysical and photochemical properties,[36] and have also been used as photoredox catalysts for some transformations. The Meggers group wondered whether our chiral bis-cyclometalated iridium Lewis acid catalyst could also be used in visible-light-induced photoredox reactions. In 2014, the Meggers group found that the **Ir**(**S**) could serve as a highly effective chiral Lewis acid and at the same time as a photoredox catalyst for the visible-light induced enantioselective α-alkylation of 2-acyl imidazoles using electron-deficient benzyl bromides or phenacyl bromides.[37] Figure 15 shows that the desired products could be delivered in high yield (up to 100%) and with excellent enantioselectivity (up to 99% *ee*) in the presence of 2 mol% of Λ-**Ir**(**S**) under visible-light irradiation.

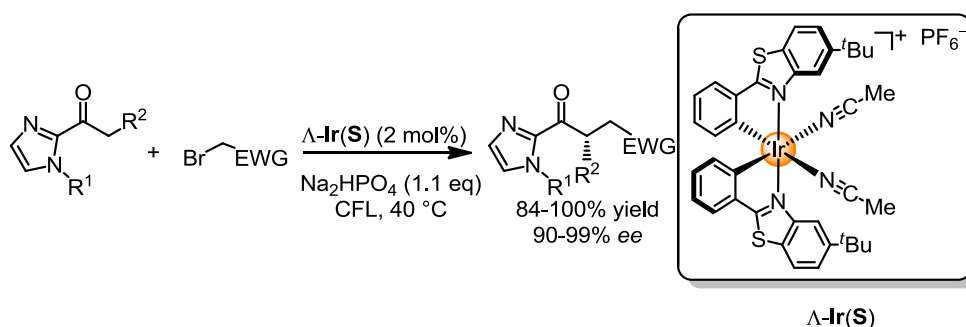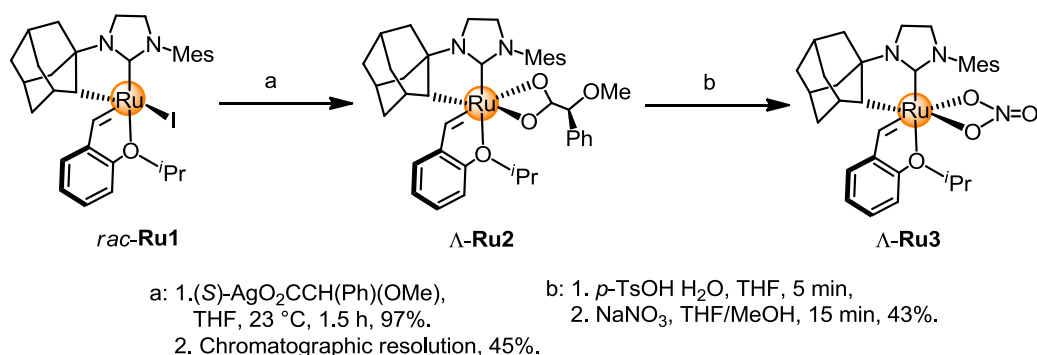

Λ-**Ir**(**S**)

Figure 15 Enantioselective α-alkylation of 2-acyl imidazoles catalyzed by Λ-**Ir**(**S**).

The Meggers group then demonstrated that this single catalyst was sufficient for many reactions including the α-alkylation of 2-acyl imidazoles with perfluoroalkyl iodides,[38] the α-trichoromethylation of 2-acyl imidazoles and 2-acyl pyridines,[39] α-aminoalkylation[40] in air and

radical/radical coupling reactions.[41] It was fascinating that these simple iridium complexes are able to perform several functions and catalyze many asymmetric transformations.

Recently, the Grubbs group reported an example of a reactive octahedral chiral-at-ruthenium complex.[42] This ruthenium(II) complex could be resolved using a chiral auxiliary-mediated strategy. Accordingly, the reaction of racemic iodide *rac*-**Ru1** with chiral silver carboxylate (*S*)-AgO$_2$CCH(Ph)(OMe) gave a 1:1 mixture of diastereomers, Λ-**Ru2** and Δ-**Ru2**. Chromatographic separation of the mixture afforded enantiopure complex Λ-Ru**2** in 45% yield and >95:5 *dr*. Subsequent treatment of Λ-Ru**2** with *p*-toluenesulfonic acid and sodium nitrate delivered Λ-**Ru3** in 43% yield (Scheme 11).

a: 1.(*S*)-AgO$_2$CCH(Ph)(OMe), THF, 23 °C, 1.5 h, 97%.
2. Chromatographic resolution, 45%.

b: 1. *p*-TsOH H$_2$O, THF, 5 min,
2. NaNO$_3$, THF/MeOH, 15 min, 43%.

Scheme 11 Asymmetric synthesis of octahedral chiral-at-ruthenium complex.

The authors then demonstrated that this complex could act as an efficient catalyst for diastereo- and enantioselective ring-opening/cross-metathesis. Figure 16 shows that the diene product can be obtained in 64% yield with 95% Z selectivity and 93% *ee* in the presence of 1 mol% of Λ-**Ru3**. The catalysis apparently occurred after dissociation of the nitrate ligand.

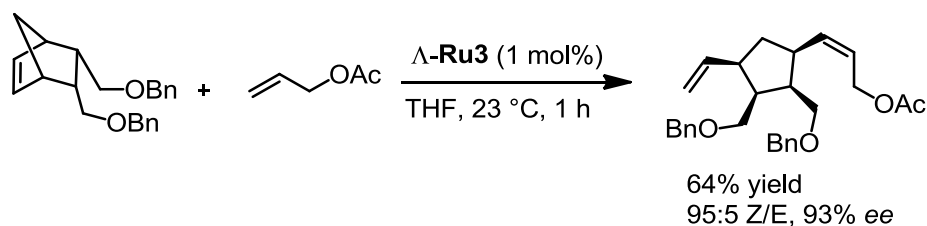64% yield
95:5 Z/E, 93% *ee*

Figure 16 Diastereo- and enantioselective ring-opening/cross-metathesis catalyzed by an octahedral chiral-at-ruthenium complex.

1.4 Conclusions

Octahedral coordination geometry provides a unique structural opportunity for the synthesis of chiral complexes bearing a stereogenic metal center. In the above-described examples, chiral

octahedral complexes with chiral ligands can be simply and diastereoselectively synthesized though the restricted coordination of chiral ligands. However, these complexes are typically combined with carefully tailored chiral ligands for achieving high enantioselectivities in asymmetric catalysis.

Octahedral chiral-at-metal complexes, in which the coordinating ligands are all achiral, have been given less attention. These complexes can be resolved by using chiral counterion-mediated asymmetric synthesis or chiral auxiliary-mediated asymmetric synthesis. Only few examples with low to moderate enantioselectivities have been reported in this area. Recently, the Meggers group has successfully developed two classes of octahedral chiral-at-metal complexes by using chiral auxiliary-mediated strategy. These complexes can achieve excellent enantioselectivities even with very low catalyst loadings. It is promising to develop more examples of chiral octahedral metal complexes with different ligands and metals, and then apply them in various asymmetric transformations. We believe that this field will continue to grow rapidly.

Reference

1. P. J. Walsh, M. C. Kozlowski, *Fundamentals of Asymmetric Catalysis*, University Science Books: Sausalito, CA, 2009.

2. J. Halpern, B. M. Trost, *Proc. Natl. Acad. Sci. USA* **2004**, *101*, 5347.

3. a) T. Hayashi, M. Kumada, *Acc. Chem. Res.* **1982**, *15*, 395−401; b) G. C. Fu, *Acc. Chem. Res.* **2004**, *37*, 542−547; c) G. C. Fu, *Acc. Chem. Res.* **2006**, *39*, 853−860; d) G. L. Hamilton, E. J. Kang, M. Mba, F. D. Toste, *Science* **2007**, *317*, 496−499.

4. a) W. S. Knowles, M. J. Sabacky, *Chem. Commun.* **1968**, 1361−1362; b) T. Ohkuma, H. Ooka, S. Hashiguchi, T. Ikariya, R. Noyori, *J. Am. Chem.Soc.* **1995**, *117*, 2675–2676; c) W. S. Knowles, *Angew. Chem. Int. Ed.* **2002**, *41*, 1998−2007; d) R. Noyori, *Angew. Chem. Int. Ed.* **2002**, *41*, 2008−2022.

5. K. B. Sharpless, *Angew. Chem. Int. Ed.* **2002**, *41*, 2024−2032.

6. a) E. N. Jacobsen, A. Pflatz, H. Yamamoto, *Comprehensive asymmetric catalysis*, Springer, Berlin Heidelberg New York 1999; b) I. Ojima, *Catalytic asymmetric synthesis*. Wiley-VCH, New York, 2000; c) B. M. Trost, *PNAS*, **2004**, *101*, 5348–5355; d) R. P. Thummel, G. Chelucci, *Chem. Rev*. **2002**, *102*, 3129–3170.

7. a) H. Brunner, *Angew. Chem. Int. Ed.* **1999**, *38*, 1194–1208; b) M. Chavarot, S. Ménage, O. Hamelin, F. Charnay, J. Pécaut, M. Fontecave, *Inorg. Chem.* **2003**, *42*, 4810−4816.

8. a) M. Fontecave, O. Hamelin, S. Ménage, *Top. Organomet. Chem.* **2005**, *15*, 271−288; b) E. B. Bauer, *Chem. Soc. Rev*. **2012**, *41*, 3153–3167; c) L. Gong, L. -A. Chen, E. Meggers, *Angew. Chem. Int. Ed.* **2014**, *53*, 10868−10874.

9. A. P. Smirnoff, *Helv. Chim. Acta* **1920**, *3*, 177−195.

10. A. von Zelewsky, *Coor. Chem. Rev*. **1999**, *190–192*, 811–825.

11. P. Knight, P. Scott, *Coor. Chem. Rev.* **2003**, *242*, 125–143.

12. For reviews on stereoselective synthesis in coordination chemistry, see: a) J.-L. Pierre, *Coord. Chem. Rev.* **1998**, *178–180*, 1183–1192; b) U. Knof, A. von Zelewsky, *Angew. Chem. Int. Ed.* **1999**, *38*, 302–322; c) C. Ganter, *Chem. Soc. Rev.* **2003**, *32*, 130–138; d) J. Lacour, V. Hebbe-Viton, *Chem. Soc. Rev.* **2003**, *32*, 373–382.

13. a) Y. N. Belokon, A. G. Bulychev, V. I. Maleev, M. North, I. L. Malfanov, N. S. Ikonnikov, *Mendeleev Commun.* **2004**, *14*, 249–250; b) Y. N. Belokon, V. I. Maleev, I. L. Mal'fanov, T. F. Savel'eva, N. S. Ikonnikov, A. G. Bulychev, D. L. Usanov, D. A. Kataev, M. North, Russ. *Chem. Bull. Int. Ed.* **2006**, *55*, 821–827; c) Y. N. Belokon, V. I. Maleev, D. A. Kataev, I. L. Mal'fanov, A. G. Bulychev, M. A. Moskalenko, T. F. Saveleva, T. V. Skrupskaya, K. A. Lyssenko, I. A. Godovikov, M. North, *Tetrahedron:Asymmetry* **2008**, *19*, 822–831.

14. a) Y. N. Belokon, V. I. Maleev, D. A. Kataev, T. F. Saveleva, T. V. Skrupskaya, Y. V. Nelyubina, M. North, *Tetrahedron: Asymmetry* **2009**, *20*, 1746–1752; b) Y. N. Belokon, V. I. Maleev, M. North, V. A. Larionov, T. F. Savel'yeva, A. Nijland, Y. V. Nelyubina, *ACS Catal.* **2013**, *3*, 1951–1955.

15. N. Kurono, K. Arai, M. Uemura, T. Ohkuma, *Angew. Chem. Int. Ed.* **2008**, *47*, 6643–6646.

16. T. Ohkuma, N. Kurono, *Synlett* **2012**, 1865–1881.

17. N. Kurono, N. Nii, Y. Sakaguchi, M. Uemura, T. Ohkuma, *Angew. Chem. Int. Ed.* **2011**, *50*, 5541–5544.

18. a) V. I. Tararov, D. E. Hibbs, M. B. Hursthouse, N. S. Ikonnikov, K. M. A. Malik, M. North, C. Orizu, Y. N. Belokon, *Chem. Commun.* **1998**, 387–388; b) Y. N. Belekon, S. Caveda-Cepas, B. Green, N. S. Ikonnikov, V. N. Khrustalev, V. S. Larichev, M. A. Moscalenko, M. North, C. Orizu, V. I. Tararov, M. Tasinazzo, G. I. Timofeeva, L. V. Yashkina, *J. Am. Chem. Soc.* **1999**, *121*, 3968–3973.

19. N. Takenaka, G. Xia, H. Yamamoto, *J. Am. Chem. Soc.* **2004**, *126*, 13198–13199.

20. J. P. Abell, H. Yamamoto, *Chem. Soc. Rev.* **2010**, *39*, 61–69.

21. a) O. Y. Lyakin, R. V. Ottenbacher, K. P. Bryliakov, E. P. Talsi, *ACS Catal.* **2012**, *2*, 1196–1202; b) O. Cussó, I. Garcia-Bosch, X. Ribas, J. Lloret-Fillol, M. Costas, *J. Am. Chem. Soc.* **2013**, *135*, 14871–14878; c) O. Cussó, M. Cianfanelli, X. Ribas, R. J. M. Klein Gebbink, M. Costas, *J. Am. Chem. Soc.* **2016**, *138*, 2732–2738; d) C. Zang, Y. Liu, Z.-J. Xu, C.-W. Tse, X. Guan, J. Wei, J.-S. Huang, C.-M. Che, *Angew. Chem. Int. Ed.* **2016**, *55,* 10253–10257; e) D. Shen, C. Saracini, Y.-M. Lee, W. Sun, S. Fukuzumi, W. Nam, *J. Am. Chem. Soc.* **2016**, *138*, 15857–15860; f) M. Milan, M. Bietti, M. Costas, *ACS Cent. Sci.* **2017**, *3*, 196–204.

22. K. Suzuki, P. D. Oldenburg, L.Que, Jr. *Angew. Chem. Int. Ed.* **2008**, *47*, 1887–1889.

23. A. Werner, *Ber. Dtsch. Chem. Ges.* **1911**, *44*, 1887.

24. C. Ganzmann, J. A. Gladysz, *Chem. Eur. J.* **2008**, *14*, 5397−5400.

25. O. Hamelin, M. Rimboud, J. Pécaut, M. Fontecave, *Inorg. Chem.* **2007**, *46*, 5354−5360.

26. a) H. Hua, A. von Zelewsky, *Inorg. Chem.* **1995**, *34*, 5791−5797; b) X. Hua, A. von Zelewsky, *Inorg. Chem.* **1995**, *34*, 992−994.

27. L.-A. Chen, W. Xu, B. Huang, J. Ma, L. Wang, J. Xi, K. Harms, L. Gong, E. Meggers, *J. Am. Chem. Soc.* **2013**, *135*, 10598–10601.

28. a) L.-A. Chen, X. Tang, J. Xi, W. Xu, L. Gong, E. Meggers, *Angew. Chem. Int. Ed.* **2013**, *52*, 14021–14025; b) J. Ma, X. Ding, Y. Hu, Y. Huang, L. Gong, E. Meggers, *Nat. Commun.* **2014**, *5*, 5531; c) H. Huo, C. Fu, C. Wang, K. Harms, E. Meggers, *Chem. Commun.* **2014**, *50*, 10409–10411; d) X. Ding, H. Lin, L. Gong, E. Meggers, *Asian J. Org. Chem.* **2015**, *4*, 434–437; e) Y. Hu, Z. Zhou, L. Gong, E. Meggers, *Org. Chem. Front.* **2015**, *2*, 968–972; f) J. Liu, L. Gong, E. Meggers, *Tetrahedron Lett.* **2015**, *56*, 4653–4656; g) Q. Ma, L. Gong, E. Meggers, *Org. Chem. Front.* **2016**, *3*, 1319–1325; h) K. Huang, Q. Ma, X. Shen, L. Gong, E. Meggers, *Asian J. Org. Chem.* **2016**, *5*, 1198–1203; i)W. Xu, M. Arieno, H. Löw, K. Huang, X. Xie, T. Cruchter, Q. Ma, J. Xi, B. Huang, O. Wiest, L. Gong, E. Meggers, *J. Am. Chem. Soc.* **2016**, *138*, 8774–8780; j) W. Xu, X. Shen, Q. Ma, L. Gong, E. Meggers, *ACS Catal.* **2016**, *6*, 7641–7646.

29. O. Hamelin, F. Charnay, J. Pécaut, M. Fontecave, *Chem. Eur. J.* **2004**, 10, 2548−2554.

30. H. Huo, C. Fu, K. Harms, E. Meggers, *J. Am. Chem. Soc.* **2014**, *136*, 2990–2993.

31. X. Shen, H. Huo, C. Wang, B. Zhang, K. Harms, E. Meggers, *Chem. Eur. J.* **2015**, *21*, 9720–9726.

32. C. Wang, L.-A. Chen, H. Huo, X. Shen, K. Harms, L. Gong, E. Meggers, *Chem. Sci.* **2015**, *6*, 1094–1100.

33. J. Ma, X. Shen, K. Harms, E. Meggers, *Dalton Trans.* **2016**, *45*,8320–8323.

34. X. Shen, K. Harms, M. Marsch, E. Meggers, *Chem. Eur. J.* **2016**, *22*, 9102–9105.

35. a) K. Zeitler, *Angew. Chem. Int. Ed.* **2009**, *48*, 9785–9789; b) J. M. R. Narayanam, C. R. J. Stephenson, *Chem. Soc. Rev.* **2011**, *40*, 102–113; c) C. K. Prier, D. A. Rankic, D. W. C. MacMillan, *Chem. Rev.* **2013**, *113*, 5322–5363; d) D. M. Schultz, T. P. Yoon, *Science* **2014**, *343*, 1239176.

36. L. Flamigni, A. Barbieri, C. Sabatini, B. Ventura, F. Barigelletti, *Top. Curr. Chem.* **2007**, *281*, 143–203.

37. H. Huo, X. Shen, C. Wang, L. Zhang, P. Röse, L.-A. Chen, K. Harms, K. Marsch, G. Hilt, E. Meggers, *Nature* **2014**, *515*, 100–103.

38. H. Huo, X. Huang, X. Shen, K. Harms, E. Meggers, *Synlett* **2016**, *27*, 749–753.

39. H. Huo, C. Wang, K. Harms, E. Meggers, *J. Am. Chem. Soc.* **2015**, *137*, 9551–9554.

40. C. Wang, Y. Zheng, H. Huo, P. Röse, L. Zhang, K. Harms, G. Hilt, E. Meggers, *Chem. Eur. J.* **2015**, *21*, 7355–7359.

41. C. Wang, J. Qin, X. Shen, R. Riedel, K. Harms, E. Meggers, *Angew. Chem. Int. Ed.* **2016**, *55*, 685–688.

42. J. Hartung, R. H. Grubbs, *J. Am. Chem. Soc.* **2013**, *135*, 10183–10185.

Chapter 2: Aim of the Work

1) Expanding the family of bis-cyclometalated octahedral chiral-at-metal iridium and rhodium complexes

Asymmetric catalysis as an elegant and atom economic strategy provides a powerful tool to introduce chirality into a molecule in the field of asymmetric synthesis. Recently, our group developed reactive octahedral chiral-at-metal iridium and rhodium complexes as Lewis acid catalysts which can effectively catalyze a variety of different asymmetric reactions, such as, Friedel-Crafts reactions,[1] Michael additions[2], cycloadditions[2] and transfer hydrogenations[3].

Our previous studies showed that **Ir**(**S**) is a somehow superior catalyst compared to **Ir**(**O**) in many transformations,[2] and the **Rh**(**S**) gives a higher enantioselectivity over **Rh**(**O**) in many light-activated reactions.[4] This is probably attributed to the increased length of the C-S bond over C-O bond which further places the two *tert*-butyl groups closer to the two labile coordination sites and then provides a higher asymmetric induction. Based on these results, we hypothesize that further increasing the length of C-X bond might result in superior catalysts over **Ir**(**S**) and **Rh**(**S**) catalysts. Herein, we would like to synthesize octahedral chiral-at-metal **Ir**(**Se**) and **Rh**(**Se**) complexes in which the two bidentate ligands are replaced by two benzoselenazole ligands, and subsequently, investigate their catalytic reactivities.

2) Introducing chiral cyclometalating ligands into chiral octahedral complexes and investigation of their catalytic activity

Recently our group reported a new family of chiral-at-metal Lewis acid catalysts (Λ/Δ-**Ir/Rh**(**O/S**)) in which the metal center is chiral resulting from the asymmetric coordination of achiral ligands. They are synthetically accessible though auxiliary-mediated method which namely a chiral bidetate ligand is temporarily incorporated into the metal center by exchanging the two labile acetonitrile ligands to facilitate the resolution of racemic complexes by chromatography or precipitation. After protonation by acid, the chiral-at-metal complexes can be obtained in an enantiomerically pure fashion.

However, all our developed Lewis acid catalysts are based on achiral ligands. So, the purposes of this part of the work are: Firstly, how the chiral cyclometalating ligands can influnce the catalytic

properties of chiral octahedral metal complexes, and secondly, we would like to simplify the synthetic route of chiral complexes featuring metal-centered chirality by employing chiral ligands.

3) Exploring new chiral-at-ruthenium complexes

Our group recently has successfully developed the chiral auxiliary-mediated strategy for the synthesis of octahedral chiral-at-metal Lewis acids iridium and rhodium catalysts. So, we were wondering whether our strategy is applicable to chiral octahedral metal complexes of other elements such as ruthenium. Although octahedral chiral-at-ruthenium complexes have already been investigated as catalysts for asymmetric reactions, only few examples were reported by now.[5] Herein, we wish to apply our strategy to asymmetric synthesis of octahedral chiral-at-ruthenium complexes. Besides, the cost of ruthenium is significantly cheaper than iridium and rhodium.

References

1   H. Huo, C. Fu, K. Harms, E. Meggers, *J. Am. Chem. Soc*. **2014**, *136*, 2990–2993.

2   X. Shen, K. Harms, M. Marsch, E. Meggers, *Chem. Eur. J.* **2016**, *22*, 9102–9105.

3   C. Tian, L. Gong, E. Meggers, *Chem. Commun.* **2016**, *52*, 4207–4210.

4   a) J. Ma, X. Shen, K. Harms, E. Meggers, *Dalton Trans*. **2016**, *45*,8320–8323; b) H. Huo, C. Fu, K. Harms, E. Meggers, *J. Am. Chem. Soc*. **2016**,*138*, 6936–6939.

5   a) M. Chavarot, S. Ménage, O. Hamelin, F. Charnay, J. Pécaut, M. Fontecave, *Inorg. Chem.* **2003**, *42*, 4810−4816; b) O. Hamelin, M. Rimboud, J. Pécaut, M. Fontecave, *Inorg. Chem.* **2007**, *46*, 5354−5360; c) J. Hartung, R. H. Grubbs, *J. Am. Chem. Soc.* **2013**, *135*, 10183–10185.

Chapter 3: Results and Discussion

3.1 Expanding the Family of Bis-Cyclometalated Octahedral Chiral-at-Metal Iridium and Rhodium Catalysts

3.1.1 Design of catalysts

In recent years, the Meggers group has successfully developed a class of octahedral chiral-at-metal **Ir(O)**[1], **Ir(S)**[2], **Rh(O)**[3] and **Rh(S)**[4] complexes in which the metal center is cyclometalated by two achiral bidentate ligands and two labile acetonitrile ligands in a propeller type fashion and thereby provides the sole source of chirality. Our studies revealed that **Ir(S)** or **Rh(S)** is often superior over **Ir(O)** or **Rh(O)**, providing better enantioselectivities.[5,6] We owed the better asymmetric induction to the increased bond length of C-S over C-O, which places the two *tert*-butyl groups even closer to the substrate coordination sites. Encouraged by theses results, we were wondering that by replacing the C-S bond with longer C-Se bond might result in better chiral Lewis acid catalysts. Thus, we synthesized the analogous complexes **Ir(Se)** and **Rh(Se)**, and compared their catalytic properties with our previous catalysts (Figure 17).
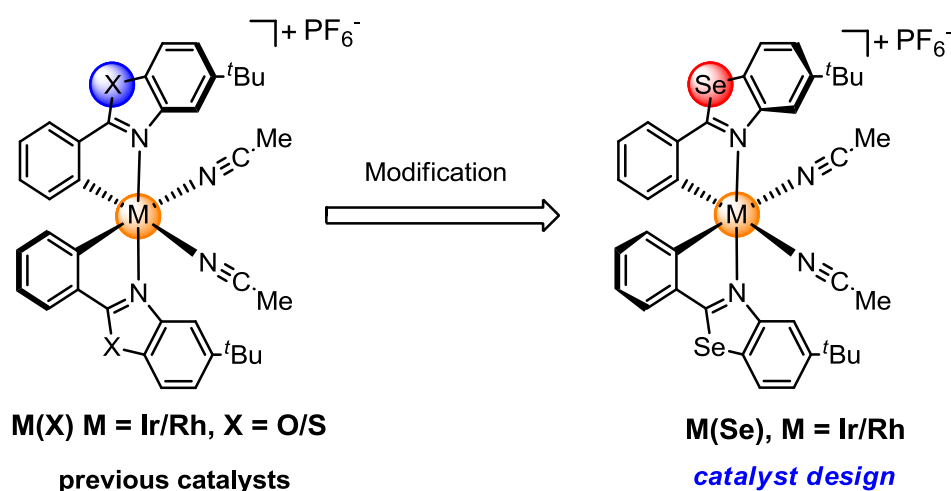
Figure 17 Catalyst design for octahedral chiral-at-metal complexes.

3.1.2 Synthesis of catalysts

The 5-(*tert*-butyl)-2-phenylbenzo[d][1,3]selenazole (**1**) was smoothly synthesized in three steps (see 5.2.1 for details). The complexes were prepared according to procedures similar to that used for the

synthesis of **Ir(S)**[5] and **Rh(S)**[4]. Accordingly, IrCl$_3$ or RhCl$_3$ hydrate was reacted with 5-(*tert*-butyl)-2-phenylbenzo[d][1,3]selenazole (**1**) in a mixture of 2-ethoxyethanol and water under reflux condition, followed by a treatment of 1.2 equivalents of AgPF$_6$ in CH$_3$CN to provide the iridium complex *rac*-**Ir(Se)** or rhodium complex *rac*-**Rh(Se)** respectively (Scheme 12, 13). The resolution of *rac*-**Ir(Se)** was conducted under our established method[5]. As shown in Scheme 12, the reaction of complex *rac*-**Ir(Se)** with chiral salicylthiazoline ligand (*S*)-**2** afforded the two diastereomeric complexes Λ-(*S*)-**3** and Δ-(*S*)-**3** as a mixture which can be separated by standard silica gel chromatography. Upon protonation of Λ-(*S*)-**3** or Δ-(*S*)-**3** by NH$_4$PF$_6$ in acetonitrile at 50 °C resulted in a substitution of chiral auxiliary ligand by two acetonitrile ligands under complete retention of configuration afforded the enantiomers Λ-**Ir(Se)** or Δ-**Ir(Se)**, respectively.
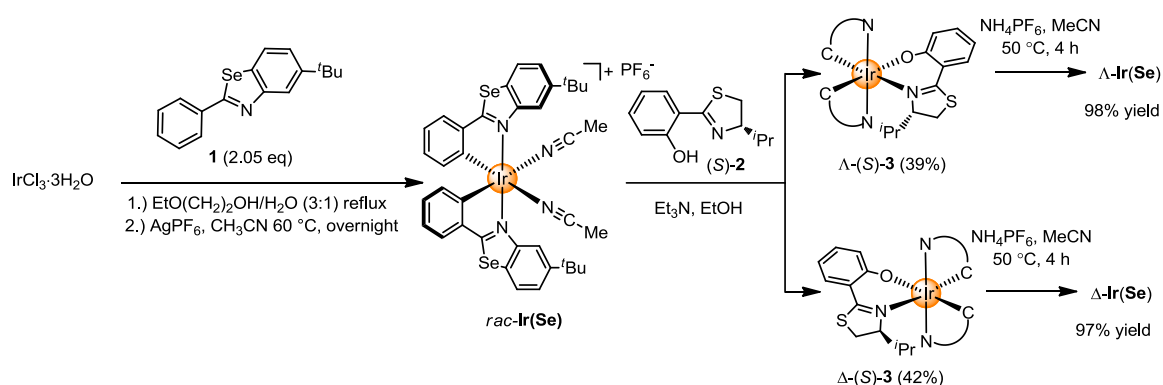
Scheme 12 Chiral auxiliary-mediated synthesis of the enantiopure iridium(III) complexes Λ-**Ir(Se)** and Δ-**Ir(Se)**.

Similarly, the resolution of complex *rac*-**Rh(Se)** could be easily achieved by employing the (*R*)-3-fluoro-2-(4-phenyl-4,5-dihydrooxazol-2-yl)phenol ((*R*)-**2′**) as chiral auxiliary which was used for the resolution of *rac*-**Rh(S)** (Scheme 13)[4]. Accordingly, the reaction of *rac*-**Rh(Se)** with (*R*)-**2′** in the presence of K$_2$CO$_3$ in EtOH at 70 °C afforded the mixture of complexes Λ-(*R*)-**4** and Δ-(*R*)-**4** which can be separated by standard silica gel chromatography combined with washing procedure. Upon protonation of Λ-(*R*)-**4** and Δ-(*R*)-**4** by TFA in acetonitrile at room temperature resulted in a substitution of chiral auxiliary ligand by two acetonitrile ligands under complete retention of configuration, affording the enantiomers Λ-**Rh(Se)** or Δ-**Rh(Se)**, respectively.
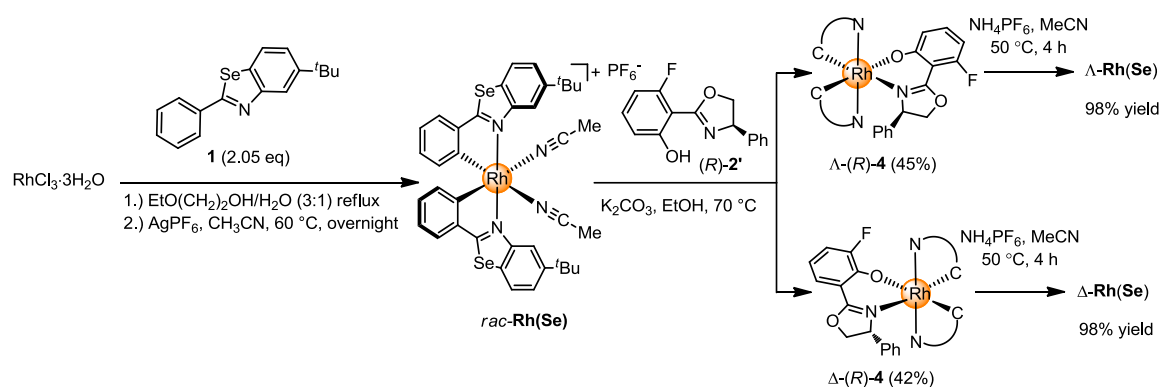
Scheme 13 Chiral auxiliary-mediated synthesis of the enantiopure rhodium(III) complexes Λ-**Rh**(**Se**) and Δ-**Rh**(**Se**).

All these newly developed enantiopure complexes can also be purified by standard flash silica gel chromatography and are configurationally stable under air and in the presence of moisture. These four enantiopure complexes were verified by CD-spectroscopy (see appendices 6.6.2). A structure of *rac*-**Ir**(**Se**) was obtained by single crystal X-ray diffraction (Figure 18, right) which clearly shows that it possesses almost identical structure compared with **Ir**(**O**) and **Ir**(**S**). The selected bond lengths and bond angles for complexes **Ir**(**O**), **Ir**(**S**) and **Ir**(**Se**) are shown in Table 1. As expected, with the atom radium of the X (X = O/S/Se) atoms increasing, the lengths of the bonds between the transition metal iridium and N atoms from the cyclometalating ligands are increasing. The bonds to the N atoms from the coordinated acetonitrile ligands are much longer in **Ir**(**Se**) than that of in **Ir**(**O**) and **Ir**(**S**), indicating more exchange labile acetonitrile ligands in **Ir**(**Se**). Besides, the distance between the quaternary carbon atoms of the *tert*-butyl groups and the plane formed by Ir atom and two N atoms from the coordinated acetonitrile ligands in **Ir**(**Se**) (4.49 Å) is shorter than that in **Ir**(**O**) (5.12 Å) and **Ir**(**S**) (4.60 Å) which indicates **Ir**(**Se**) might provide better asymmetric induction.
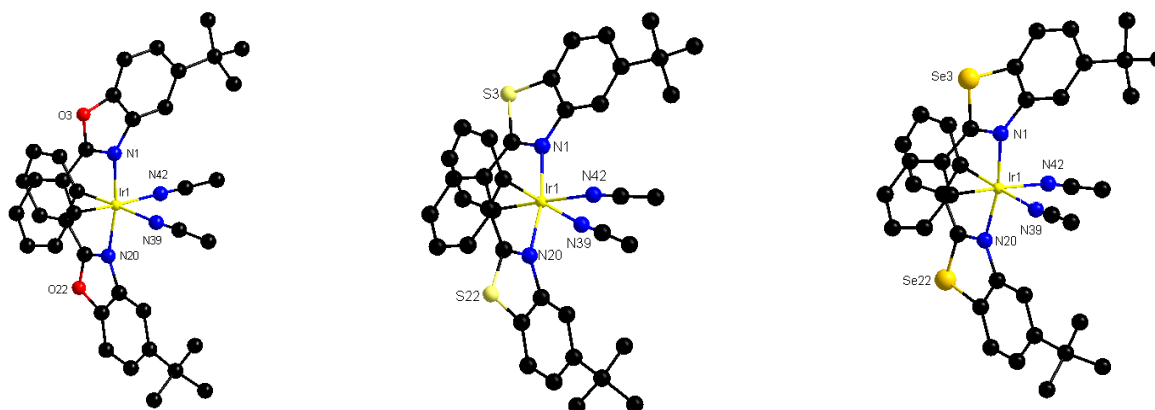
Figure 18 Crystal structures of **Ir**(**O**) (left), **Ir**(**S**) (middle) and **Ir**(**Se**) (right). The hexafluorophosphate counteranion and hydrogen atoms are omitted for clarity.

Table 1 Selected bond lengths (Å) and bond angles (°) for complexes **Ir(O)**, **Ir(S)** and **Ir(Se)**.

Complex	Ir(O)	Ir(S)	Ir(Se)
	Bond lengths		
Ir(1)-N(1)	2.044(7)	2.065(6)	2.074(4)
Ir(1)-N(20)	2.055(8)	2.072(7)	2.079(4)
Ir(1)-N(39)	2.101(8)	2.119(6)	2.126(5)
Ir(1)-N(42)	2.112(6)	2.123(7)	2.141(5)
	Bond angles		
N(1)- Ir(1)-N(20)	170.9(3)	169.6(3)	169.6(2)
N(1)- Ir(1)-N(39)	90.1(3)	86.9(2)	84.62(18)
N(1)- Ir(1)-N(42)	96.2(2)	101.4(3)	102.9(2)
N(20)- Ir(1)-N(39)	97.2(3)	100.4(2)	102.62(18)
N(20)- Ir(1)-N(42)	89.6(2)	86.2(3)	84.4(2)
N(39)- Ir(1)-N(42)	87.6(3)	88.7(3)	92.0(2)

3.1.3 Catalytic reactions

Next, we investigated several well established reactions in our lab to compare the catalytic ability of homologous catalysts Λ-**Ir/Rh(O)**, Λ-**Ir/Rh(S)** and Λ-**Ir/Rh(Se)**.

1) Asymmetric Michael addition

The Michael addition of 2-acyl imidazole **5** with malononitrile **6** was investigated firstly[5]. As shown in Figure 19, the addition of malononitrile **6** to 2-acyl imidazole **5** catalyzed by 1 mol% Λ-**Ir(O)** in THF at room temperature afforded the adduct product (*S*)-**7** in 96% yield with 88% *ee*. Our new Λ-**Ir(Se)** resulted in the same *ee* but Λ-**Ir(S)** gave 2% higher.
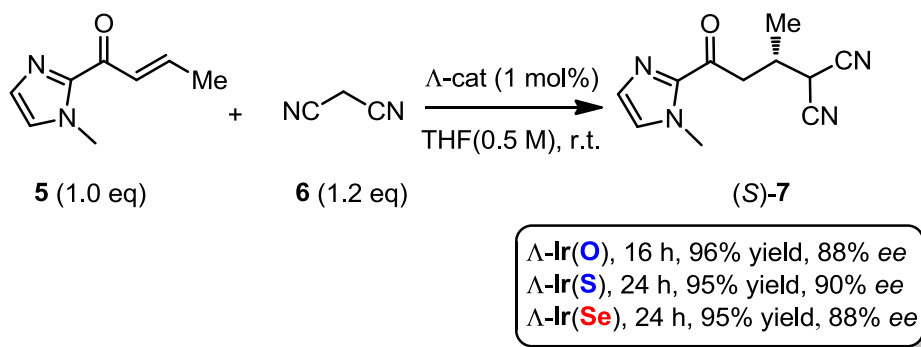
Figure 19 Asymmetric Michael addition of malononitrile.

2) Asymmetric photoredox catalysis

Several visible-light-induced reactions were also examined. Photoinduced enantioselective α-alkylation of 2-acyl imidazoles was investigated firstly.[2] As shown in Figure 20, under visible-light irradiation, when Λ-**Ir(S)** (2 mol%) was used as catalyst, the enantioselective α-alkylation of 2-acyl imidazole **8a** with phenacyl bromide **9** provided the desired product (*R*)-**10** in 91% yield and with 90% *ee* within 6 hours at 40 °C. However, when Λ-**Ir(Se)** was employed as catalyst, the reaction became slower under the same conditions and the conversion was very low after 6 hours. Prolonging the reaction time to 22 hours gave 82% yield with only 78% *ee*.
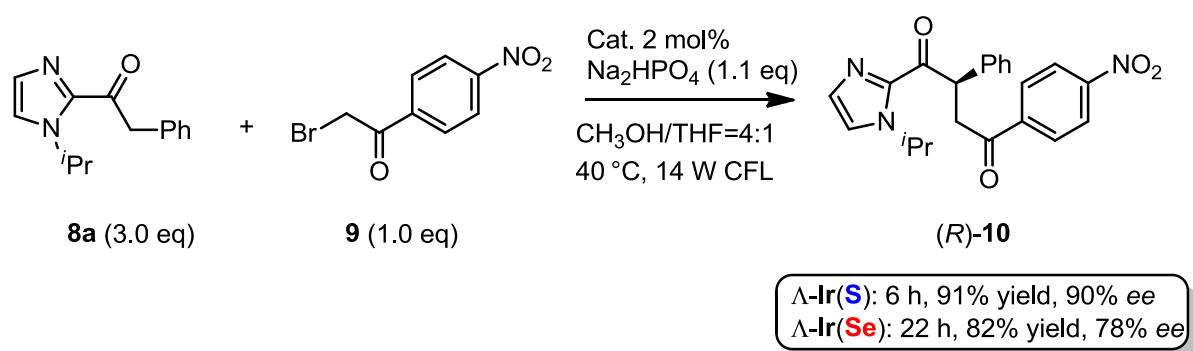
Figure 20 Asymmetric photoactivated α-alkylation of 2-acyl imidazole.

As shown in Figure 21, visible light activated asymmetric aminoalkylation of 2-trifluoroacetyl imidazoles was also investigated.[8] Λ-**Ir(S)** (2 mol%) was able to catalyze the reaction of 2-trifluoroacetyl imidazole **11a** and tertiary amine **12** to give the adduct product (*S*)-**13** in 75% yield and with high enantioselectivity of 95% *ee* under optimized conditions. However, by using Λ-**Ir(Se)** as catalyst under the same reaction conditions, the reaction was much slower and the product was obtained only in 37% yield with identical enantioselectivity after 21 hours.
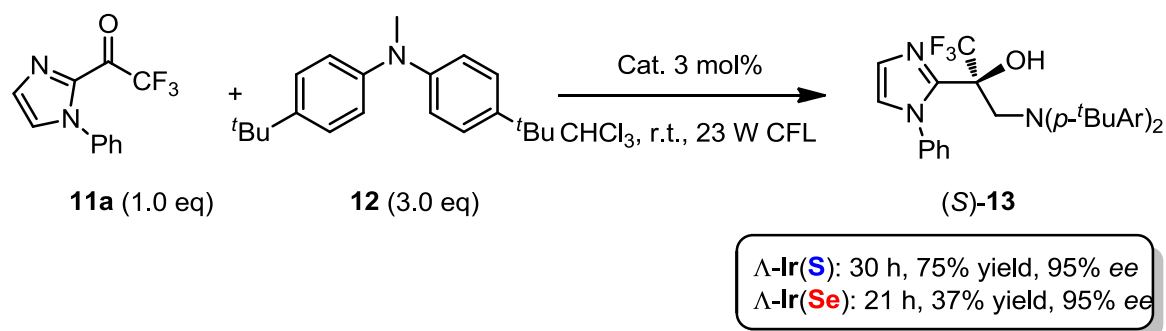
Figure 21 Asymmetric photoactivated aminoalkylation of 2-trifluoroacetyl imidazole.

Photoexcited asymmetric α-amination of 2-acyl imidazoles was also examined as shown in Figure

22.[9] Our previous study showed that Λ-**Rh**(**S**) was a better catalyst than Λ-**Rh**(**O**). The enantioselective radical amination of 2-acyl imidazole **8b** with ODN-carbamate **14** could provide the corresponding product **15** in 96% yield and with >99.5% *ee* in the presence of Λ-**Rh**(**S**). When Λ-**Rh**(**Se**) was used as a catalyst, the target product **15** was obtained only in 82% yield and with 97% *ee*.
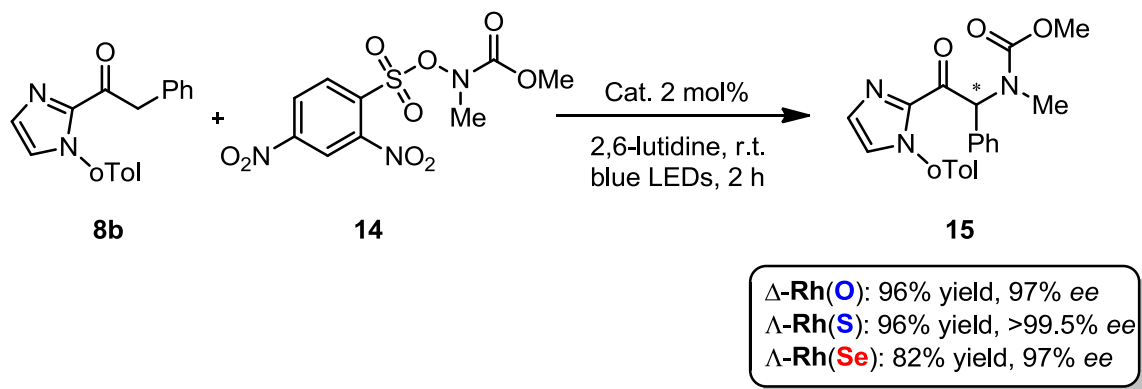
Figure 22 Asymmetric photoactivated α-amination of 2-acyl imidazole.

In the above-described examples, all the results indicated that the benzoselenazole complexes **Ir**(**Se**) and **Rh**(**Se**) are not better asymmetric catalysts compared to our previous benzoxazole and benzothiazole complexes.

3.1.4 Conclusions

In conclusion, we successfully synthesized new octahedral chiral-at-metal benzoselenazole complexes Λ/Δ-**Ir**/**Rh**(**Se**) by following our established method. This work not only expanded the family of bis-cyclometalated iridium(III) and rhodium(III) complexes but also demonstrated that our methodology for the synthesis and resolution of racemic octahedral complexes are quite general and robust. Unfortunately, the new complexes Λ/Δ-**Ir**/**Rh**(**Se**) did not show better catalytic activity compared to benzoxazole complexes Λ/Δ-**Ir**/**Rh**(**O**) and benzothiazole complexes Λ/Δ-**Ir**/**Rh**(**S**) when applying them in asymmetric catalysis. The worse reactivity might be attributed to the sluggish coordination of substrate to catalyst.

References

1   H. Huo, C. Fu, K. Harms, E. Meggers, *J. Am. Chem. Soc*. **2014**, *136*, 2990–2993.

2   H. Huo, X. Shen, C. Wang, L. Zhang, P. Röse, L.-A. Chen, K. Harms, M. Marsch, G. Hilt, E. Meggers, *Nature* **2014**, *515*, 100–103.

3   C. Wang, L.-A. Chen, H. Huo, X. Shen, K. Harms, L. Gong, E. Meggers, *Chem. Sci*. **2015**, *6*, 1094–1100.

4   J. Ma, X. Shen, K. Harms, E. Meggers, *Dalton Trans*. **2016**, *45*, 8320–8323.

5   X. Shen, H. Huo, C. Wang, B. Zhang, K. Harms, E. Meggers, *Chem. Eur. J*. **2015**, *21*, 9720–9726.

6   H. Huo, C. Wang, K. Harms, E. Meggers, *J. Am. Chem. Soc.* **2015**, *137*, 9551–9554.

7   a) M. Neumann, S. Füldner, B. König, K. Zeitler, *Angew. Chem. Int. Ed.* **2011**, *50*, 951–954; b) M. Cherevatskaya, M. Neumann, S. Füldner, C. Harlander, S. Kümmel, S. Dankesreiter, A. Pfitzner, K. Zeitler, B. König, *Angew. Chem. Int. Ed.* **2012**, *51*, 4062–4066; c) P. Riente, A. Mata Adams, J. Albero, E. Palomares, M. A. Pericàs, *Angew. Chem. Int. Ed.* **2014**, *53*, 9613–9616; d) D. A. Nicewicz, D. W. C. MacMillan, *Science* **2008**, *322*, 77–80; e) D. A. Nagib, M. E. Scott, D. W. C. MacMillan, *J. Am. Chem. Soc*. **2009**, *131*, 10875–10877; f) H.-W. Shih, M. N. Vander Wal, R. L. Grange, D. W. C. MacMillan, *J. Am. Chem. Soc*. **2010**, *132*, 13600–13603; g) M. A. Cismesia, T. P. Yoon, *Chem. Sci.* **2015**, *6*, 5426–5434; h) Y. Zhu, L. Zhang, S. Luo, *J. Am. Chem. Soc.* **2014**, *136*, 14642–14645; i) J. J. Murphy, D. Bastida, S. Paria, M. Fagnoni, P. Melchiorre. *Nature* **2016**, *532*, 218–222 ; j) D. A. DiRocco, T. Rovis, *J. Am. Chem. Soc.* **2012**, *134*, 8094–8097; k) L. J. Rono, H. G. Yayla, D. Y. Wang, M. F. Armstrong and R. R. Knowles, *J. Am. Chem. Soc*. **2013**, *135*, 17735–17738; l) G. Bergonzini, C. S. Schindler, C.-J. Wallentin, E. N. Jacobsen, C. R. J. Stephenson, *Chem. Sci.* **2013**, *5*, 112–116; m) D. Uraguchi, N. Kinoshita, T. Kizu, T. Ooi, *J. Am. Chem. Soc*. **2015**, *137*, 13768−13771; n) J. Du, K. L. Skubi, D. M. Schultz, T. P. Yoon, *Science* **2014**, *344*, 392–396.

8   C. Wang, J. Qin, X. Shen, R. Riedel, K. Harms, E. Meggers, *Angew. Chem. Int. Ed*. **2016**, *55*, 685–688.

9   X. Shen, K. Harms, M. Marsch, E. Meggers, *Chem. Eur. J.* **2016**, *22*, 9102–9105.

3.2 Synthesis, Characterization and Reactivity of Bis-Cyclometalated Iridium(III)/Rhodium(III) Complexes Containing Pinene-Derived Ligands

3.2.1 Design of catalysts

Recently, our group introduced a new class of chiral Lewis acids in which a central iridium(III) or rhodium(III) is cyclometalated by two achiral ligands, thereby generating a propeller-type C_2-symmetry with metal-centered chirality[1,2] which constitutes the exclusive source of chirality (Figure 23).[3,4] This structural element displays high constitutional and configurational stability, while two additional acetonitrile ligands are labile and provide coordinative access for substrates to coordinate to the Lewis acidic metal center. These complexes are powerful chiral Lewis acid catalysts for a variety of transformations, some activated by visible light. However, all so far synthesized catalysts (Λ- and Δ-configured **Ir(O/S/Se)** and **Rh(O/S/Se)**) are limited to achiral ligands as cyclometalating components. Our objective for this part of work was therefore twofold: Firstly, we wanted to investigate how the catalytic properties of these cyclometalated complexes depend on the the nature of the cyclometalating unit, and secondly, we were interested in simplifying the synthesis of these chiral complexes by employing chiral cyclometalating ligands instead of achiral ones, thereby drawing from a large body of work regarding diastereoselective coordination chemistry with chiral ligands and the resolution of diastereomeric mixtures of chiral metal complexes.[1] After doing some literature research, we decided to use chiral arylpyridine as an adequate candidate, because it can be readily synthesized from natural product and be widely used in asymmetric transformations (Figure 23).[5-9]
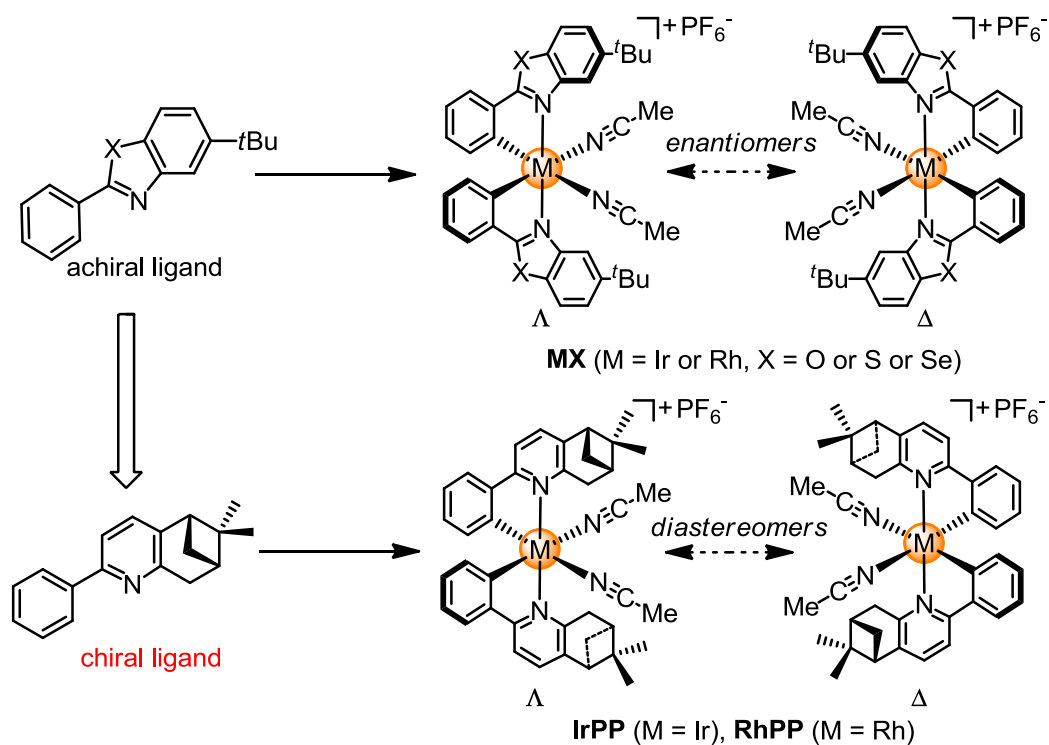
Figure 23 New design for the metal-centered chirality complexes with chiral ligands.

3.2.2 Synthesis of catalysts

The work was started by using readily available pinene-modified chiral pyridine ligands which were developed by von Zelewsky and others.[5-9] Accordingly, the reaction of 2-phenyl-5,6-(*S,S*)-pinenopyridine[7] with RhCl$_3$ hydrate or IrCl$_3$ hydrate in a mixture of 2-ethoxyethanol/water (3:1) at 125 °C for 36 hours afforded the respective chloro-bridged dimers ΛΛ/ΔΔ-**2$_{Rh}$** or ΛΛ/ΔΔ-**2$_{Ir}$**[9] as mixtures of diastereomers (Scheme 14). Consistent with related studies using cyclometalating pinene-derived pryridine ligands, the dinuclear complexes are mainly formed as the homochiral ΛΛ- and ΔΔ-diastereomers and within the coordination sphere the kinetically favored *trans* arrangement of the pyridine ligands is observed exclusively.[8] The assigned absolute configurations were confirmed by the crystal structures of bis-acetontrile complexes which were obtained from the corresponding dimers and also verified by CD-spectroscopies. The diastereomers ΔΔ-**2$_{Rh}$** and ΔΔ-**2$_{Ir}$** were formed in slight excess of their ΛΛ-counterparts according to the crude ^{1}H NMR. Conveniently, the diastereomeric dimers could be easily seperated by standard silica gel chromatography using ethyl acetate/*n*-hexane (v/v = 1:20) as the mobile phase. The subsequent reaction of the individual diastereomers with AgPF$_6$ in CH$_3$CN at 40 °C converted the chloro-bridged dimers into the individual monomeric bis-acetonitrile complexes Λ-**RhPP**, Δ-**RhPP**, Λ-**IrPP** and Δ-**IrPP**. The high diastereomeric purity (>99% *dr*) of these

complexes was confirmed by ^{1}H NMR and was verified by CD-spectroscopy (Figtures 24–27). Single crystals of all four complexes suitable for X-ray diffraction could be easily obtained by slow diffusion of *n*-hexane into CH_2Cl_2 solution and their crystal stuctures are shown in Figures 28–31, which confirm their relative and absolute configurations and reveal the propeller-type ligand arrangement with a combination of metal-centered and ligand-derived chirality. All complexes display high constitutional and configurational stability without any significant decomposition or isomerization upon leaving the complexes dissolved in CH_2Cl_2 on the benchtop for several weeks or stored in refrigerator for several months.
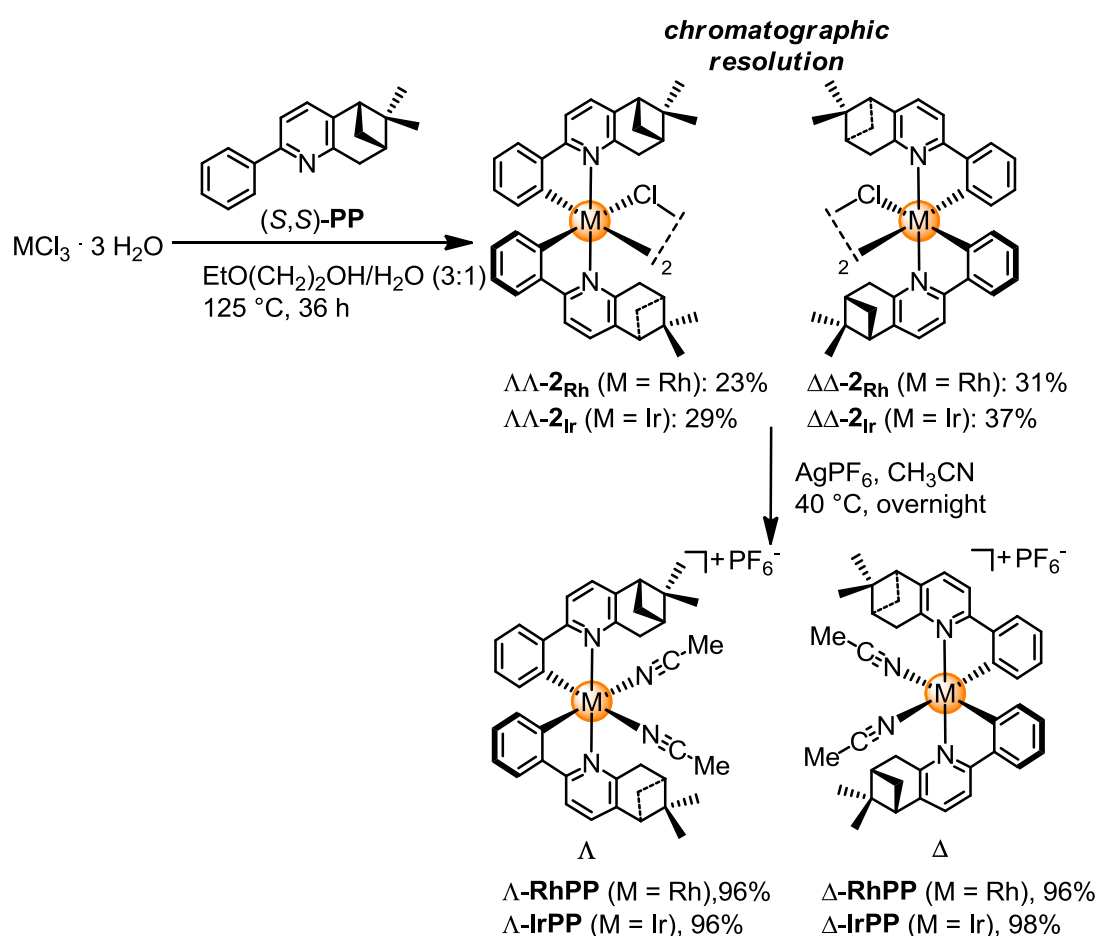
Scheme 14 Two steps synthesis of chiral octahedral iridium(III) and rhodium(III) complexes.
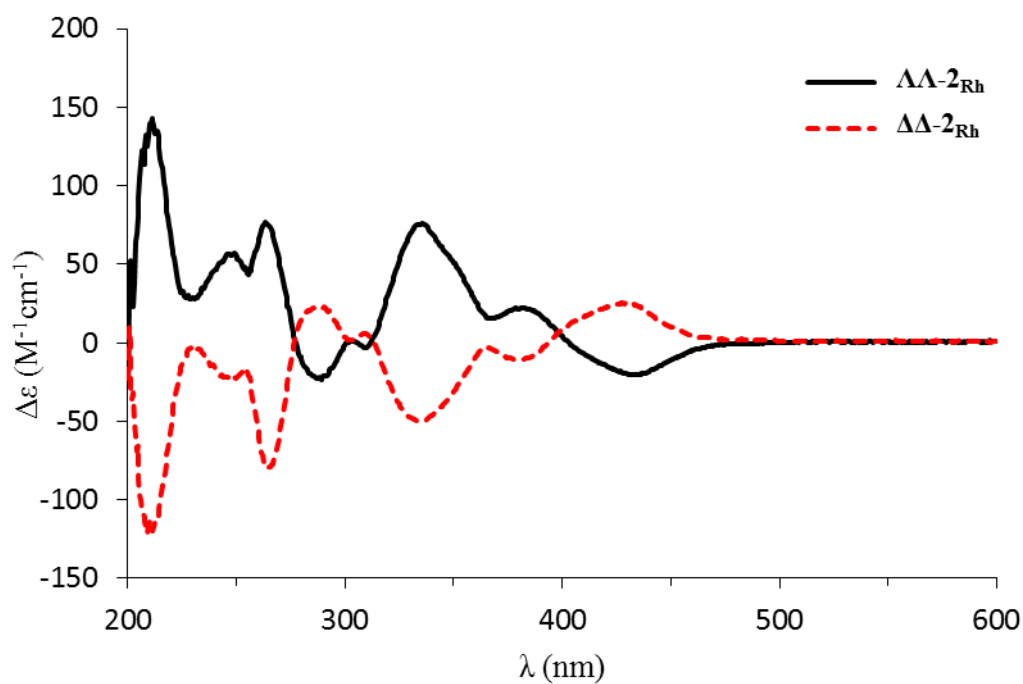
Figure 24 CD spectra of complexes $\Lambda\Lambda$-2_{Rh} and $\Delta\Delta$-2_{Rh} recorded in CH_3OH (0.2 mM).
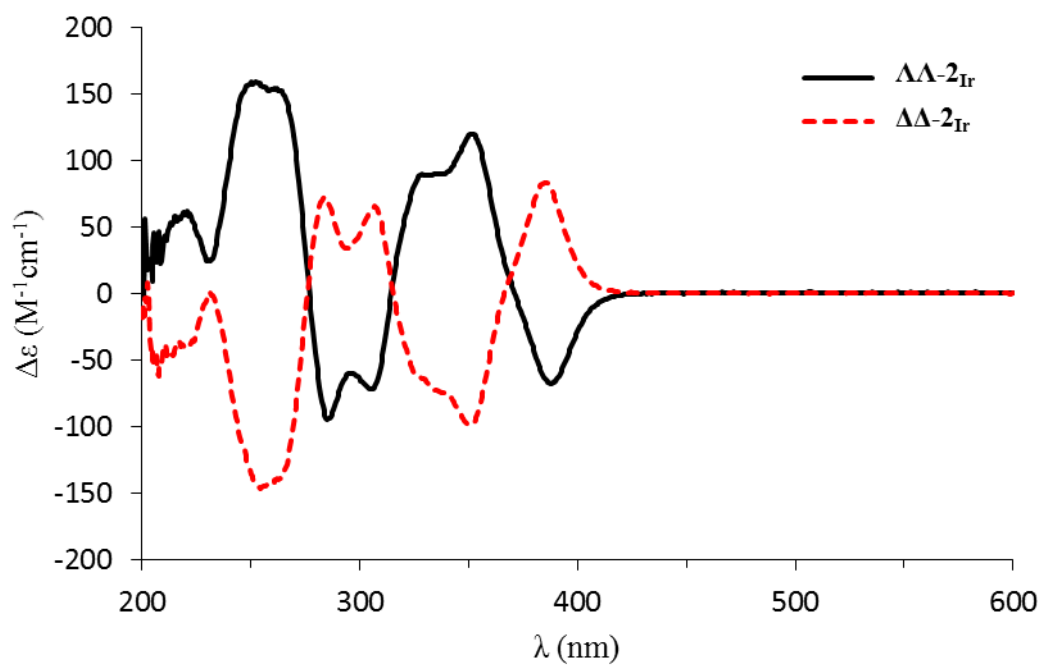
Figure 25 CD spectra of complexes $\Lambda\Lambda$-2_{Ir} and $\Delta\Delta$-2_{Ir} recorded in CH_3OH (0.2 mM).
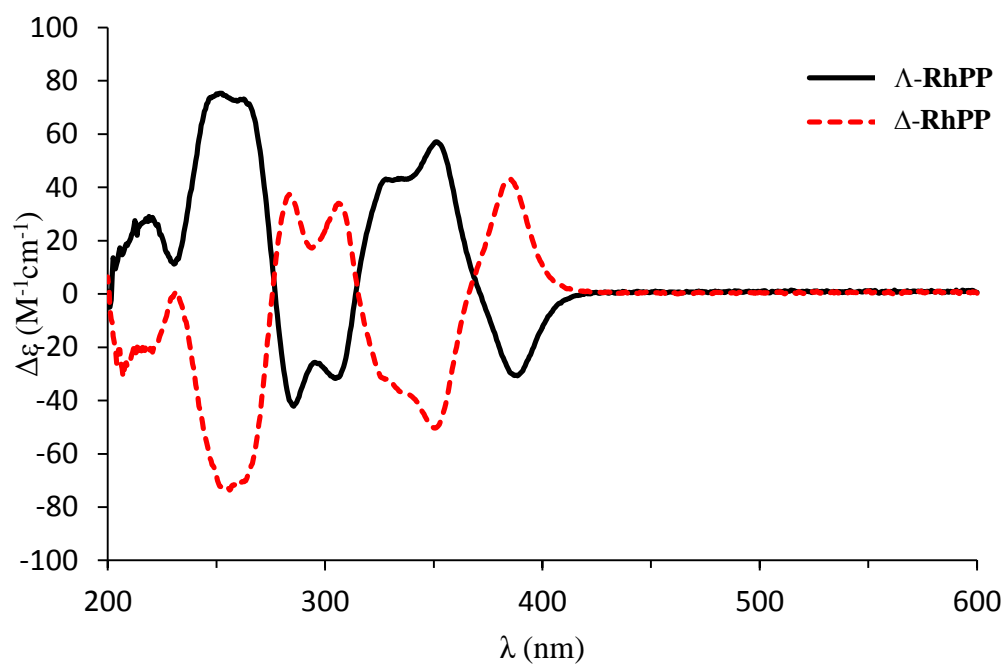
Figure 26 CD spectra of complexes **Λ-RhPP** and **Δ-RhPP** recorded in CH$_3$OH (0.2 mM).
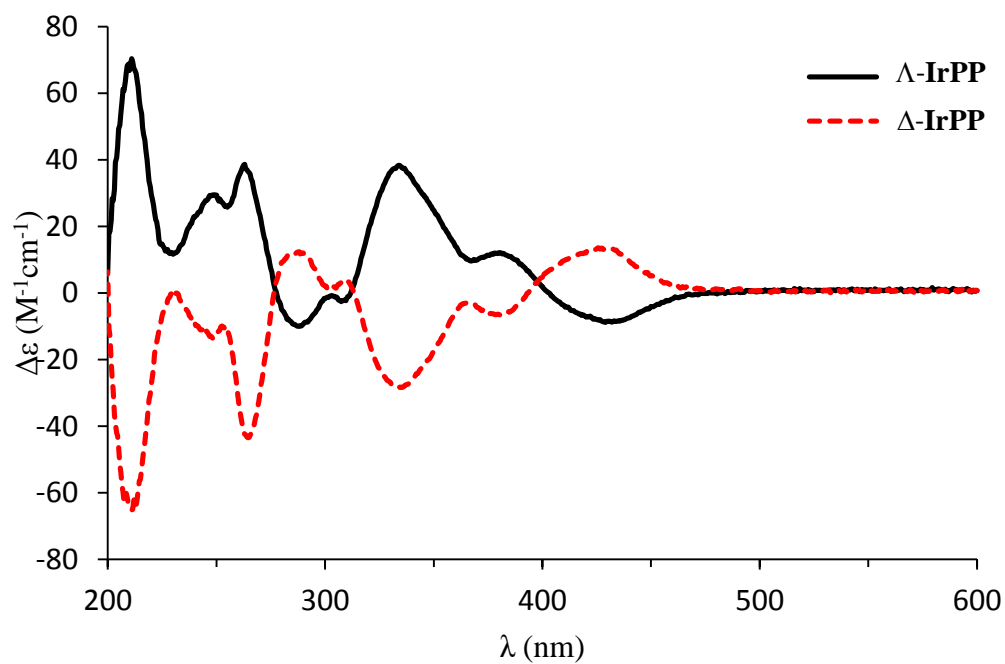
Figure 27 CD spectra of complexes **Λ-IrPP** and **Δ-IrPP** recorded in CH$_3$OH (0.2 mM).
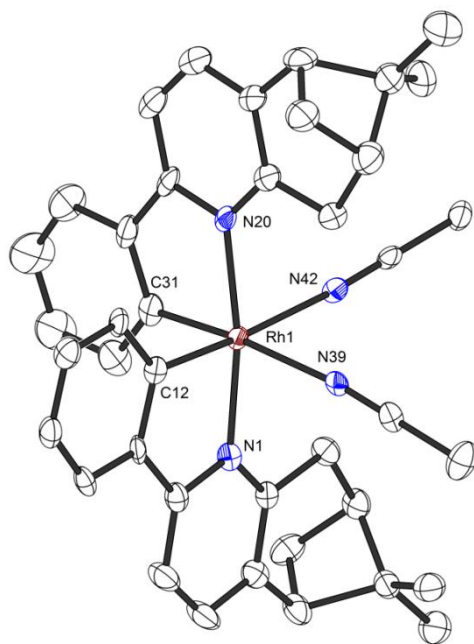
Figure 28 Crystal structure of Λ**-RhPP**. ORTEP drawing with 50% probability thermal ellipsoids. The hexafluorophosphate counteranion is omitted for clarity.
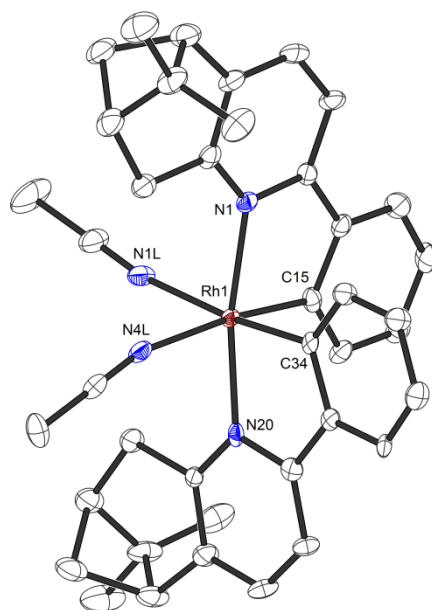
Figure 29 Crystal structure of Δ**-RhPP**. ORTEP drawing with 50% probability thermal ellipsoids. The hexafluorophosphate counteranion is omitted for clarity.
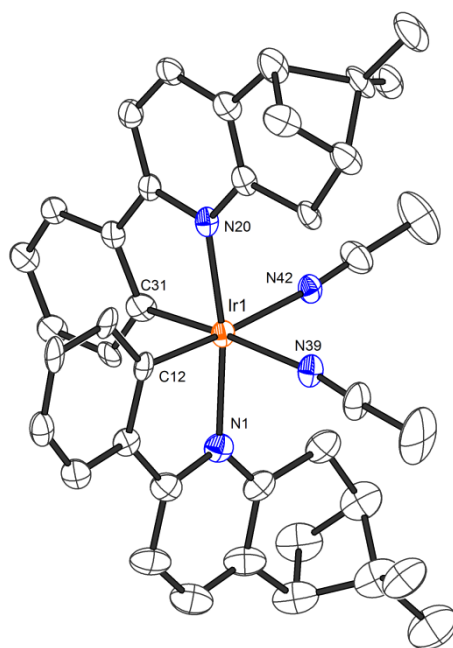
Figure 30 Crystal structure of Λ**-IrPP**. ORTEP drawing with 50% probability thermal ellipsoids. The hexafluorophosphate counteranion is omitted for clarity.
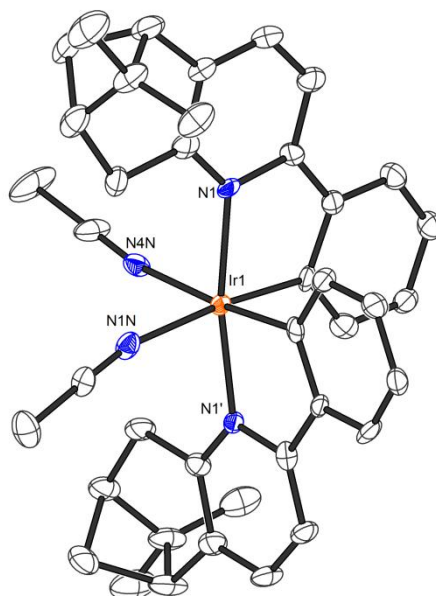
Figure 31 Crystal structure of Δ**-IrPP**. ORTEP drawing with 50% probability thermal ellipsoids. The hexafluorophosphate counteranion is omitted for clarity.

3.2.3 Catalytic reactions

With the four diastereomerically and enantiomerically pure transition metal complexes in hand, we next investigated their catalytic ability by testing several reactions. Firstly, the Friedel-Crafts addition of 2-acyl imidazole with indole was examined as shown in Figure 32.[3c] The new catalyst Λ-**IrPP** can catalyze the addition of indole to α,β-unsaturated 2-acyl imidazole **5** affording the Friedel-Crafts product (*S*)-**16** in only 38% yield and 35% *ee* after 24 h, This result was quite disappointing compared to the previous results (Λ-**Ir(S)** as catalyst, 40 h, 94% yield and 99% *ee*).
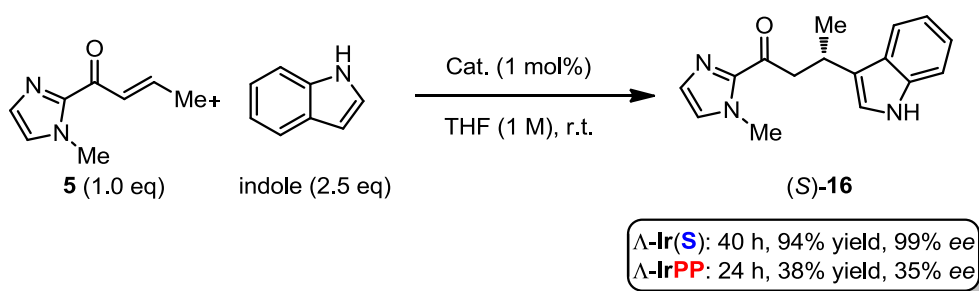
Figure 32 Comparison of different Lewis acid catalysts Λ-**Ir(S)** and Λ-**IrPP** for asymmetric conjugate addition.

The Michael addition of 2-acyl imidazole with malononitrile was next investigated.[4c] Figure 33 shows that the addition of malononitrile **6** to substrate **5** catalyzed by 1 mol% Λ-**Ir(S)** in THF at room temperature afforded the adduct **7** with 95% yield and 90% *ee* after 24 hours. Although our new catalysts only provided 78% *ee* (by Λ-**IrPP**) and less than 10% *ee* (by Δ-**IrPP**) respectively, we gladly found that the reactions were much faster. The substrate **5** was completely consumed only within one hour. That probably means that the rate of ligand exchange in **IrPP** is much faster than that in **Ir(S)**.
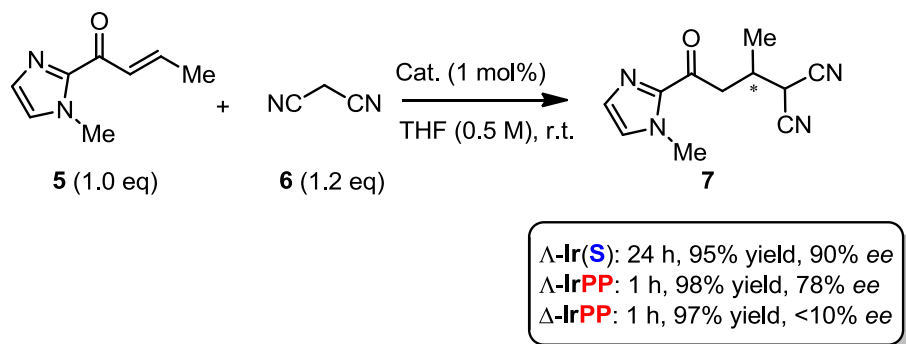
Figure 33 Comparison of different Lewis acid catalysts for asymmetric conjugate additions.

We therefore tried two following reactions regarding weak coordinating substrates (Figure 34). For the addition of malononitrile to the substrate **17**, no desired product was observed even after 48 hours at room temperature. Surprisingly, for the alkynylation of trifluoropyruvates **18** with phenylacetylene,

14% isolated yield of product **19** was obtained in the presence of 3 mol% *rac*-**RhPP** and KOAc (3 eq). After intensive screening of reaction parameters such as different bases, solvents, concentrations and temperatures and so on, the best results we can achieve were 41% yield and 38% *ee* with 3 mol% Λ-**RhPP** as a catalyst.
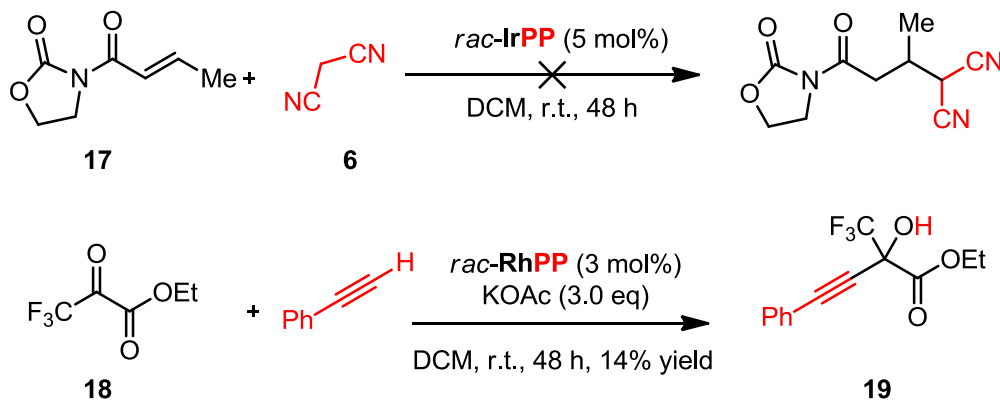
Figure 34 Two reactions with weak coordinating substrates.

When 1-phenyl-2-trifluoroacetyl imidazole (**11a**) was chosen as substrate instead of trifluoropyruvate **18**, as shown in Table 2, we found that **RhPP** can serve as an excellent catalyst for the enantioselective alkynylation of 1-phenyl-2-trifluoroacetyl imidazole (**11a**).[10-13]

The reaction of ketone **11a** with phenylacetylene at room temperature for 24 hours provided the propargyl alcohol (*R*)-**20a** in 89% yield and with 95% *ee* by using 3 mol% of Δ-**RhPP** in the presence of 1.2 equivalents of Et₃N (Table 2, entry 1). Replacing the *N*-phenyl substituent with an isopropyl group (**11b**) improved the yield of (*R*)-**20b** to 94% and enantioselectivity to 97% *ee* (entry 2). The best results were achieved with 1-phenyl-2-trifluorocetyl imidazole (**11c**), providing the propargyl alcohol (*R*)-**20c** in 92% yield and with 99% *ee* (entry 3). It is noteworthy that using the diastereomeric catalyst Λ-**RhPP** afforded the mirror-imaged product (*S*)-**20c** with an identical enantioselectivity of 99% *ee* and only with a slightly reduced yield of 90% (entry 4). This comparison of Δ-**RhPP** with Λ-**RhPP** unambiguously demonstrates that the asymmetric induction in the course of the catalysis is mainly controlled by the metal-centered chirality and not the chirality of the ligand. Notably control experiments confirmed that both the catalyst and a base were necessary for achieving a conversion (entries 5 and 6). Reduced loadings of Δ-**RhPP** (entries 7 and 8) and the base triethylamine (entry 9) did not affect the enantioselectivity but the reaction rate. Conveniently, the catalytic reaction can even be performed in an open flask since it is not sensitive to air or small amount of water (entries 10 and 11). For comparison, the iridium-congeners Λ- and Δ-**IrPP** (entries 12 and 13) provided inferior results whereas our

previously developed catalysts **Rh(O)**, **Ir(O)** or **Ir(S)** were not able to catalyze the transformation at all (entries 14–16). Thus, although the absolute configuration at the ligand does not affect the rate and degree of asymmetric induction, the nature of the ligand is obviously crucial for an effective catalysis as cyclometalated phenylbenzoxazoles (**Rh(O)** and **Ir(O)**) or phenylbenzothiazoles (**Ir(S)**) do not provide active catalysts.

Table 2 Initial Experiments[a]

11a-c
R = Ph (**11a**, **20a**), ^{i}Pr (**11b**, **20b**), Me (**11c**, **20c**)
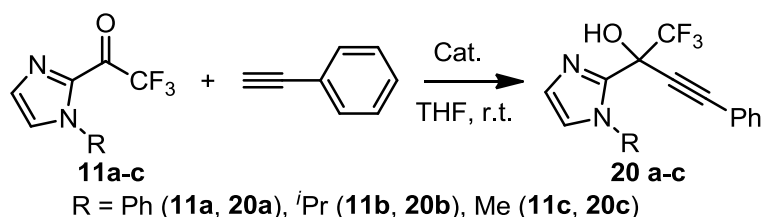
Entry	Catalyst[b]	Substrate	Base	Conditions	T (h)	Yield (%)[c]	ee (%)[d]
1	Δ-**RhPP** (3.0)	**11a**	Et$_3$N (1.2 eq)	nitrogen	24	89	95 (R)
2	Δ-**RhPP** (3.0)	**11b**	Et$_3$N (1.2 eq)	nitrogen	24	94	98 (R)
3	Δ-**RhPP** (3.0)	**11c**	Et$_3$N (1.2 eq)	nitrogen	24	92	99 (R)
4	Λ-**RhPP** (3.0)	**11c**	Et$_3$N (1.2 eq)	nitrogen	24	90	99 (S)
5	Δ-**RhPP** (3.0)	**11c**	none	nitrogen	24	0	n.a.
6	none	**11c**	Et$_3$N (1.2 eq)	nitrogen	24	0	n.a.
7	Δ-**RhPP** (2.0)	**11c**	Et$_3$N (1.2 eq)	nitrogen	24	80	99 (R)
8	Δ-**RhPP** (1.0)	**11c**	Et$_3$N (1.2 eq)	nitrogen	24	51	99 (R)
9	Δ-**RhPP** (3.0)	**11c**	Et$_3$N (0.3 eq)	nitrogen	24	60	99 (R)
10	Δ-**RhPP** (3.0)	**11c**	Et$_3$N (1.2 eq)	air	24	93	99 (R)
11	Δ-**RhPP** (3.0)	**11c**	Et$_3$N (1.2 eq)	air, 1% H$_2$O	24	88	99 (R)
12	Δ-**IrPP** (3.0)	**11c**	Et$_3$N (1.2 eq)	nitrogen	24	37	29 (R)
13	Λ-**IrPP** (3.0)	**11c**	Et$_3$N (1.2 eq)	nitrogen	24	84	15 (S)
14	Λ/Δ-**Rh(O)** (3.0)	**11c**	Et$_3$N (1.2 eq)	nitrogen	24	0	n.a.
15	Λ/Δ-**Ir(O)** (3.0)	**11c**	Et$_3$N (1.2 eq)	nitrogen	24	0	n.a.
16	Λ/Δ-**Ir(S)** (3.0)	**11c**	Et$_3$N (1.2 eq)	nitrogen	24	0	n.a.

[a]Conditions: trifluoromethyl ketone (0.20 mmol), phenylacetylene (0.60 mmol) and catalyst (3.0 mol%) in THF (0.2 mL) were stirred at room temperature for 24 hours. [b]Catalyst loading in mol% provided in brackets. [c]Isolated yields. [d]Chiral HPLC analysis. n.a. = not applicable.

After these promising initial results regarding the enantioselective alkynylation with Δ-**RhPP**, we performed a substrate scope evaluation under optimized conditions with the trifluoroketone **11c** and a variety of arylacetylenes. As shown in Figure 35, our method tolerates a variety of substituted phenylacetylenes, containing alkyl and aryl with electron-donating and electron-withdrawing substituents. Heteroarylacetylenes such as 2-pyridylacetylene and 3-thiophenylacetylene are also suitable substrates for this asymmetric transformation. Overall, yields range from 79−99% and enantioselectivities from 97−99% *ee* for the propargyl alcohols (*R*)-**20c-p**.
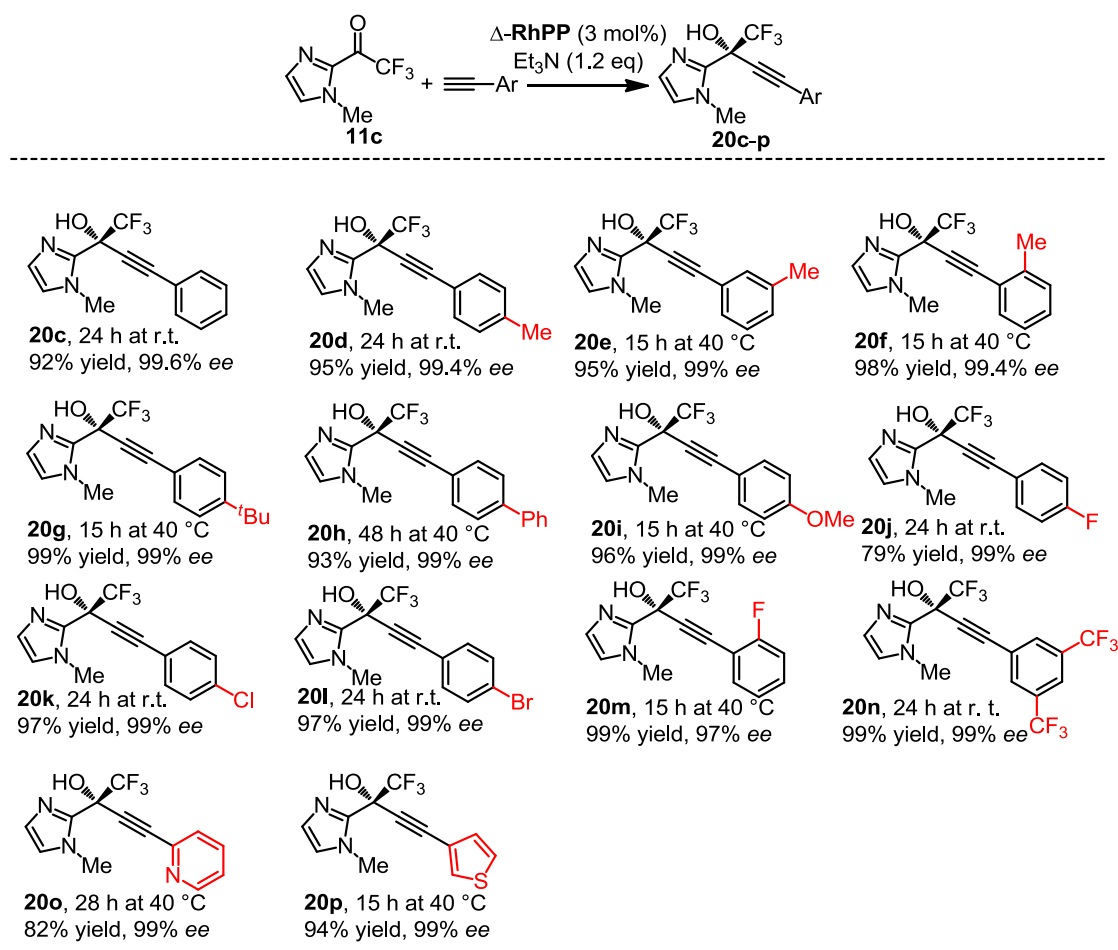
Figure 35 Substrate scope with respect to arylacetylenes.

Δ-**RhPP** also catalyzes the reaction of trifluoroketone **11c** with aliphatic acetylenes as shown in Figure 36 to provide the propargyl alcohols (*R*)-**20q-v** in satisfactory yields (55−88%) and with

excellent enantioselectivities (94−99% *ee*). Next several other substrates with respect to the imidazole substrates are also investigated under the same or some modified conditions (Figure 37).
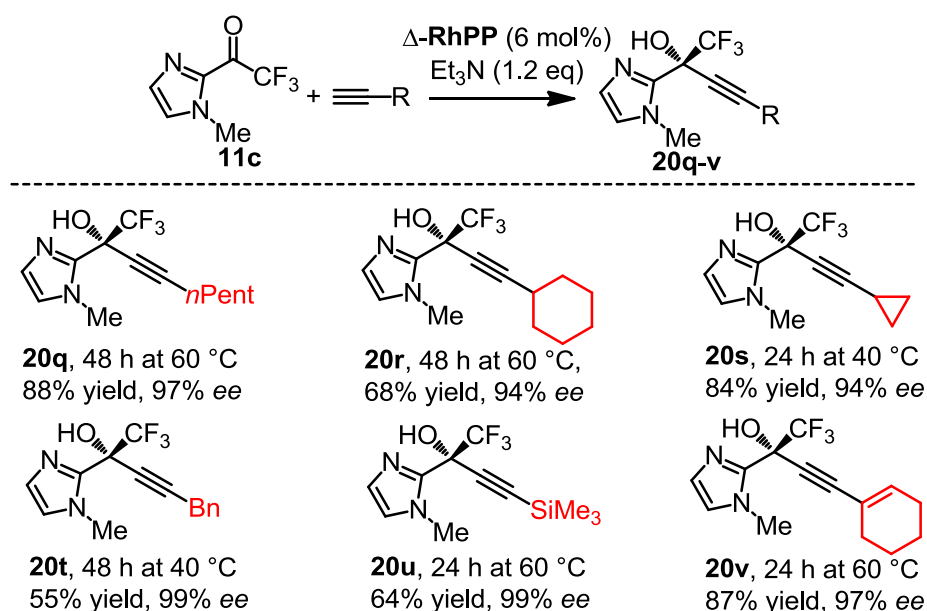
Figure 36 Substrate scope with respect to alkylacetylenes and trimethylsilylacetylene.

The benzimidazole substrate **11d** can also react with phenylacetylene to give the corresponding alcohol **20w** in moderate yield and with excellent enantioselectivity (99% *ee*). The substrate **11e** with methoxyphenyl group on imidazole moiety can provide satisfying results (95% yield, 94% *ee*). Importantly, the CF_3 group can be replaced by a CF_2CF_3 group, affording the expected product **20y** in good yield and with excellent enantioselectivity (97% *ee*) by prolonging the reaction time to 48 h and at the same time increasing the temperature to 60 °C.
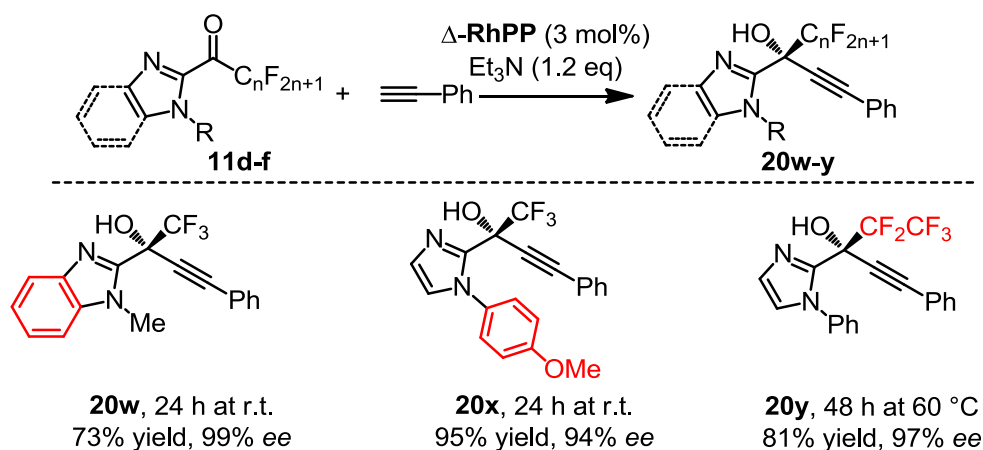
Figure 37 Substrate scope with respect to other 2-fluoroacetyl imidazoles.

However, it is important to note that satisfactory yields and excellent enantioselectivities of this reaction are limited to ketones which contain both the CF_3 group as well as the imidazole moiety. For

example, replacing the imidazole moiety with a phenyl or ethylcarboxylate or benzoyl leads to get no or low yield and enantioselectivity, while changing the CF_3 group with an ethyl group completely abolishes the conversion (Figure 38). These results imply that a successful catalysis relies on a strong electronic activation of the carbonyl group by a neighboring CF_3 in combination with the efficient coordination of the substrate to the rhodium catalyst.
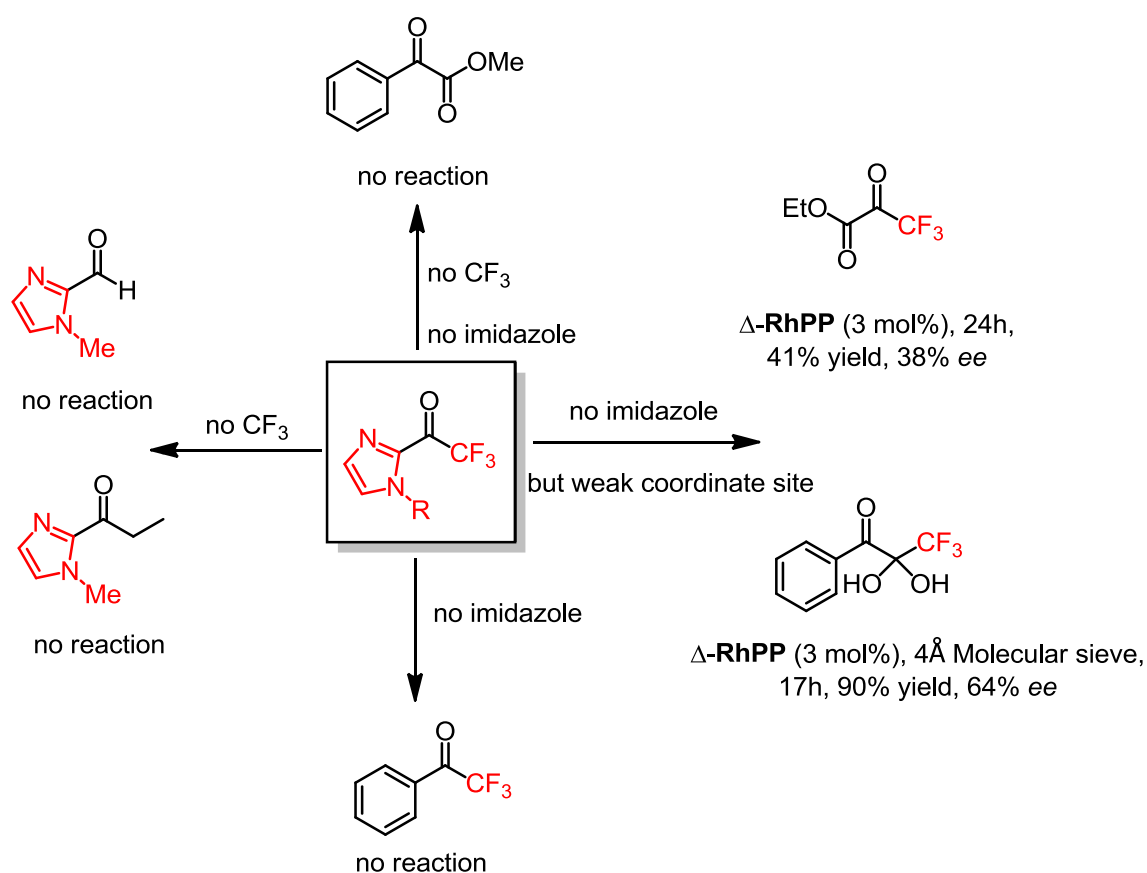
Figure 38 Control experiments with other substrates.

Since our previously developed chiral-at-metal complexes **Ir(O)** and **Ir(S)** had been proven as multi-function catalysts for photoredox catalysis, we wondered whether our new **IrPP** could perform the same properties or not. Two light-activated asymmetric reactions which had been well established in our group were investigated as shown in Figure 39. Firstly, the enantioselective α-alkylation of 2-acyl imidazole **8c** with benzyl bromide **21** catalyzed by the complex Λ-**Ir(S)** (2 mol%), under visible-light irradiation, provided the desired product (*R*)-**22** in 98% yield and with 99% *ee* within 2 hours at 40 °C.[3b] However, the reaction became very slow when Λ-**IrPP** was employed as a catalyst. The reaction did not finish after 2 hours and only 30% *ee* was obtained.
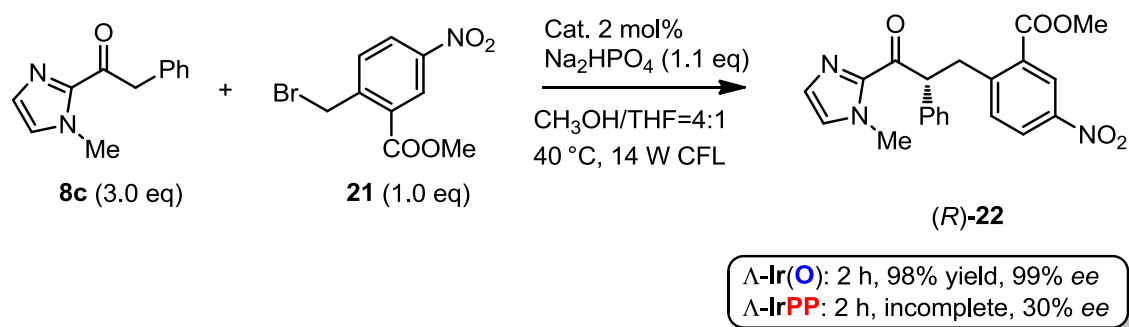
Figure 39 Comparison of Λ-**Ir(O)** and Λ-**IrPP** for enantioselective α-alkylation of 2-acyl imidazole with benzyl bromide.

Secondly, visible light induced asymmetric α-aminoalkylation of 2-acyl imidazole was also examined (Figure 40).[3e] The reaction of 2-acyl imidazole **8d** and silyl amine **23** gave the addition product (*R*)-**24** in 92% yield and with high enantioselectivity of 97% *ee* within 6.5 hours when Λ-**Ir(O)** (2 mol%) was employed as catalyst. However, employing Λ-**IrPP** as catalyst, the reaction became very sluggish. Prolonging the reaction time to 21 hours, the product was only obtained in 17% yield and with very low enantioselectivity (7% *ee*) under the same reaction conditions.
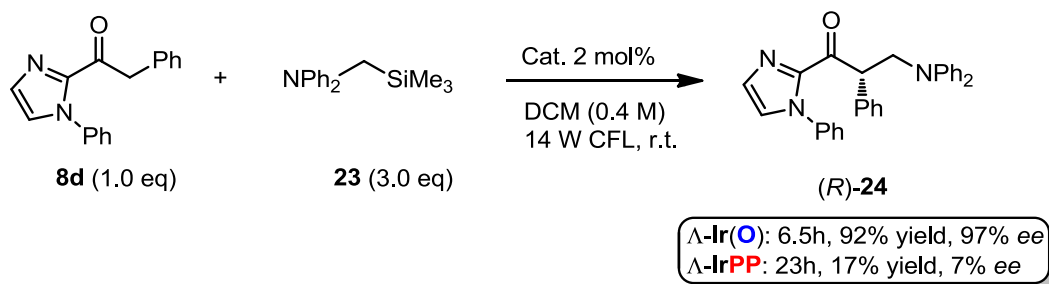
Figure 40 Comparison of Λ-**Ir(O)** and Λ-**IrPP** for asymmetric α-aminoalkylation of 2-acyl imidazole.

3.2.4 Conclusions

In conclusion, we developed four new bis-cyclometalated rhodium(III) and iridium(III) complexes and found that the rhodium complex could serve as a highly effective catalyst for the catalytic enantioselective alkynylation of 2-trifluoroacetyl imidazoles. The rhodium complex contains pinene-derived chiral ligands that permit the straightforward synthesis of the complexes as enantiomerically pure single diastereomers. Interestingly, although the asymmetric induction over the course of the catalysis is mainly controlled by the metal-centered chirality, the synthesized rhodium complexes feature a catalytic activity that is surprisingly distinct from our previous benzoxazole- and benzothiazole-based catalysts.

References

1   For reviews on different aspects of metal-centered chirality, see: a) J.-L. Pierre, *Coord. Chem. Rev.* **1998**, *178−180*, 1183−1192; b) U. Knof, A. von Zelewsky, *Angew. Chem. Int. Ed.* **1999**, *38*, 302−322; c) P. D. Knight, P. Scott, *Coord. Chem. Rev.* **2003**, *242*, 125−143; d) H. Amouri, M. Gruselle, *Chirality in Transition Metal Chemistry*, Wiley, Chichester, UK, 2008; e) E. Meggers, *Eur. J. Inorg. Chem.* **2011**, 2911−2926; f) J. Crassous, *Chem. Commun.* **2012**, *48*, 9684−9692; g) E. C. Constable, *Chem. Soc. Rev.* **2013**, *42*, 1637−1651; h) A. von Zelewsky, *Chimia* **2014**, *68*, 297−298.

2   For reviews covering chiral-at-metal complexes and their catalytic applications, see: a) H. Brunner, *Angew. Chem. Int. Ed.* **1999**, *38*, 1194−1208; b) P. Knight, P. Scott, *Coord. Chem. Rev.* **2003**, *242*, 125−143; c) C. Ganter, *Chem. Soc. Rev.* **2003**, *32*, 130−138; d) M. Fontecave, O. Hamelin, S. Ménage, *Top. Organomet. Chem.* **2005**, *15*, 271−288; e) E. B. Bauer, *Chem. Soc. Rev.* **2012**, *41*, 3153−3167; f) L. Gong, L.-A. Chen, E. Meggers, *Angew. Chem. Int. Ed.* **2014**, *53*, 10868−10874.

3   a) H. Huo, C. Fu, K. Harms, E. Meggers, *J. Am. Chem. Soc.* **2014**, *136*, 2990−2993; b) H. Huo, X. Shen, C. Wang, L. Zhang, P. Röse, L.-A. Chen, K. Harms, M. Marsch, G. Hilt, E. Meggers, *Nature* **2014**, *515*, 100−103; c) X. Shen, H. Huo, C. Wang, B. Zhang, K. Harms, E. Meggers, *Chem. Eur. J.* **2015**, *21*, 9720−9726; d) C. Wang, J. Qin, X. Shen, R. Riedel, K. Harms, E. Meggers, *Angew. Chem. Int. Ed.* **2016**, *55*, 685−688; e) C. Wang, Y. Zheng, H. Huo, P. Röse, L. Zhang, K. Harms, G. Hilt, E. Meggers, *Chem. Eur. J.* **2015***, 21*, 7355−7359.

4   a) C. Wang, L.-A. Chen, H. Huo, X. Shen, K. Harms, L. Gong, E. Meggers, *Chem. Sci.* **2015**, *6*, 1094−1100; b) Y. Tan, W. Yuan, L. Gong, E. Meggers, *Angew. Chem. Int. Ed.* **2015**, *54*, 13045−13048; c) X. Shen, K. Harms, M. Marsch, E. Meggers, *Chem. Eur. J.* **2016**, *22*, 9102−9105. d) H. Huo, K. Harms, E. Meggers, *J. Am. Chem. Soc.* **2016**, *138*, 6936−6939.

5   a) P. Hayoz, A. von Zelewsky, *Tetrahedron Lett.* **1992**, *33*, 5165–5168; b) P. Hayoz, A. von Zelewsky, H. Stoeckli-Evans, *J. Am. Chem. Soc.* **1993**, *115*, 5111−5114; c) H. Mürner, A. von Zelewsky, H. Stoeckli-Evans, *Inorg. Chem.* **1996**, *35*, 3931−3935; d) M. Gianini, A. Forster, P. Haag, A. von Zelewsky, H. Stoeckli-Evans, *Inorg. Chem.* **1996**, *35*, 4889−4895; e) M. Gianini, A. von Zelewsky, H. Stoeckli-Evans, *Inorg. Chem.* **1997**, *36*, 6094−6098; f) P. Collomb, A. von Zelewsky, *Tetrahedron: Asymmetry* **1998**, *9*, 3911–3917; g) L. Ghizdavu, A. V. Zelewsky, H.

Stoeckli-Evans, *Eur. J. Inorg. Chem.* **2001**, 993−1003; h) D. Lötscher, S. Rupprecht, P. Collomb, P. Belser, H. Viebrock, A. von Zelewsky, P. Burger, *Inorg. Chem.* **2001**, *40*, 5675−5681; i) C. Hamann, A. von Zelewsky, A. Neels, H. Stoeckli-Evans, *Dalton Trans.* **2004**, 402−406; j) C. Schaffner-Hamann, A. von Zelewsky, A. Barbieri, F. Barigelletti, G. Muller, J. P. Riehl, A. Neels, *J. Am. Chem. Soc.* **2004**, *126*, 9339−9348; k) M. Düggeli, C. Bonte, A. von Zelewsky, *Inorg. Chim. Acta* **2005**, *358*, 41−49; l) L. Yang, A. von Zelewsky, H. Stoeckli-Evans, *Chem. Commun.* **2005**, 4155−4157.

6   For metal complexes with related pinene-modified chiral pyridine ligands, see also: a) G. Chelucci, D. Berta, D. Fabbri, G. A. Pinna, A. Saba, F. Ulgheri, *Tetrahedron: Asymmetry* **1998**, *9*, 1933–1940; b) J.-P. Djukic, C. Michon, A. Maisse-Francois, R. Allagapen, M. Pfeffer, K. H. Dötz, A. de Cian, J. Fischer, *Chem. Eur. J.* **2000**, *6*, 1064–1077; c) A. V. Malkov, M. Bell, M. Vassieu, V. Bugatti, P. Kočovský, *J. Mol. Catal. A* **2003**, *196*, 179–186; d) Y.-J. Chen, R.-X. Lin, C. Chen, *Tetrahedron: Asymmetry* **2004**, *15*, 3561–3571; e) J.-P. Djukic, M. Duquenne, A. Berger, M. Pfeffer, *Inorg. Chim. Acta* **2006**, *359*, 1754–1760; f) X. Meng, Y. Gao, X. Li, D. Xu, *Cat. Commun.* **2009**, *10*, 950–954; g) G. Chelucci, M. Marchetti, A. V. Malkov, F. Friscourt, M. E. Swarbrick, P. Kočovský, *Tetrahedron* **2011**, *67*, 5421–5431; h) X. Meng, X. Li, D. Xu, *Tetrahedron: Asymmetry* **2009**, *20*, 1402–1406; i) L. Vaquer, A. Poater, J. de Tovar, J. García-Antón, M. Solà, A. Llobet, X. Sala, *Inorg. Chem.* **2013**, *52*, 4985–4992; j) J. Jung, J. Jo, M. Laskar, D. Lee, *Chem. Eur. J.* **2013**, *19*, 5156–5168; k) A. V. Malkov, S. Stončius, M. Bell, F. Castelluzzo, P. Ramírez-López, L. Biedermannová, V. Langer, L. Rulíšek, P. Kočovský, *Chem. Eur. J.* **2013**, *19*, 9167–9185; l) R.-Y. Chen, A. P. Dhondge, G.-H. Lee, C. Chen, *Adv. Synth. Catal.* **2015**, *357*, 961–966; m) C. Schmitz, W. Leitner, G. Franciò, *Eur. J. Org. Chem.* **2015**, 2889–2901.

7   a) P. Collomb, A. von Zelewsky, *Tetrahedron: Asymmetry* **1995**, *6*, 2903–2904; b) G. Chelucci, M. Antonietta Cabras, *Tetrahedron: Asymmetry* **1996**, *7*, 965–966;

8   a) L. Ghizdavu, B. Kolp, A. von Zelewsky, H. Stoeckli-Evans, *Eur. J. Inorg. Chem.* **1999**, 1271–1279; b) L. Ghizdavu, O. Lentzen, S. Schumm, A. Brodkorb, C. Moucheron, A. Kirsch-De Mesmaeker, *Inorg. Chem.* **2003**, *42*, 1935–1944.

9 The synthesis of the racemic dinuclear complex ΛΛ/ΔΔ-**2_Ir** and a derived non-racemic acetoacetonato complex has been reported. See: L. Yang, A. von Zelewsky, H. P. Nguyen, G. Muller, G. Labat, H. Stoeckli-Evans, *Inorg. Chim. Acta* **2009**, *362*, 3853−3856.

10 For other reports on the catalytic, enantioselective alkynylation of trifluoromethyl ketones, see: a) R. Motoki, D. Tomita, M. Kanai, M. Shibasaki, *Tetrahedron Lett.* **2006**, *47*, 8083–8086; b) R. Motoki, M. Kanai, M. Shibasaki, *Org. Lett.* **2007**, *9*, 2997–3000; c) K. Aikawa, Y. Hioki, K. Mikami, *Org. Lett.* **2010**, 12, 5716–5719; d) G.-W. Zhang, W. Meng, H. Ma, J. Nie, W.-Q. Zhang, J.-A. Ma, *Angew. Chem. Int. Ed.* **2011**, *50*, 3538–3542; e) T. Ohshima, T. Kawabata, Y. Takeuchi, T. Kakinuma, T. Iwasaki, T. Yonezawa, H. Murakami, H. Nishiyama, K. Mashima, *Angew. Chem. Int. Ed.* **2011**, *50*, 6296–6300; f) T. Wang, J.-L. Niu, S.-L. Liu, J.-J. Huang, J.-F. Gong, M.-P. Song, *Adv. Synth. Catal.* **2013**, *355*, 927–937; g) V. Dhayalan, R. Murakami, M. Hayashi, *Asian J. Chem.* **2013**, *25*, 7505−7508; h) A. M. Cook, C. Wolf, *Angew. Chem. Int. Ed.* **2016**, *55*, 2929–2933.

11 For chiral-auxiliary-mediated methods on the enantioselective alkynylation of trifluoromethyl ketones, see: a) A. S. Thompson, E. G. Corley, M. F. Huntington, E. Grabowski, *Tetrahedron Lett.* **1995**, *36*, 8937–8940; b) A. Thompson, E. G. Corley, M. F. Huntington, E. J. J. Grabowski, J. F. Remenar, D. B. Collum, *J. Am. Chem. Soc.* **1998**, *120*, 2028–2038; c) L. Tan, C.-y. Chen, R. D. Tillyer, E. J. J. Grabowski, P. J. Reider, *Angew. Chem. Int. Ed.* **1999**, *38*, 711–713; d) F. Xu, R. A. Reamer, R. Tillyer, J. M. Cummins, E. J. J. Grabowski, P. J. Reider, D. B. Collum, J. C. Huffman, *J. Am. Chem. Soc.* **2000**, *122*, 11212–11218; e) R. Motoki, D. Tomita, M. Kanai, M. Shibasaki, *Tetrahedron Lett.* **2006**, *47*, 8083–8086; f) B. Jiang, Y. Feng, *Tetrahedron Lett.* **2002**, *43*, 2975–2977.

12 For a recent review on the asymmetric construction of stereogenic centers containing a trifluoromethyl substituent, see: J. Nie, H. -C. Guo, D. Cahard, J.-A. Ma, *Chem. Rev.* **2011**, *111*, 455–529.

13 For the synthesis, properties and applications of trifluoromethyl ketones, see: C. B. Kelly, M. A. Mercadante, N. E. Leadbeater, *Chem. Commun.* **2013**, *49*, 11133−11148.

3.3 Octahedral Chiral-at-Ruthenium Complexes for Asymmetric Catalysis

3.3.1 Design of catalysts

Transition metal complexes represent one of the most powerful and versatile classes of homogeneous catalysts. Applied to asymmetric catalysis, metal ions are typically combined with carefully tailored chiral ligands.[1] In a more simplistic design, only achiral ligands are employed but their assembly around the central metal creates metal-centered chirality[2] which is then responsible for the asymmetric induction during catalysis.[3] Our group recently realized this approach with the design of bis-cyclometalated iridium[4] and rhodium[5] complexes as chiral Lewis acids which provide excellent enantioselectivities and high turnover numbers for a variety of reactions. However, at the onset of this work it was unclear to what extend this design principle is general and applicable to chiral octahedral metal complexes of other elements. In pioneering work, Fontecave and co-workers reported that Λ- and Δ-[Ru(2,9-dimethyl-1,10-phenanthroline)(MeCN)$_2$]$^{2+}$ catalyzed the oxidation of organic sulfides to their sulfoxides, albeit with a maximum of just 18% *ee*.[3a] Much higher enantioselectivities for the synthesis of sulfoxides were achieved by Ye using chiral-at-metal Λ- and Δ-[Ru(2,2'-bipyridine)$_2$(py)$_2$]$^{2+}$ as recyclable chiral auxiliaries.[6] Hartung and Grubbs reported a chiral-at-ruthenium catalyst for diastereo- and enantioselective ring-opening/cross-metathesis. The complex contains additional carbon-centered stereogenicity and catalysis is supposed to occur via a trigonal bipyramidal intermediate.[7] After a period of efforts, we finally chose the inert and strong σ-donating *N*-heterocyclic carbenes (NHCs) as ligands which might make the ruthenium complex is configurationally stable and has more labile acetonitrile ligands due to its strong *trans*-effect (Figure 41).
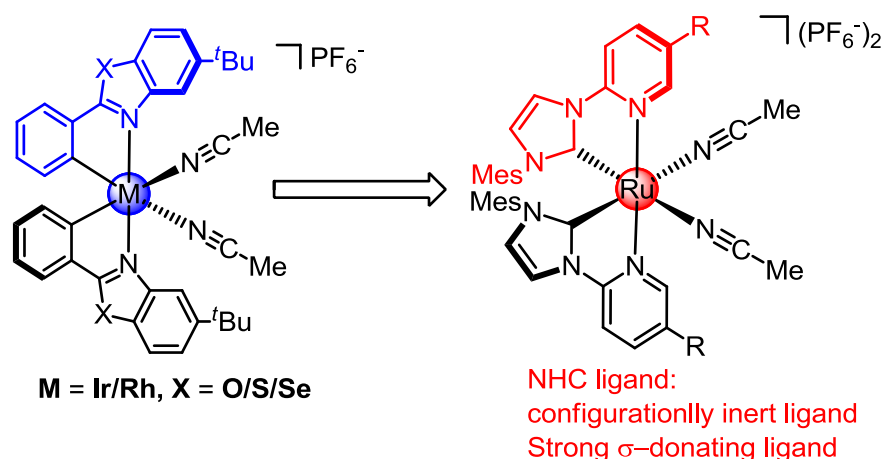
Figure 41 Design of octahedral chiral-at-ruthenium catalysts.

3.3.2 Synthesis of catalysts

The racemic complex *rac*-**Ru1** was synthesized according to the procedure reported by Hahn and co-workers with some modifications.[8] Accordingly, the octahedral ruthenium complex *rac*-**Ru1** was synthesized by reacting RuCl$_3$ hydrate with the *N*-(2-pyridyl)-imidazolium salt **25** in ethylene glycol at 200 °C, followed by treatment with AgPF$_6$ to afford the racemic complex *rac*-**Ru1** in 92% yield (Scheme 15). The single crystals of *rac*-**Ru1** suitable for X-ray were obtained by diffusion of hexane in CH$_2$Cl$_2$ solution at room temperature (Figure 42). This racemic mixture was then reacted with the chiral salicyloxazoline ligand (*S*)-**2″** to provide Λ-(*S*)-**Ru1** as a single diastereomer in 36% yield after the standard chromatography. In analogy, using the auxiliary (*R*)-**2″** instead, the complex Δ-(*R*)-**Ru1** was obtained. The individual diastereomerically pure complexes were next treated with TFA in CH$_3$CN to generate **Ru1** as individual Λ- and Δ-enantiomer. Λ-**Ru2** and Δ- **Ru2** can be obtained by the same protocol (see chapter 5.3 for details). CD spectra of Λ-**Ru1** and Δ- **Ru1** are shown in Figure 44 and were used to assign the absolute configuration by comparison with related enantiopure ruthenium complexes,[9] and confirmed by an X-ray crystal structure of a derivative of Δ-**Ru2** (Figure 43).
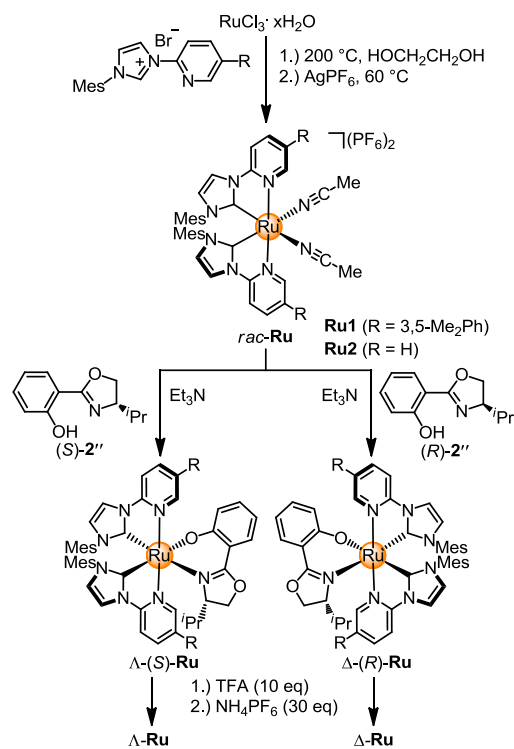
Scheme 15 Synthesis of enantiopure complexes Λ- and Δ-**Ru**.
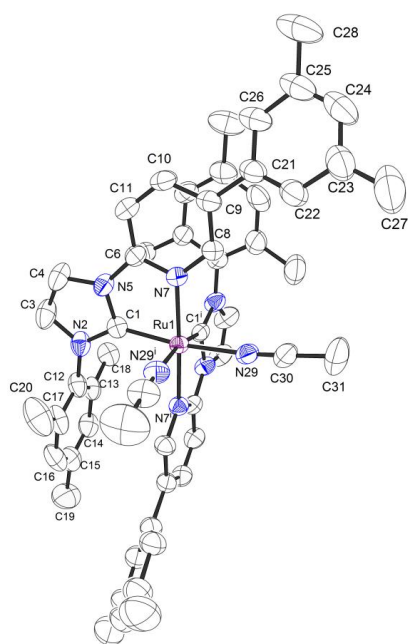
Figure 42 Crystal structure of *rac*-**Ru1**. ORTEP drawing with 50% probability thermal ellipsoids. The hexafluorophosphate counteranion and all hydrogens are omitted for clarity.
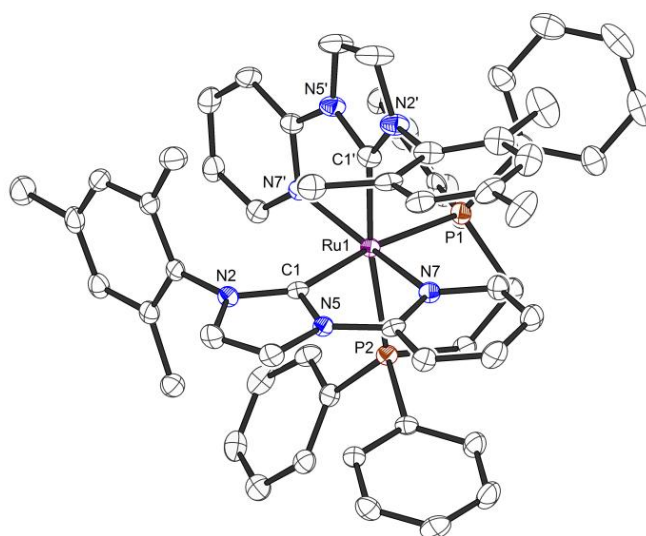
Figure 43 Crystal structure of Δ-**Ru2-DPPE**. ORTEP drawing with 50% probability thermal ellipsoids. The hexafluorophosphate counteranion and all hydrogens are omitted for clarity.
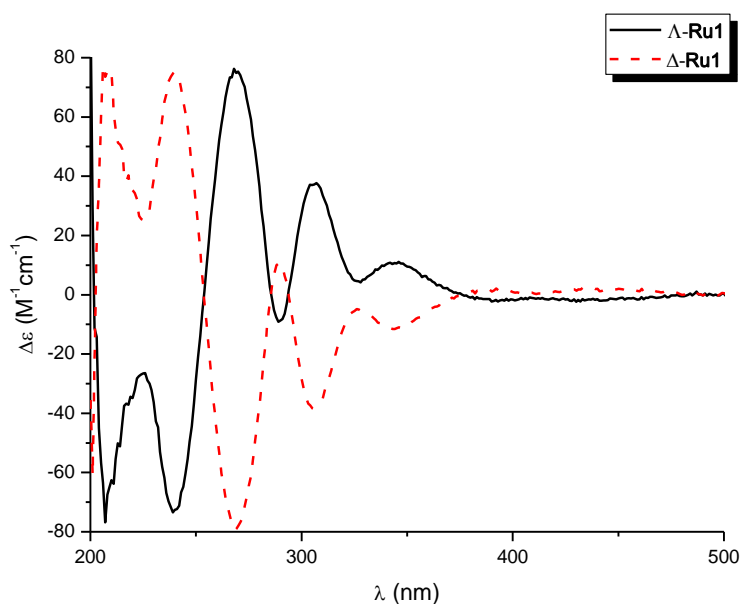
Figure 44 CD spectra of Λ- and Δ-**Ru1**(0.2 mM in CH$_3$OH).

Importantly, we found that the enantiopure complexes are constitutionally and configurationally surprisingly stable. For example, a solution of Λ-**Ru1** (20 mg) in 3 mL THF was stirred at 60 $^{\circ}$C for 3 days. After cooling to room temperature, 2 drops of CH$_3$CN were added, and the solvent was removed, then the residue was analyzed by ^{1}H NMR which shows no obvious change (Figure 45). The resulting

complex was also used to catalyze the model reaction (see 3.3.4 for details) under the same conditions, giving the almost identical results (94% yield, 99% *ee*).

After 3 days in THF at 60 °C

NMR spectrum of Λ-**Ru1** in CD$_2$Cl$_2$
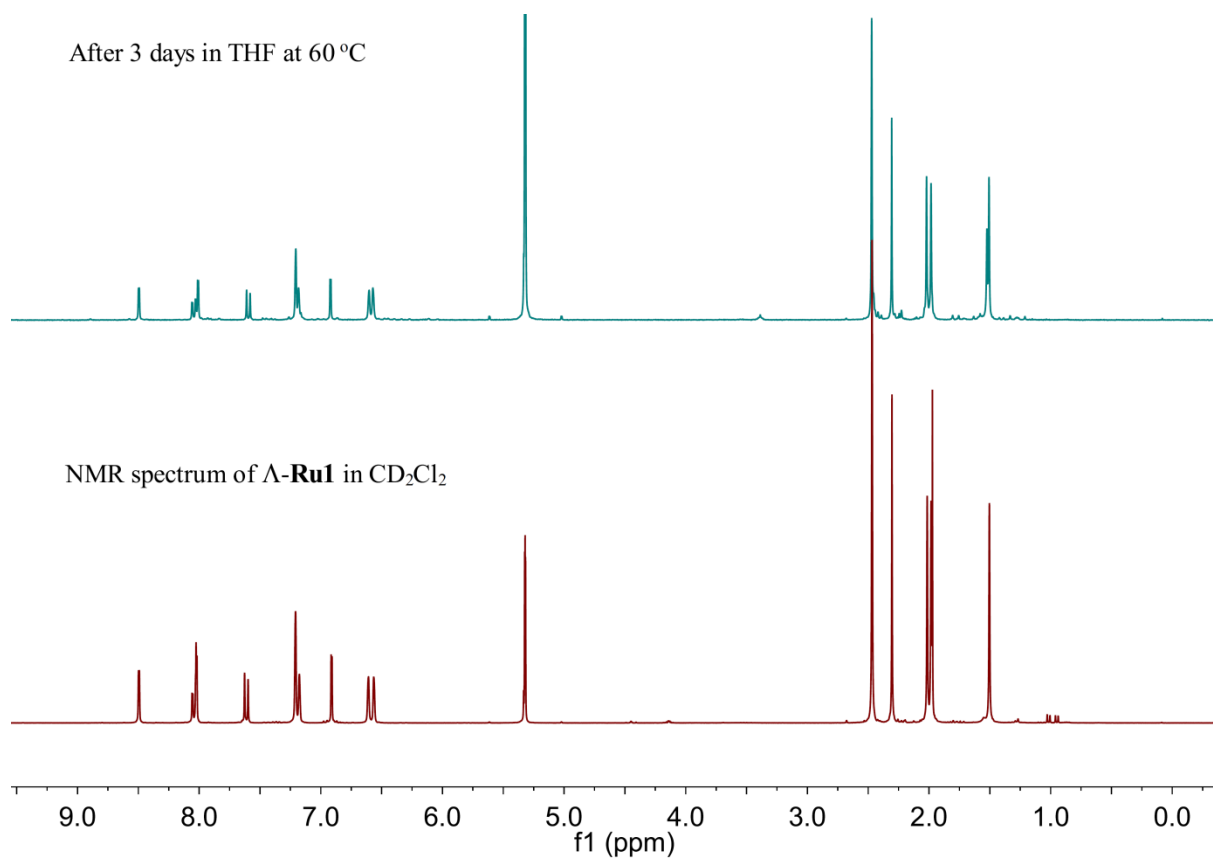
Figure 45 ^{1}H NMR spectra of Λ-**Ru1** recorded in CD$_2$Cl$_2$ (fresh and 3 days in CD$_2$Cl$_2$).

3.3.3 Studies of the *trans*-effect in the ruthenium complexes

The *trans*-effect of the NHC-ligands in the catalysts **Ru1** and **Ru2** was investigated by comparison with the related complex [Ru(2,2'-bipyridine)$_2$(MeCN)$_2$]$^{2+}$.

[Ru(bpy)$_2$(MeCN)$_2$]$^{2+}$

Ru1 (R = 3,5-Me$_2$Ph)
Ru2 (R = H)
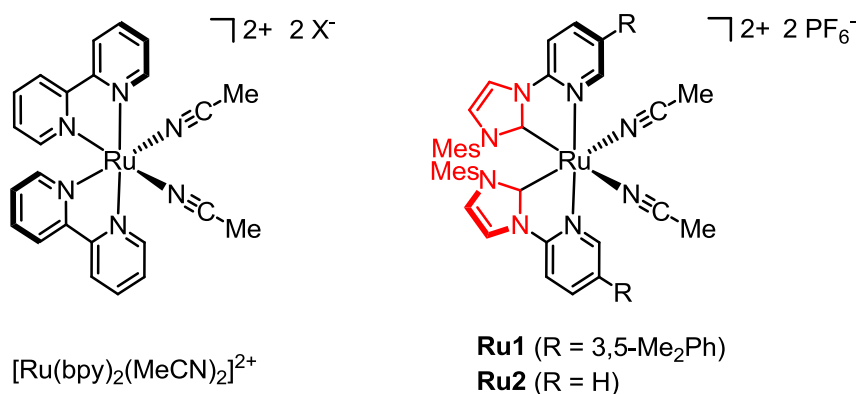
Figure 46 The structures of ruthenium complexes.

a.) Structural *trans*-effect

We determined the X-ray crystal structure of the racemic catalyst *rac*-**Ru1** (see **3.3.1**). Several X-ray crystal structures are available for the complex $[Ru(bpy)_2(MeCN)_2]^{2+}$ with different counterions as listed in Table 3.[10-13] The comparison demonstrates that the Ru-N coordinative bonds with the MeCN ligands in $[Ru(bpy)_2(MeCN)_2]^{2+}$ are in the range of 2.012–2.049 Å and thereby significantly shorter compared to the Ru-N (MeCN) bonds in *rac*-**Ru1** (2.098 Å). This is clear evidence of the structural *trans*-effect exerted by the two NHC-ligands in *trans* to the two MeCN ligands.

Table 3 Investigation of the structural *trans*-effect by comparison of the Ru-N bond lengths of the coordinated MeCN ligands.

Complexes	Ru-N bonds to MeCN (Å)	References
$[Ru(bpy)_2(MeCN)_2](PF_6)_2$	2.033, 2.033	Heeg, et al.,[10]
$[Ru(bpy)_2(MeCN)_2](PF_6)_2$	2.012, 2.012	Xu, et al.,[11]
$[Ru(bpy)_2(MeCN)_2](BF_4)_2$	2.042, 2.049	Wang, et al.,[12]
$[Ru(bpy)_2(MeCN)_2](ClO_4)_2$	2.0397, 2.0447	Chattopydhyay, et al.,[13]
rac-**Ru1**	2.098, 2.098	Our work

b.) Kinetic *trans*-effect

We compared *rac*-**Ru2** and $[Ru(bpy)_2(MeCN)_2]^{2+}$ with respect to the rate of replacing the MeCN ligands with the bidentate ligand 2,2'-bipyridine. For this, a mixture of $[Ru(bpy)_2(MeCN)_2](PF_6)_2$ or *rac*-**Ru2** (20.0 mg), and 2,2'-bipyridine (1.75 eq) in CD_2Cl_2 (1.0 mL or 0.8 mL) was stirred at room temperature and then analyzed by ^{1}H NMR spectroscopy after 0.5 h, 3 h, 8 h, and 24 h, respectively. As shown in Figure 47, there is no ligand replacement of the coordinated MeCN ligands by 2,2'-bipyridine can be monitored at room temperature for $[Ru(bpy)_2(MeCN)_2](PF_6)_2$ even after 24 hours, whereas the complex *rac*-**Ru2** under the same conditions displays a significant conversion already after 30 min. This much higher lability of the CH_3CN ligands in *rac*-**Ru2** can be attributed to the kinetic *trans*-effect of the NHC ligands in *rac*-**Ru2**.
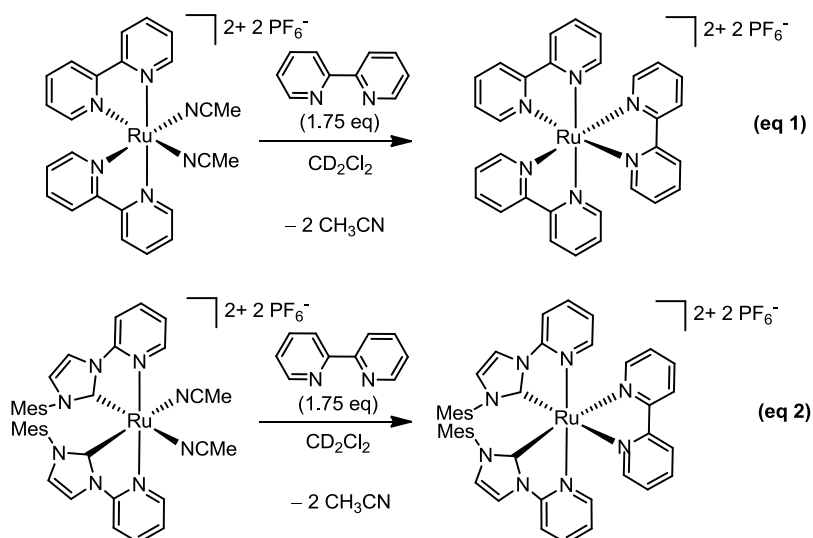
Figure 47 The acetonitrile exchange experiments in the presence of bipyridine.
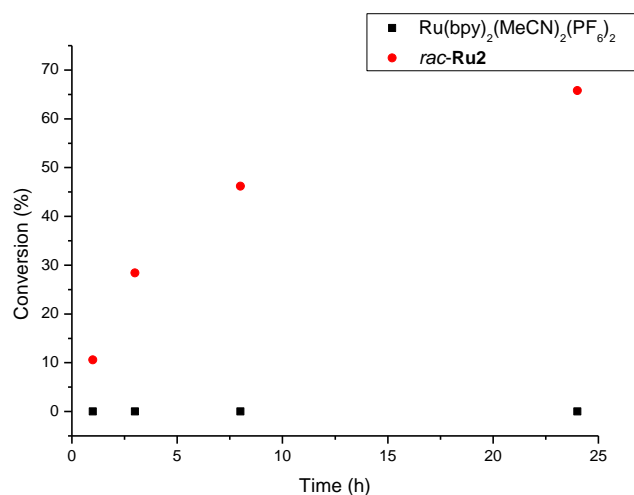
Figure 48 Investigation of kinetic *trans*-effect.

3.3.4 Catalytic reactions

With the chiral catalysts in hand, we firstly tested the reaction of 2-trifluoroacetly imidazole **11c** with phenylacetylene. However, the reaction cannot give any traces of desired product **20c** under our optimal conditions.
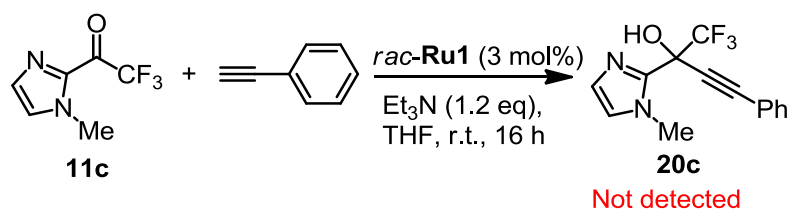
Figure 49 Alkynylation of 2-trifluoroacetyl imidazole catalyzed by *rac*-**Ru1**.

Since our new catalysts have very strong *trans*-effect that means they might active more general substrates. Therefore, trifluoroacetophenone **25a** was employed to examine. To our delight, we found that **Ru1** is an excellent catalyst for the enantioselective alkynylation of trifluoromethyl ketones.[14,15]

Table 4 Initial Catalysis Experiments[a]
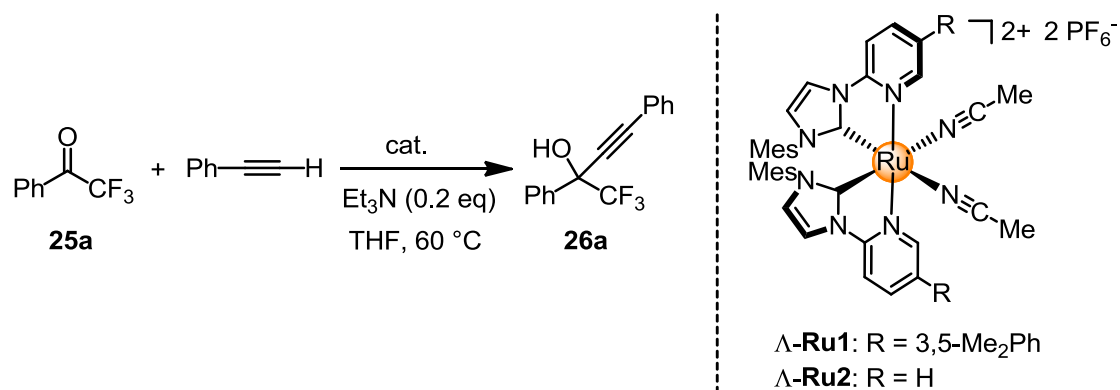
Entry	Catalyst	Loading (mol%)	Time (h)	Yield (%)[b]	ee (%)[c]
1	Λ-**Ru1**	3	16	97	99 (*S*)
2	Λ-**Ru1**	1	16	93	99 (*S*)
3	Λ-**Ru1**	0.5	16	95	99 (*S*)
4	Λ-**Ru1**	0.2	30	98	99(*S*)
5	Δ- **Ru1**	0.5	16	95	99 (*R*)
6	Λ-**Ru2**	0.5	16	93	97 (*S*)
7	Δ-**Ir(S)**	3	20	15	15 (*R*)
8	Δ-**Rh(S)**	3	20	28	93 (*R*)

[a]Conditions: **25a** (0.20 mmol), phenylacetylene (0.60 mmol) with catalyst (0.2–3.0 mol%) and Et$_3$N (20 mol%) in THF (0.4 mL) were stirred at 60 °C. [b]Isolated yields. [c]Chiral HPLC analysis.

As shown in Table 4, the reaction of trifluoroacetophenone (**25a**) with phenylacetylene in the presence of Et$_3$N (0.2 eq) and 3.0 mol% Λ-**Ru1** provides the propargyl alcohol (*S*)-**26a** in 97% yield and with 99% *ee* (entry 1). The catalyst loading can be reduced down to 0.2 mol% without any loss in yield or enantioselectivity (entries 2−4). As to be expected, mirror-imaged Δ-**Ru1** provides the mirror-imaged product (*R*)-**26a** with otherwise identical performance (entry 5). The catalyst devoid of the 3,5-Me$_2$Ph substituents (Λ-**Ru2**) leads to a reduced enantioselectivity of 97% *ee* (entry 6), confirming the steric role of the substituents at the pyridine ligands. Interestingly, previously reported

chiral-at-metal iridium and rhodium catalysts only display very sluggish reactivity for the alkynylation of trifluoromethyl ketones and a diminished enantioselectivity even at catalyst loadings of 3.0 mol% (entries 7 and 8).

A substrate scope with respect to terminal alkynes is shown in Figure 50, providing the propargylalcohols (*S*)-**26b**-**m** in yields of 66-99% and with outstanding enantioselectivities of 96 to >99% *ee*. The catalyst tolerates equally well phenylacetylenes with substituents in the phenyl moiety, 2-ethynylthiophene, the conjugated alkenyl acetylene 1-ethynylcyclohexene, aliphatic acetylenes, and trimethylsilylacetylene. Typically, catalyst loadings of just 0.5 mol% Λ-**Ru1** are sufficient except for *ortho*-substituted phenylacetylenes which react more sluggish, presumably due to steric reasons.
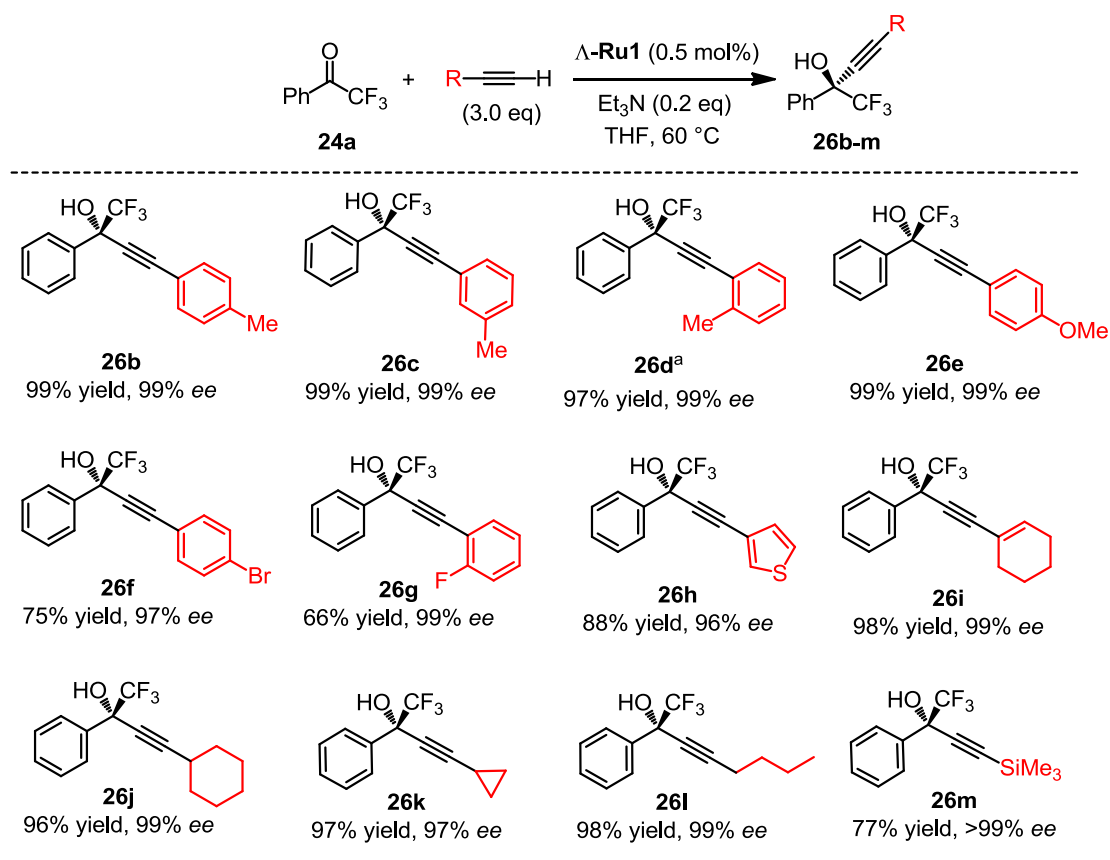
Figure 50 Substrate scope with respect to terminal alkynes. [a]1.0 mol% catalyst loading instead.

The scope of this reaction with respect to trifluoromethyl ketones is outlined in Figure 51. Trifluoroacetophenone with different substituents in the phenyl moiety provided the corresponding propargyl alcohols in high yields and with almost perfect enantioselectivity except for *ortho*-methyl trifluoroacetophenone which reacts sluggish, reinforcing that the catalyst is sensitive to steric effects. It is also noteworthy that an aliphatic trifluoromethyl ketone and ethyl trifluoropyruvate are not

suitable substrate for this catalysis. However, replacing one fluorine of the trifluormethyl group with chlorine by using 2-chloro-2,2-difluoroacetophenone as the substrate yields the corresponding propargyl alcohol in 99% yield and 99% *ee*.
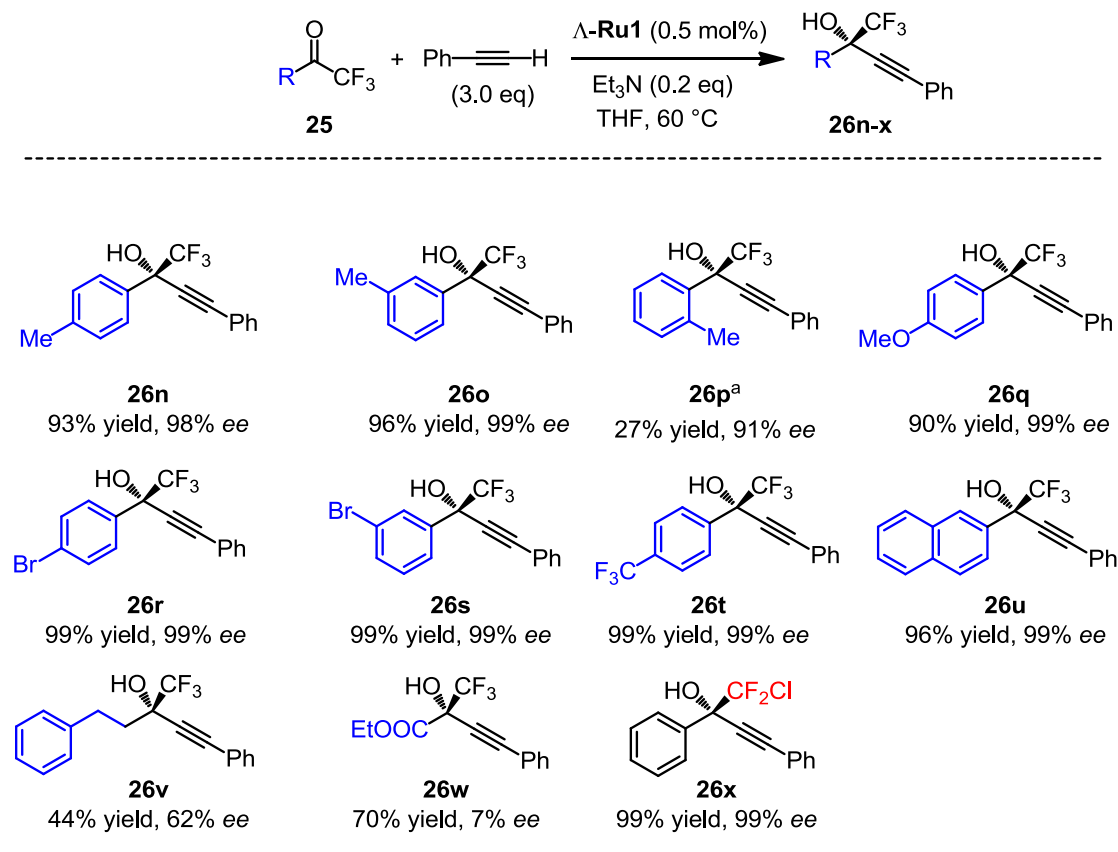
Figure 51 Substrate scope with respect to trifluoromethyl ketones. [a]1.0 mol% catalyst loading instead.

3.3.5 Applications

After getting these exciting results, we turned our attention to search for some applications. The synthetic methodology we developed here is very valuable because propargylic alcohols constitute highly versatile synthetic building blocks[16]; furthermore, fluorinated compounds play an increasingly important role in drug development. For example, efavirenz[17], containing a quaternary stereocenter bearing a CF_3 and alkynyl group, is a potent HIV reverse transcriptase inhibitor and a key drug for the treatment of AIDS. So, we decided to pursue this direction.

Initially, we identified the reaction of 1-(2-amino-5-chlorophenyl)-2,2,2-trifluoroethanone (**27a**) with cyclopropylacetylene in the presence of Et$_3$N (0.2 eq) in THF (0.5 M) at 60 ^{o}C for 48 h catalyzed by chiral-at-metal Δ-**Ru1** (3 mol%) provided the Merck intermediate (*S*)-**28a** with 58% yield and 91.6% *ee* (Table 5, entry 1). Although this method provides a convenient catalytic, enantioselective access to

the key Merck intermediate (*S*)-**28a**, the yield and the enantioselectivity are only modest and we were not able to significantly improve these results. Unexpectedly, excellent enantioselectivity (99.0% *ee*) was obtained when Δ-**Ru2** was employed as catalyst under the same reaction conditions, although the yield was disappointingly very low (entry 2). We therefore switched our attention to a related substrate in which the electron donating amino group (**27a**) is replaced with an electron withdrawing nitro group (**27b**), with the expectation that this modification would accelerate the alkynylation **27b**→(*S*)-**28b** and a straightforward iron-based reduction of (*S*)-**28b** to (*S*)-**28a** has been reported.[18] Gratifyingly, using just 0.5 mol% Δ-**Ru1**, the propargylic alcohol (*S*)-**2c** was obtained in a yield of 93% with 99.6% *ee* after 16 hours at 60 ℃ (entry 3). Interestingly, using a simplified catalyst devoid of the two 3,5-dimethylphenyl moieties (Δ-**Ru2**), almost unchanged yield and enantioselectivity were observed (entry 4). Since the synthesis of Δ-**Ru2** is less time consuming and less expensive compared to Δ-**Ru1**, the simplified catalyst Δ-**Ru2** is apparently the catalyst of choice for the conversion **27b**→(*S*)-**28b**. Even at a reduced catalyst loading of 0.2 mol%, a yield of 95% with 99.4% *ee* was obtained (entry 5), while at a further reduced catalyst loading of 0.1 mol% the yield deteriorated (entry 6). Interestingly for practical reasons, at a catalyst loading of 0.5 mol% Δ-**Ru2**, the reaction can be executed at room temperature to afford (*S*)-**2c** with 96% yield and 99.4% *ee* after 16 hours (entry 7). A lower catalyst loading of 0.2 mol% leads to a decreased yield (entry 8). The reaction is sensitive to air (entry 9) but not to the presence of small amounts of water (entry 10).
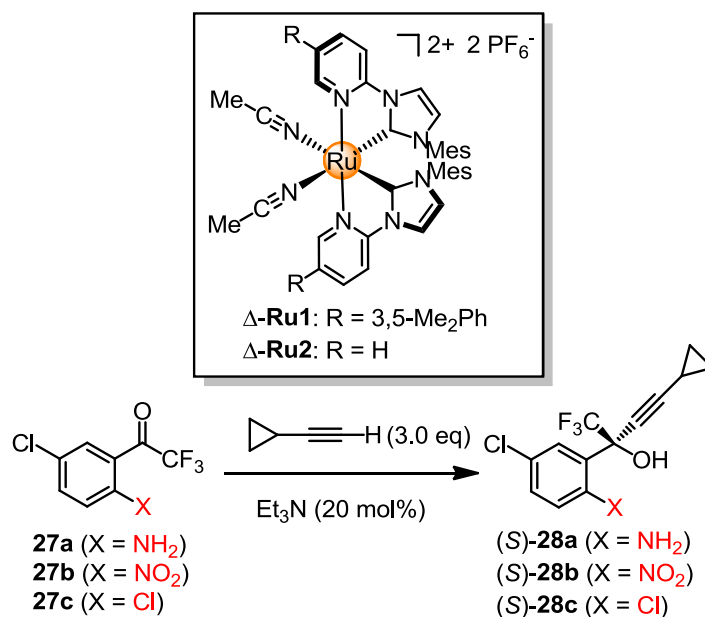
Scheme 16 The synthesis of intermediates of the drug efavirenz with chiral-at-ruthenium complexes.

Table 5 Optimization of the reaction conditions with substrates **27a** and **27b**[a]

Entry	Catalyst[b]	X	T (°C)	t (h)	Yield (%)[c]	ee (%)[d]
1[e]	Δ-**Ru1** (3.0)	NH$_2$	60	48	58	91.6
2[e]	Δ-**Ru2** (3.0)	NH$_2$	60	48	25	99.0
3	Δ-**Ru1** (0.5)	NO$_2$	60	16	93	99.6
4	Δ-**Ru2** (0.5)	NO$_2$	60	16	92	99.4
5	Δ-**Ru2** (0.2)	NO$_2$	60	16	95	99.4
6	Δ-**Ru2** (0.1)	NO$_2$	60	64	42	99.2
7	Δ-**Ru2** (0.5)	NO$_2$	r.t.	16	96	99.4
8	Δ-**Ru2** (0.2)	NO$_2$	r.t.	48	55	99.4
9[f]	Δ-**Ru2** (0.2)	NO$_2$	60	16	21	98.2
10[g]	Δ-**Ru2** (0.2)	NO$_2$	60	16	96	99.0

[a]Reaction conditions: **27a** or **27b** (0.20 mmol), cyclopropylacetylene (0.60 mmol), catalyst, and Et$_3$N (20 mol%) in THF (0.4 mL, 0.5 M). [b]Catalyst loadings in mol% provided in brackets. [c]Isolated yields. [d]Determined by HPLC on a chiral stationary phase. [e]2 mmol cyclopropylacetylene was used instead. [f]Performed under air. [g]Performed in the presence of 1% H$_2$O.

Lonza intermediate is also an important intermediate which can be converted to efavirenz in one step[19]. So we next investigated the catalytic, enantioselective alkynylation of the chlorinated Lonza intermediate **27c** with cyclopropylacetylene. Accordingly, with Δ-**Ru1** at 0.5 mol% catalyst loading, the reaction of **27c** with cyclopropylacetylene at 60 °C provided the propargylic alcohol (*S*)-**28c** in 99% yield and with 90% *ee* (Table 6, entry 1). Interestingly, same as for the nitro substrate **27b**, the simplified catalyst Δ-**Ru2** provides superior results (entries 2−6). With a catalyst loading of just 0.2 mol% at room temperature, (*S*)-**28c** provided in 95% yield and with 95% *ee* (entry 5). Attempts to lower the catalyst loading to 0.1 mol% led to a decreased yield, even after prolonging the reaction time to 64 hours (entry 6). Control experiments reveal that the reaction is sensitive to air (entry 7) but not to small amounts of water (entry 8) which means that the reaction must be performed under inert gas conditions but the solvents do not need to be dry.

Table 6 Optimization of the reaction conditions with substrate **27c**[a]

Entry	Catalyst[b]	T (°C)	t (h)	Yield (%)[c]	ee (%)[d]
1	Δ-**Ru1** (0.5)	60	16	99	90.2
2	Δ-**Ru2** (0.5)	60	16	99	93.8
3	Δ-**Ru2** (0.2)	60	24	93	93.7
4	Δ-**Ru2** (0.5)	r.t.	16	99	95.2
5	Δ-**Ru2** (0.2)	r.t.	16	95	95.0
6	Δ-**Ru2** (0.1)	r.t.	64	71	95.0
7[e]	Δ-**Ru2** (0.2)	r.t.	16	11[f]	n.d. [g]
8[h]	Δ-**Ru2** (0.2)	r.t.	16	96	95.2

[a]Reaction conditions: **27c** (0.20 mmol), cyclopropylacetylene (0.60 mmol), catalyst, and Et$_3$N (20 mol%) in THF (0.4 mL, 0.5 M) were stirred at indicated temperature for the indicated time. [b]Catalyst loadings in mol% provided in brackets. [c]Isolated yields. [d]Determined by HPLC on a chiral stationary phase. [e]Performed under air. [f]NMR yield with tetrachloroethane as internal standard. [g]Not determined. [h]Performed in the presence of 1mol% H$_2$O.

Two gram-scale reactions were carried out to highlight the practical utility of this protocol. As shown in Figure 52, employing **27b** or **27c** as substrate under the optimal conditions, respectively, the reaction exhibited excellent efficiency, providing the propargylic alcohol products in high isolated yield without any loss of enantioselectivity.
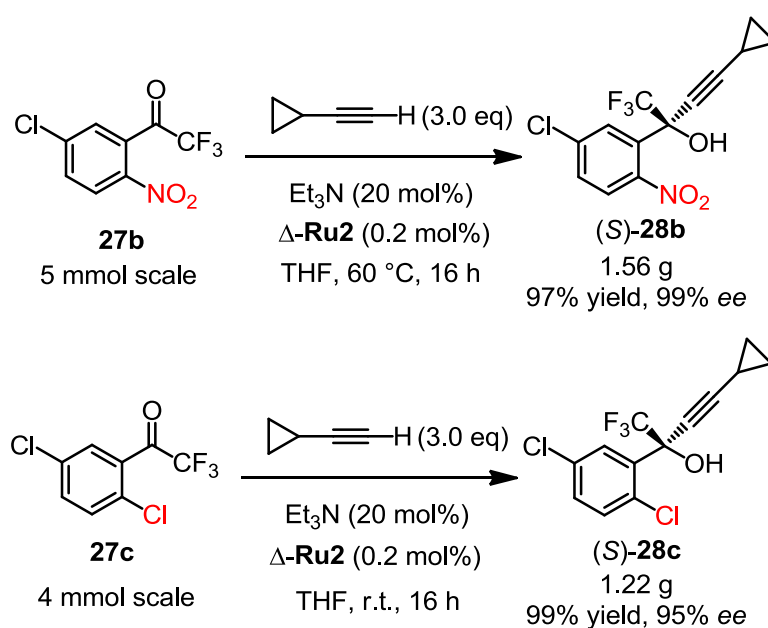
Figure 52 Gram-scale reactions under optimized reaction conditions.

3.3.6 Proposed mechanism

Mechanistically, we propose that the reaction proceeds through an intermediate ruthenium acetylide which then tranfers the acetylide to the presumable ruthenium-coordinated trifluoroketone (Figure 53).[16a] The observed excellent asymmetric induction suggests that the trifluoromethyl ketone substrate coordinates to the ruthenium ahead of the acetylide transfer. During this transfer, the metal-centered chirality provides a suprisingly high asymmetric induction, thus reinforcing our catalyst design strategy. The rigidity of the propeller-type coordination sphere most likely contributes to the observed excellent enantioselectivities but is also responsible for sensitivity to steric effects. It is worth noting that catalytic amounts of base are necessary in this reaction, which apparently serves as a proton shuttle.
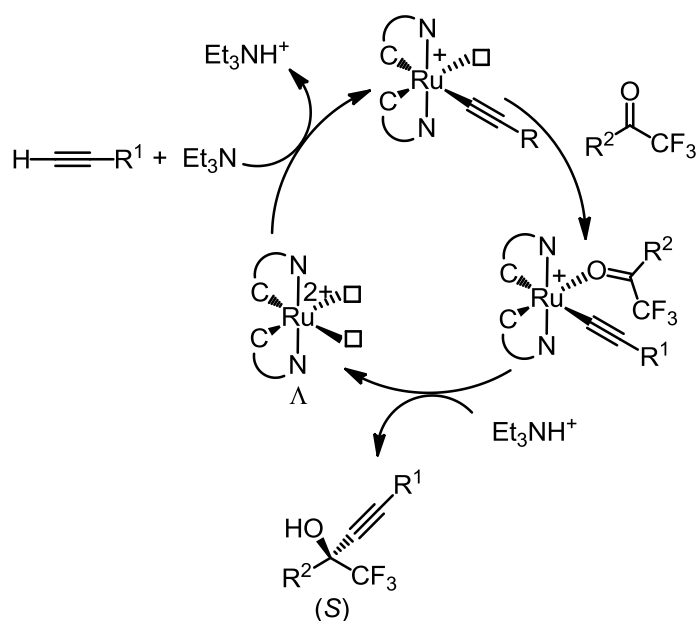
Figure 53 Proposed mechanism. □ = vacant coordination site.

3.3.7 Conclusions

In summary, the first example of an octahedral chiral-at-metal ruthenium complex with high catalytic activity and excellent enantioselectivity was presented. Key components of this new class of asymmetric catalysts are the two N-(2-pyridyl)-subsituted *N*-heterocyclic carbene (PyNHC) chelate ligands.[20,21] First, the PyNHC ligands are tightly coordinating ligands which provide a strong ligand field important for the constitutional and configurational stability of the bis-(PyNHC)Ru unit. Second, the propeller shape and high rigidity of the bis-(PyNHC)Ru provides an excellent asymmetric induction. And third, the strong σ-donating NHC-ligands[22] in *trans* to the coordinated acetonitrile

ligands are crucial for labilizing the coordinated acetonitrile ligands (*trans*-effect) thereby ensuring a high catalytic activity. We also demonstrated that highly efficient catalytic enantioselective synthesis of key chiral propargylic alcohol intermediates toward enantiomerically pure efavirenz. The Merck propargylic alcohol intermediate (*S*)-**28a** can be obtained indirectly after reduction of the nitro-derivative (*S*)-**28b**, which itself is formed through a catalytic, enantioselective alkynylation in 97% yield and with 99% *ee*. The Lonza propargylic alcohol intermediate (*S*)-**28c** can be accessed through a catalytic, enantioselective alkynylation in 99% yield and with 95% *ee* with a turnover number reaching almost 500 and relying only on the addition of catalytic amounts of the base triethylamine. These synthetic routes might constitute significant improvements over existing protocols and could contribute to lowering the cost for the production of the important anti-HIV drug efavirenz.

References

1   P. J. Walsh, M. C. Kozlowski, *Fundamentals of Asymmetric Catalysis*; University Science Books: Sausalito, California, 2009.

2   For reviews on different aspects of metal-centered chirality, see: a) J.-L. Pierre, *Coord. Chem. Rev.* **1998**, *178−180*, 1183−1192; b) U. Knof, A. von Zelewsky, *Angew. Chem. Int. Ed.* **1999**, *38*, 302−322; (c) M. Fontecave, O. Hamelin, S. Ménage, *Top. Organomet. Chem.* **2005**, *15*, 271−288; d) E. Meggers, *Eur. J. Inorg. Chem.* **2011**, 2911−2926; e) E. B. Bauer, *Chem. Soc. Rev.* **2012**, *41*, 3153−3167; f) J. Crassous, *Chem. Commun.* **2012**, *48*, 9684−9686; g) L. Gong, L.-A. Chen, E. Meggers, *Angew. Chem. Int. Ed.* **2014**, *53*, 10868−10874; h) Z.-Y. Cao, W. D. G. Brittain, J. S. Fossey, Zhou, F. *Catal. Sci. Technol.* **2015**, *5*, 3441−3451.

3   For precedence of asymmetric, octahedrally coordinated catalysts featuring solely metal-centered chirality, see: a) M. Chavarot, S. Ménage, O. Hamelin, F. Charnay, J. Pécaut, M. Fontecave, *Inorg. Chem.* **2003**, *42*, 4810−4816; b) O. Hamelin, M. Rimboud, J. Pécaut, M. Fontecave, *Inorg. Chem.* **2007**, *46*, 5354−5360; c) C. Ganzmann, J. A. Gladysz, *Chem. Eur. J.* **2008**, *14*, 5397−5400; d) L.-A. Chen, W. Xu, B. Huang, J. Ma, L. Wang, J. Xi, K. Harms, L. Gong, E. Meggers, *J. Am. Chem. Soc.* **2013**, *135*, 10598−10601.

4   a) H. Huo, C. Fu, K. Harms, E. Meggers, *J. Am. Chem. Soc.* **2014**, *136*, 2990−2993; b) H. Huo, X. Shen, C. Wang, L. Zhang, P. Röse, L.-A. Chen, K. Harms, M. Marsch, G. Hilt, E. Meggers, *Nature* **2014**, *515*, 100−103; c) X. Shen, H. Huo, C. Wang, B. Zhang, K. Harms, E. Meggers, *Chem. Eur. J.*

2015, *21*, 9720−9726; d) C. Wang, J. Qin, X. Shen, R. Riedel, K. Harms, E. Meggers, *Angew. Chem. Int. Ed.* **2016**, *55*, 685−688.

5   a) C. Wang, L.-A. Chen, H. Huo, X. Shen, K. Harms, L. Gong, E. Meggers, *Chem. Sci.* **2015**, *6*, 1094−1100; b) Y. Tan, W. Yuan, L. Gong, E. Meggers, *Angew. Chem. Int. Ed.* **2015**, *54*, 13045−13048; c) X. Shen, K. Harms, M. Marsch, E. Meggers, *Chem. Eur. J.* **2016**, *22*, 9102−9105; d) H. Huo, K. Harms, E. Meggers, *J. Am. Chem. Soc.* **2016**, *138*, 6936−6939.

6   a) Z.-Z. Li, S.-Y. Yao, J.-J. Wu, B.-H. Ye, *Chem. Commun.* **2014**, *50*, 5644−5647; b) Z.-Z. Li, S.-Y. Yao, B.-H. Ye, *ChemPlusChem* **2015**, *80*, 141−150; c) Z.-Z. Li, A.-H. Wen, S.-Y. Yao, B.-H. Ye, *Inorg. Chem.* **2015**, *54*, 2726−2733; d) Z.-Z. Li, S.-Y. Yao, A.-H. Wen, B.-H. Ye, *Eur. J. Inorg. Chem.* **2015**, 4335−4342.

7   a) J. Hartung, R. H. Grubbs, *J. Am. Chem. Soc.* **2013**, *135*, 10183−10185; b) J. Hartung, P. K. Dornan, R. H. Grubbs, *J. Am. Chem. Soc*. **2014**, *136*, 13029−13037.

8   O. Kaufhold, F. E. Hahn, T.Pape, A. Hepp, *J. Organomet. Chem.* **2008**, *693*, 3435−3440.

9   a) R. T. Watson, J. L. Jackson, J. D. Harper, K. A. Kane-Maguire, L. A. Kane-Maguire, N. A. Kane-Maguire, *Inorg. Chim. Acta* **1996**, *249*, 5−7; b) L. Gong, S. P. Mulcahy, D. Devarajan, K. Harms, G. Frenking, E. Meggers, *Inorg. Chem.* **2010**, *49*, 7692−7699.

10 M. J. Heeg, R. Kroener, E. Deutsch, *Acta Cryst. C* **1985**, *41*, 684−686.

11 F. Xu, W.Huang, *Acta Cryst. E* **2007**, *63*, m2114.

12 Y. Wang, F.Xu, W. Huang, *Acta Cryst. E* **2012**, *68*, m68.

13 S. K. Chattopadhyay, K. Mitra, S. Biswas, S. Naskar, D. Mishra, B. Adhikary, R. G. Harrison, J. F. Cannon, *Transition Met. Chem.* **2004**, *29*, 1.

14 For precedence on enantioselective, catalytic alkynylations of trifluoromethyl ketones, see: a) R. Motoki, D. Tomita, M. Kanai, M. Shibasaki, *Tetrahedron Lett.* **2006**, *47*, 8083−8086; b) R. Motoki, M. Kanai, M. Shibasaki, *Org. Lett.* **2007**, *9*, 2997−3000; c) K. Aikawa, Y. Hioki, K. Mikami, *Org. Lett.* **2010**, *12*, 5716−5719; d) G.-W. Zhang, W. Meng, H. Ma, J. Nie, W.-Q. Zhang, J.-A. Ma, *Angew. Chem. Int. Ed.* **2011**, *50*, 3538−3542; e) T. Ohshima, T. Kawabata, Y. Takeuchi, T. Kakinuma, T. Iwasaki, T. Yonezawa, H. Murakami, H. Nishiyama, K. Mashima, *Angew. Chem. Int. Ed.* **2011**, *50*, 6296−6300; f) T. Wang, J.-L. Niu, S.-L. Liu, J.-J. Huang, J.-F. Gong, M.-P. Song, *Adv. Synth. Catal.* **2013**, *355*, 927–937; g) V. Dhayalan, R. Murakami, M. Hayashi, *Asian J. Chem.*

2013, *25*, 7505−7508; h) A. M. Cook, C. Wolf, *Angew. Chem. Int. Ed.* **2016**, *55*, 2929–2933; i) J.-i. Ito, S. Ubukata, S. Muraoka, H. Nishiyama, *Chem. Eur. J.* **2016**, *22*, 16801−16804.

15 J. Nie, H.-C. Guo, D. Cahard, J.-A. Ma, *Chem. Rev.* **2011**, *111*, 455−529.

16 a) B. M. Trost, A. H. Weiss, *Adv. Synth. Catal.* **2009**, *351*, 963−983; b) K. Müller, C. Faeh, F. Diederich, *Science* **2007**, *317*, 1881−1886; c) S. Purser, P. R. Moore, S. Swallow, V. Gouverneur, *Chem. Soc. Rev.* **2008**, *37*, 320−330; d) E. P. Gillis, K. J. Eastman, M. D. Hill, D. J. Donnelly, N. A. Meanwell, *J. Med. Chem.* **2015**, *58*, 8315−8359.

17 S. M. E. Vrouenraets, F. W. N. M. Wit, J. van Tongeren, J. M. A. Lange, *Expert Opin. Pharmacother.* **2007**, *8*, 851−871.

18 S. Okusu, K. Hirano, Y. Yasuda, J. Tanaka, E. Tokunaga, H. Fukaya, N. Shibata, *Org. Lett.* **2016**, *18*, 5568−5571.

19 D. Dai, X. Long, B. Luo, A. Kulesza, J. Reichwagen, Y. Guo, Process for Preparation of Efavirenz by Cyclization. WO 2012097510, 2012.

20 S. U. Son, K. H. Park, Y.-S. Lee, B. Y. Kim, C. H. Choi, M. S. Lah, Y. H. Jang, D.-J. Jang, Y. K. Chung, *Inorg. Chem.* **2004**, *43*, 6896−6898.

21 a) Y. Cheng, J.-F. Sun, H.-L. Yang, H.-J. Xu, Y.-Z. Li, X.-T. Chen, Z.-L. Xue, *Organometallics* **2009**, *28*, 819−823; b) M. Dakkach, X. Fontrodona, T. Parella, A. Atlamsani, I. Romero, M. Rodríguez, *Adv. Synth. Catal.* **2011**, *353*, 231−238; c) M. R. Norris, J. J. Concepcion, D. P. Harrison, R. A. Binstead, D. L. Ashford, Z. Fang, J. L. Templeton, T. J. Meyer, *J. Am. Chem. Soc.* **2013**, *135*, 2080−2083; d) V. Leigh, W. Ghattas, R. Lalrempuia, H. Muller-Bunz, M. T. Pryce, M. Albrecht, *Inorg. Chem.* **2013**, *52*, 5395−5402; e) G. J. Barbante, P. S. Francis, C. F. Hogan, P. R. Kheradmand, D. J. D. Wilson, P. J. Barnard, *Inorg. Chem.* **2013**, *52*, 7448−7459; f) B.; Saha, G. Sengupta, A. Sarbajna, I. Dutta, J. K. Bera, *J. Organomet. Chem.* **2014**, *771*, 124−130; g) J. Olguín, M. Díaz-Fernández, J. La Cruz-Cruz, M. A. Paz-Sandoval, *J. Organomet. Chem.* **2016**, *824*, 33−41.

22 H. Cai, J. Nie, Y. Zheng, J.-A. Ma, *J. Org.Chem.* **2014**, *79*, 5484−5493.

Chapter 4: Summary and Outlook

4.1 Summary

1) **Expanding the family of bis-cyclometalated octahedral chiral-at-metal iridium and rhodium catalysts**

Several octahedral chiral-at-metal complexes **Ir**(**Se**) and **Rh**(**Se**) were successfully synthesized for expanding our previously developed Lewis acid catalysts based on our established procedures. Accordingly, the chiral Lewis acid complexes Λ/Δ-**Ir**(**Se**) and Λ/Δ-**Rh**(**Se**) were synthesized though the chiral auxiliary-mediated strategy which was developed by our group. The reaction of *rac*-**Ir**(**Se**) or *rac*-**Rh**(**Se**) with the appropriate chiral auxiliary afforded the corresponding auxiliary complexes Λ-(*S*)-**3** and Δ-(*S*)-**3** or Λ-(*R*)-**4** and Δ-(*R*)-**4** as a mixture of diastereomers, respectively. The generated diastereomeric complexes could be resolved by standard silica gel chromatography. Then the individual enantiomers Λ/Δ-**Ir**(**Se**) and Λ/Δ-**Rh**(**Se**) were generated after the protonation by acid.
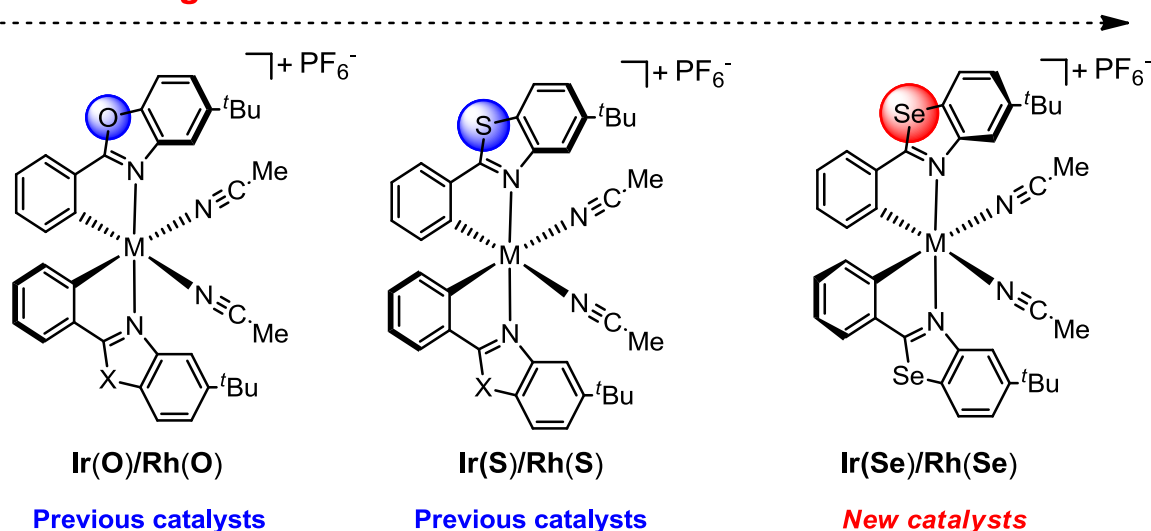
Figure 54 Expansion of catalysts library.
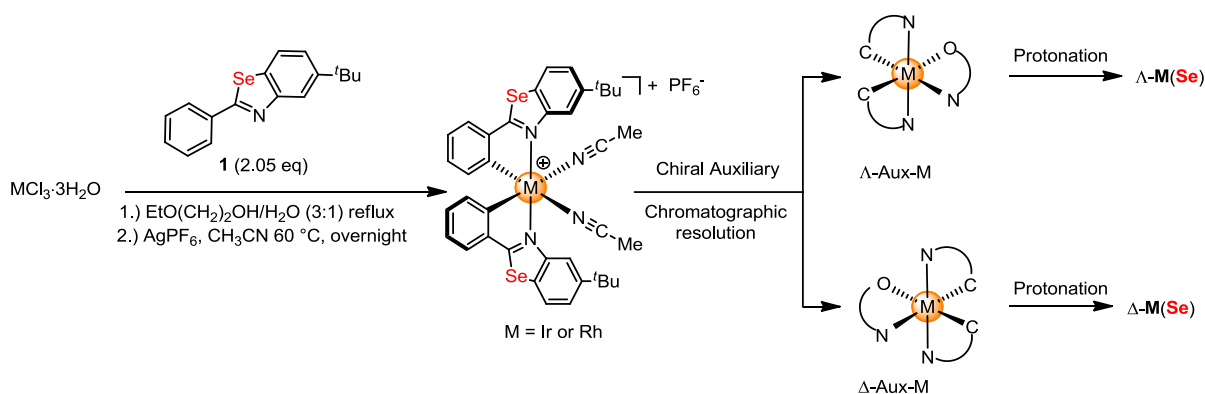
Scheme 17 Chiral auxiliary-mediated asymmetric synthesis of the enantiopure chiral-at-metal complexes.

We then investigated some reactions to compare their catalytic reactivity with the previous ones. Michael addition reaction and three photo-induced reactions were tested as summarized below. Unfortunately, the new catalysts did not have better or even similar performance. Except for Michael addition reaction, Λ-**Ir**(**Se**) or Λ-**Rh**(**Se**) showed worse activity. We assumed that maybe the coordination of substrate with **Ir**(**Se**) or **Rh**(**Se**) is more difficult than its congeners due to higher steric hinderance.
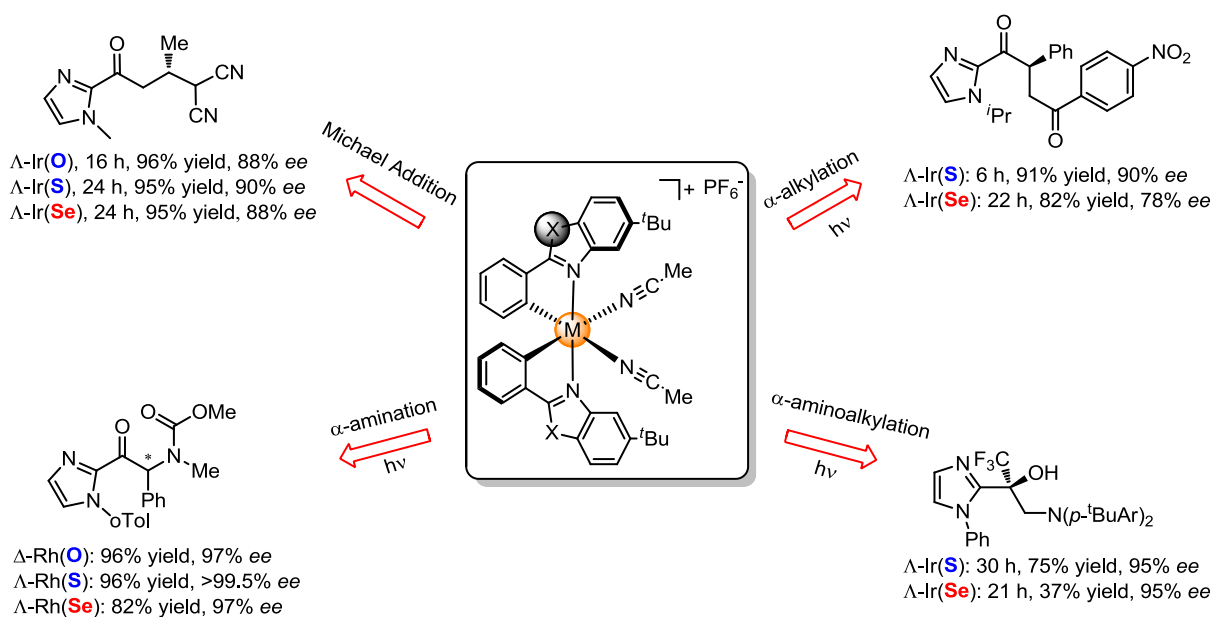
Figure 55 Comparison of catalytic reactions catalyzed by Lewis acid catalysts.

2) Synthesis, characterization and reactivity of bis-cyclometalated iridium(III)/rhodium(III) complexes containing pinene-derived ligands

Chiral ligands mediated four new bis-cyclometalated rhodium(III) and iridium(III) complexes were firstly synthesized in a diastereomerically and enantiomerically pure fashion in our group. Reactivity studies demonstrated that the rhodium complex contains pinene-derived chiral ligands can serve as a highly effective catalyst to catalyze the enantioselective alkynylation of 2-trifluoroacetyl imidazoles. The propargyl alcohols were obtained in 55–99% yields with excellent enantioselectivities (94–>99% *ee*). Interestingly, the asymmetric induction is mainly controlled by the metal-centered chirality not the chirality of ligands during the catalytic cycle, and at the same time the rhodium complexes show higher catalytic activity compared to our previous achiral ligand-based catalysts. Besides, the introduction of chiral ligand shortens the asymmetric synthesis of chiral octahedral complexes.
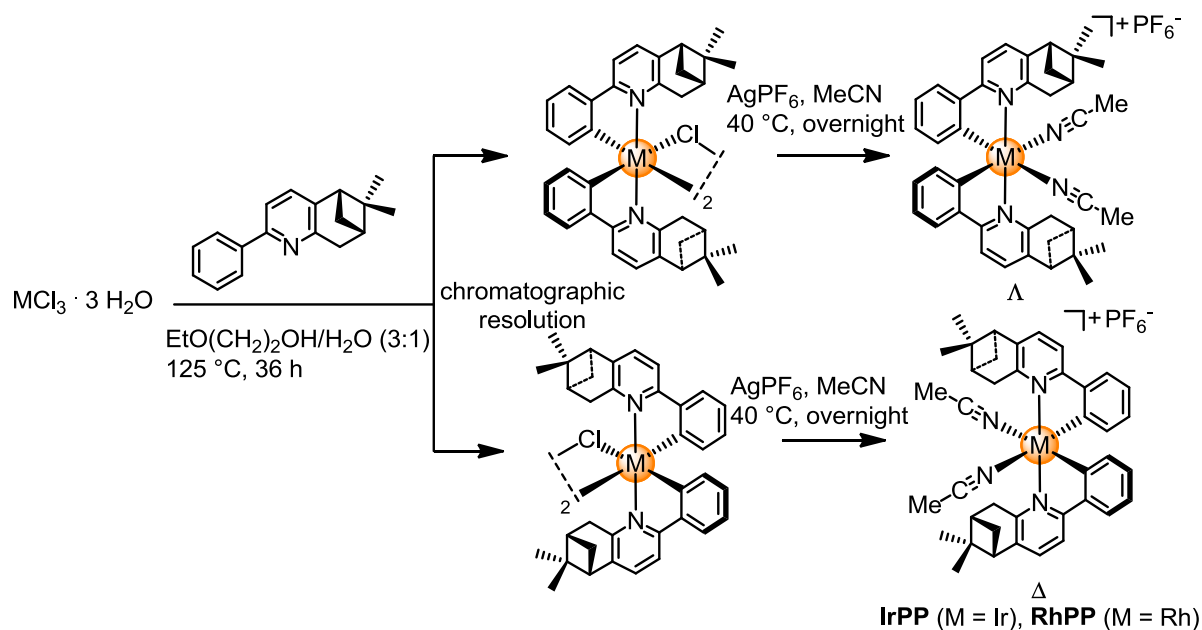
Scheme 18 Synthesis of chiral octahedral iridium(III) and rhodium(III) complexes with chiral ligands.
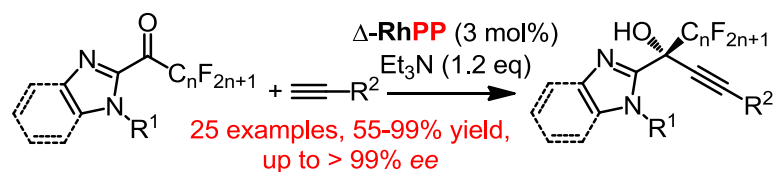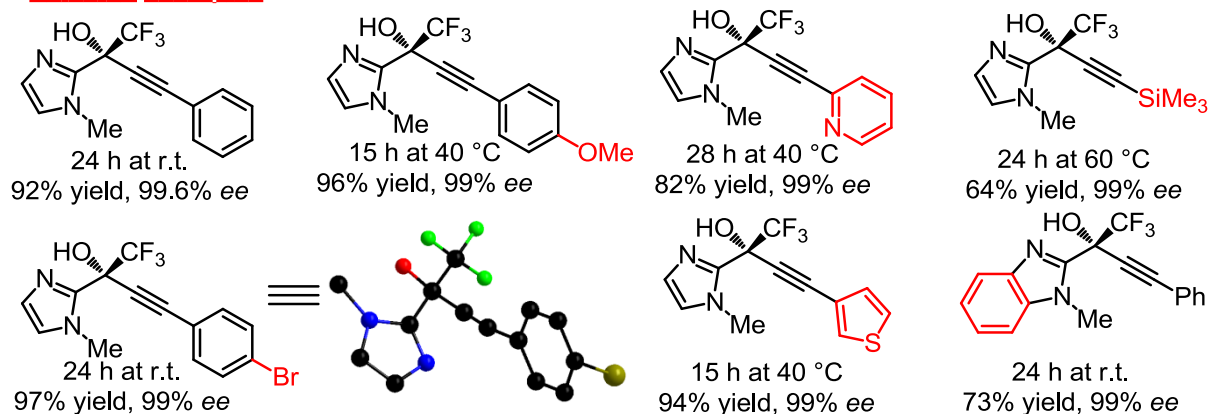
Figure 56 Selected examples of asymmetric alkynylation of 2-trifluoroacetly imidazoles.

3) Octahedral chiral-at-ruthenium complexes for highly effective asymmetric catalysis

The first example of an octahedral chiral-at-metal ruthenium complex with stable constitution and configuration was introduced here. The success of the synthesis of these new catalysts is attributed to the introduction of two PyNHC ligands. On the one hand, the PyNHC ligands as rigid coordinating ligands provide a suitable environment for the formation of the stable bis-(PyNHC)Ru complex. On the other hand, the strong σ-donating NHC-ligands make the coordinated acetonitrile ligands labile enough to accelerate the ligand exchange through the *trans*-effect. As a result, we found that the new class of catalysts can efficiently catalyze the enantioselective alkynylation of trifluoromethyl ketones to provide the propargylic alcohols in high yields (up to 99% yield) with excellent enantioselectivities (up to > 99% *ee*). Importantly, our new catalysts can be applied to access two kinds of propargylic alcohol intermediates which can convert to enantiomerically anti-HIV drug efavirenz easily. The Merck intermediate and the Lonza intermediate were obtained in high yields and with high enantioselectivities. The gram-scale reactions indicated that the synthetic routes might contribute to lowering the cost for the production of the important anti-HIV drug efavirenz.
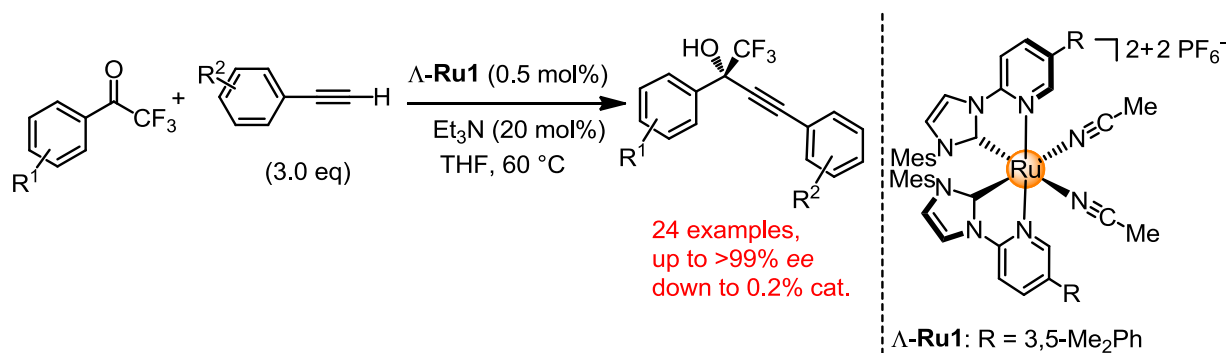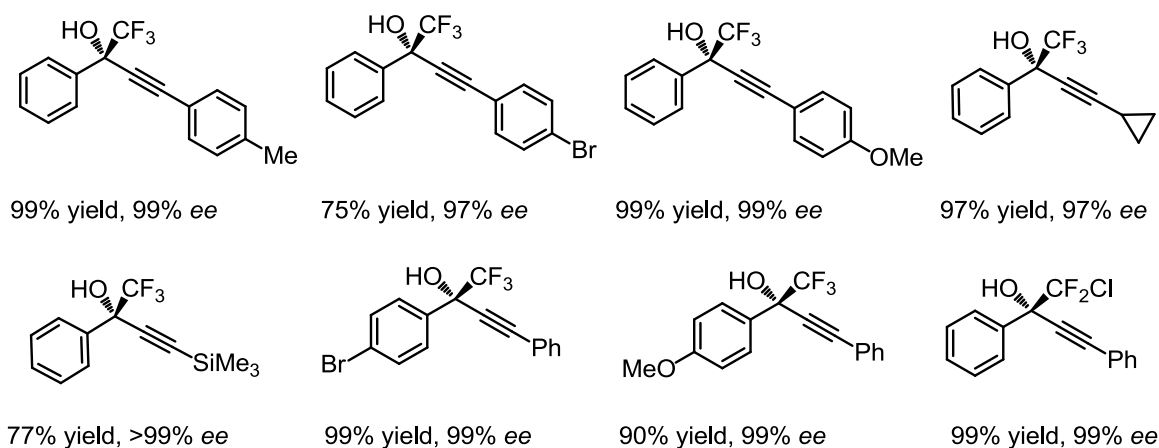
Figure 57 Selected examples of asymmetric alkynylation of trifluoroacetly ketones.
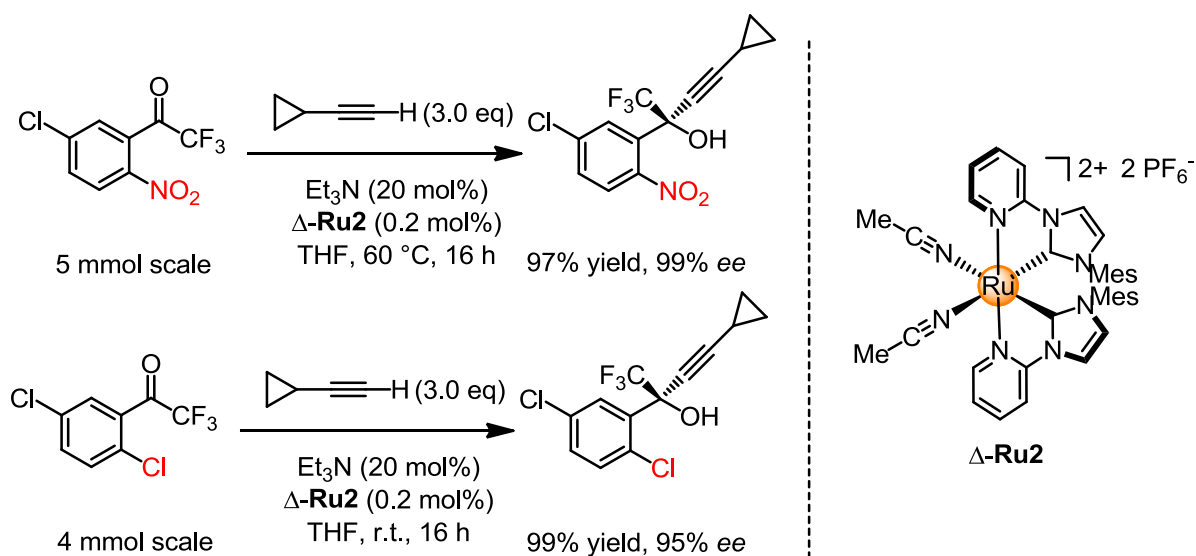
Figure 58 Gram-scale synthesis of key intermediates of the anti-HIV drug efavirenz.

4.2 Outlook

My thesis work mainly focused on the development of new octahedral metal complexes with metal-centered chirality and their applications in asymmetric catalysis. Several further investigations can be considered as follows:

1) **Explore C(sp^3)-H activation reactions catalyzed by octahedral chiral-at-ruthenium complexes:** Asymmetric C(sp^3)-H activation is one of the most attractive and promising projects in organic catalysis nowadays. Ruthenium imido complexes and ruthemium oxo complexes as high reactivity intermediates responsible for C(sp^3)-H activation. Since our newly developed chiral-at-ruthenium complexes show highly strong *trans*-effect, it is promising to try some chiral-at-ruthenium involved asymmetric C(sp^3)-H activation reactions.

2) **Explore asymmetric photoreactions catalyzed by octahedral chiral-at-ruthenium complexes:** Ru(bpy)$_3^{2+}$ has been widely used as photoredox catalyst and combined with an asymmetric catalyst, such as organocatalysts or metal-based complexes, to provide the required stereocontrol and the activation of one substrate in asymmetric photoreactions. It is worthy to investigate the coordination behaviors of octahedral chiral-at-ruthenium complexes and measure the redox potentials of ruthenium-based complexes, including the substrate-coordinated complexes. Then we can adjust the redox potential of them through introducing electron rich or deficient groups at the fixed position of achiral ligand. And finally, our chiral-at-ruthenium complexes might serve as a single catalyst to catalyze some asymmetric photoreactions.

3) **Explore octahedral base-metal centered catalysts**: Recently, the development of first-row transition metals catalysts became more attractive topic because they are nontoxic, inexpensive and earth-abundant. Despite the fact that many base-metal catalysts display high reactivity and selectivity, chiral octahedral complexes of base metals such as iron, cobalt and nickel which furnish asymmetric catalysis is far less studied. Based on our experiences on asymmetric synthesis of octahedral chiral-at-metal complexes, it is promising to apply our strategies for the synthesis of base-metal centered complexes and then inverstigate their properties.

Chapter 5: Experimental Part

5.1 Materials and Methods

All reactions were carried out under an atmosphere of nitrogen with magnetic stirring unless indicated otherwise. The catalytic reactions were performed in Schlenk tube.

Solvents and Reagents

Solvents were distilled under nitrogen from calcium hydride ($CHCl_3$, CH_2Cl_2, CH_3CN and DMF), magnesium turnings/iodine (MeOH) or sodium/benzophenone (Et_2O, THF and toluene). HPLC grade solvents, such as 2-methoxyethanol, ethanol, ethylene glycol and DMSO are used directly without further drying. All reagents were purchased from Acros, Alfa aesar, Sigma Aldrich, TCI, ChemPur and Fluorochem and used without further purification.

Chromatographic Methods

The course of the reactions and the column chromatographic elution were monitored by thin layer chromatography (TLC) [Macherey-Nagel (ALUGRAM®Xtra Sil G/UV254)]. Flash column chromatography was performed with silica gel from Merck (particle size 0.040-0.063 mm).

Nuclear Magnetic Resonance Spectroscopy (NMR)

^1H NMR, proton decoupled ^{13}C NMR, and proton coupled ^{19}F NMR spectra were recorded on Bruker Avance 300 system (^1H NMR: 300 MHz, ^{13}C NMR: 75 MHz, ^{19}F NMR: 282 MHz) spectrometers at ambient temperature. Chemical shifts are given in ppm on the δ scale, and were determined after calibration to the residual signals of the solvents, which were used as an internal standard. NMR standards were used are as follows: ^1H NMR spectroscopy: $\delta = 7.26$ ppm ($CDCl_3$), $\delta = 5.32$ ppm (CD_2Cl_2), $\delta = 3.31$ ppm (CD_3OD); ^{13}C NMR spectroscopy: $\delta = 77.0$ ppm ($CDCl_3$), $\delta = 54.0$ ppm (CD_2Cl_2), $\delta = 118.26, 1.32$ ppm (CD_3CN), $\delta = 49.0$ ppm (CD_3OD). ^{19}F NMR spectroscopy: $\delta = 0$ ppm ($CFCl_3$). The characteristic signals were specified from the low field to high field with the chemical shifts (δ in ppm). ^1H NMR spectra peak multiplicities indicated as singlet (s), doublet (d), doublet of doublet (dd), doublet of doublet of doublet (ddd), triplet (t), doublet of triplet (dt), quartet (q),

multiplet (m). The coupling constant *J* indicated in hertz (Hz).

High-Performance Liquid Chromatography (HPLC)

Chiral HPLC was performed with an Agilent 1200 Series or Agilent 1260 Series HPLC System. All the HPLC conditions were detailed in the individual procedures. The type of the columns, mobile phase and the flow rate were specified in the individual procedures.

Infrared Spectroscopy (IR)

IR measurements were recorded on a Bruker Alpha-P FT-IR spectrometer. The absorption bands were indicated a wave numbers v (cm^{-1}). All substances were measured as films or solids.

Mass Spectrometry (MS)

High-resolution mass spectra were recorded on a Bruker En Apex Ultra 7.0 TFT-MS instrument using ESI or APCI or FD technique. Ionic masses are given in units of m/z for the isotopes with the highest natural abundance.

Circular Dichroism Spectroscopy (CD)

CD spectra were recorded on a JASCO J-810 CD spectropolarimeter. The parameters we used as follows: from 600 nm to 200 nm; data pitch (0.5 nm); band with (1 nm); response (1 second); sensitivity (standard); scanning speed (50 nm/min); accumulation (3 times). The concentration of the compounds for the measurements was 0.2 mM. The formula for converting θ to ε is shown as below.

$$\Delta\varepsilon = \frac{\theta[m\deg]}{32980 \times c\,(mol/L) \times L(cm)}$$

c = concentration of the sample; L = thickness of the measurement vessel

Crystal Structure Analysis

Crystal X-ray measurements and the crystal structure analysis were carried out by Dr. Klaus Harms (Chemistry Department, Philipps University of Marburg). X-ray data were collected with a Bruker 3 circuit D8 Quest diffractometer with MoKa radiation (microfocus tube with multilayer optics) and Photon 100 CMOS detector. Scaling and absorption correction was performed by using the SADABS[1]

software package of Bruker. Structures were solved using direct methods in SHELXS[2] and refined using the full matrix least squares procedure in SHELXL-2013[3] or SHELXL-2014[4]. The Flack parameter is a factor used to estimate the absolute configuration of the coumounds.[5] The hydrogen atoms were placed in calculated positions and refined as riding on their respective C atom, and Uiso(H) was set at 1.2 Ueq(Csp^2) and 1.5 Ueq(Csp^3). Disorder of PF_6 ions, solvent molecules or methylene groups were refined using restraints for both the geometry and the anisotropic displacement factors.

Optical Rotation Polarimeter

Optical rotations were measured on a Krüss P8000-T or Perkin-Elmer 241 polarimeter with $[\alpha]_D^{25}$ values reported in degrees with concentrations reported in g/100 mL.

Melting Point determination Apparatus

The uncorrected melting points were determined on a Mettler Toledo MP 70 using one end closed capillary tubes.

5.2 Expanding the Family of Bis-Cyclometalated Chiral-at-Metal Iridium and Rhodium Catalysts

1) Synthesis of benzoselenazole ligand

5-(*tert*-butyl)-2-phenylbenzo[d][1,3]selenazole (1)
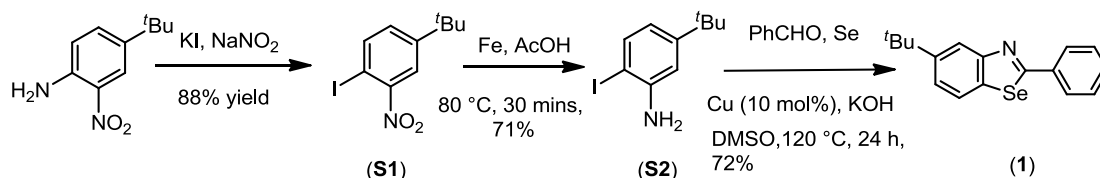
The compound **S1** was synthesized following a published procedure with slight modifications.[6] To a solution of *p*-TsOH H$_2$O (7.70 g, 44.7 mmol) in CH$_3$CN (60 mL) was added 4-(*tert*-butyl)-2-nitroaniline (2.894 g, 14.7 mmol). The resulting suspension of amine salt was cooled to 10–15 ℃ and to this was added, gradually, a solution of NaNO$_2$ (2.06 g, 29.8 mmol) and KI (6.18 g, 37.2 mmol) in H$_2$O (9 mL). The reaction mixture was stirred at room temperature and monitored by TLC until the starting material was completely consumed. The reaction mixture was then poured into H$_2$O. Saturated aqueous solution of NaHCO$_3$ was added until pH reached 9–10. Then the mixture was treated with Na$_2$S$_2$O$_3$ (2 M, 30 mL).The resulted mixture was extracted with CH$_2$Cl$_2$ and purified by flash chromatography to obtain the product **S1** (4.023 g, 13.2 mmol, yield: 88%, R$_f$ = 0.85, EtOAc/*n*-hexane = 1:5) as a yellow oil.

^{1}H NMR (300 MHz, CDCl$_3$) δ 7.92 (d, J = 8.3 Hz, 1H), 7.84 (d, J = 2.3 Hz, 1H), 7.28 (dd, J = 4.9, 2.5 Hz, 1H), 1.33 (s, 1H).

^{13}C NMR (75 MHz, CDCl$_3$) δ 153.6, 153.1, 141.5, 131.0, 122.8, 82.4, 35.1, 31.0.

IR (film): v (cm^{-1}) 2962, 2871, 1526, 1471, 1349, 1283, 1254, 1115, 1016, 892, 828, 749, 699, 663, 516.

HRMS (ESI, *m/z*) calcd for C$_{10}$H$_{12}$INO$_2$Na$_1$ [M+Na]$^+$: 327.9805, found: 327.9805.

The compound **S2** was synthesized following a published procedure with slight modifications.[7] AcOH (46 mL) was added to the mixture of **S1** (3.27 g, 10.8 mmol) and Fe power (3.2 g, 57.3 mmol) in EtOH (46 mL). The mixture was degassed for 15 min, and then heated at 100 ℃ for 40 min. The reaction mixture was diluted with 100 mL water and extracted with CH$_2$Cl$_2$ and purified by flash

chromatography to obtain the product **S2** (2.089 g, 7.59 mmol, yield: 70%, R_f = 0.8, EtOAc/*n*-hexane = 1:5) as a white solid.

^{1}H NMR (300 MHz, CDCl$_3$) δ 7.58–7.52 (m, 1H), 6.79 (d, *J* = 2.2 Hz, 1H), 6.54 (dd, *J* = 8.4, 2.3 Hz, 1H), 4.04 (s, 2H), 1.28 (s, 9H).

^{13}C NMR (75 MHz, CDCl$_3$) δ 153.2, 146.5, 138.6, 117.9, 112.3, 80.7, 34.6, 31.3.

IR (film): v (cm^{-1}) 3463, 3369, 2958, 2867, 1604, 1558, 1478, 1404, 1363, 1310, 1238, 1202, 1155, 1114, 1074, 1005, 930, 862, 800, 698, 641, 586, 546, 455.

HRMS (ESI, *m/z*) calcd for C$_{10}$H$_{15}$IN [M+1]$^+$: 276.0244, 277.0276, found: 276.0248, 277.0282.

The compound **1** was synthesized following a published procedure with slight modifications.[8] To a solution of **S2** (1.376 g, 5.0 mmol) and benzaldehyde (0.637mg, 6 mmol) in dry DMSO (15 mL), Se power (1.18g, 15 mmol), Cu power (31.8 mg, 0.5 mmol) and KOH (0.561 mg, 10.0 mmol) were added. The resulting was degassed for 15 min and stirred at 120 ^{o}C for 24 h under N$_2$ atmosphere. The reaction mixture was cooled to room temperature and diluted with saturated aq. NH$_4$Cl and extracted with CH$_2$Cl$_2$. The organic layer was dried over Na$_2$SO$_4$ and the solvent was removed under reduced pressure. The residue was purified by flash chromatography to obtain the product **1** (1.136 g, 3.6 mmol, yield: 72%, R_f = 0.9, EtOAc/*n*-hexane = 1:5) as a yellow solid.

^{1}H NMR (300 MHz, CDCl$_3$) δ 8.19 (d, *J* = 1.9 Hz, 1H), 8.08–7.98 (m, 2H), 7.86 (d, *J* = 8.4 Hz, 1H), 7.53–7.45 (m, 3H), 7.40 (dd, *J* = 8.4, 2.0 Hz, 1H), 1.44 (s, 9H).

^{13}C NMR (75 MHz, CDCl$_3$) δ 172.5, 156.2, 150.1, 136.4, 135.0, 130.9, 129.1, 127.9, 124.2, 123.4, 121.5, 34.9, 31.6.

IR (film): v (cm^{-1}) 2957, 2865, 1540, 1511, 1475, 1448, 1400, 1361, 1307, 1281, 1248, 1207, 1159, 1098, 1074, 1045, 1024, 945, 914, 882, 847, 814, 761, 722, 685, 652, 614, 583, 476.

HRMS (ESI, *m/z*) calcd for C$_{17}$H$_{18}$N$_1$Se$_1$ [M+1]$^+$: 316.0600, found: 316.0604.

2) Synthesis of benzoselenazole iridium and rhodium complexes *rac*-Ir(Se) and *rac*-Rh(Se)

rac-**Ir(Se)**: The new complex *rac*-**Ir(Se)** was synthesized according to a procedure reported by our group with slight modification.[9] Accordingly, 5-*tert*-butyl-2-phenylbenzo[*d*]selenazole **1** (100 mg, 0.318 mmol) was added to IrCl$_3$•3H$_2$O (54.8 mg, 0.155 mmol) in a mixture of 2-ethoxyethanol and water (3:1, 6.88 mL). The reaction mixture was heated at 120 ℃ for 24 h under an atmosphere of

nitrogen. The resulting precipitate was collected by centrifugation, washed with methanol and dried to obtain a mixture as a pale orange solid. To the orange solid in CH_3CN (20 mL) was added $AgPF_6$ (59 mg, 0.233 mmol) in one portion, and then stirred at 60 ℃ overnight. After cooling to room temperature, the mixture was filtered. The filtrate was collected, evaporated to dryness and purified by column chromatograph on silica gel (CH_2Cl_2/CH_3CN = 100:1 to 20:1) to give *rac*-**Ir**(**Se**) (55.1 mg, 0.053 mmol, 34% yield for two steps, R_f = 0.4, CH_3CN/CH_2Cl_2 = 1:10) as an orange solid.

^{1}H NMR (300 MHz, CD_2Cl_2) δ 8.51 (d, J = 1.8 Hz, 2H), 8.04 (d, J = 8.5 Hz, 2H), 7.70–7.61 (m, 4H), 6.96 (td, J = 7.5, 1.0 Hz, 2H), 6.75 (td, J = 7.6, 1.3 Hz, 2H), 6.26 (d, J = 7.6 Hz, 2H), 2.31 (s, 6H), 1.46 (s, 18H).

^{13}C NMR (75 MHz, CD_2Cl_2) δ 187.4, 152.9, 151.7, 144.5, 142.1, 133.1, 131.8, 130.1, 127.3, 126.3, 125.4, 124.0, 122.1, 119.1, 35.7, 31.9, 4.2.

^{19}F NMR (282 MHz, CD_2Cl_2) δ −71.7, −74.2.

IR (film): v (cm^{-1}) 3053, 2957, 2868, 1618, 1580, 1551, 1441, 1410, 1364, 1286, 1249, 1159, 1100, 1024, 982, 927, 833, 759, 731, 717, 662, 553, 460.

HRMS (ESI, *m/z*) calcd for $C_{34}H_{32}IrN_2Se_2$ [M]$^+$: 819.0524, found: 819.0528.

rac-**Rh**(**Se**): The metal complex *rac*-**Rh**(**Se**) was synthesized according to a procedure reported by our group with some modification.[10] Accordingly, 5-*tert*-butyl-2-phenylbenzo[*d*]selenazole **1** (213 mg, 0.678 mmol) was added to $RhCl_3 \bullet 3H_2O$ (69 mg, 0.331 mmol) in a mixture of 2-ethoxyethanol and water (3:1). The reaction mixture was heated at 110 ℃ for 24 h under an atmosphere of nitrogen. Cooling to room temperatue and water was added. The resulting precipitate was collected by centrifugation, dried to obtain a mixture as a pale brown solid. To the brown solid in CH_3CN (5 mL) was added $AgPF_6$ (125.6 mg, 0.496 mmol) in one portion, and then stirred at 60 ℃ overnight. After cooling to room temperature, the mixture was filtered. The filtrate was collected, evaporated to dryness and purified by column chromatograph on silica gel (CH_2Cl_2/CH_3CN = 20:1) to give *rac*-**Rh**(**Se**) (92 mg, 0.113 mmol, 34% yield for two steps, R_f = 0.4, CH_3CN/CH_2Cl_2 = 1:10) as a pale yellow solid.

^{1}H NMR (300 MHz, CD_2Cl_2) δ 8.62 (s, 2H), 8.04 (d, J = 8.5 Hz, 2H), 7.71–7.59 (m, 4H), 7.03 (td, J = 7.5, 0.9 Hz, 2H), 6.85 (td, J = 7.7, 1.4 Hz, 2H), 6.29 (d, J = 7.8 Hz, 2H), 2.15 (s, 6H), 1.44 (s, 18H).

^{13}C NMR (75 MHz, CD_2Cl_2) δ 182.7, 152.9, 151.5, 143.7, 133.9, 131.4, 130.8, 127.6, 126.0, 125.5,

125.0, 122.6, 122.5, 119.4, 35.7, 31.8, 3.7.

^{19}F NMR (282 MHz, CD$_2$Cl$_2$) δ –71.6, –74.1.

HRMS (ESI, m/z) calcd for C$_{34}$H$_{32}$N$_2$RhSe^{2+} [M–PF$_6$]$^+$: 730.9945, found: 730.9952.

IR (film): v (cm^{-1}) 3573, 2958, 2867, 1618, 1577, 1468, 1436, 1364, 1289, 1253, 1160, 1102, 1025, 979, 926, 836, 755, 712, 660, 554, 456.

3) Iridium auxiliary complexes Λ-(S)-3 and Δ-(S)-3
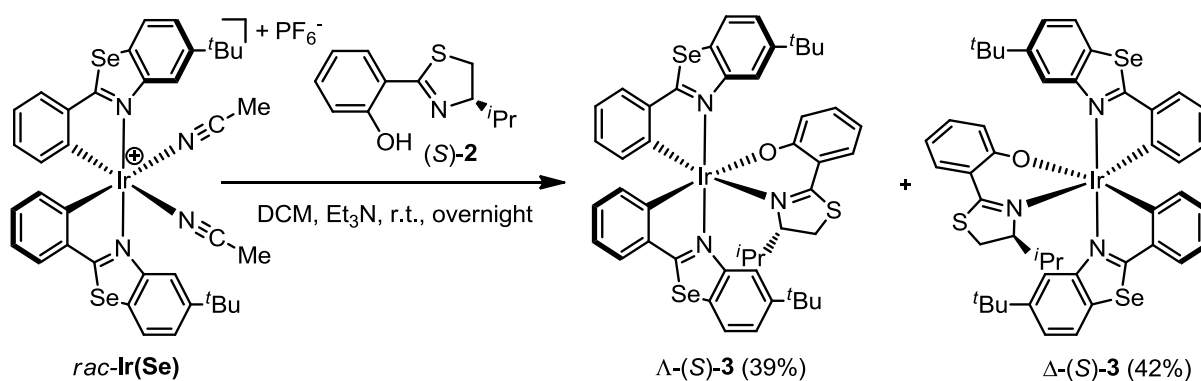
The new iridium auxiliary complexes Λ-(S)-**3** and Δ-(S)-**3** were synthesized according to our reported method with some modification.[9] To a solution of *rac*-**Ir(Se)** (164 mg, 0.16 mmol) in CH$_2$Cl$_2$ (8.0 mL), the chiral auxiliary (S)-**2** (35.5 μL, 0.188 mmol) and Et$_3$N (65.6 μL, 0.470 mmol) were added. The mixture was stirred at room temperature overnight. The solvent was removed and the residue was subjected to a flash silica gel chromatography (EtOAc/n-hexane = 1:25 to 1:10) to separate the two diastereomers. The first eluting diastereomer was assigned as Λ-(S)-**3** (red solid, 64.6 mg, 0.062 mmol, 39%, R$_f$ = 0.75, EtOAc/n-hexane = 1:5) and the second eluting diastereomer was assigned as Δ-(S)-**3** (red solid, 68.9 mg, 0.066 mmol, 42%, R$_f$ = 0.5, EtOAc/n-hexane = 1:5).

Λ-(S)-**3**: ^{1}H NMR (300 MHz, CD$_2$Cl$_2$) δ 9.30 (d, J = 1.8 Hz, 1H), 7.86 (dd, J = 12.7, 5.1 Hz, 2H), 7.74 (dd, J = 11.6, 8.1 Hz, 2H), 7.61 (d, J = 7.6 Hz, 1H), 7.42 (ddd, J = 8.3, 4.3, 1.7 Hz, 2H), 7.00 (d, J = 7.8 Hz, 2H), 6.90 (dd, J = 7.9, 7.2 Hz, 3H), 6.69 (dt, J = 15.0, 7.5 Hz, 2H), 6.55 (d, J = 8.5 Hz, 1H), 6.24 (d, J = 7.7 Hz, 1H), 6.04 (t, J = 7.4 Hz, 1H), 4.39 (dd, J = 7.7, 2.2 Hz, 1H), 3.43–3.30 (m, 1H), 2.96 (dd, J = 11.7, 1.8 Hz, 1H), 1.47 (s, 9H), 1.17 (s, 9H), 0.40 (d, J = 7.0 Hz, 3H), 0.10 (d, J = 6.9 Hz, 3H).

^{13}C NMR (75 MHz, CD$_2$Cl$_2$) δ 186.5, 185.3, 171.0, 170.1, 154.0, 152.9, 152.1, 152.0, 151.0, 149.9, 146.5, 145.9, 137.1, 133.5, 132.8, 132.5, 130.7, 129.9, 129.4, 129.0, 127.7, 127.5, 125.5, 124.8, 124.3, 124.0, 123.6, 122.54, 122.47, 121.2, 120.7, 118.2, 113.6, 83.7, 35.5, 35.4, 32.1, 31.7, 30.3, 28.6, 20.3,

15.1.

CD (MeOH): λ, nm (Δε, $M^{-1}cm^{-1}$) 463 (−25), 345 (+43), 315 (−15), 287 (−12), 269 (+16), 253 (−7), 241 (+17), 229 (−43), 215 (+146).

Δ-(S)-**3**: ^{1}H NMR (300 MHz, CD_2Cl_2) δ 9.05 (d, J = 1.8 Hz, 1H), 8.03 (d, J = 1.7 Hz, 1H), 7.89 (d, J = 8.4 Hz, 1H), 7.78 (d, J = 8.5 Hz, 1H), 7.67 (d, J = 7.6 Hz, 1H), 7.59 (dt, J = 8.1, 4.1 Hz, 1H), 7.46 (dd, J = 8.5, 1.9 Hz, 1H), 7.37 (dd, J = 8.5, 1.8 Hz, 1H), 7.26 (dd, J = 8.0, 1.7 Hz, 1H), 6.94–6.79 (m, 3H), 6.72 (td, J = 7.5, 1.2 Hz, 1H), 6.66–6.57 (m, 2H), 6.50–6.44 (m, 1H), 6.33 (d, J = 7.5 Hz, 1H), 6.22–6.14 (m, 1H), 3.51 (ddd, J = 8.5, 7.3, 4.4 Hz, 1H), 2.95 (dd, J = 11.2, 7.1 Hz, 1H), 2.50 (dd, J = 11.2, 8.7 Hz, 1H), 1.28 (s, 9H), 1.12 (s, 9H), 0.75 (d, J = 6.7 Hz, 3H), 0.24 (d, J = 7.0 Hz, 3H).

^{13}C NMR (75 MHz, CD_2Cl_2) δ 187.1, 186.0, 171.2, 168.9, 153.5, 153.1, 152.6, 151.0, 148.9, 145.7, 145.6, 136.1, 133.6, 132.7, 132.1, 130.7, 130.6, 129.7, 129.6, 127.8, 127.0, 125.2, 125.0, 124.4, 124.3, 123.9, 122.4, 122.3, 121.12, 121.09, 119.8, 113.3, 84.1, 35.6, 35.5, 31.9, 31.6, 31.2, 29.7, 21.1, 18.5.

CD (MeOH): λ, nm (Δε, $M^{-1}cm^{-1}$) 350 (−34), 319 (+19), 285 (+16), 271 (−8), 253 (+11), 229 (+88), 216 (−127).

IR (film): v (cm^{-1}) 3050, 2953, 2863, 1732, 1591, 1552, 1522, 1460, 1435, 1408, 1354, 1284, 1238, 1197, 1151, 1121, 1010, 976, 925, 883, 844, 809, 746, 732, 715, 661, 634, 579, 557.

HRMS (ESI, m/z) calcd for $C_{46}H_{46}IrN_3OSSe_2Na$ $[M+Na]^+$: 1062.1221, found: 1062.1221.

3) Rhodium auxiliary complexes Λ-(R)-4 and Δ-(R)-4
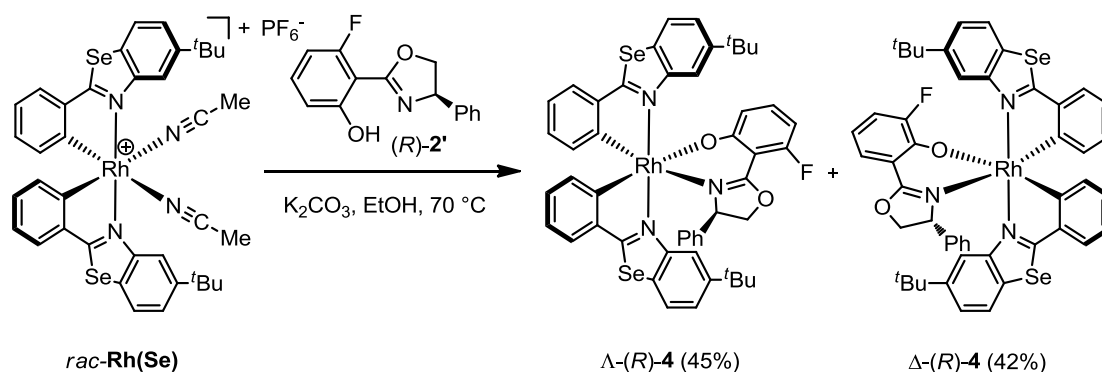
The new rhodium auxiliary complexes Λ-(R)-**4** and Δ-(R)-**4** were synthesized according to a reported method with some modification.[10] A mixture of *rac*-**Rh(Se)** (72.2 mg, 0.076 mmol), the chiral auxiliary (R)-**2′** (23.8 mg, 0.084 mmol) and K_2CO_3 (31.3 mg, 0.226 mmol) in EtOH (6.7 mL) was heated at 70 °C for 18 h. Afterwards, the reaction mixture was cooled to room temperature and concentrated to dryness. The residue was extracted by CH_2Cl_2, and the filtrate was evaporated to give the mixture of two diastereoisomers, which was then washed by EtOH (8 × 8 mL) to give Δ-(R)-**4** (17.1 mg, 0.016 mmol, 42% yield, R_f = 0.5, EtOAc/*n*-hexane = 1:4) as a yellow solid. The filtrate was concentrated and subjected to a flash chromatography on silica gel (*n*-hexane/CH_2Cl_2 = 1:10) to give

Λ-(*R*)-**4** (18.3 mg, 0.017 mmol, 45% yield, R_f = 0.35, EtOAc/*n*-hexane = 1:4) as a yellow solid. Note: Λ-(*R*)-**4** is soluble in EtOH; Δ-(*R*)-**4** is insoluble in EtOH.

Λ-(*R*)-**4**: ^{1}H NMR (300 MHz, CD$_2$Cl$_2$) δ 9.34 (d, *J* = 1.9 Hz, 1H), 8.53 (d, *J* = 1.8 Hz, 1H), 7.95 (d, *J* = 8.4 Hz, 1H), 7.80 (d, *J* = 8.5 Hz, 1H), 7.59 (dd, *J* = 7.6, 1.2 Hz, 1H), 7.50 (dd, *J* = 8.5, 2.0 Hz, 1H), 7.43 (dd, *J* = 8.5, 1.9 Hz, 1H), 7.06 (dd, *J* = 7.5, 1.4 Hz, 1H), 6.98–6.89 (m, 4H), 6.87–6.78 (m, 3H), 6.75–6.67 (m, 1H), 6.58–6.46 (m, 2H), 6.37–6.30 (m, 2H), 6.22 (d, *J* = 8.6 Hz, 1H), 5.76 (ddd, *J* = 11.5, 7.9, 0.9 Hz, 1H), 4.41–4.27 (m, 1H), 4.14–4.05 (m, 1H), 3.88 (dd, *J* = 12.5, 8.3 Hz, 1H), 1.37 (s, 9H), 1.23 (s, 9H).

^{13}C NMR (75 MHz, CD$_2$Cl$_2$) δ 182.11, 182.07, 175.4, 175.3, 169.4, 169.0, 168.5, 168.1, 167.6, 164.9, 161.5, 152.8, 152.8, 151.3, 144.3, 143.8, 138.2, 135.4, 133.6, 133.1, 132.9, 130.3, 130.13, 130.07, 129.7, 128.3, 127.9, 127.6, 127.4, 127.1, 125.2, 125.1, 124.63, 124.56, 123.5, 122.6, 121.1, 119.4, 119.31, 119.27, 104.5, 104.4, 98.8, 98.5, 75.0, 70.7, 35.8, 35.6, 31.9, 31.7.

Δ-(*R*)-**4**: ^{1}H NMR (300 MHz, CD$_2$Cl$_2$) δ 9.14 (d, *J* = 1.7 Hz, 1H), 8.06 (d, *J* = 1.5 Hz, 1H), 7.79 (d, *J* = 8.5 Hz, 1H), 7.62 (d, *J* = 8.4 Hz, 1H), 7.56 (d, *J* = 7.1 Hz, 1H), 7.52–7.41 (m, 2H), 7.37 (dd, *J* = 8.5, 1.8 Hz, 1H), 7.02–6.70 (m, 8H), 6.43–6.30 (m, 4H), 5.97 (d, *J* = 7.7 Hz, 1H), 5.71 (dt, *J* = 30.2, 15.2 Hz, 1H), 4.96–4.78 (m, 2H), 4.10–3.89 (m, 1H), 1.46 (s, 9H), 1.28 (s, 9H).

^{13}C NMR (75 MHz, CD$_2$Cl$_2$) δ 183.01, 182.97, 181.39, 181.35, 175.5, 175.4, 170.6, 170.2, 168.2, 167.8, 166.33, 166.29, 165.4, 162.0, 153.1, 152.8, 151.6, 151.2, 144.8, 141.4, 136.1, 133.6, 133.1, 132.9, 131.1, 130.0, 129.8, 129.6, 128.3, 128.0, 127.4, 127.2, 125.5, 124.4, 124.0, 123.9, 123.5, 122.9, 122.4, 120.3, 120.2, 118.6, 98.9, 98.5, 76.2, 69.7, 35.4, 31.91, 31.86.

IR (film): ν (cm^{-1}) 3053, 2955, 2862, 1618, 1577, 1530, 1441, 1369, 1286, 1219, 1156, 1094, 1026, 972, 919, 843, 812, 787, 749, 697, 661, 624, 578, 527, 458.

HRMS (ESI, *m/z*) calcd for C$_{49}$H$_{44}$FN$_3$O$_2$RhSe$_2$ [M+H]$^+$: 988.0810, found: 988.0809.

Λ-(*R*)-**4**:

CD (MeOH): λ, nm ($\Delta\varepsilon$, M^{-1}cm^{-1}) 429 (−23), 343 (+18), 300 (−43), 276 (+27), 263 (+19), 255 (−22).

Δ-(*R*)-**4**:

CD (MeOH): λ, nm ($\Delta\varepsilon$, M^{-1}cm^{-1}) 422 (+27), 351 (−46), 304 (+47), 277 (−30), 264 (−9), 244 (−39).

4) Synthesis of non-racemic iridium/rhodium catalysts
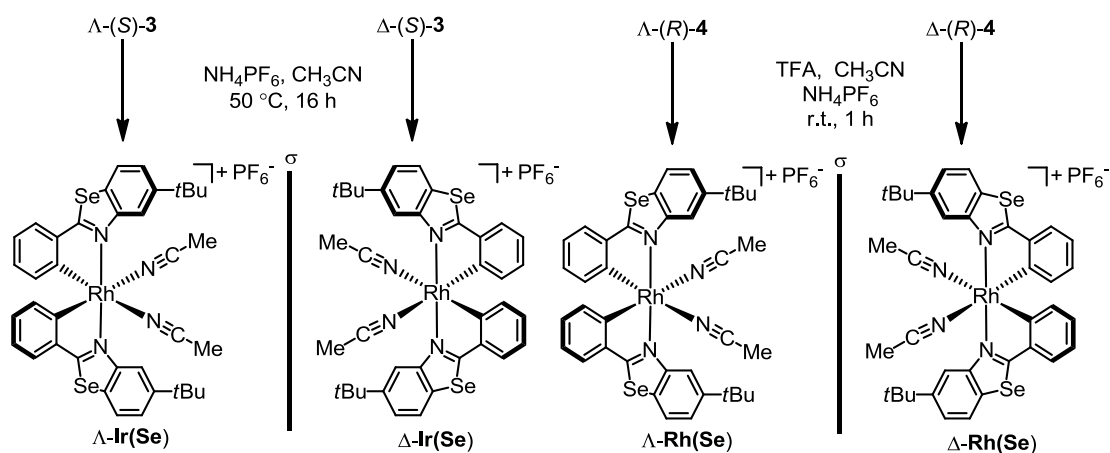
A suspension of the iridium auxiliary complex Λ-(*S*)-**3** (61.7 mg, 0.060 mmol) or Δ-(*S*)-**3** (65.3 mg, 0.063 mmol) and NH$_4$PF$_6$ (96.8 mg, 0.6 mmol) or NH$_4$PF$_6$ (102.7 mg, 0.63 mmol) in acetonitrile (10.0 mL) was heated at 50 °C for 16 h. The reaction mixture was concentrated to dryness and subjected to flash silica gel chromatography (CH$_2$Cl$_2$/CH$_3$CN = 100:1 to 15:1) to give the enantiopure catalyst Λ-**Ir(Se)** (52.7 mg, 0.058 mmol, 98%) or Δ-**Ir(Se)** (55.1 mg, 0.061 mmol, 97%) as a orange solid. All other spectroscopic data of enantiopure ruthenium catalysts were in agreement with the racemic catalysts. The absolute configurations were assigned by comparison with the analogue complexes Λ-**Ir(S)** and Δ-**Ir(S)**.[9]

Λ-**Ir(Se)**: CD (MeOH): λ, nm (Δε, M^{-1}cm^{-1}) 469 (−15), 362 (+43), 293 (−34), 260 (+17), 228 (−87), 216 (+199).

Δ-**Ir(Se)**: CD (MeOH): λ, nm (Δε, M^{-1}cm^{-1}) 470 (+14), 362 (−45), 292 (+32), 260 (−21), 228 (+84), 216 (−209).

To a suspension of Λ-(*S*)-**4** (47.0 mg, 0.048 mmol) or Δ-(*R*)-**4** (32.2 mg, 0.033 mmol), in CH$_3$CN (3 mL) was added TFA (10 eq) in one portion and stirred at room temperature for 0.5 h. The reaction mixture was evaporated to dryness, redissolved in CH$_3$CN, followed by the addition of excess NH$_4$PF$_6$ (30 eq), and then stirred at room temperature for another 0.5 h. The mixture was filtered by a thin pad of silica gel, the pale yellow filtrate was concentrated, and then subjected to the column chromatography on silica gel (CH$_2$Cl$_2$/CH$_3$CN = 100:1 to 5:1) to give the enantiopure catalysts Λ-**Rh(Se)** (38.4 mg, 0.047 mmol, 98% yield) or Δ-**Rh(Se)** (26.0 mg, 0.032 mmol, 98% yield) as pale yellow solid. All other spectroscopic data of enantiopure ruthenium catalysts were in agreement with the racemic catalysts. The absolute configurations were assigned by comparison with the analogue

complexes Λ-**Rh**(**S**) and Δ-**Rh**(**S**).[10]

Λ-**Rh**(**Se**): CD (MeOH): λ, nm (Δε, M^{-1}cm^{-1}) 412 (−47), 371 (+71), 358 (+65), 306 (−112), 269 (+34), 246 (+55), 231 (−31), 212 (+93).

Δ-**Rh**(**Se**): CD (MeOH): λ, nm (Δε, M^{-1}cm^{-1}) 413 (+38), 371 (−63), 355 (−58), 305 (+92), 266 (−32), 244 (−50), 230 (+22), 212 (−83).

5.3 Synthesis, Characterization and Reactivities of Bis-Cyclometalated Iridium(III)/Rhodium(III) Complexes Containing Pinene-Derived Ligands

5.3.1 Synthesis of the iridium and rhodium catalysts IrPP and RhPP

a) Synthesis of the 2-phenyl-5,6-(*S,S*)-pinenopyridine ligand

(1*R*)-(+)-α-Pinene   pinocarvone   (*S,S*)-**PP**
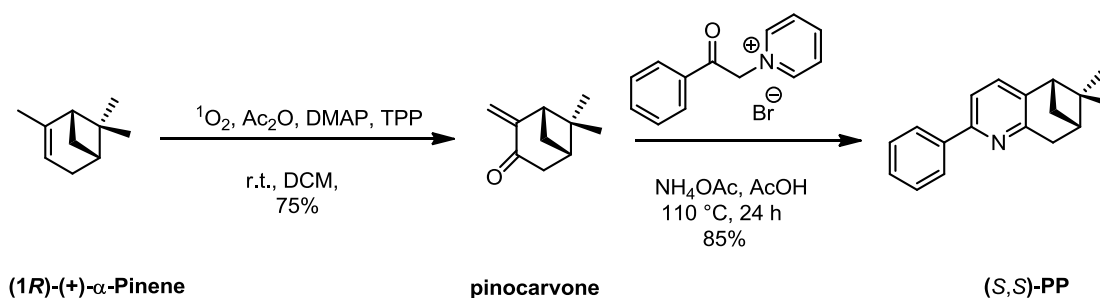
Pinocarvone: Pinocarvone was synthesized following a published procedure with some modifications.[11] Acetic anhydride (1.324 g, 13.0 mmol) and pyridine (0.500 g, 6.3 mmol) were added to the mixture of tetraphenylporphine (TPP) (8.0 mg, 1.3 μmol), DMAP (31.0 mg, 0.3 mmol) and (1*R*)-(+)-α-pinene (1.720 g, 12.6 mmol) in CH$_2$Cl$_2$ (11 mL). The suspension was stirred at room temperature for 18 h under ^{1}O$_2$ which is generated by 2 × 20W white lights. The mixture was then diluted with CH$_2$Cl$_2$ and washed successively with saturated NaHCO$_3$, 1 *N* HCl, and saturated CuSO$_4$. The organic fraction was thoroughly washed with water and dried over Na$_2$SO$_4$. After concentration, the residue was purified by silica gel column (EtOAc/*n*-hexane = 1:30) to yield pinocarvone as a purple oil (1.416 g, 9.4 mmol, 75%, R$_f$ = 0.5, EtOAc/*n*-hexane = 1:10).

^{1}H NMR (300 MHz, CD$_2$Cl$_2$) δ 5.90 (d, *J* = 1.8 Hz, 1H), 4.99 (d, *J* = 1.8 Hz, 1H), 2.83–2.58 (m, 3H), 2.57–2.40 (m, 1H), 2.23–2.17 (m, 1H), 1.36 (s, 3H), 1.28 (d, *J* = 10.3 Hz, 1H), 0.80 (s, 3H).

^{13}C NMR (75 MHz, CD$_2$Cl$_2$) δ 199.9, 150.1, 117.2, 49.0, 43.0, 41.3, 39.3, 33.0, 26.3, 21.9.

All spectroscopic data are in agreement with the literature.[12]

(*S*,*S*)-**PP**: (*S*,*S*)-**PP** was synthesized following a published procedure with slight modifications.[12] The mixture of phenacylpyridinium bromide (2.781 g, 10.0 mmol), anhydrous ammonium acetate (6.630 g, 86.0 mmol) and pinocarvone (1.362 g, 9.1 mmol) in acetic acid (6.6 mL) was heated at 110 °C for 24 h. After cooling to room temperature, water was then added and the mixture was extracted with ethyl acetate. The combined organic layers were washed successively with water, brine and dried over Na_2SO_4 and concentrated. The residue was purified by silica gel chromatograph (EtOAc/*n*-hexane = 1:30) to yield 2-phenyl-5,6-(*S*,*S*)-pinenopyridine (*S*,*S*)-**PP** as a white solid (1.917 g, 7.7 mmol, 85%, R_f = 0.5, EtOAc/*n*-hexane = 1:10).

^{1}H NMR (300 MHz, CDCl$_3$) δ 7.99 (dd, *J* = 8.3, 1.3 Hz, 2H), 7.57–7.33 (m, 4H), 7.33–7.21 (m, 1H), 3.23 (d, *J* = 2.7 Hz, 2H), 2.81 (t, *J* = 5.7 Hz, 1H), 2.73 (dt, *J* = 9.4, 5.8 Hz, 1H), 2.52–2.29 (m, 1H), 1.45 (s, 3H), 1.34 (d, *J* = 9.5 Hz, 1H), 0.72 (s, 3H).

^{13}C NMR (75 MHz, CDCl$_3$) δ 156.9, 154.9, 140.5, 140.1, 133.7, 128.7, 128.3, 126.8, 117.3, 46.5, 40.4, 39.7, 36.9, 32.1, 26.2, 21.5.

All spectroscopic data are in agreement with the literature.[13]

b) Synthesis of the metal complexes

Iridium dimer complexes: Iridium dimer complexes were synthesized following a published procedure with slight modifications.[14] The mixture of (*S*,*S*)-**PP** (374.0 mg, 1.50 mmol) and iridium chloride hydrate (176.3 mg, 0.50 mmol) in a mixture of 2-ethoxyethanol/water (3:1, 23 mL) was heated at 125 °C for 36 h under nitrogen. After removal of the solvent, the residue was subjected to flash silica gel chromatography (EtOAc/*n*-hexane = 1:20) to separate the diastereomers. The first eluting diastereomer was assigned as ΛΛ-**2$_{Ir}$** (red solid, 106.4 mg, 0.073 mmol, 29%) and the second eluting diastereomer was assigned as ΔΔ-**2$_{Ir}$** (red solid, 134.8 mg, 0.093 mmol, 37%). The Λ- and Δ-configurations of the diastereomers were confirmed by the single crystal structures of Λ-**IrPP** and Δ-**IrPP**.

ΛΛ-**2$_{Ir}$**: ^{1}H NMR (300 MHz, CD$_2$Cl$_2$) δ 7.66 (d, *J* = 8.0 Hz, 4H), 7.54 (dd, *J* = 7.8, 1.3 Hz, 4H), 7.42 (d, *J* = 8.0 Hz, 4H), 6.95–6.83 (m, 4H), 6.71–6.60 (m, 4H), 6.04 (dd, *J* = 7.9, 0.9 Hz, 4H), 4.69 (dd, *J* = 18.5, 2.4 Hz, 4H), 2.90 (t, *J* = 5.7 Hz, 4H), 2.77 (dd, *J* = 18.6, 3.0 Hz, 4H), 2.71–2.61 (m, 4H), 2.31–2.25 (m, 4H), 1.42 (s, 12H), 1.23 (d, *J* = 9.6 Hz, 4H), 0.93 (s, 12H).

^{13}C NMR (75 MHz, CD$_2$Cl$_2$) δ 164.3, 161.1, 145.6, 142.8, 135.5, 134.9, 133.3, 128.5, 123.8, 122.7,

115.6, 47.6, 41.0, 39.3, 37.9, 32.5, 26.0, 22.4.

CD (MeOH): λ, nm (Δε, M^{-1}cm^{-1}) 386 (−67), 352 (+120), 306 (−71), 285 (−94), 255 (+157), 230 (+25).

ΔΔ-**2$_{Ir}$**: ^{1}H NMR (300 MHz, CD$_2$Cl$_2$) δ 7.68 (d, J = 8.0 Hz, 4H), 7.56 (dd, J = 7.8, 1.4 Hz, 4H), 7.45 (d, J = 8.0 Hz, 4H), 6.90 (ddd, J = 8.3, 7.5, 1.1 Hz, 4H), 6.68–6.56 (m, 4H), 6.11–6.00 (m, 4H), 4.72 (dd, J = 18.5, 3.3 Hz, 4H), 2.91 (t, J = 5.7 Hz, 4H), 2.81–2.71 (m, 4H), 2.66 (dd, J = 18.5, 2.4 Hz, 4H), 2.32–2.26 (m, 4H), 1.47 (d, J = 9.6 Hz, 4H), 1.40 (s, 12H), 0.70 (s, 12H).

^{13}C NMR (75 MHz, CD$_2$Cl$_2$) δ 163.8, 160.7, 145.5, 142.9, 135.6, 135.3, 133.8, 128.2, 123.9, 122.7, 115.6, 47.4, 40.9, 40.3, 37.2, 31.8, 26.3, 21.9.

CD (MeOH): λ, nm (Δε, M^{-1}cm^{-1}) 386 (+84), 351 (−99), 307 (+66), 284 (+73), 255 (−146), 231 (+2).

IR (film): v (cm^{-1}) 3049, 2922, 2868, 2019, 1595, 1576, 1462, 1437, 1420, 1385, 1218, 1122, 1074, 1028, 949, 836, 822, 773, 734, 719, 669, 449.

HRMS (ESI, m/z) calcd for C$_{72}$H$_{72}$Cl$_1$N$_2$Ir$_2$ [M/2−Cl]$^+$: 689.2508, found: 689.2517.

Rhodium dimer complexes: The mixture of (*S*,*S*)-**PP** (748.0 mg, 3.0 mmol) and rhodium chloride hydrate (209.3 mg, 0.79 mmol) in a mixture of 2-ethoxyethanol/water (3:1, 46 mL) was heated at 125 ℃ for 36 h under nitrogen. After removal of the solvent, the residue was subjected to flash silica gel chromatography (EtOAc/*n*-hexane = 1:20) to separate the diastereomers. The first eluting diastereomer was assigned as ΛΛ-**2$_{Rh}$** (orange solid, 115.3 mg, 0.091 mmol, 23%) and the second eluting diastereomer as ΔΔ-**2$_{Rh}$** (orange solid, 156.9 mg, 0.124 mmol, 31%). The Λ- and Δ-configurations of the diastereomers were confirmed by the single crystal structures of Λ-**RhPP** and Δ-**RhPP**.

ΛΛ-**2$_{Rh}$**: ^{1}H NMR (300 MHz, CD$_2$Cl$_2$) δ 7.72–7.58 (m, 8H), 7.50–7.41 (m, 4H), 7.00 (tt, J = 12.6, 6.3 Hz, 4H), 6.83–6.71 (m, 4H), 6.18 (dt, J = 13.0, 6.5 Hz, 4H), 4.63 (dd, J = 18.6, 2.5 Hz, 4H), 2.90–2.82 (m, 8H), 2.72–2.65 (m, 4H), 2.33–2.27 (m, 4H), 1.42 (s, 12H), 1.21 (d, J = 9.6 Hz, 4H), 0.90 (s, 12H).

^{13}C NMR (75 MHz, CD$_2$Cl$_2$) δ 161.3, 160.5, 159.2, 158.7, 145.4, 143.2, 135.5, 134.7, 128.8, 124.1, 123.8, 115.9, 47.6, 40.8, 39.5, 37.9, 32.7, 26.0, 22.3.

CD (MeOH): λ, nm (Δε, M^{-1}cm^{-1}) 436 (−20), 367 (+15), 336 (+76), 289 (−23), 264 (+77), 211 (+143).

ΔΔ-**2$_{Rh}$** : ^{1}H NMR (300 MHz, CD$_2$Cl$_2$) δ 7.72–7.61 (m, 8H), 7.49 (d, J = 8.0 Hz, 4H), 7.02 (td, J = 7.6,

1.1 Hz, 4H), 6.77 (td, J = 7.6, 1.5 Hz, 4H), 6.25 (dt, J = 7.9, 1.1 Hz, 4H), 4.71 (dd, J = 18.6, 3.3 Hz, 4H), 2.90 (t, J = 5.7 Hz, 4H), 2.84–2.68 (m, 8H), 2.35–2.29 (m, 4H), 1.47 (d, J = 9.7 Hz, 4H), 1.41 (s, 12H), 0.70 (s, 12H).

^{13}C NMR (75 MHz, CD$_2$Cl$_2$) δ 161.1, 160.2, 159.5, 159.0, 145.3, 143.3, 135.7, 135.1, 128.6, 124.2, 123.9, 116.0, 47.4, 40.9, 40.2, 37.2, 31.9, 26.2, 21.9.

CD (MeOH): λ, nm ($\Delta\varepsilon$, M^{-1}cm^{-1}) 434 (+24), 367 (−33), 335 (−50), 289 (+23), 264 (−80), 212 (−120).

IR (film): ν (cm^{-1}) 3052, 2922, 1735, 1592, 1574, 1466, 1436, 1420, 1385, 1219, 1123, 1073, 1022, 948, 837, 822, 773, 734, 666, 650, 625, 427.

HRMS (ESI, m/z) calcd for C$_{72}$H$_{72}$Cl$_2$N$_2$Rh$_2$ [M−Cl]$^+$: 1233.3550, found: 1233.3554.

Λ-**IrPP** and Δ-**IrPP**: A suspension of ΛΛ-**2$_{Ir}$** (103.0 mg, 0.07 mmol) and AgPF$_6$ (45.0 mg, 0.18 mmol) in acetonitrile (14.2 mL, 5 mM), or ΔΔ-**2$_{Ir}$** (73.0 mg, 0.05 mmol) and AgPF$_6$ (32.0 mg, 0.13 mmol) in acetonitrile (10.0 mL, 5 mM) was heated at 40 °C overnight under nitrogen in the dark. The reaction mixture was concentrated to dryness and subjected to flash silica gel chromatography (CH$_2$Cl$_2$/CH$_3$CN = 100:1 to 20:1) to give the diastereomeric pure catalyst Λ-**IrPP** (125.0 mg, 0.14 mmol, 96%, R$_f$ = 0.3, CH$_3$CN/CH$_2$Cl$_2$ = 1:20) or Δ-**IrPP** (90.0 mg, 0.10 mmol, 98%, R$_f$ = 0.3, CH$_3$CN/CH$_2$Cl$_2$ = 1:20) as a yellow solid.

Λ-**IrPP**: ^{1}H NMR (300 MHz, CD$_2$Cl$_2$) δ 7.68 (d, J = 8.1 Hz, 2H), 7.56–7.43 (m, 4H), 6.90 (td, J = 7.6, 1.2 Hz, 2H), 6.73 (td, J = 7.5, 1.3 Hz, 2H), 6.16 (dd, J = 7.7, 0.9 Hz, 2H), 3.55 (dd, J = 18.2, 2.7 Hz, 2H), 3.37 (dd, J = 18.2, 3.1 Hz, 2H), 2.96 (t, J = 5.7 Hz, 2H), 2.88–2.74 (m, 2H), 2.56–2.50 (m, 2H), 2.20 (s, 6H), 1.50 (s, 6H), 1.39 (d, J = 9.7 Hz, 2H), 0.80 (s, 6H).

^{13}C NMR (75 MHz, CD$_2$Cl$_2$) δ 166.0, 160.8, 146.2, 143.3, 140.9, 137.0, 132.1, 129.6, 124.0, 123.4, 116.8, 47.6, 41.2, 41.0, 39.2, 31.9, 25.6, 21.3, 3.5.

CD (MeOH): λ, nm ($\Delta\varepsilon$, M^{-1}cm^{-1}) 432 (−9), 334 (+38), 288 (−10), 263 (+39), 211 (+70).

Δ-**IrPP**: ^{1}H NMR (300 MHz, CD$_2$Cl$_2$) δ 7.69 (d, J = 8.1 Hz, 2H), 7.55–7.47 (m, 4H), 6.90 (td, J = 7.6, 1.1 Hz, 2H), 6.70 (td, J = 7.5, 1.3 Hz, 2H), 6.22 (dd, J = 7.7, 0.9 Hz, 2H), 3.64 (dd, J = 18.2, 3.2 Hz, 2H), 3.23 (dd, J = 18.2, 2.6 Hz, 2H), 3.01–2.90 (m, 2H), 2.88–2.77 (m, 2H), 2.54–2.48 (m, 2H), 2.21 (s, 6H), 1.48 (s, 6H), 1.34 (d, J = 9.8 Hz, 2H), 0.86 (s, 6H).

^{13}C NMR (75 MHz, CD$_2$Cl$_2$) δ 165.9, 160.7, 146.3, 143.4, 141.0, 137.1, 132.6, 129.3, 124.0, 123.4, 116.8, 47.7, 41.4, 40.8, 38.9, 32.3, 26.0, 21.8, 3.4.

CD (MeOH): λ, nm (Δε, M^{-1}cm^{-1}) 432 (+12), 334 (−28), 288 (+12), 264 (−43), 211 (−65).

IR (film): v (cm^{-1}) 2927, 1596, 1470, 1440, 1388, 1218, 1190, 1127, 1032, 833, 782, 747, 556.

HRMS (ESI, m/z) calcd for C$_{36}$H$_{36}$IrN$_2$ [M−(CH$_3$CN)$_2$−PF$_6$]$^+$: 689.2508, found: 689.2519.

Λ-RhPP and **Δ-RhPP**: A suspension of ΛΛ-**2$_{Rh}$** (135.0 mg, 0.11 mmol) and AgPF$_6$ (67.0 mg, 0.27 mmol) in acetonitrile (20.5 mL, 5 mM), or ΔΔ-**2$_{Rh}$** (107.0 mg, 0.08 mmol) and AgPF$_6$ (53.0 mg, 0.21 mmol) in acetonitrile (16.8 mL, 5 mM), was heated at 40 °C overnight under nitrogen in the dark. The reaction mixture was concentrated to dryness and subjected to a flash silica gel chromatography (CH$_2$Cl$_2$/CH$_3$CN = 100:1 to 20:1) to give the diastereomeric pure catalyst Λ-**RhPP** (168.0 mg, 0.20 mmol, 96%, R$_f$ = 0.3, CH$_3$CN/CH$_2$Cl$_2$ = 1:20) or Δ-**RhPP** (133.0 mg, 0.16 mmol, 96%, R$_f$ = 0.3, CH$_3$CN/CH$_2$Cl$_2$ = 1:20) as a yellow solid.

Λ-**RhPP**: ^{1}H NMR (300 MHz, CD$_2$Cl$_2$) δ 7.69 (d, J = 8.0 Hz, 2H), 7.56 (d, J = 8.0 Hz, 4H), 6.98 (td, J = 7.5, 1.1 Hz, 2H), 6.79 (td, J = 7.7, 1.4 Hz, 2H), 6.18 (d, J = 7.8 Hz, 2H), 3.56 (dd, J = 18.3, 2.5 Hz, 2H), 3.35 (dd, J = 18.3, 3.0 Hz, 2H), 2.96 (t, J = 5.7 Hz, 2H), 2.89–2.69 (m, 2H), 2.64–2.39 (m, 2H), 2.05 (s, 6H), 1.49 (s, 6H), 1.36 (d, J = 9.7 Hz, 2H), 0.79 (s, 6H).

^{13}C NMR (75 MHz, CD$_2$Cl$_2$) δ 162.5, 159.9, 159.4, 159.0, 145.6, 143.9, 136.7, 133.1, 129.6, 124.2, 124.1, 121.3, 117.0, 47.6, 40.8, 39.9, 39.2, 32.1, 25.7, 21.4, 3.2.

CD (MeOH): λ, nm (Δε, M^{-1}cm^{-1}) 389 (−31), 352 (57), 328 (+43), 305 (−32), 286 (−42), 258 (+73).

Δ-**RhPP**: ^{1}H NMR (300 MHz, CD$_2$Cl$_2$) δ 7.71 (d, J = 8.0 Hz, 2H), 7.66–7.45 (m, 4H), 6.99 (td, J = 7.6, 1.1 Hz, 2H), 6.77 (td, J = 7.7, 1.4 Hz, 2H), 6.25 (d, J = 7.8 Hz, 2H), 3.63 (dd, J = 18.3, 3.1 Hz, 2H), 3.23 (dd, J = 18.3, 2.4 Hz, 2H), 2.96 (t, J = 5.7 Hz, 2H), 2.88–2.76 (m, 2H), 2.51 (dt, J = 9.0, 2.9 Hz, 2H), 2.06 (s, 6H), 1.47 (s, 6H), 1.32 (d, J = 9.8 Hz, 2H), 0.83 (s, 6H).

^{13}C NMR (75 MHz, CD$_2$Cl$_2$) δ 162.3, 159.9, 159.7, 159.2, 145.6, 143.8, 136.7, 133.3, 129.3, 124.3, 124.1, 121.1, 117.1, 47.6, 41.1, 39.8, 39.1, 32.4, 26.0, 21.8, 3.1.

CD (MeOH): λ, nm (Δε, M^{-1}cm^{-1}) 386 (+43), 351 (−50), 328 (−32), 307 (+34), 286 (+37), 258 (−72).

IR (film): v (cm^{-1}) 2937, 1595, 1577, 1471, 1439, 1422, 1219, 1126, 1029, 833, 780, 746, 556, 431.

HRMS (ESI, m/z) calcd for C$_{36}$H$_{36}$RhN$_2$ [M−(CH$_3$CN)$_2$−PF$_6$]$^+$: 599.1934, found: 599.1930.

5.3.2. Synthesis of 2-fluoroacetyl imidazoles

General procedure for the preparation of the 2-trifluoroacetyl imidazoles: 11a was synthesized according to our recently published procedure.[15] **11b−11f** were synthesized according to reported procedures with some modifications.[16] Accordingly, trifluoroacetic anhydride (1.2 eq) was added dropwisely to a stirred solution of imidazole in toluene (0.1 M referring to the imidazole) at −20 ℃ over 20 min, and then Et$_3$N (1.2 eq) was added slowly. After stirring for 6–8 h, the resulting mixture was slowly warmed to room temperature and stirred overnight. After removal of the solvent *in vacuo*, the residue was purified by flash chromatography on silica gel (EtOAc/*n*-hexane = 1:10 to 1:5).

2,2,2-Trifluoro-1-(1-isopropyl-1*H*-imidazol-2-yl)ethanone (11b)
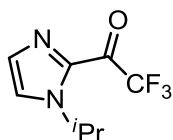
Following the general procedure, 1-isopropyl-1*H*-imidazole (1.102 g, 10.0 mmol) was converted to **11b** (1.630 g, 7.9 mmol, yield: 79%, R$_f$ = 0.5, EtOAc/*n*-hexane = 2:1) as a colorless oil.

^{1}H NMR (300 MHz, CDCl$_3$) δ 7.43 (d, *J* = 0.5 Hz, 1H), 7.40–7.30 (m, 1H), 5.36 (hept, *J* = 6.6 Hz, 1H), 1.45 (dd, *J* = 6.7, 3.2 Hz, 6H).

^{13}C NMR (75 MHz, CDCl$_3$) δ 170.5 (q, *J* = 35 Hz), 137.3, 132.4, 124.0, 116.5 (q, *J* = 287.5 Hz), 50.2, 23.2.

^{19}F NMR (282 MHz, CDCl$_3$) δ −72.1 (s, 3F).

IR (film): v (cm^{-1}) 3117, 2986, 1694, 1463, 1402, 1343, 1260, 1196, 1149, 1091, 942, 901, 837, 785, 738, 682, 654, 612, 552, 522.

HRMS (EI, *m/z*) calcd for C$_8$H$_9$F$_3$N$_2$O [M]$^+$: 206.0667, found: 206.0660.

2,2,2-Trifluoro-1-(1-methyl-1*H*-imidazol-2-yl)ethanone (11c)
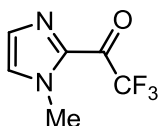
Following the general procedure, 1-methyl-1*H*-imidazole (0.821 g, 10.0 mmol) was converted to **11c** (1.478 g, 8.3 mmol, yield: 83%, R$_f$ = 0.55, EtOAc/*n*-hexane = 2:1) as a white solid.

^{1}H NMR (300 MHz, CDCl$_3$) δ 7.37 (d, *J* = 0.9 Hz, 1H), 7.23 (d, *J* = 0.9 Hz, 1H), 4.07 (s, 3H).

^{13}C NMR (75 MHz, CDCl$_3$) δ 138.2, 132.0, 129.2, 118.3, 114.4, 36.3.

All spectroscopic data are in agreement with the literature.[16]

2,2,2-Trifluoro-1-(1-methyl-1*H*-benzo[d]imidazol-2-yl)ethanone (11d)
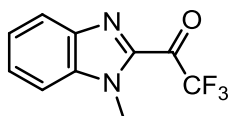
Following the general procedure, 1-methyl-1*H*-benzoimidazol (0.661 g, 5.0 mmol) was converted to 2-acyl imidazole **11d** (1.034 g, 4.5 mmol, yield: 90%, R$_f$ = 0.3, EtOAc/*n*-hexane = 2:1) as a white solid.

^{1}H NMR (300 MHz, CDCl$_3$) δ 7.99 (d, *J* = 8.3 Hz, 1H), 7.65–7.31 (m, 3H), 4.17 (s, 3H).

^{13}C NMR (75 MHz, CDCl$_3$) δ 174.1 (q, *J* = 35 Hz), 142.6, 140.9, 137.2, 128.2, 125.01, 121.4 (q, *J* = 155 Hz), 118.3, 114.5, 110.8, 32.5.

^{19}F NMR (282 MHz, None) δ –72.8 (s, 3F).

IR (film): *v* (cm^{-1}) 3538, 1719, 1478, 1457, 1194, 1173, 1150, 1117, 1077, 1011, 950, 912, 750, 737, 633, 551, 536, 448, 402.

HRMS (APCI, *m/z*) calcd for C$_{10}$H$_7$F$_3$N$_2$OH [M+H]$^+$: 229.0583, found: 229.0582.

2,2,2-Trifluoro-1-(1-(4-methoxyphenyl)-1*H*-imidazol-2-yl)ethanone (11e)
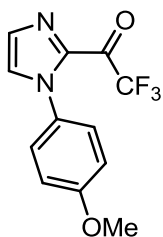
Following the general procedure, 1-(4-methoxyphenyl)-1*H*-imidazole (1.742 g, 10.0 mmol) was converted to 2-acyl imidazole **11e** (0.811 g, 3.0 mmol, yield: 30%, R$_f$ = 0.5, EtOAc/*n*-hexane = 2:1) as a white solid.

^{1}H NMR (300 MHz, CDCl$_3$) δ 7.47 (d, *J* = 0.9 Hz, 1H), 7.33 (d, *J* = 0.9 Hz, 1H), 7.25–7.18 (m, 2H), 7.01–6.94 (m, 2H), 3.87 (s, 3H).

^{13}C NMR (75 MHz, CDCl$_3$) δ 160.3, 138.0, 132.2, 129.7, 129.5, 126.8, 123.8, 118.2, 114.4, 55.6.

^{19}F NMR (282 MHz, None) δ –73.4 (s, 3F).

IR (film): *v* (cm^{-1}) 3208, 3154, 2942, 2841, 1699, 1605, 1510, 1456, 1355, 1252, 1134, 1073, 933, 828,

777, 633, 538.

HRMS (APCI, *m/z*) calcd for $C_{12}H_9F_3N_2O_2H$ [M+H]$^+$: 271.0689, found: 271.0688.

2,2,3,3,3-Pentafluoro-1-(1-phenyl-1*H*-imidazol-2-yl)propan-1-one (11f)
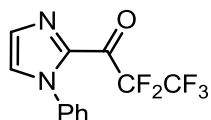
Following the general procedure, using perfluoropropionic acid anhydride instead, 1-(4-methoxyphenyl)-1*H*-imidazole (1.441 g, 10.0 mmol) was converted to 2-acyl imidazole **11f** (1.587 g, 5.5 mmol, yield: 55%, R_f = 0.3, EtOAc/*n*-hexane = 2:1) as a white solid.

^{1}H NMR (300 MHz, CDCl$_3$) δ 7.49–7.36 (m, 4H), 7.28 (s, 1H), 7.26–7.15 (m, 2H).

^{13}C NMR (75 MHz, CDCl$_3$) δ 172.1, 138.5, 137.1, 132.3, 129.6, 129.4, 125.7, 120.0, 116.2, 112.1, 108.3, 104.8.

^{19}F NMR (282 MHz, None) δ –81.0 (s, 3F), –116.7 (s, 2F).

IR (film): v (cm^{-1}) 3099, 1692, 1591, 1497, 1453, 1402, 1349, 1306, 1204, 1141, 1091, 994, 920, 826, 757, 682, 531, 424.

HRMS (APCI, *m/z*) calcd for $C_{12}H_7F_5N_2OH$ [M+H]$^+$: 291.0551, found: 291.0549.

5.3.3. Rhodium-catalyzed alkynylation reactions
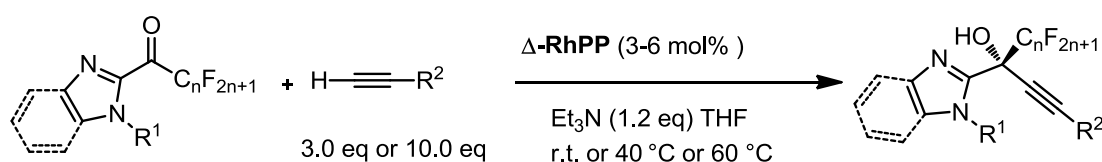
General catalytic procedure: A dried 10 mL Schlenk tube was charged with the catalyst Δ-**RhPP** (3–6 mol%) and the corresponding trifluoromethyl ketones (0.20 mmol, 1.0 eq). The tube was purged with nitrogen and THF (0.2 mL), and then Et$_3$N (33.27 μL, 1.2 eq) was added via syringe, followed by the corresponding alkynes (3.0 eq or 10.0 eq). The tube was sealed and the reaction was stirred at the indicated temperature for the indicated time (monitored by TLC) under nitrogen atmosphere. Afterwards, the solvent was removed under reduced pressure. The residue was purified by flash chromatography on silica gel (EtOAc/hexane = 1:10 to 1:5) to afford the products **20a-y**. Racemic samples were obtained by carrying out the reactions with *rac*-**RhPP**. The enantiomeric excess was determined by chiral HPLC analysis.

(*R*)-1,1,1-Trifluoro-4-phenyl-2-(1-phenyl-1*H*-imidazol-2-yl)but-3-yn-2-ol (20a)
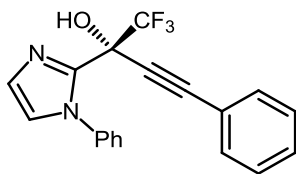
Starting from trifluoromethyl ketone **11a** (48.0 mg, 0.20 mmol) and phenylacetylene (61.3 mg, 0.60 mmol) according to the general procedure to give **20a** as a white solid (61.0 mg, 0.178 mmol, yield: 89%, R_f = 0.5, EtOAc/*n*-hexane = 1:2). Enantiomeric excess was established by HPLC analysis using a Chiralpak AD-H column, *ee* = 95% (HPLC: AD-H, 254 nm, hexane/isopropanol = 90:10, flow rate 1.0 mL/min, 25 °C, t_r (major) = 8.8 min, t_r (minor) = 25.2 min). $[\alpha]_D^{25}$ = +102.3° (*c* 0.7, CH$_2$Cl$_2$).

^{1}H NMR (300 MHz, CD$_3$OD) δ 7.58–7.38 (m, 5H), 7.37–7.20 (m, 6H), 7.14–7.08 (m, 1H).

^{13}C NMR (75 MHz, CD$_3$OD) δ 142.9, 139.8, 132.8, 130.5, 130.0, 129.7, 129.4, 128.7, 127.9, 126.6, 122.8, 122.3, 89.4, 83.7, 71.0 (q, *J* = 33.0 Hz).

^{19}F NMR (282 MHz, CD$_3$OD) δ −78.56 (s, 3F).

IR (film): *v* (cm^{-1}) 2291, 1595, 1497, 1467, 1418, 1259, 1202, 1172, 1133, 1125, 1071, 1043, 1027, 994, 936, 903, 785, 761, 746, 722, 689, 584, 562, 538, 529, 502.

HRMS (ESI, *m/z*) calcd for C$_{19}$H$_{14}$F$_3$N$_2$O [M+H]$^+$: 343.1053, found: 343.1058.

(*R*)-1,1,1-Trifluoro-2-(1-isopropyl-1*H*-imidazol-2-yl)-4-phenylbut-3-yn-2-ol (20b)
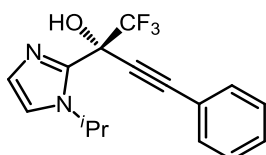
Starting from trifluoromethyl ketone **11b** (41.2 mg, 0.20 mmol) and phenylacetylene (61.3 mg, 0.60 mmol) according to the general procedure to give **20b** as a white solid (58.2 mg, 0.189 mmol, yield: 94%, R_f = 0.5, EtOAc/*n*-hexane = 1:2). Enantiomeric excess established by HPLC analysis using a Chiralpak AD-H column, *ee* = 97% (HPLC: AD-H, 254 nm, hexane/isopropanol = 90:10, flow rate 1.0 mL/min, 25 °C, t_r (minor) = 6.6 min, t_r (major) = 10.1 min). $[\alpha]_D^{25}$ = +41.2° (*c* 0.6, CH$_2$Cl$_2$).

^{1}H NMR (300 MHz, CD$_3$OD) δ 7.62–7.49 (m, 2H), 7.47–7.31 (m, 4H), 6.99 (d, *J* = 1.0 Hz, 1H), 5.46–5.29 (m, 1H), 1.46 (d, *J* = 6.7 Hz, 6H).

^{13}C NMR (75 MHz, CD$_3$OD) δ 141.5, 132.9, 130.6, 129.7, 128.3, 124.7 (q, *J* = 284.0 Hz), 122.4, 120.0, 88.6, 84.0, 71.6 (q, J = 33.8 Hz), 50.3, 24.0, 23.7.

^{19}F NMR (282 MHz, CD$_3$OD) δ –79.04 (s, 3F).

IR (film): v (cm^{-1}) 2981, 2254, 1493, 1467, 1248, 1185, 1170, 1125, 1109, 1017, 941, 908, 789, 752, 705, 692, 650, 640, 628, 580, 554, 529, 456, 425.

HRMS (ESI, m/z) calcd for C$_{16}$H$_{16}$F$_3$N$_2$O [M+H]$^+$: 309.1209, found: 309.1214.

(*R*)-1,1,1-Trifluoro-2-(1-methyl-1*H*-imidazol-2-yl)-4-phenylbut-3-yn-2-ol (20c)
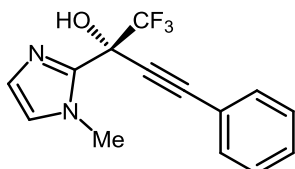
Starting from trifluoromethyl ketone **11c** (35.6 mg, 0.20 mmol) and phenylacetylene (61.3 mg, 0.60 mmol) according to the general procedure to give **20c** as a white solid (51.4 mg, 0.18 mmol, yield: 92%, R$_f$ = 0.5, EtOAc/*n*-hexane = 1:2). Enantiomeric excess established by HPLC analysis using a Chiralpak AD-H column, *ee* = 99.6% (HPLC: AD-H, 254 nm, hexane/isopropanol = 90:10, flow rate 1.0 mL/min, 25 °C, t$_r$ (minor) = 7.1 min, t$_r$ (major) = 9.2 min). [α]$_D^{25}$ = +42.5° (*c* 0.6, CH$_2$Cl$_2$).

^{1}H NMR (300 MHz, CD$_3$OD) δ 7.62–7.49 (m, 2H), 7.47–7.29 (m, 3H), 7.13 (d, *J* = 1.2 Hz, 1H), 6.96 (d, *J* = 1.2 Hz, 1H), 3.94 (s, 3H).

^{13}C NMR (75 MHz, CD$_3$OD) δ 142.1, 133.0, 130.6, 129.6, 127.6, 125.9, 124.8 (q, *J* = 284.3 Hz), 122.5, 88.7, 83.8, 71.9 (q, *J* = 33.8 Hz), 35.7.

^{19}F NMR (282 MHz, CD$_3$OD) δ –80.99 (s, 3F).

IR (film): v (cm^{-1}) 2233, 1482, 1402, 1284, 1242, 1209, 1192, 1172, 1157, 1120, 1106, 1034, 1018, 999, 942, 912, 788, 756, 709, 683, 616, 582, 531, 551, 421, 398.

HRMS (ESI, m/z) calcd for C$_{14}$H$_{12}$F$_3$N$_2$O [M+H]$^+$: 281.0902, found: 281.0899.

(*R*)-1,1,1-Trifluoro-2-(1-methyl-1*H*-imidazol-2-yl)-4-(*p*-tolyl)but-3-yn-2-ol (20d)
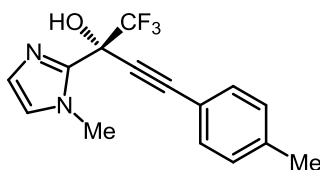
Starting from trifluoromethyl ketone **11c** (35.6 mg, 0.20 mmol) and 1-ethynyl-4-methylbenzene (69.7 mg, 0.60 mmol) according to the general procedure to give **20d** as a white solid (55.6 mg, 0.189 mmol,

yield: 95%, R_f = 0.5, EtOAc/n-hexane = 1:2). Enantiomeric excess established by HPLC analysis using a Chiralpak AD-H column, ee = 99.4% (HPLC: AD-H, 254 nm, hexane/isopropanol = 90:10, flow rate 1.0 mL/min, 25 °C, t_r (minor) = 8.9 min, t_r (major) = 13.3 min). $[\alpha]_D^{25}$ = +32.7° (c 0.4, CH$_2$Cl$_2$).

^{1}H NMR (300 MHz, CD$_3$OD) δ 7.43 (d, J = 13.3 Hz, 2H), 7.18 (d, J = 7.9 Hz, 2H), 7.12 (d, J = 1.2 Hz, 1H), 7.02–6.89 (m, 1H), 3.93 (s, 3H), 2.34 (s, 3H).

^{13}C NMR (75 MHz, CD$_3$OD) δ 142.2, 141.2, 132.9, 130.3, 127.6, 125.9, 124.9 (q, J = 284.0 Hz) 119.4, 89.0, 83.1, 71.9 (q, J = 33.0 Hz), 35.7, 21.5.

^{19}F NMR (282 MHz, CD$_3$OD) δ –79.43 (s, 3F).

IR (film): v (cm^{-1}) 2240, 1512, 1482, 1411, 1278, 1244, 1190, 1173, 1150, 1103, 1057, 1027, 1019, 942, 912, 820, 759, 702, 676, 612, 551, 532, 523, 504, 453, 427, 411.

HRMS (ESI, m/z) calcd for C$_{15}$H$_{14}$F$_3$N$_2$O [M+H]$^+$: 295.1053, found: 295.1057.

(R)-1,1,1-Trifluoro-2-(1-methyl-1H-imidazol-2-yl)-4-(m-tolyl)but-3-yn-2-ol (20e)
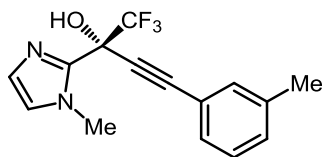
Starting from trifluoromethyl ketone **11c** (35.6 mg, 0.20 mmol) and 1-ethynyl-3-methylbenzene (69.7 mg, 0.60 mmol) according to the general procedure to give **20e** as a white solid (55.8 mg, 0.190 mmol, yield: 95%, R_f = 0.5, EtOAc/n-hexane = 1:2). Enantiomeric excess established by HPLC analysis using a Chiralpak AD-H column, ee > 99% (HPLC: AD-H, 254 nm, hexane/isopropanol = 90:10, flow rate 1.0 mL/min, 25 °C, t_r = 29.0 min). $[\alpha]_D^{25}$ = +43.1° (c 0.6, CH$_2$Cl$_2$).

^{1}H NMR (300 MHz, CD$_3$OD) δ 7.45–7.30 (m, 2H), 7.30–7.18 (m, 2H), 7.13 (d, J = 1.1 Hz, 1H), 6.95 (d, J = 1.0 Hz, 1H), 3.94 (s, 3H), 2.32 (s, 3H).

^{13}C NMR (75 MHz, CD$_3$OD) δ 142.2, 139.6, 133.4, 131.4, 130.1, 129.5, 127.6, 125.9, 124.8 (q, J = 283.8 Hz), 122.3, 89.0, 83.4, 71.9 (q, J = 33.0 Hz), 35.6, 21.2.

^{19}F NMR (282 MHz, CD$_3$OD) δ –79.81 (s, 3F).

IR (film): v (cm^{-1}) 2234, 1485, 1247, 1172, 1149, 1105, 1034, 943, 915, 894, 796, 765, 691, 682, 635, 426.

HRMS (ESI, m/z) calcd for C$_{15}$H$_{14}$F$_3$N$_2$O [M+H]$^+$: 295.1053, found: 295.1057.

(R)-1,1,1-Trifluoro-2-(1-methyl-1H-imidazol-2-yl)-4-(o-tolyl)but-3-yn-2-ol (20f)
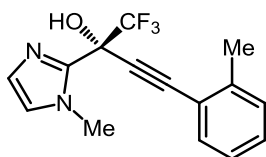
Starting from trifluoromethyl ketone **11c** (35.6 mg, 0.20 mmol) and 1-ethynyl-2-methylbenzene (69.7 mg, 0.60 mmol) according to the general procedure to give **20f** as a white solid (57.5 mg, 0.196 mmol, yield: 98%, R_f = 0.5, EtOAc/n-hexane = 1:2). Enantiomeric excess established by HPLC analysis using a Chiralpak AD-H column, ee = 99.4% (HPLC: AD-H, 254 nm, hexane/isopropanol = 90:10, flow rate 1.0 mL/min, 25 °C, t_r (minor) = 10.5 min, t_r (major) = 12.3 min). $[\alpha]_D^{25}$ = +45.9° (c 0.7, CH$_2$Cl$_2$).

^{1}H NMR (300 MHz, CD$_3$OD) δ 7.57–7.41 (m, 1H), 7.34–7.15 (m, 3H), 7.12 (d, J = 1.2 Hz, 1H), 6.95 (d, J = 1.2 Hz, 1H), 3.95 (s, 3H), 2.43 (s, 3H).

^{13}C NMR (75 MHz, CD$_3$OD) δ 142.2, 142.1, 133.2, 130.7, 130.6, 127.6, 126.8, 125.8, 123.0, 122.1, 119.2, 87.8, 87.7, 71.9 (q, J = 33.0 Hz), 35.6, 20.6.

^{19}F NMR (282 MHz, CD$_3$OD) δ −79.63 (s, 3F).

IR (film): v (cm^{-1}) 2924, 2853, 2229, 1535, 1415, 1301, 1285, 1245, 1216, 1193, 1168, 1154, 1121, 1088, 1012, 887, 861, 826, 794, 766, 749, 711, 682, 638, 611, 569, 548, 494, 430, 389.   HRMS (ESI, m/z) calcd for C$_{15}$H$_{13}$F$_3$N$_2$ONa [M+Na]$^+$: 317.0883, found: 317.0872.

(R)-4-(4-(tert-Butyl)phenyl)-1,1,1-trifluoro-2-(1-methyl-1H-imidazol-2-yl)but-3-yn-2-ol (20g)
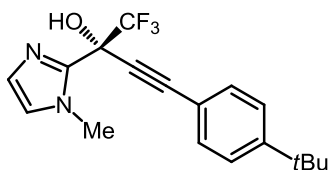
Starting from trifluoromethyl ketone **11c** (35.6 mg, 0.20 mmol) and 1-(tert-butyl)-4-ethynylbenzene (94.9 mg, 0.60 mmol) according to the general procedure to give **20g** as a white solid (67.1 mg, 0.199 mmol, yield: 99%, R_f = 0.6, EtOAc/n-hexane = 1:2). Enantiomeric excess established by HPLC analysis using a Chiralpak AD-H column, ee > 99% (HPLC: AD-H, 254 nm, hexane/isopropanol = 90:10, flow rate 1.0 mL/min, 25 °C, t_r = 12.4 min). $[\alpha]_D^{25}$ = +32.1° (c 0.8, CH$_2$Cl$_2$).

^{1}H NMR (300 MHz, CD$_3$OD) δ 7.54–7.44 (m, 2H), 7.44–7.37 (m, 2H), 7.12 (d, J = 1.1 Hz, 1H), 6.95

(d, J = 1.0 Hz, 1H), 3.94 (s, 3H), 1.30 (s, 9H).

^{13}C NMR (75 MHz, CD$_3$OD) δ 154.2, 142.3, 132.8, 127.5, 126.6, 125.9, 123.0, 119.5, 88.9, 83.2, 71.8 (q, J = 33.0 Hz), 35.70, 35.66, 31.50.

^{19}F NMR (282 MHz, CD$_3$OD) δ –79.38 (s, 3F).

IR (film): v (cm^{-1}) 2963, 2235, 1506, 1478, 1391, 1253, 1185, 1170, 1118, 1104, 1052, 1024, 942, 909, 833, 751, 713, 688, 657, 615, 563, 530, 513.

HRMS (ESI, m/z) calcd for C$_{18}$H$_{20}$F$_3$N$_2$O [M+H]$^+$: 337.1533, found: 337.1523.

(*R*)-4-([1,1'-Biphenyl]-4-yl)-1,1,1-trifluoro-2-(1-methyl-1*H*-imidazol-2-yl)but-3-yn-2-ol (20h)
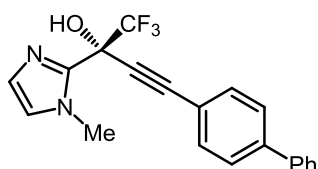
Starting from trifluoromethyl ketone **11c** (35.6 mg, 0.20 mmol) and 4-ethynyl-1,1'-biphenyl (106.4 mg, 0.60 mmol) according to the general procedure to give **20h** as a white solid (66.5 mg, 0.187 mmol, yield: 93%, R$_f$ = 0.5, EtOAc/n-hexane = 1:2). Enantiomeric excess established by HPLC analysis using a Chiralpak AD-H column, *ee* = 99% (HPLC: AD-H, 254 nm, hexane/isopropanol = 90:10, flow rate 1.0 mL/min, 25 °C, t$_r$ (minor) = 13.3 min, t$_r$ (major) = 22.6 min). [α]$_D^{25}$ = +20.4° (*c* 0.8, CH$_2$Cl$_2$).

^{1}H NMR (300 MHz, CD$_3$OD) δ 7.65–7.54 (m, 6H), 7.50–7.37 (m, 2H), 7.36–7.27 (m, 1H), 7.12 (d, J = 1.2 Hz, 1H), 7.01–6.92 (m, 1H), 3.94 (s, 3H).

^{13}C NMR (75 MHz, CD$_3$OD) δ 143.5, 142.1, 141.2, 133.5, 130.0, 129.0, 128.1, 127.9, 127.6, 126.7, 126.0, 123.0, 121.3, 88.6, 84.4, 72.2, 71.8, 72.0 (q, J = 31.0 Hz), 35.7.

^{19}F NMR (282 MHz, CD$_3$OD) δ –80.26 (s, 3F).

IR (film): v (cm^{-1}) 2924, 2233, 1448, 1290, 1251, 1173, 1087, 1029, 1014, 944, 912, 838, 757, 692, 618, 559, 517, 504, 458.

HRMS (ESI, m/z) calcd for C$_{20}$H$_{16}$F$_3$N$_2$O [M+H]$^+$: 357.1209, found: 357.1214.

(*R*)-1,1,1-Trifluoro-4-(4-methoxyphenyl)-2-(1-methyl-1*H*-imidazol-2-yl)but-3-yn-2-ol (20i)
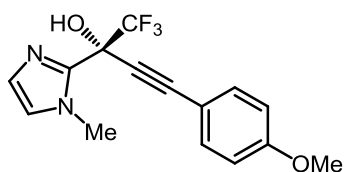
Starting from trifluoromethyl ketone **11c** (35.6 mg, 0.20 mmol) and 1-ethynyl-4-methoxybenzene (79.6 mg, 0.60 mmol) according to the general procedure to give **20i** as a white solid (59.3 mg, 0.191 mmol, yield: 96%, R_f = 0.5, EtOAc/*n*-hexane = 1:2). Enantiomeric excess established by HPLC analysis using a Chiralpak AD-H column, *ee* = 99.4% (HPLC: AD-H, 254 nm, hexane/isopropanol = 90:10, flow rate 1.0 mL/min, 25 °C, t_r (minor) = 13.1 min, t_r (major) = 18.6 min). $[\alpha]_D^{25}$ = +34.9° (*c* 0.6, CH$_2$Cl$_2$).

^{1}H NMR (300 MHz, CD$_3$OD) δ 7.57–7.40 (m, 2H), 7.12 (d, *J* = 1.2 Hz, 1H), 7.03–6.87 (m, 3H), 3.94 (s, 3H), 3.80 (s, 3H).

^{13}C NMR (75 MHz, CD$_3$OD) δ 162.2, 142.3, 134.6, 127.5, 125.9, 124.9 (q, *J* = 284.3 Hz), 115.2, 114.4, 89.0, 82.4, 71.8 (q, *J* = 33.0 Hz), 55.9, 35.6.

^{19}F NMR (282 MHz, CD$_3$OD) δ −79.46 (s, 3F).

IR (film): *v* (cm^{-1}) 2969, 2941, 2844, 2233, 1606, 1568, 1512, 1480, 1462, 1446, 1407, 1296, 1253, 1211, 1192, 1181, 1157, 1120, 1075, 1051, 993, 967, 943, 887, 837, 819, 760, 748, 737, 677, 611, 564, 501, 457, 421.

HRMS (ESI, *m/z*) calcd for C$_{15}$H$_{14}$F$_3$N$_2$O$_2$ [M+H]$^+$: 311.1013, found: 311.1004.

(*R*)-1,1,1-Trifluoro-2-(1-methyl-1*H*-benzo[d]imidazol-2-yl)-4-phenylbut-3-yn-2-ol (20j)
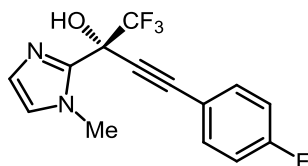
Starting from trifluoromethyl ketone **11c** (35.6 mg, 0.20 mmol) and 1-ethynyl-4-fluorobenzene (61.3 mg, 0.60 mmol) according to the general procedure to give **20j** as a white solid (47.0 mg, 0.157 mmol, yield: 79%, R_f = 0.5, EtOAc/*n*-hexane = 1:2). Enantiomeric excess established by HPLC analysis using a Chiralpak AD-H column, *ee* > 99% (HPLC: AD-H, 254 nm, hexane/isopropanol = 90:10, flow rate 1.0 mL/min, 25 °C, t_r = 11.4 min). $[\alpha]_D^{25}$ = +42.6° (*c* 0.4, CH$_2$Cl$_2$).

^{1}H NMR (300 MHz, CD$_3$OD) δ 7.71–7.51 (m, 2H), 7.21–7.05 (m, 3H), 6.96 (d, J = 1.2 Hz, 1H), 3.94 (s, 3H).

^{13}C NMR (75 MHz, CD$_3$OD) δ 166.3, 163.0, 142.0, 135.4, 135.3, 127.6, 126.0, 124.8 (q, J = 282.8 Hz), 118.8, 117.0, 116.7, 87.6, 83.7, 72.0 (q, J = 33.0 Hz), 35.7.

^{19}F NMR (282 MHz, CD$_3$OD) δ –81.04 (s, 3F), –112.13 (s, 1F).

IR (film): v (cm^{-1}) 2227, 1600, 1509, 1227, 1213, 1188, 1177, 1140, 1081, 1016, 947, 916, 840, 769, 754, 711, 677, 613, 535, 503, 478, 466, 392.

HRMS (ESI, m/z) calcd for C$_{14}$H$_{11}$F$_3$N$_2$O [M+H]$^+$: 299.0802, found: 299.0805.

(*R*)-4-(4-Chlorophenyl)-1,1,1-trifluoro-2-(1-methyl-1*H*-imidazol-2-yl)but-3-yn-2-ol (20k)
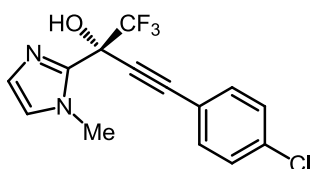
Starting from trifluoromethyl ketone **11c** (35.6 mg, 0.20 mmol) and 1-chloro-4-ethynylbenzene (61.3 mg, 0.60 mmol) according to the general procedure to give **20k** as a white solid (60.8 mg, 0.194 mmol, yield: 97%, R$_f$ = 0.5, EtOAc/*n*-hexane = 1:2). Enantiomeric excess established by HPLC analysis using a Chiralpak AD-H column, ee = 99.0% (HPLC: AD-H, 254 nm, hexane/isopropanol = 90:10, flow rate 1.0 mL/min, 25 °C, t$_r$ (minor) = 8.5 min, t$_r$ (major) = 13.1 min). [α]$_D^{25}$ = +30.4° (*c* 0.6, CH$_2$Cl$_2$).

^{1}H NMR (300 MHz, CD$_3$OD) δ 7.62–7.48 (m, 2H), 7.48–7.34 (m, 2H), 7.13 (d, J = 1.2 Hz, 1H), 6.96 (d, J = 1.0 Hz, 1H), 3.93 (s, 3H).

^{13}C NMR (75 MHz, CD$_3$OD) δ 141.9, 136.7, 134.5, 129.9, 127.7, 126.0, 124.8 (q, J = 284.0 Hz), 121.2, 87.4, 84.9, 72.1 (q, J = 33.0 Hz), 35.7.

^{19}F NMR (282 MHz, CD$_3$OD) δ –80.14 (s, 3F).

IR (film): v (cm^{-1}) 2235, 1592, 1491, 1480, 1400, 1291, 1246, 1194, 1107, 1089, 1017, 986, 916, 895, 831, 793, 762, 716, 687, 648, 607, 581, 530, 469, 438, 424.

HRMS (ESI, m/z) calcd for C$_{14}$H$_{11}$ClF$_3$N$_2$O [M+H]$^+$: 315.0507, found: 315.0509.

(*R*)-4-(4-Bromophenyl)-1,1,1-trifluoro-2-(1-methyl-1*H*-imidazol-2-yl)but-3-yn-2-ol (20l)
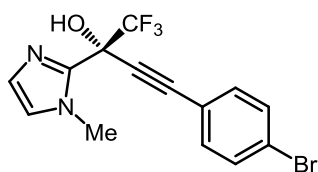
Starting from trifluoromethyl ketone **11c** (35.6 mg, 0.20 mmol) and 1-bromo-4-ethynylbenzene (61.3 mg, 0.60 mmol) according to the general procedure to give **20l** as a white solid (70.0 mg, 0.195 mmol, yield: 97%, R_f = 0.5, EtOAc/*n*-hexane = 1:2). Enantiomeric excess established by HPLC analysis using a Chiralpak AD-H column, *ee* = 99% (HPLC: AD-H, 254 nm, hexane/isopropanol = 90:10, flow rate 1.0 mL/min, 25 °C, t_r (minor) = 9.0 min, t_r (major) = 15.0 min). $[\alpha]_D^{25}$ = +30.3° (*c* 0.8, CH$_2$Cl$_2$).

^{1}H NMR (300 MHz, CD$_3$OD) δ 7.61–7.51 (m, 2H), 7.47 (d, *J* = 8.5 Hz, 2H), 7.14 (d, *J* = 1.1 Hz, 1H), 7.01–6.91 (m, 1H), 3.93 (s, 3H).

^{13}C NMR (75 MHz, CD$_3$OD) δ 141.9, 134.6, 132.9, 127.7, 126.0, 124.8, 124.7 (q, *J* = 284.3 Hz), 121.6, 87.5, 85.0, 72.1 (q, *J* = 33.8 Hz), 35.7.

^{19}F NMR (282 MHz, CD$_3$OD) δ –79.47 (s, 3F).

IR (film): v (cm^{-1}) 3120, 2805, 2244, 1486, 1243, 1188, 1175, 1151, 1103, 1072, 1023, 942, 912, 836, 822, 794, 757, 681, 622, 526, 460, 417.

HRMS (ESI, *m/z*) calcd for C$_{14}$H$_{11}$BrF$_3$N$_2$O [M+H]$^+$: 359.0012, found: 359.0002.

(*R*)-1,1,1-Trifluoro-4-(2-fluorophenyl)-2-(1-methyl-1*H*-imidazol-2-yl)but-3-yn-2-ol (20m)
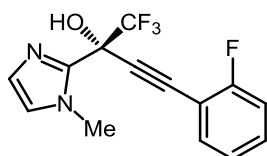
Starting from trifluoromethyl ketone **11c** (35.6 mg, 0.20 mmol) and 1-ethynyl-2-fluorobenzene (72.1 mg, 0.60 mmol) according to the general procedure to give **20m** as a white solid (59.2 mg, 0.199 mmol, yield: 99%, R_f = 0.5, EtOAc/*n*-hexane = 1:2). Enantiomeric excess established by HPLC analysis using a Chiralpak AD-H column, *ee* = 97% (HPLC: AD-H, 254 nm, hexane/isopropanol = 98:2, flow rate 1.0 mL/min, 25 °C, t_r (minor) = 7.6 min, t_r (major) = 8.7 min). $[\alpha]_D^{25}$ = +34.5° (*c* 0.5, CH$_2$Cl$_2$).

^{1}H NMR (300 MHz, CD$_3$OD) δ 7.63–7.52 (m, 1H), 7.50–7.39 (m, 1H), 7.20–7.10 (m, 3H), 6.95 (d, *J* = 1.0 Hz, 1H), 3.95 (s, 3H).

^{13}C NMR (75 MHz, CD$_3$OD) δ 164.6, 161.3, 140.5, 133.5, 131.4, 131.3, 126.2, 124.5, 124.1, 123.8 (q, J = 284.0 Hz), 115.4, 115.1, 109.6, 109.3, 87.4, 80.9, 70.4 (q, J = 33.8 Hz), 34.2. ^{19}F NMR (282 MHz, CD$_3$OD) δ −80.07 (s, 3F), −111.56 (s, 1F).

IR (film): v (cm^{-1}) 2240, 1574, 1492, 1450, 1284, 1249, 1226, 1176, 1091, 1060, 1011, 916, 891, 837, 763, 707, 683, 636, 614, 579, 532, 503, 479, 436, 408.

HRMS (ESI, m/z) calcd for C$_{14}$H$_{11}$N$_2$O [M+H]$^+$: 299.0802, found: 299.0806.

(*R*)-4-(3,5-Bis(trifluoromethyl)phenyl)-1,1,1-trifluoro-2-(1-methyl-1*H*-imidazol-2-yl)but-3-yn-2-ol (20n)
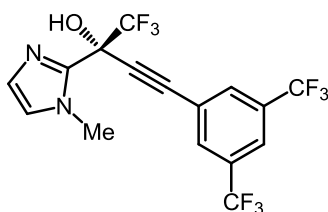
Starting from trifluoromethyl ketone **11c** (35.6 mg, 0.20 mmol) and 1-ethynyl-3,5-bis(trifluoromethyl)benzene (142.9 mg, 0.60 mmol) according to the general procedure to give **20n** as a white solid (82.8 mg, 0.199 mmol, yield: 99%, R$_f$ = 0.5, EtOAc/*n*-hexane = 1:2). Enantiomeric excess established by HPLC analysis using a Chiralpak AD-H column, *ee* > 99% (HPLC: AD-H, 254 nm, hexane/isopropanol = 98:2, flow rate 1.0 mL/min, 25 °C, t$_r$ = 10.4 min). [α]$_D^{25}$ = −4.8° (*c* 0.7, CH$_2$Cl$_2$).

^{1}H NMR (300 MHz, CD$_3$OD) δ 8.23–8.15 (m, 2H), 8.04 (d, J = 13.6 Hz, 1H), 7.15 (d, J = 1.1 Hz, 1H), 6.99 (d, J = 1.2 Hz, 1H), 3.94 (s, 3H).

^{13}C NMR (75 MHz, CD$_3$OD) δ 141.5, 133.4 (m), 127.9, 126.4, 125.3, 124.7 (q, J = 284.5 Hz), 124.3 (q, J = 270.5 Hz), 123.9 (m), 87.5, 85.2, 72.6 (q, J = 33.5 Hz), 35.8.

^{19}F NMR (282 MHz, CD$_3$OD) δ −64.4 (s, 6F), −80.0 (s, 3F).

IR (film): v (cm^{-1}) 2925, 2236, 1593, 1577, 1463, 1437, 1380, 1277, 1176, 1132, 1105, 1054, 1030, 945, 918, 898, 775, 740, 700, 683, 616, 589, 438, 422, 404, 394.

HRMS (ESI, m/z) calcd for C$_{16}$H$_{10}$F$_9$N$_2$O [M+H]$^+$: 417.0655, found: 417.0648.

(R)-1,1,1-Trifluoro-2-(1-methyl-1H-imidazol-2-yl)-4-(pyridin-2-yl)but-3-yn-2-ol (20o)
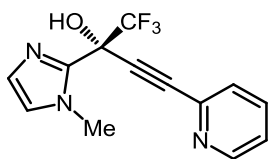
Starting from trifluoromethyl ketone **11c** (35.6 mg, 0.20 mmol) and 2-ethynylpyridine (61.9 mg, 0.60 mmol) according to the general procedure to give **20o** as a yellow oil (46.3 mg, 0.165 mmol, yield: 82%, R_f = 0.5, EtOAc/n-hexane = 1:2). Enantiomeric excess established by HPLC analysis using a Chiralpak AD-H column, ee > 99% (HPLC: AD-H, 254 nm, hexane/isopropanol = 90:10, flow rate 1.0 mL/min, 25 °C, t_r = 5.6 min). $[\alpha]_D^{25}$ = +37.4° (c 0.6, CH$_2$Cl$_2$).

^{1}H NMR (300 MHz, CD$_3$OD) δ 8.55 (ddd, J = 5.0, 1.7, 0.9 Hz, 1H), 7.87 (td, J = 7.8, 1.8 Hz, 1H), 7.70 (dt, J = 7.9, 1.0 Hz, 1H), 7.45 (ddd, J = 7.7, 5.0, 1.2 Hz, 1H), 7.15 (d, J = 1.1 Hz, 1H), 6.97 (d, J = 1.2 Hz, 1H), 3.95 (s, 3H).

^{13}C NMR (75 MHz, CD$_3$OD) δ 150.9, 142.3, 141.6, 138.6, 129.4, 127.8, 126.1, 125.7, 124.7 (q, J = 284.3 Hz), 71.9 (q, J = 33.3 Hz), 87.0, 84.0, 35.7.

^{19}F NMR (282 MHz, CD$_3$OD) δ −79.55 (s, 3F).

IR (film): v (cm^{-1}) 2236, 1585, 1483, 1465, 1430, 1279, 1250, 1175, 1109, 1092, 1055, 1027, 942, 912, 844, 777, 738, 717, 682, 635, 617, 594, 537, 503, 401.

HRMS (ESI, m/z) calcd for C$_{13}$H$_{11}$F$_3$N$_3$O [M+H]$^+$: 282.0849, found: 282.0853.

(R)-1,1,1-Trifluoro-2-(1-methyl-1H-imidazol-2-yl)-4-(thiophen-3-yl)but-3-yn-2-ol (20p)
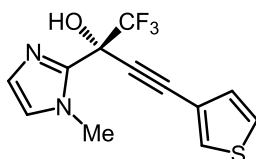
Starting from trifluoromethyl ketone **11c** (35.6 mg, 0.20 mmol) and 3-ethynylthiophene (64.9 mg, 0.60 mmol) according to the general procedure to give **20p** as a white solid (53.9 mg, 0.188 mmol, yield: 94%, R_f = 0.5, EtOAc/n-hexane = 1:2). Enantiomeric excess established by HPLC analysis using a Chiralpak OJ-H column, ee = 99.0% (HPLC: OJ-H, 254 nm, hexane/isopropanol = 85:15, flow rate 1.0 mL/min, 25 °C, t_r (minor) = 11.4 min, t_r (major) = 14.2 min). $[\alpha]_D^{25}$ = +44.1° (c 0.6, CH$_2$Cl$_2$).

^{1}H NMR (300 MHz, CD$_3$OD) δ 7.80–7.70 (m, 1H), 7.50–7.38 (m, 1H), 7.21 (dd, J = 5.0, 1.0 Hz, 1H), 7.12 (d, J = 1.0 Hz, 1H), 6.95 (d, J = 0.9 Hz, 1H), 3.93 (s, 3H).

^{13}C NMR (75 MHz, CD$_3$OD) δ 142.1, 132.0, 130.7, 127.6, 127.1, 125.9, 124.8 (q, J = 284.3 Hz), 71.9 (q, J = 33.0 Hz), 121.5, 84.2, 83.3, 35.6.

^{19}F NMR (282 MHz, CD$_3$OD) δ –79.41 (s, 3F).

IR (film): v (cm^{-1}) 2236, 1478, 1285, 1244, 1194, 1173, 1080, 1050, 1027, 1002, 941, 912, 885, 872, 789, 760, 722, 688, 658, 626, 610, 532, 500, 417.

HRMS (ESI, m/z) calcd for C$_{12}$H$_{10}$F$_3$N$_2$OS [M+H]$^+$: 287.0460, found: 287.0468.

(*R*)-1,1,1-Trifluoro-2-(1-methyl-1*H*-imidazol-2-yl)oct-3-yn-2-ol (20q).
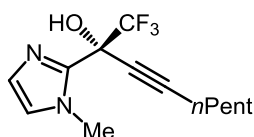
Starting from trifluoromethyl ketone **11c** (35.6 mg, 0.20 mmol) and hex-1-yne (164.3 mg, 2.0 mmol) according to the general procedure to give **20q** as a white solid (45.5 mg, 0.175 mmol, yield: 88%, R$_f$ = 0.3, EtOAc/*n*-hexane = 1:2). Enantiomeric excess established by HPLC analysis using a Chiralpak AD-H column, *ee* = 97% (HPLC: AD-H, 220 nm, hexane/isopropanol = 95:5, flow rate 1.0 mL/min, 25 °C, t$_r$ (minor) = 8.4 min, t$_r$ (major) = 11.7 min). [α]$_D^{25}$ = +35.0° (*c* 0.5, CH$_2$Cl$_2$).

^{1}H NMR (300 MHz, CD$_3$OD) δ 7.09 (d, J = 1.2 Hz, 1H), 6.91 (d, J = 1.2 Hz, 1H), 3.89 (s, 3H), 2.33 (t, J = 6.9 Hz, 2H), 1.62–1.37 (m, 4H), 0.93 (t, J = 7.2 Hz, 3H).

^{13}C NMR (75 MHz, CD$_3$OD) δ 142.7, 127.3, 125.6, 124.8 (q, J = 283.7 Hz), 90.4, 75.3, 71.1 (q, J = 33.0 Hz), 35.6, 31.2, 22.9, 19.0, 13.8.

^{19}F NMR (282 MHz, CD$_3$OD) δ –79.64 (s, 3F).

IR (film): v (cm^{-1}) 2960, 2936, 2874, 2247, 1688, 1484, 1466, 1257, 1165, 1141, 1072, 991, 943, 915, 906, 839, 751, 718, 699, 683, 614.

HRMS (ESI, m/z) calcd for C$_{12}$H$_{16}$F$_3$N$_2$O [M+H]$^+$: 261.1220, found: 261.1210.

(*R*)-4-Cyclohexyl-1,1,1-trifluoro-2-(1-methyl-1*H*-imidazol-2-yl)but-3-yn-2-ol (20r)
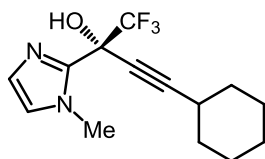
Starting from trifluoromethyl ketone **11c** (35.6 mg, 0.20 mmol) and ethynylcyclohexane (216.4 mg,

2.0 mmol) according to the general procedure to give **20r** as a white solid (38.8 mg, 0.136 mmol, yield: 68%, R_f = 0.3, EtOAc/*n*-hexane = 1:2). Enantiomeric excess established by HPLC analysis using a Chiralpak AD-H column, *ee* = 94% (HPLC: AD-H, 220 nm, hexane/isopropanol = 95:5, flow rate 1.0 mL/min, 25 °C, t_r (minor) = 7.7 min, t_r (major) = 11.0 min). $[\alpha]_D^{25}$ = +5.7° (*c* 0.5, CH$_2$Cl$_2$).

^{1}H NMR (300 MHz, CD$_3$OD) δ 7.09 (d, *J* = 1.2 Hz, 1H), 6.90 (d, *J* = 1.2 Hz, 1H), 3.89 (s, 3H), 2.62–2.45 (m, 1H), 1.90–1.80 (m, 2H), 1.79–1.62 (m, 2H), 1.62–1.44 (m, 3H), 1.44–1.23 (m, 3H).

^{13}C NMR (75 MHz, CD$_3$OD) δ 142.7, 127.3, 125.6, 124.8 (q, *J* = 283.7 Hz), 94.1, 75.4, 71.0 (q, *J* = 33.0 Hz), 35.6, 33.1, 30.1, 26.9, 25.7.

^{19}F NMR (282 MHz, CD$_3$OD) δ −80.30 (s, 3F).

IR (film): v (cm^{-1}) 2936, 2925, 2856, 2245, 1488, 1443, 1389, 1191, 1157, 1093, 1046, 1013, 941, 924, 906, 848, 759, 708, 688, 591, 536, 514, 456.

HRMS (ESI, *m/z*) calcd for C$_{14}$H$_{18}$F$_3$N$_2$O [M+H]$^+$: 287.1377, found: 287.1363.

(*R*)-4-Cyclopropyl-1,1,1-trifluoro-2-(1-methyl-1*H*-imidazol-2-yl)but-3-yn-2-ol (20s)
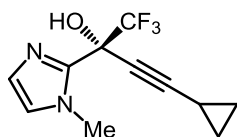
Starting from trifluoromethyl ketone **11c** (35.6 mg, 0.20 mmol) and ethynylcyclopropane (132.2 mg, 2 mmol) according to the general procedure to give **20s** as a white solid (41.0 mg, 0.168 mmol, yield: 84%, R_f = 0.2, EtOAc/*n*-hexane = 1:2). Enantiomeric excess established by HPLC analysis using a Chiralpak AD-H column, *ee* = 94% (HPLC: AD-H, 220 nm, hexane/isopropanol = 95:5, flow rate 1.0 mL/min, 25 °C, t_r (minor) = 6.9 min, t_r (major) = 8.3 min). $[\alpha]_D^{25}$ = +48.7° (*c* 0.5, CH$_2$Cl$_2$).

^{1}H NMR (300 MHz, CD$_3$OD) δ 7.08 (d, *J* = 1.2 Hz, 1H), 6.90 (d, *J* = 1.2 Hz, 1H), 3.87 (s, 3H), 1.44–1.35 (m, 1H), 0.90–0.80 (m, 2H), 0.79–0.71 (m, 2H).

^{13}C NMR (75 MHz, CD$_3$OD) δ 142.6, 127.3, 125.7, 124.8 (q, *J* = 283.8 Hz), 93.4, 71.2 (q, *J* = 33.0 Hz), 70.1, 35.6, 8.6, 8.5, −0.01.

^{19}F NMR (282 MHz, CD$_3$OD) δ −80.41(s, 3F).

IR (film): v (cm^{-1}) 2236, 1494, 1454, 1362, 1288, 1277, 1191, 1172, 1164, 1143, 1088, 1035, 947, 925, 907, 848, 816, 758, 738, 714, 687, 610, 491.

HRMS (ESI, *m/z*) calcd for C$_{11}$H$_{12}$F$_3$N$_2$O [M+H]$^+$: 245.0907, found: 245.0897.

(*R*)-1,1,1-Trifluoro-2-(1-methyl-1*H*-imidazol-2-yl)-5-phenylpent-3-yn-2-ol (20t)
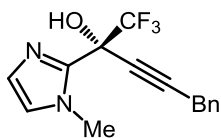
Starting from trifluoromethyl ketone **11c** (35.6 mg, 0.20 mmol) and prop-2-yn-1-ylbenzene (69.7 mg, 0.60 mmol) according to the general procedure to give **20t** as a white solid (32.4 mg, 0.110 mmol, yield: 55%, R_f = 0.4, EtOAc/*n*-hexane = 1:2). Enantiomeric excess established by HPLC analysis using a Chiralpak AD-H column, *ee* = 99% (HPLC: AD-H, 220 nm, hexane/isopropanol = 90:10, flow rate 1.0 mL/min, 25 °C, t_r (minor) = 8.6 min, t_r (major) = 14.3 min). $[\alpha]_D^{25}$ = +25.0° (*c* 0.3, CH_2Cl_2).

^{1}H NMR (300 MHz, CD_3OD) δ 7.45–7.25 (m, 4H), 7.25–7.16 (m, 1H), 7.08 (d, *J* = 1.2 Hz, 1H), 6.92 (d, *J* = 1.2 Hz, 1H), 3.86 (s, 3H), 3.75 (s, 2H).

^{13}C NMR (75 MHz, CD_3OD) δ 142.5, 137.0, 129.6, 129.0, 127.8, 127.4, 125.7, 124.8 (q, *J* = 284 Hz), 88.2, 77.3, 71.4 (q, *J* = 33.8 Hz), 35.6, 25.5.

^{19}F NMR (282 MHz, CD_3OD) δ –79.55 (s, 3F).

IR (film): v (cm^{-1}) 2256, 1604, 1495, 1453, 1409, 1338, 1285, 1187, 1165, 1142, 1061, 945, 926, 909, 762, 723, 693, 619, 607, 535, 478, 456.

HRMS (ESI, *m/z*) calcd for $C_{15}H_{14}F_3N_2O$ [M+H]$^+$: 295.1064, found: 295.1053.

(*R*)-1,1,1-Trifluoro-2-(1-methyl-1*H*-imidazol-2-yl)-4-(trimethylsilyl)but-3-yn-2-ol (20u)
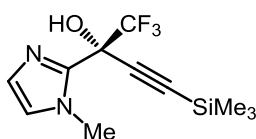
Starting from trifluoromethyl ketone **11c** (53.5 mg, 0.30 mmol) and ethynyltrimethylsilane (88.4 mg, 0.90 mmol) according to the general procedure to give **20u** as a white solid (52.7 mg, 0.191 mmol, yield: 64%, R_f = 0.4, EtOAc/*n*-hexane = 1:2). Enantiomeric excess established by HPLC analysis using a Chiralpak OD-H column, *ee* > 99% (HPLC: OD-H, 220 nm, hexane/isopropanol = 98:2, flow rate 1.0 mL/min, 25 °C, t_r = 10.7 min). $[\alpha]_D^{25}$ = +54.5° (*c* 0.6, CH_2Cl_2).

^{1}H NMR (300 MHz, CD_3OD) δ 7.10 (d, *J* = 1.2 Hz, 1H), 6.92 (d, *J* = 1.2 Hz, 1H), 3.89 (s, 3H), 0.22 (s, 9H).

^{13}C NMR (75 MHz, CD_3OD) δ 141.9, 127.5, 125.8, 124.6 (q, *J* =283.8 Hz), 99.3, 94.7, 71.2 (q, *J* =

33.0 Hz), 35.5, −0.6.

^{19}F NMR (282 MHz, CD$_3$OD) δ −79.64 (s, 3F).

IR (film): v (cm^{-1}) 2965, 2240, 1491, 1380, 1288, 1277, 1265, 1251, 1205, 1192, 1172, 1140, 1110, 1055, 1030, 947, 913, 844, 764, 749, 730, 709, 699, 603, 520, 460, 418.

HRMS (ESI, m/z) calcd for C$_{11}$H$_{16}$F$_3$N$_2$OSi [M+H]$^+$: 277.0979, found: 277.0982.

(*R*)-4-(Cyclohex-1-en-1-yl)-1,1,1-trifluoro-2-(1-methyl-1*H*-imidazol-2-yl)but-3-yn-2-ol (20v)
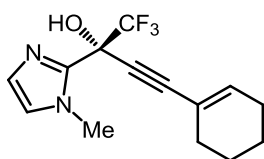
Starting from trifluoromethyl ketone **11c** (35.6 mg, 0.20 mmol) and 1-ethynylcyclohex-1-ene (64.9 mg, 0.60 mmol) according to the general procedure to give **20v** as a white solid (49.5 mg, 0.174 mmol, yield: 87%, R$_f$ = 0.4, EtOAc/*n*-hexane = 1:2). Enantiomeric excess established by HPLC analysis using a Chiralpak AD-H column, *ee* = 97% (HPLC: AD-H, 220 nm, hexane/isopropanol = 95:5, flow rate 1.0 mL/min, 25 °C, t$_r$ (minor) = 10.3 min, t$_r$ (major) = 12.8 min). [α]$_D^{25}$ = +36.5° (*c* 0.5, CH$_2$Cl$_2$).

^{1}H NMR (300 MHz, CD$_3$OD) δ 7.09 (d, J = 1.2 Hz, 1H), 6.91 (d, J = 1.1 Hz, 1H), 6.34–6.19 (m, 1H), 3.89 (s, 3H), 2.40–1.93 (m, 4H), 1.87–1.40 (m, 4H).

^{13}C NMR (75 MHz, CD$_3$OD) δ 142.4, 138.6, 127.4, 125.7, 124.8 (q, J = 283.8 Hz), 120.6, 90.6, 81.2, 71.5 (q, J = 33.3 Hz), 35.6, 29.5, 26.6, 23.2, 22.4.

^{19}F NMR (282 MHz, CD$_3$OD) δ −79.93 (s, 3F).

IR (film): v (cm^{-1}) 3138, 2944, 2852, 2216, 1721, 1484, 1361, 1288, 1189, 1173, 1137, 1090, 1054, 1013, 947, 910, 765, 734, 720, 695, 533.

HRMS (ESI, m/z) calcd for C$_{14}$H$_{16}$F$_3$N$_2$O [M+H]$^+$: 285.1209, found: 285.1207.

(*R*)- 1,1,1-Trifluoro-2-(1-methyl-1*H*-benzo[d]imidazol-2-yl)-4-phenylbut-3-yn-2-ol (20w)
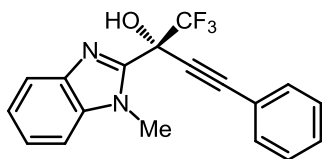
Starting from trifluoromethyl ketones **11d** (45.6 mg, 0.2 mmol) and phenylacetylene (61.3 mg, 0.60 mmol) according to the general procedure to give **20w** as a white solid (48.4 mg, 0.146 mmol, yield:

73%, $R_f = 0.5$, EtOAc/n-hexane = 1:2). Enantiomeric excess established by HPLC analysis using a Chiralpak AD-H column, *ee* = 98.8% (HPLC: AD-H, 254 nm, hexane/isopropanol = 90:10, flow rate 1.0 mL/min, 25 °C, t_r (major) = 13.2 min, t_r (minor) = 16.2 min). $[\alpha]_D^{25} = 34.6°$ (*c* 0.4, CH_2Cl_2).

^{1}H NMR (300 MHz, MeOD) δ 7.74 (d, *J* = 7.5 Hz, 1H), 7.61–7.49 (m, 3H), 7.46–7.24 (m, 5H), 4.12 (s, 3H).

^{13}C NMR (75 MHz, MeOD) δ 148.5, 142.2, 138.0, 133.0, 130.5, 129.6, 125.1, 124.8 (q, J = 284.3), 124.0, 122.9, 120.6, 111.2, 89.5, 83.3, 72.4 (q, J = 33.0 Hz), 32.7.

^{19}F NMR (282 MHz, None) δ –78.78 (s).

IR (film): v (cm^{-1}) 2243, 1492, 1474, 1445, 1385,1331, 1287, 1244, 1186, 1167, 1113, 1072, 1029, 1020, 1007, 997, 946, 818, 762, 734, 691, 636, 618, 587, 553, 539, 480, 437, 418.

HRMS (ESI, *m/z*) calcd for $C_{18}H_{13}F_3N_2OH$ [M+H]$^+$: 331.1053, found: 331.1056.

(*R*)-1,1,1-Trifluoro-2-(1-(4-methoxyphenyl)-1*H*-imidazol-2-yl)-4-phenylbut-3-yn-2-ol (20x)
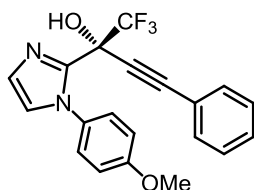
Starting from trifluoromethyl ketones **11e** (54.0 mg, 0.2 mmol) and phenylacetylene (61.3 mg, 0.60 mmol) according to the general procedure to give **20x** as a white solid (70.7 mg, 0.190 mmol, yield: 95%, $R_f = 0.5$, EtOAc/n-hexane = 1:2). Enantiomeric excess established by HPLC analysis using a Chiralpak AD-H column, *ee* = 94.3% (HPLC: AD-H, 254 nm, hexane/isopropanol = 90:10, flow rate 1.0 mL/min, 25 °C, t_r (minor) = 8.8 min, t_r (major) = 13.1 min). $[\alpha]_D^{25} = 85.9$ (*c* 1.0, CH_2Cl_2).

^{1}H NMR (300 MHz, MeOD) δ 7.44–7.20 (m, 1H), 7.17 (d, *J* = 1.2 Hz, 1H), 7.08 (d, *J* = 1.0 Hz, 1H), 6.96–6.86 (m, 1H), 3.75 (s, 1H).

^{13}C NMR (75 MHz, MeOD) δ 161.4, 143.0, 132.8, 132.3, 130.4, 129.9, 129.4, 127.7, 126.7, 124.6 (q, *J* = 284.3 Hz), 122.4, 114.9, 89.5, 83.7, 70.8 (q, *J* = 33.0 Hz), 56.00.

^{19}F NMR (282 MHz, None) δ –78.56.

IR (film): v (cm^{-1}) 2336, 1512, 1491, 1463, 1443, 1301, 1251, 1202, 1166, 1070, 941, 898, 834, 757, 726, 718, 687, 629, 560, 542, 529, 502, 462.

HRMS (ESI, *m/z*) calcd for $C_{20}H_{15}F_3N_2O_2H$ [M+H]$^+$: 373.1158, found: 373.1169.

(*R*)- 4,4,5,5,5-Pentafluoro-1-phenyl-3-(1-phenyl-1*H*-imidazol-2-yl)pent-1-yn-3-ol (20y)
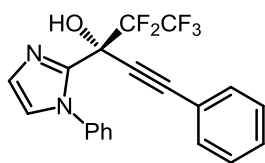
Starting from pentafluoroketones **11f** (58.0 mg, 0.2 mmol) and phenylacetylene (61.3 mg, 0.60 mmol) according to the general procedure to give **20y** as a white solid (63.2 mg, 0.161 mmol, yield: 81%, R_f = 0.3, EtOAc/*n*-hexane = 1:2). Enantiomeric excess established by HPLC analysis using a Chiralpak AD-H column, *ee* = 96.8% (HPLC: AD-H, 254 nm, hexane/isopropanol = 90:10, flow rate 1.0 mL/min, 25 °C, t_r (minor) = 8.1 min, t_r (major) = 19.5 min). $[\alpha]_D^{25}$ = 12.8° (*c* 0.8, CH_2Cl_2).

^{1}H NMR (300 MHz, MeOD) δ 7.46–7.38 (m, 5H), 7.38–7.28 (m, 5H), 7.17 (d, *J* = 1.3 Hz, 1H), 7.13 (d, *J* = 1.3 Hz, 1H).

^{13}C NMR (75 MHz, MeOD) δ 142.9, 140.1, 132.8, 131.1, 130.5, 129.9, 129.6, 129.4, 128.9, 128.1, 127.2, 122.5, 122.3, 90.3, 83.9, 71.7.

^{19}F NMR (282 MHz, None) δ –78.42, –116.89, –117.84, –120.28, –121.23.

IR (film): v (cm^{-1}) 2246, 1597, 1498, 1457, 1445, 1330, 1212, 1179, 1154, 1142, 1124, 1097, 1075, 1058, 988, 936, 841, 773, 756, 689, 643, 569, 537, 517, 434, 418.

HRMS (ESI, *m*/*z*) calcd for $C_{20}H_{13}F_5N_2OH$ [M+H]$^+$: 393.1021, found: 393.1027.

5.4 Octahedral Chiral-at-Ruthenium Complexes for Asymmetric Catalysis

5.4.1. Synthesis and characterization of catalysts

a) Synthesis of the NHCs ligands
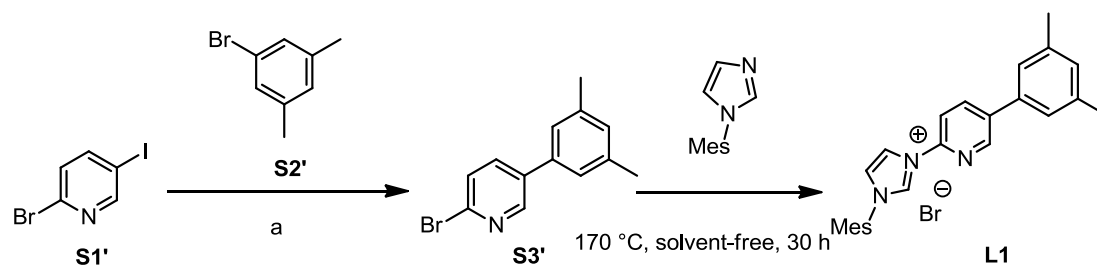
a: (i) 1.11 equiv of n-BuLi/THF,-78 °C, 30min
   (ii) 0.73 equiv of ZnCl₂/THF,-78 °C to RT, 30min
   (iii) 1.0 equiv of **S2'**, 1.6 mol% Pd(PPh₃)₄/THF, reflux, 18 h

2-Bromo-5-(3,5-dimethylphenyl)pyridine (S3′) was synthesized following a published procedure with slight modifications.[17] The 2-bromo-5-iodopyridine (**S1′**) (925.3 mg, 5.0 mmol) was dissolved in 2.0 mL of THF and was cooled to −78 °C. n-Butyllithium (n-BuLi) (3.47 mL, 5.55 mmol, 1.6 M in hexane) was added over a 30 min period. The lithiate was then warmed to −40 $^{\circ}$C and stirred for 15 min before being cooled again to −78 °C. A solution of ZnCl₂ (pre-dried under vacuum) (497 mg, 3.65 mmol) was separately prepared in 4.0 mL THF. This solution was then added to the lithiate over a 5 min period at −78 ℃. The reaction mixture was left to warm to room temperature upon which it was added to a solution of 1-bromo-3,5-dimethylbenzene (**S2′**) (925 mg, 5.0 mmol) and Pd(PPh₃)₄ (93 mg, 0.08 mmol, 1.60 mol%) in 5 mL THF. The final reaction mixture was degassed and heated to reflux for 18 h. The brown solution was then cooled to room temperature and 2/3 of the THF was evaporated under reduced pressure and its volume replaced by CH₂Cl₂. The solution was then treated with a mixture of sat. NaHCO₃ and EDTA solutions (1:1) (3 × 70 mL). All the aqueous phases were combined and extracted with CH₂Cl₂. The organic phases were combined, dried over MgSO₄ and concentrated. Purification on a silica gel column (EtOAc/hexane = 1:50) resulted in the compound **S3′** as a white solid (712 mg, 54% yield, R_f = 0.5, EtOAc/n-hexane = 1:10).

¹H NMR (300 MHz, CDCl₃) δ 8.56 (d, J = 2.1 Hz, 1H), 7.79−7.67 (m, 1H), 7.52 (d, J = 8.2 Hz, 1H), 7.14 (s, 2H), 7.06 (s, 1H), 2.40 (d, J = 5.7 Hz, 6H).

¹³C NMR (75 MHz, CDCl₃) δ 148.7, 140.8, 139.0, 137.1, 136.6, 136.4, 130.3, 128.0, 125.0, 21.5.

IR (film): v (cm⁻¹) 3013, 2910, 2854, 1598, 1447, 1343, 1074, 1017, 826, 694, 404.

HRMS (ESI, *m/z*) calcd for $C_{13}H_{13}BrN$ [M+H]$^+$: 262.0226, 264.0206, found: 262.0228, 264.0207.

L1 was synthesized following a published procedure with slight modifications.[18] 1-Mesitylimidazole (391 mg, 2.1 mmol) and 2-bromo-5-(3,5-dimethylphenyl)pyridine (**S3′**) (524 mg, 2.0 mmol) were stirred in a sealed tube at 170 °C for 30 h. After cooling to room temperature, the resulting brown solid was washed with diethyl ether for several times until no starting materials were visible by TLC, and then the solvent was removed to give **L1** as a white solid (498 mg, 56% yield). MP: 304 °C.

^{1}H NMR (300 MHz, CDCl$_3$) δ 11.38 (s, 1H), 9.28 (d, J = 8.4 Hz, 1H), 8.93 (s, 1H), 8.69 (s, 1H), 8.26 (d, J = 7.1 Hz, 1H), 7.36 (s, 1H), 7.20 (s, 2H), 7.09 (s, 1H), 7.05 (s, 2H), 2.40 (s, 6H), 2.35 (s, 3H), 2.20 (s, 6H).

^{13}C NMR (75 MHz, CDCl$_3$) δ 146.9, 144.7, 141.7, 139.1, 139.03, 138.97, 136.0, 135.9, 134.1, 130.71, 130.67, 130.1, 125.1, 124.1, 120.3, 116.3, 21.4, 21.2, 18.0.

IR (film): v (cm^{-1}) 2900, 2774, 1604, 1534, 1480, 1378, 1331, 1243, 1081, 1052, 1029, 963, 864, 831, 753, 730, 700, 669, 636, 582, 549, 413.

HRMS (ESI, *m/z*) calcd for $C_{25}H_{26}N_3$ [M−HBr]$^+$: 368.2121, found: 368.2111.
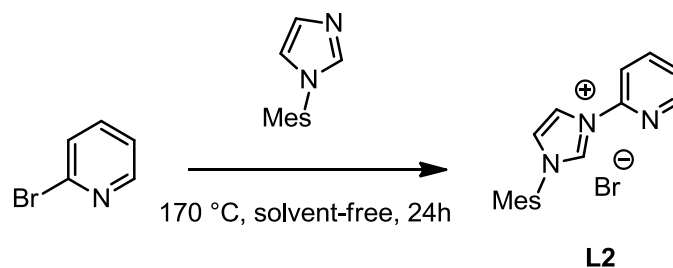
L2 was prepared according to a reported literature procedure.[19]

b) Synthesis of *rac*-Ru1 and *rac*-Ru2

R=3,5-Me$_2$Ph: *rac*-**Ru1**
R=H: *rac*-**Ru2**
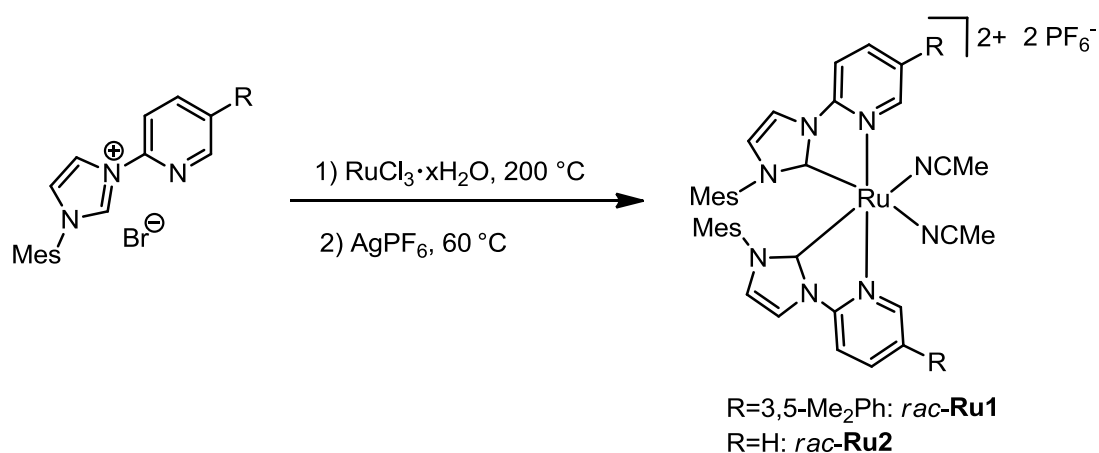
rac-**Ru1 Complex**: A solution of RuCl$_3$•xH$_2$O (25.0 mg, 0.12 mmol) and **L1** (108 mg, 0.24 mmol) in ethylene glycol (2.4 mL) was heated at 200 ℃ for 8 h, and the reaction mixture was treated with saturated aqueous NH$_4$PF$_6$ after cooling down to room temperature. A yellow precipitate formed which was separated by filtration and dissolved in CH$_2$Cl$_2$, washed with water and dried to obtain a red-orange solid. To the red-orange solution in CH$_3$CN (3 mL) was added AgPF$_6$ (38 mg, 0.15 mmol) in one portion, and then stirred at 60 ℃ overnight. After cooling to room temperature, the mixture was filtered. The filtrate was collected, evaporated to dryness and purified by column chromatograph on silica gel (CH$_2$Cl$_2$/CH$_3$CN = 10:1) to give *rac*-**Ru1** (133 mg, 0.110 mmol, 92% yield for two steps, R$_f$ = 0.4, CH$_3$CN/CH$_2$Cl$_2$ = 1:10) as a pale yellow solid. MP: 241–243 ℃ (decomp.).

^{1}H NMR (300 MHz, CD$_2$Cl$_2$) δ 8.49 (d, J = 1.9 Hz, 2H), 8.04 (dd, J = 9.8, 2.2 Hz, 4H), 7.61 (d, J = 8.6 Hz, 2H), 7.19 (d, J = 9.4 Hz, 6H), 6.91 (d, J = 2.3 Hz, 2H), 6.59 (d, J = 13.2 Hz, 2H), 2.47 (s, 12H), 2.30 (s, 6H), 2.01 (s, 6H), 1.98 (s, 6H), 1.50 (s, 6H).

^{13}C NMR (75 MHz, CD$_2$Cl$_2$) δ 189.5, 152.2, 149.1, 140.5, 139.9, 137.0, 135.8, 135.1, 135.0, 134.3, 134.2, 131.4, 130.3, 129.6, 125.9, 124.9, 124.8, 118.0, 111.8, 21.7, 21.1, 17.7, 17.4, 3.9. ^{19}F NMR (282 MHz, CD$_2$Cl$_2$) δ −71.31, −73.83.

IR (film): v (cm^{-1}) 2924, 1609, 1499, 1425, 1372, 1306, 1256, 1114, 1035, 932, 828, 697, 604, 554, 438.

rac-**Ru2 Complex**: A solution of RuCl$_3$•xH$_2$O (52.0 mg, 0.25 mmol) and **L2** (172 mg, 0.50 mmol) in ethylene glycol (5.0 mL) was heated at 200 ℃ for 4 h, and the reaction mixture was treated with saturated aqueous NH$_4$PF$_6$ after cooling down to room temperature. A yellow precipitate formed which was separated by filtration and dissolved in CH$_2$Cl$_2$, washed with water and dried to obtain a yellow

solid. To the yellow solution in CH_3CN (5 mL) was added $AgPF_6$ (79 mg, 0.31 mmol) in one portion, and then stirred at 60 ℃ overnight. After cooling to room temperature, the mixture was filtered. The filtrate was collected, evaporated to dryness and purified by column chromatograph on silica gel (CH_2Cl_2/CH_3CN = 10:1) to give *rac*-**Ru2** (224 mg, 0.224 mmol, 89% yield for two steps, R_f = 0.4, CH_3CN/CH_2Cl_2 = 1:10) as a pale yellow solid. MP: 184−186 ℃ (decomp.).

^{1}H NMR (300 MHz, CD_2Cl_2) δ 8.36 (d, J = 4.8 Hz, 2H), 7.93 (d, J = 2.3 Hz, 2H), 7.90–7.74 (m, 2H), 7.47 (d, J = 8.2 Hz, 2H), 7.17–7.00 (m, 2H), 6.91 (d, J = 2.3 Hz, 2H), 6.75 (s, 2H), 6.52 (s, 2H), 2.28 (s, 6H), 2.19 (s, 6H), 1.98 (s, 6H), 1.45 (s, 6H).

^{13}C NMR (75 MHz, CD_2Cl_2) δ 190.4, 153.2, 152.5, 140.6, 138.6, 135.6, 134.1, 134.0, 130.4, 129.8, 125.8, 124.9, 123.3, 117.6, 111.3, 21.1, 17.6, 17.4, 3.9.

^{19}F NMR (282 MHz, CD_2Cl_2) δ −72.21, −74.73.

IR (film): v (cm^{-1}) 3146, 2946, 2281, 1613, 1486, 1449, 1420, 1335, 1305, 1259, 826, 770, 741, 553, 455.

c) Synthesis of enantiomerically pure ruthenium catalysts
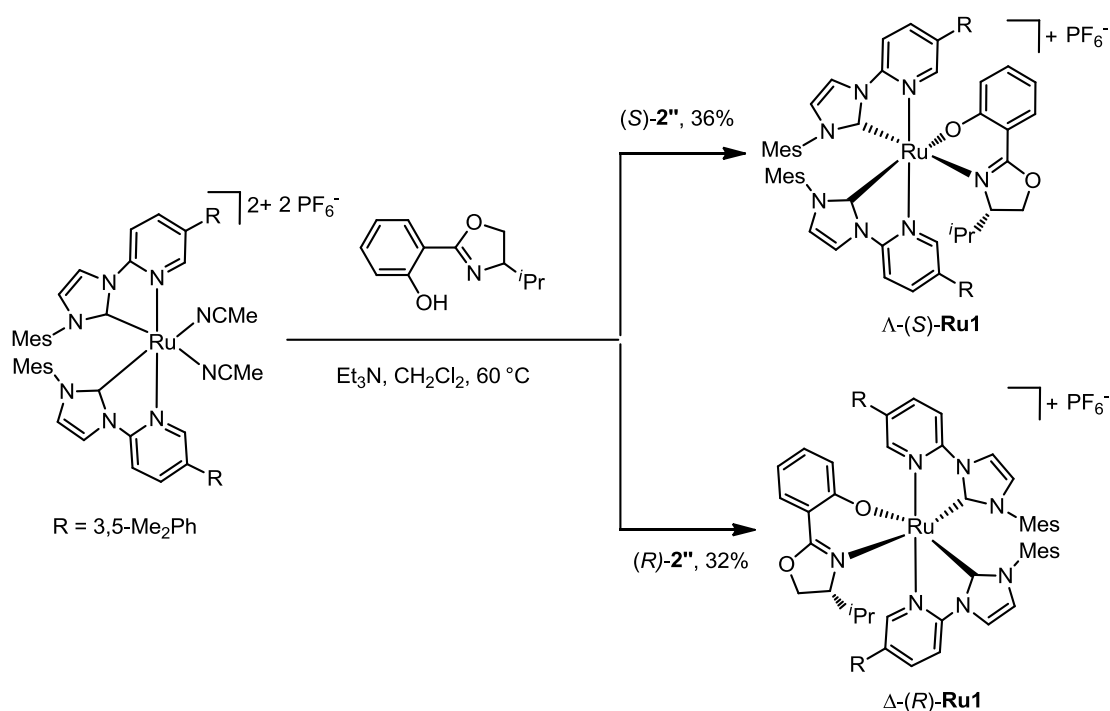
Λ-(*S*)-**Ru1** and Δ-(*R*)-**Ru1:** A mixture of *rac*-**Ru1** (100.0 mg, 0.083 mmol), the chiral auxiliary (*S*)-**2″** or (*R*)-**2″** (42.4 mg, 0.207 mmol) and triethylamine (84.0 mg, 0.830 mmol) in CH_2Cl_2 (1.37 mL) was heated at 60 ℃ for 20 h. The reaction mixture was cooled to room temperature and concentrated to dryness. The residue was subjected to a flash silica gel chromatography (CH_3CN /CH_2Cl_2 = 1:200) to

separate the first eluting diastereomer, which was assigned as Λ-(*S*)-**Ru1** (red solid, 35.6 mg, 0.030 mmol, 36%) or Δ-(*R*)-**Ru1** (red solid, 31.8 mg, 0.027 mmol, 32%), respectively. MP: 181−183 ℃ (decomp.).

^{1}H NMR (300 MHz, CD$_2$Cl$_2$) δ 8.67 (d, *J* = 2.0 Hz, 1H), 8.17 (d, *J* = 1.9 Hz, 1H), 7.95 (d, *J* = 2.3 Hz, 1H), 7.88 (dd, *J* = 9.5, 2.2 Hz, 2H), 7.65 (dd, *J* = 8.6, 2.0 Hz, 1H), 7.52 (dd, *J* = 8.1, 1.8 Hz, 1H), 7.47 (d, *J* = 8.6 Hz, 1H), 7.30 (d, *J* = 8.6 Hz, 1H), 7.10–7.02 (m, 3H), 6.98 (s, 2H), 6.88−6.89 (m, 3H), 6.84 (d, *J* = 2.2 Hz, 1H), 6.54 (d, *J* = 8.8 Hz, 2H), 6.48 (d, *J* = 6.7 Hz, 3H), 6.31−6.22 (m, 1H), 4.32 (dd, *J* = 9.1, 3.0 Hz, 1H), 4.10 (t, *J* = 9.0 Hz, 1H), 3.97 (dt, *J* = 8.9, 3.0 Hz, 1H), 2.40 (s, 6H), 2.36 (s, 6H), 2.30 (s, 3H), 2.06 (s, 3H), 1.99 (s, 3H), 1.96 (s, 3H), 1.60 (s, 3H), 1.42 (s, 3H), 0.58 (d, *J* = 6.9 Hz, 3H), 0.42–0.25 (m, 1H), −0.05 (d, *J* = 6.8 Hz, 3H).

^{13}C NMR (75 MHz, CD$_2$Cl$_2$) δ 197.7, 196.4, 172.0, 165.4, 153.0, 152.9, 148.7, 148.3, 139.7, 139.64, 139.57, 139.4, 137.3, 135.8, 135.5, 135.3, 135.2, 135.0, 134.4, 134.3, 134.2, 134.0, 133.9, 130.8, 130.5, 130.0, 129.6, 129.2, 125.8, 125.3, 124.53, 124.48, 124.0, 116.8, 116.1, 113.0, 110.9, 110.7, 110.1, 75.3, 66.7, 30.2, 21.73, 21.71, 21.09, 21.03, 19.01, 18.8, 18.1, 17.6, 13.7.

^{19}F NMR (282 MHz, CD$_2$Cl$_2$) δ −72.56, −75.07.

HRMS (ESI, *m/z*) calcd for C$_{62}$H$_{64}$N$_7$O$_2$Ru [M−PF$_6$]$^+$: 1040.4175, found: 1040.4182.

Λ-(*S*)-**Ru1**: CD (MeOH): λ, nm ($\Delta\varepsilon$, M^{-1}cm^{-1}) 473 (−7), 407 (+34), 365 (−5), 332 (+16), 291 (−36), 269 (+37), 247 (−13), 227 (+27), 208 (−64), 200 (+95). IR (film): *v* (cm^{-1}) 3138, 2960, 2918, 1606, 1535, 1494, 1472, 1419, 1376, 1323, 1279, 1251, 1222, 1066, 1035, 925, 837, 749, 690, 598, 555, 428, 392.

Δ-(*R*)-**Ru1**: CD (MeOH): λ, nm ($\Delta\varepsilon$, M^{-1}cm^{-1}) 471 (+6), 407 (−18), 367 (+5), 334 (−9), 292 (+16), 269 (−6), 249 (+9), 244 (+8). IR (film): *v* (cm^{-1}) 2959, 2919, 2861, 1605, 1493, 1471, 1419, 1373, 1309, 1252, 1223, 1150, 1066, 1034, 925, 835, 753, 689, 598, 554, 430.
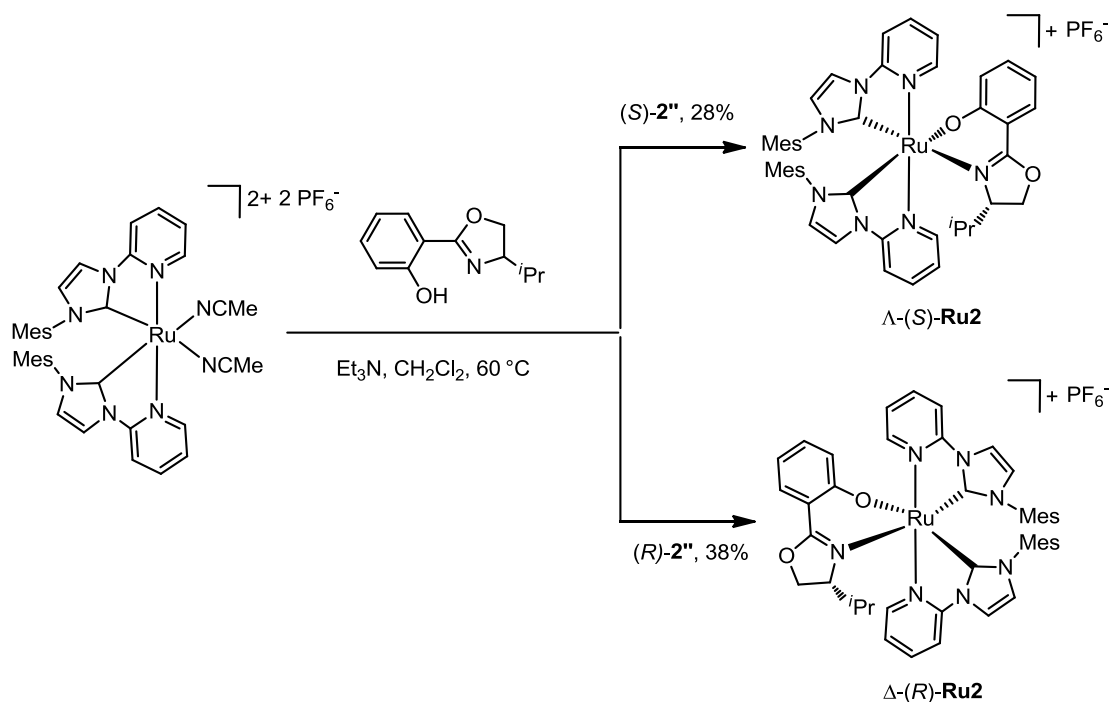
Λ-(*S*)-**Ru2**: A mixture of *rac*-**Ru2** (109.4 mg, 0.11 mmol), the chiral auxiliary (*S*)-**2″** (56.0 mg, 0.27 mmol) and triethylamine (110.5 mg, 1.09 mmol) in CH_2Cl_2 (1.82 mL) was heated at 60 °C for 20 h. The reaction mixture was cooled to room temperature and concentrated to dryness. The residue was subjected to a flash silica gel chromatography (CH_3CN /CH_2Cl_2= 1:600 to 1:200) to separate the first eluting diastereomer (orange solid, 29.5 mg, 0.03 mmol, 28%) which was assigned as Λ-(*S*)-**Ru2**.

Δ-(*R*)-**Ru2**: The catalyst Δ-(*R*)-**Ru2** was similarly synthesized with Λ-(*S*)-**Ru2**. A mixture of *rac*-**Ru2** (109.4 mg, 0.11 mmol), the chiral auxiliary (*R*)-**2″** (56.0 mg, 0.27 mmol) and triethylamine (110.5 mg, 1.09 mmol) in CH_2Cl_2 (1.82 mL) was heated at 60 °C for 30 h. The reaction mixture was cooled to room temperature and concentrated to dryness. The residue was subjected to a flash silica gel chromatography (CH_3CN /CH_2Cl_2= 1:600 to 1:200) to separate the first eluting diastereomer (orange solid, 40.9 mg, 0.04 mmol, 38%) which was assigned as Δ-(*R*)-**Ru2**.

^{1}H NMR (300 MHz, CD_2Cl_2) δ 8.36 (d, *J* = 4.5 Hz, 1H), 7.99–7.72 (m, 3H), 7.65 (t, *J* = 7.5 Hz, 1H), 7.62–7.41 (m, 2H), 7.32 (dd, *J* = 31.3, 8.2 Hz, 2H), 7.01–6.98 (m, 1H), 6.89–6.68 (m, 6H), 6.47 (d, *J* = 18.2 Hz, 2H), 6.30–6.28 (m, 1H), 6.04 (s, 1H), 4.23–4.14 (m, 2H), 3.96 (s, 1H), 2.27–2.10 (m, 12H), 1.54 (s, 3H), 1.35 (s, 3H), 0.51 (d, *J* = 6.6 Hz, 3H), 0.22–0.04 (m, 1H), –0.07 (d, *J* = 6.3 Hz, 1H).

^{13}C NMR (75 MHz, CD_2Cl_2) δ 154.3, 154.2, 150.9, 139.8, 137.7, 136.5, 136.4, 135.2, 135.1, 134.8, 134.6, 134.0, 133.4, 130.6, 130.2, 129.8, 129.7, 129.5, 125.7, 125.2, 121.4, 121.2, 116.7, 115.8, 110.6, 109.9, 75.0, 66.4, 30.5, 21.1, 21.0, 19.1, 18.7, 18.1, 18.0, 17.5, 13.6.

^{19}F NMR (282 MHz, CD$_2$Cl$_2$) δ −72.62, −75.14.

Λ-(*S*)-**Ru2**: CD (MeOH): λ, nm ($\Delta\varepsilon$, M^{-1}cm^{-1}) 396 (+25), 352 (−6), 327 (+6), 303 (−11), 280 (+19), 260 (−11), 232 (+70).

Δ-(*R*)-**Ru2**: CD (MeOH): λ, nm ($\Delta\varepsilon$, M^{-1}cm^{-1}) 398 (−15), 353 (+7), 328 (−2), 302 (+12), 280 (−10), 258 (+11), 240 (−9).

IR (film): v (cm^{-1}) 3171, 3138, 2962, 2921, 2867, 1607, 1536, 1479, 1445, 1414, 1379, 1321, 1280, 1252, 1225, 1155, 1130, 1069, 925, 832, 762, 685, 553, 529, 453.

HRMS (ESI, *m/z*) calcd for C$_{46}$H$_{48}$N$_7$O$_2$Ru [M−PF$_6$]$^+$: 832.2918, found: 832.2922.

R = H or 3,5-Me$_2$Ph
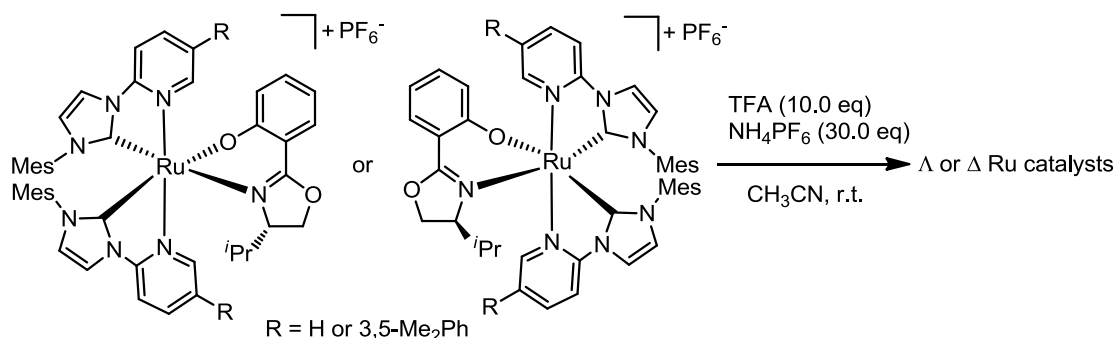
To a suspension of Λ-(*S*)-**Ru1** (27.2 mg, 0.023 mmol), Δ-(*R*)-**Ru1** (20.1 mg, 0.017 mmol), Λ-(*S*)-**Ru2** (33.0 mg, 0.034 mmol) or Δ-(*R*)-**Ru2** (40.9 mg, 0.042 mmol) in CH$_3$CN (3 mL) was added TFA (10 eq) in one portion and stirred at room temperature for 0.5 h. The reaction mixture was evaporated to dryness, redissolved in CH$_3$CN, followed by the addition of excess NH$_4$PF$_6$ (30 eq), and then stirred at room temperature for another 0.5 h. The mixture was filtered by a thin pad of silica gel, the pale yellow filtrate was concentrated, and then subjected to the column chromatography on silica gel (CH$_2$Cl$_2$/CH$_3$CN = 100:1 to 5:1) to give the enantiopure catalyst Λ-**Ru1** (25.6 mg, 0.021 mmol, 92% yield), Δ-**Ru1** (19.5 mg, 0.016 mmol, 95% yield), Λ-**Ru2** (25.8 mg, 0.026 mmol, 76% yield) or Δ-**Ru2** (37.1 mg, 0.037 mmol, 88% yield) as pale yellow solid. All other spectroscopic data of enantiopure ruthenium catalysts were in agreement with the racemic catalysts.

CD (CH$_3$OH) for Λ-**Ru1**: λ, nm ($\Delta\varepsilon$, M^{-1}cm^{-1}) 346 (+11), 328 (+4), 307 (+38), 289 (−9), 268 (+76), 239 (−73), 226 (−26), 207 (−76).

CD (CH$_3$OH) for Δ-**Ru1**: λ, nm ($\Delta\varepsilon$, M^{-1}cm^{-1}) 344 (−12), 329 (−5), 306 (−39), 290 (+11), 269 (−79), 240 (+75), 225 (+25), 206 (+77).

CD (CH$_3$OH) for Λ-**Ru2**: λ, nm ($\Delta\varepsilon$, M^{-1}cm^{-1}) 351 (+4), 312 (−4), 283 (+23), 264 (−21), 235 (+23),

218 (−1).

CD (MeOH) for Δ-**Ru2**: λ, nm (Δε, M^{-1}cm^{-1}) 314 (+8), 283 (−22), 264 (+32), 233 (−15).

5.4.2 Assignment of the absolute configuration of enantiopure ruthenium complexes

High quality single crystals for X-ray diffraction were obtained by converting the single enantiomer Δ-**Ru2** into Δ-**Ru2-DPPE**.
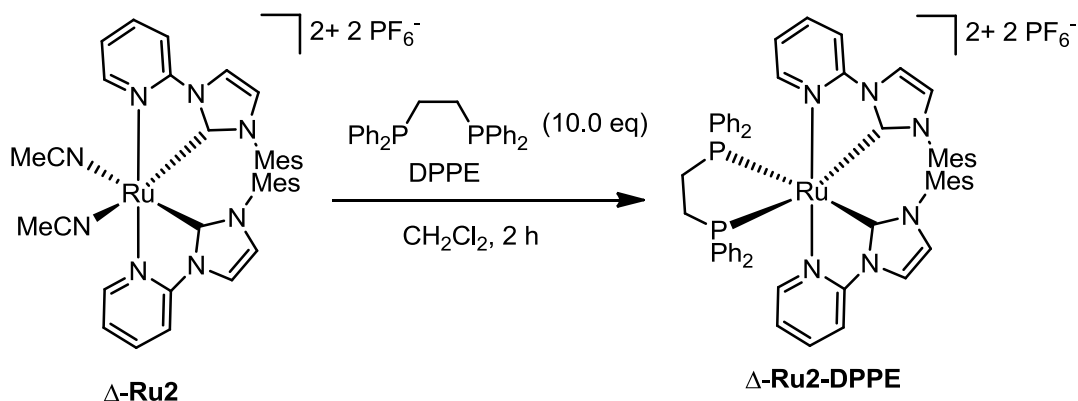
Δ-**Ru2-DPPE** was obtained by reacting Δ-**Ru2** (20.0 mg, 0.02 mmol) with 1,2-bis(diphenylphosphino)ethane (DPPE) (79.7 mg, 0.2 mmol) at room temperature for 2 hours in CH$_2$Cl$_2$ (2.0 mL). The solution was then evaporated and the resulting solid was washed with Et$_2$O and a pure pale yellow solid was obtained (24.4 mg, yield: 92%). MP: 217–219 ℃ (decomp.).

^{1}H NMR (300 MHz, CD$_2$Cl$_2$) δ 8.09 (d, J = 2.2 Hz, 2H), 7.78 (d, J = 5.3 Hz, 2H), 7.62–7.45 (m, 4H), 7.40 (t, J = 6.8 Hz, 4H), 7.31–7.23 (m, J = 7.4, 6.2 Hz, 8H), 7.13–6.94 (m, 6H), 6.63–6.49 (m, 6H), 6.48–6.35 (m, 4H), 3.16–3.06 (m, 2H), 2.90–2.61 (m, 2H), 2.13 (s, 6H), 1.45 (s, 6H), 1.32 (s, 6H).

^{13}C NMR (75 MHz, CD$_2$Cl$_2$) δ 188.5, 187.4, 154.7, 153.3, 140.8, 139.7, 135.0, 134.5, 134.4, 133.6, 133.2, 132.9, 132.8, 132.7, 131.9, 130.9, 130.6, 130.43, 130.37, 130.31, 130.25, 130.19, 130.13, 130.08, 129.87, 129.81, 129.76, 129.2, 128.7, 123.2, 118.4, 113.3, 28.0, 27.5, 20.9, 19.0, 18.4.

^{19}F NMR (282 MHz, CD$_2$Cl$_2$) δ −72.12, −74.64.

IR (film): v (cm^{-1}) 2953, 2922, 2853, 1614, 1485, 1455, 1437, 1413, 1378, 1331, 1295, 1260, 1186, 1174, 1089, 832, 770, 740, 696, 556, 520.

Crystals of Δ-**Ru-DPPE** were obtained from slow diffusion of Et$_2$O into a solution of the complex in MeOH and CH$_2$Cl$_2$. The obtained crystal structure of Δ-**Ru-DPPE** contains a Δ-configuration at the ruthenium center.

5.4.3. Ruthenium-catalyzed alkynylation reactions
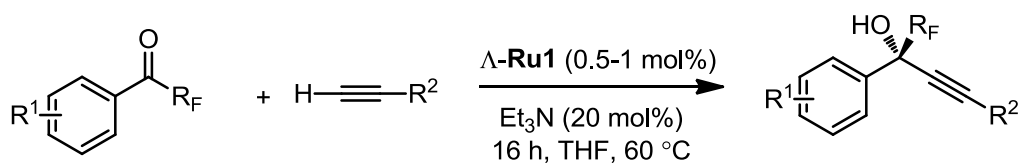
General catalytic procedure: A dried 10 mL Schlenk tube was charged with the catalyst Λ-**Ru1** (0.5−1.0 mol%) and the corresponding trifluoromethyl ketones (0.20 mmol, 1.0 eq). The tube was purged with nitrogen, THF (0.4 mL) and Et_3N (5.6 μL, 0.2 eq) were added via syringe, and followed by the corresponding alkynes (3.0 eq). The tube was sealed and the reaction was stirred at 60 °C for 16 h under nitrogen atmosphere. The solvent was removed and the residue was purified by flash chromatography on silica gel (EtOAc/hexane = 1:50) to afford the propargyl alcohols. Racemic samples were obtained by using *rac*-**Ru1**. The product (*S*)-**26a** was obtained by using Λ-**Ru1** as catalyst. The (*S*)-configuration of the product **26a** was assigned by comparison with published optical rotation and chiral HPLC retention time data.[20] All other products were assigned accordingly. Optical rotation of (*S*)-**26a:** $[\alpha]_D^{25} = -24.2°$ (*c* 1.0, CH_2Cl_2, 99.1% *ee*).   Lit.[20]: $[\alpha]_D^{25} = -25.5$ (*c* 1.1, $CHCl_3$, 88% ee for *S*-configuration). Chiral HPLC with (*S*)-**26a:** (Daicel Chiralcel OJ-H column, 254 nm, hexane/isopropanol = 90:10, flow rate 0.8 mL/min, 25 °C) t_r (minor) = 14.8 min, t_r (major) = 34.8 min. Lit.[s4]: t_r (minor) = 16.9 min, t_r (major) = 33.4 min.

(*S*)-1,1,1-Trifluoro-2,4-diphenylbut-3-yn-2-ol (26a)
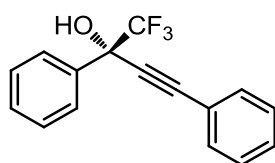
Starting from 2,2,2-trifluoro-1-phenylethanone (34.8 mg, 0.20 mmol) and phenylacetylene (61.3 mg, 0.60 mmol) according to the general procedure to give **26a** as a colorless oil (52.4 mg, 0.190 mmol, yield: 95%, R_f = 0.4, EtOAc/*n*-hexane = 1:10). Enantiomeric excess was established by HPLC analysis using a Chiralcel OJ-H column, *ee* = 99.2% (HPLC: OJ-H, 254 nm, hexane/isopropanol = 85:15, flow rate 1.0 mL/min, 25 °C, t_r (minor) = 9.5 min, t_r (major) = 25.2 min). $[\alpha]_D^{25} = -24.2°$ (*c* 1.0, CH_2Cl_2).

^{1}H NMR (300 MHz, $CDCl_3$) δ 7.86–7.83 (m, 2H), 7.61–7.52 (m, 2H), 7.51–7.33 (m, 6H), 3.11 (s, 1H).

^{13}C NMR (75 MHz, $CDCl_3$) δ 135.5, 132.2, 129.70, 129.68, 128.6, 128.4, 127.4, 127.3, 123.6 (q, *J* = 284.0 Hz), 121.1, 88.3, 84.6, 73.6 (q, *J* = 32.3 Hz).

^{19}F NMR (282 MHz, CDCl$_3$) δ −80.26.

HRMS (ESI, m/z) calcd for C$_{16}$H$_{10}$F$_3$ [M+H–H$_2$O]$^+$: 259.0729, found: 259.0728.

All spectroscopic data are in agreement with the literature.[20]

(S)-1,1,1-Trifluoro-2-phenyl-4-(p-tolyl)but-3-yn-2-ol (26b)
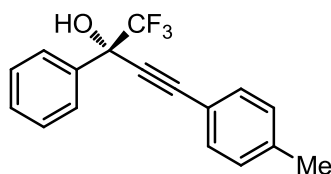
Starting from 2,2,2-trifluoro-1-phenylethanone (34.8 mg, 0.20 mmol) and 1-ethynyl-4-methylbenzene (69.7 mg, 0.60 mmol) according to the general procedure to give **26b** as a colorless oil (57.3 mg, 0.197 mmol, yield: 99%, R$_f$ = 0.4, EtOAc/n-hexane = 1:10). Enantiomeric excess established by HPLC analysis using a Chiralcel OJ-H column, ee = 99.2% (HPLC: OJ-H, 254 nm, hexane/isopropanol = 85:15, flow rate 1.0 mL/min, 25 °C, t$_r$ (minor) = 8.5 min, t$_r$ (major) = 12.3 min). [α]$_D^{25}$ = −29.2° (c 1.0, CH$_2$Cl$_2$).

^{1}H NMR (300 MHz, CDCl$_3$) δ 7.88–7.78 (m, 2H), 7.48–7.40 (m, 5H), 7.17 (d, J = 7.9 Hz, 2H), 3.06 (s, 1H), 2.38 (s, 3H).

^{13}C NMR (75 MHz, CDCl$_3$) δ 140.1, 135.6, 132.1, 129.6, 129.4, 128.4, 127.38, 127.37, 123.6 (q, J = 284.0 Hz), 88.5, 84.0, 73.6 (q, J = 32.3 Hz), 21.7.

^{19}F NMR (282 MHz, CDCl$_3$) δ −80.20.

HRMS (ESI, m/z) calcd for C$_{17}$H$_{12}$F$_3$ [M+H–H$_2$O]$^+$: 273.0886, found: 273.0885.

All spectroscopic data are in agreement with the literature.[21]

(S)-1,1,1-Trifluoro-2-phenyl-4-(m-tolyl)but-3-yn-2-ol (26c)
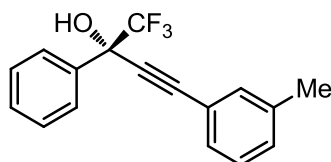
Starting from 2,2,2-trifluoro-1-phenylethanone (34.8 mg, 0.20 mmol) and 1-ethynyl-3-methylbenzene (69.7 mg, 0.60 mmol) according to the general procedure to give **26c** as a colorless oil (57.4 mg, 0.197 mmol, yield: 99%, R$_f$ = 0.4, EtOAc/n-hexane = 1:10). Enantiomeric excess established by HPLC analysis using a Chiralcel OJ-H column, ee = 99.2% (HPLC: OJ-H, 254 nm, hexane/isopropanol =

85:15, flow rate 1.0 mL/min, 25 °C, t_r (minor) = 6.9 min, t_r (major) = 11.6 min). $[\alpha]_D^{25}$ = –29.0° (*c* 1.0, CH_2Cl_2).

^{1}H NMR (300 MHz, CDCl$_3$) δ 8.03–7.65 (m, 2H), 7.49–7.38 (m, 3H), 7.37–7.30 (m, 2H), 7.24–7.17 (m, 2H), 3.07 (s, 1H), 2.34 (s, 3H).

^{13}C NMR (75 MHz, CDCl$_3$) δ 138.4, 135.5, 132.8, 130.6, 129.6, 129.3, 128.5, 128.4, 127.4, 123.6 (q, *J* = 284.0 Hz), 120.9, 88.5, 84.2, 73.6 (q, *J* = 32.3 Hz), 21.3.

^{19}F NMR (282 MHz, CDCl$_3$) δ –80.26.

IR (film): *v* (cm^{-1}) 3543, 3064, 3037, 2233, 1598, 1485, 1450, 1351, 1251, 1171, 1102, 1064, 1016, 933, 903, 783, 762, 697, 626, 589, 524, 447.

HRMS (ESI, *m/z*) calcd for C$_{17}$H$_{12}$F$_3$ [M+H–H$_2$O]$^+$: 273.0886, found: 273.0884.

All spectroscopic data are in agreement with the literature.[22]

(*S*)-1,1,1-Trifluoro-2-phenyl-4-(*o*-tolyl)but-3-yn-2-ol (26d)
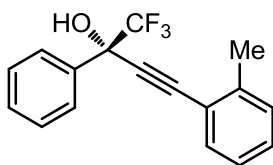
Starting from 2,2,2-trifluoro-1-phenylethanone (34.8 mg, 0.20 mmol) and 1-ethynyl-2-methylbenzene (69.7 mg, 0.60 mmol) according to the general procedure to give **26d** as a colorless oil (56.4 mg, 0.197 mmol, yield: 99%, R$_f$ = 0.4, EtOAc/*n*-hexane = 1:10). Enantiomeric excess established by HPLC analysis using a Chiralcel OJ-H column, *ee* = 99.2% (HPLC: OJ-H, 254 nm, hexane/isopropanol = 85:15, flow rate 1.0 mL/min, 25 °C, t_r (minor) = 6.5 min, t_r (major) = 8.9 min). $[\alpha]_D^{25}$ = –21.6° (*c* 1.0, CH_2Cl_2).

^{1}H NMR (300 MHz, CDCl$_3$) δ 7.97–7.73 (m, 2H), 7.56–7.37 (m, 4H), 7.35–7.09 (m, 3H), 3.06 (s, 1H), 2.47 (s, 3H).

^{13}C NMR (75 MHz, CDCl$_3$) δ 141.2, 135.5, 132.5, 129.8, 129.72, 129.66, 128.4, 127.39, 127.38, 125.9, 123.6 (q, *J* = 284.0 Hz), 120.9, 88.4, 87.4, 73.7 (q, *J* = 32.3 Hz), 20.7.

^{19}F NMR (282 MHz, CD$_3$OD) δ –80.25.

IR (film): *v* (cm^{-1}) 3543, 3067, 2922, 2228, 1599, 1486, 1451, 1351, 1242, 1175, 1124, 1097, 1063, 1007, 933, 905, 827, 759, 713, 666, 625, 599, 537, 501, 456, 429.

HRMS (EI, *m/z*) calcd for C$_{17}$H$_{13}$F$_3$O: 290.0919, found: 290.0913.

(*S*)-1,1,1-Trifluoro-4-(4-methoxyphenyl)-2-phenylbut-3-yn-2-ol (26e)
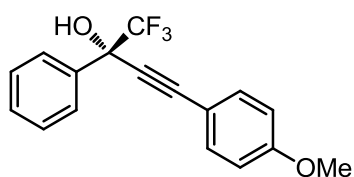
Starting from 2,2,2-trifluoro-1-phenylethanone (34.8 mg, 0.20 mmol) and 1-ethynyl-4-methoxybenzene (79.3 mg, 0.60 mmol) according to the general procedure to give **26e** as a pale yellow solid (60.4 mg, 0.197 mmol, yield: 99%, R_f = 0.7, EtOAc/*n*-hexane = 1:10). MP: 64 °C. Enantiomeric excess established by HPLC analysis using a Chiralcel OJ-H column, *ee* = 99.0% (HPLC: OJ-H, 254 nm, hexane/isopropanol = 85:15, flow rate 1.0 mL/min, 25 °C, t_r (minor) = 20.1 min, t_r (major) = 22.1 min). $[\alpha]_D^{25}$ = –38.8° (*c* 1.0, CH$_2$Cl$_2$).

^{1}H NMR (300 MHz, CDCl$_3$) δ 8.00–7.73 (m, 2H), 7.58–7.36 (m, 5H), 7.00–6.77 (m, 2H), 3.83 (s, 3H), 3.10 (s, 1H).

^{13}C NMR (75 MHz, CDCl$_3$) δ 160.7, 135.7, 133.8, 129.6, 128.4, 127.4, 123.6 (q, *J* = 283.5 Hz), 114.3, 113.1, 88.4, 83.4, 73.6 (q, *J* = 32.3 Hz), 55.5.

^{19}F NMR (282 MHz, CDCl$_3$) δ –80.20.

HRMS (ESI, *m/z*) calcd for C$_{17}$H$_{14}$F$_3$O$_2$ [M+H]$^+$: 307.0940, found: 307.0940.

All spectroscopic data are in agreement with the literature.[23]

(*S*)-4-(4-Bromophenyl)-1,1,1-Trifluoro-2-phenylbut-3-yn-2-ol (26f)
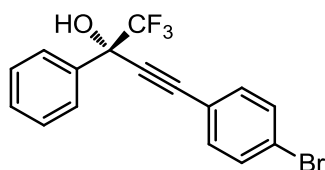
Starting from 2,2,2-trifluoro-1-phenylethanone (34.8 mg, 0.20 mmol) and 1-bromo-4-ethynylbenzene (108.6 mg, 0.60 mmol) according to the general procedure to give **26f** as a pale yellow oil (53.2 mg, 0.150 mmol, yield: 75%, R_f = 0.4, EtOAc/*n*-hexane = 1:10). Enantiomeric excess established by HPLC analysis using a Chiralcel OJ-H column, *ee* = 97.0% (HPLC: OJ-H, 254 nm, hexane/isopropanol = 85:15, flow rate 1.0 mL/min, 25 °C, t_r (major) = 11.8 min, t_r (minor) = 18.0 min). $[\alpha]_D^{25}$ = –30.4° (*c* 1.0, CH$_2$Cl$_2$).

^{1}H NMR (300 MHz, CDCl$_3$) δ 7.81–7.78 (m, 2H), 7.55–7.48 (m, 2H), 7.47–7.36 (m, 5H), 3.05 (s, 1H).

^{13}C NMR (75 MHz, CDCl$_3$) δ 135.2, 133.6, 132.0, 129.8, 128.5, 127.3, 124.2, 123.5 (q, J = 283.8 Hz), 120.0, 87.2, 85.7, 73.6 (q, J = 32.5 Hz).

^{19}F NMR (282 MHz, CDCl$_3$) δ –80.22.

HRMS (APCI, m/z) calcd for C$_{16}$H$_9$BrF$_3$ [M+H–H$_2$O]$^+$: 338.9814, found: 338.9812.

All spectroscopic data are in agreement with the literature.[20]

(*S*)-1,1,1-Trifluoro-4-(2-fluorophenyl)-2-phenylbut-3-yn-2-ol (26g)
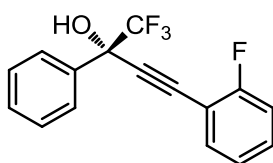
Starting from 2,2,2-trifluoro-1-phenylethanone (34.8 mg, 0.20 mmol) and 1-ethynyl-2-fluorobenzene (72.1 mg, 0.60 mmol) according to the general procedure to give **26g** as a colorless oil (38.8 mg, 0.132 mmol, yield: 66%, R$_f$ = 0.4, EtOAc/*n*-hexane = 1:10). Enantiomeric excess established by HPLC analysis using a Chiralcel OJ-H column, *ee* = 99.4% (HPLC: OJ-H, 254 nm, hexane/isopropanol = 85:15, flow rate 1.0 mL/min, 25 °C, t$_r$ (minor) = 8.8 min, t$_r$ (major) = 17.2 min). [α]$_D^{25}$ = –17.6° (*c* 1.0, CH$_2$Cl$_2$).

^{1}H NMR (300 MHz, CDCl$_3$) δ 7.87–7.75 (m, 2H), 7.68–7.33 (m, 5H), 7.23–7.03 (m, 2H), 3.11 (s, 1H).

^{13}C NMR (75 MHz, CDCl$_3$) δ 165.1, 161.7, 135.2, 133.9, 131.6, 131.5, 129.2, 128.4, 127.4, 124.3, 124.2, 123.5 (q, J = 283.8 Hz), 116.0, 115.7, 110.0, 109.8, 89.6, 81.9, 73.7 (q, J = 32.3 Hz), 35.70, 35.66, 31.50.

^{19}F NMR (282 MHz, CDCl$_3$) δ –108.91, –80.22.

IR (film): v (cm^{-1}) 3555, 3450, 3068, 2238, 1958, 1609, 1574, 1490, 1449, 1352, 1251, 1176, 1116, 1063, 1008, 935, 906, 838, 760, 717, 666, 625, 584, 549, 481, 436.

HRMS (ESI, m/z) calcd for C$_{16}$H$_9$F$_4$O [M–H]$^+$:293.0584, found: 293.0582.

(*S*)-1,1,1-Trifluoro-2-phenyl-4-(thiophen-2-yl)but-3-yn-2-ol (26h)
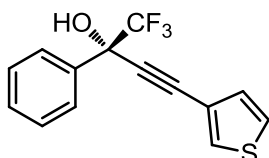
Starting from 2,2,2-trifluoro-1-phenylethanone (34.8 mg, 0.20 mmol) and 3-ethynylthiophene (64.9

mg, 0.60 mmol) according to the general procedure to give **26h** as a pale yellow oil (49.5 mg, 0.176 mmol, yield: 88%, R_f = 0.5, EtOAc/*n*-hexane = 1:10). Enantiomeric excess established by HPLC analysis using a Chiralcel OJ-H column, *ee* = 96.2% (HPLC: OJ-H, 254 nm, hexane/isopropanol = 60:40, flow rate 1.0 mL/min, 25 °C, t_r (minor) = 8.5 min, t_r (major) = 18.4 min). $[\alpha]_D^{25}$ = –46.2° (*c* 1.0, CH_2Cl_2).

^{1}H NMR (300 MHz, CDCl$_3$) δ 7.89–7.74 (m, 1H), 7.61 (dd, *J* = 3.0, 1.1 Hz, 1H), 7.50–7.41 (m, 3H), 7.33–7.31 (m, 1H), 7.20 (dd, *J* = 5.0, 1.1 Hz, 1H), 3.06 (s, 1H).

^{13}C NMR (75 MHz, CDCl$_3$) δ 135.4, 131.0, 130.0, 129.7, 128.4, 127.3, 127.3, 126.0, 123.5 (q, *J* = 283.5 Hz), 120.2, 84.4, 83.6, 73.6 (q, *J* = 32.3 Hz), 35.7.

^{19}F NMR (282 MHz, CDCl$_3$) δ –80.22.

IR (film): v (cm^{-1}) 3543.3300, 3110, 2232, 1489, 1450, 1356, 1260, 1237, 1172, 1105, 1062, 1013, 909, 869, 828, 785, 697, 625, 593, 518.

HRMS (ESI, *m/z*) calcd for $C_{14}H_8F_3OS$ [M–H]$^+$: 281.0242, found: 281.0252.

All spectroscopic data are in agreement with the literature.[20]

(*S*)-4-(Cyclohex-1-en-1-yl)-1,1,1-Trifluoro-2-phenylbut-3-yn-2-ol (26i)
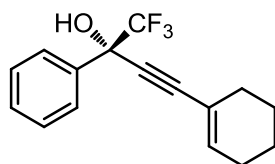
Starting from 2,2,2-trifluoro-1-phenylethanone (34.8 mg, 0.20 mmol) and 1-ethynylcyclohex-1-ene (63.7 mg, 0.60 mmol) according to the general procedure to give **26i** as a colorless oil (54.8 mg, 0.196 mmol, yield: 98%, R_f = 0.5, EtOAc/*n*-hexane = 1:10). Enantiomeric excess established by HPLC analysis using a Chiralcel OJ-H column, *ee* = 99.2% (HPLC: OJ-H, 230 nm, hexane/isopropanol = 95:5, flow rate 1.0 mL/min, 25 °C, t_r (minor) = 14.5 min, t_r (major) = 15.4 min). $[\alpha]_D^{25}$ = –15.6° (*c* 1.0, CH_2Cl_2).

^{1}H NMR (300 MHz, CDCl$_3$) δ 7.85–7.71 (m, 2H), 7.49–7.35 (m, 3H), 6.37–6.26 (m, 1H), 2.98 (s, 1H), 2.28–2.06 (m, 4H), 1.78–1.55 (m, 4H).

^{13}C NMR (75 MHz, CDCl$_3$) δ 138.1, 135.8, 129.5, 128.3, 127.4, 123.6 (q, *J* = 283.7 Hz), 119.3, 90.1, 82.0, 73.4 (q, *J* = 32.3 Hz), 28.8, 25.8, 22.2, 21.4.

^{19}F NMR (282 MHz, CDCl$_3$) δ –80.98.

HRMS (ESI, m/z) calcd for $C_{16}H_{14}F_3O$ [M–H]$^+$: 279.0991, found: 279.1007.

All spectroscopic data are in agreement with the literature.[20]

(S)-4-Cyclohexyl-1,1,1-trifluoro-2-phenylbut-3-yn-2-ol (26j)
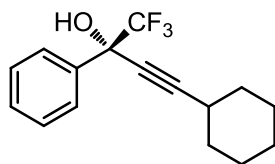
Starting from 2,2,2-trifluoro-1-phenylethanone (34.8 mg, 0.20 mmol) and ethynylcyclohexane (64.9 mg, 0.60 mmol) according to the general procedure to give **26j** as a colorless oil (54.1 mg, 0.192 mmol, yield: 96%). Enantiomeric excess established by HPLC analysis using a Chiralpak AD-H column, ee = 99.2% (HPLC: AD-H, 210 nm, hexane/isopropanol = 95:5, flow rate 1.0 mL/min, 25 °C, t_r (minor) = 6.7 min, t_r (major) = 9.5 min). $[\alpha]_D^{25}$ = –5.4° (c 1.0, CH_2Cl_2).

^{1}H NMR (300 MHz, CDCl$_3$) δ 7.89–7.67 (m, 2H), 7.55–7.33 (m, 3H), 2.89 (s, 1H), 2.70–2.42 (m, 1H), 1.89–1.69 (m, 4H), 1.60–1.31 (m, 6H).

^{13}C NMR (75 MHz, CDCl$_3$) δ 136.0, 129.4, 128.2, 127.4, 123.6 (q, J = 283.5 Hz), 93.7, 76.5, 73.0 (q, J = 32.0 Hz), 32.18, 32.16, 29.0, 25.9, 24.7.

^{19}F NMR (282 MHz, CDCl$_3$) δ –80.73.

HRMS (FD, m/z) calcd for $C_{16}H_{17}F_3O$ [M]$^+$: 282.1231, found: 282.1148.

All spectroscopic data are in agreement with the literature.[20]

(S)-4-Cyclopropyl-1,1,1-trifluoro-2-phenylbut-3-yn-2-ol (26k)
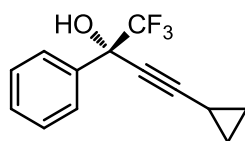
Starting from 2,2,2-trifluoro-1-phenylethanone (34.8 mg, 0.20 mmol) and cyclopropylacetylene (39.7 mg, 0.60 mmol) according to the general procedure to give **26k** as a colorless oil (46.4 mg, 0.193 mmol, yield: 97%, R_f = 0.3, EtOAc/n-hexane = 1:10). Enantiomeric excess established by HPLC analysis using a Chiralcel OJ-H column, ee = 97.0% (HPLC: OJ-H, 220 nm, hexane/isopropanol = 90:10, flow rate 1.0 mL/min, 25 °C, t_r (minor) = 15.7 min, t_r (major) = 18.1 min). $[\alpha]_D^{25}$ = –42.2° (c 1.0, CH_2Cl_2).

^{1}H NMR (300 MHz, CDCl$_3$) δ 7.88–7.61 (m, 2H), 7.47–7.33 (m, 3H), 2.88 (s, 1H), 1.48–1.23 (m, 1H), 1.07–0.70 (m, 4H).

^{13}C NMR (75 MHz, CDCl$_3$) δ 135.9, 129.4, 128.2, 127.3, 123.5(q, J = 283.5 Hz), 92.8, 73.0 (q, J = 32.0 Hz), 71.3, 8.63, 8.60, –0.50.

^{19}F NMR (282 MHz, CDCl$_3$) δ –80.49.

HRMS (FD, m/z) calcd for C$_{13}$H$_{11}$F$_3$O [M]$^+$: 240.0762, found: 240.0755.

All spectroscopic data are in agreement with the literature.[21]

(*S*)-1,1,1-Trifluoro-2-phenyloct-3-yn-2-ol (26l)
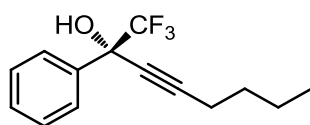
Starting from 2,2,2-trifluoro-1-phenylethanone (34.8 mg, 0.20 mmol) and hex-1-yne (49.3 mg, 0.60 mmol) according to the general procedure to give **26l** as a colorless oil (50.4 mg, 0.196 mmol, yield: 98%, R$_f$ = 0.4, EtOAc/n-hexane = 1:10). Enantiomeric excess established by HPLC analysis using a Chiralcel OJ-H column, *ee* = 99.0% (HPLC: OJ-H, 220 nm, hexane/isopropanol = 90:10, flow rate 1.0 mL/min, 25 °C, t$_r$ (minor) = 7.6 min, t$_r$ (major) = 9.3 min). [α]$_D^{25}$ = –3.6 °(c 1.0, CH$_2$Cl$_2$).

^{1}H NMR (300 MHz, CDCl$_3$) δ 7.80–7.67 (m, 2H), 7.57–7.34 (m, 3H), 2.90 (s, 1H), 2.34 (t, J = 7.0 Hz, 2H), 1.67–1.53 (m, 2H), 1.53–1.39 (m, 2H), 0.98–0.93 (t, J = 7.4 Hz, 3H).

^{13}C NMR (75 MHz, CDCl$_3$) δ 135.9, 129.4, 128.2, 127.3, 123.6 (q, J = 283.5 Hz), 89.9, 76.4, 73.1 (q, J = 32.3 Hz), 30.3, 22.1, 18.5, 13.6.

^{19}F NMR (282 MHz, CDCl$_3$) δ –80.66.

IR (film): v (cm^{-1}) 3478, 3068, 2960, 2933, 2869, 2243, 1453, 1352, 1259, 1166, 1035, 994, 936, 906, 841, 761, 725, 697, 667, 625.

HRMS (APCI, m/z) calcd for C$_{14}$H$_{14}$F$_3$ [M+H–H$_2$O]$^+$: 239.1042, found: 239.1039.

All spectroscopic data are in agreement with the literature.[21]

(*S*)-1,1,1-Trifluoro-2-phenyl-4-(trimethylsilyl)but-3-yn-2-ol (26m)
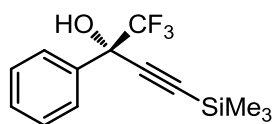
Starting from 2,2,2-trifluoro-1-phenylethanone (34.8 mg, 0.20 mmol) and ethynyltrimethylsilane (58.9 mg, 0.60 mmol) according to the general procedure to give **26m** as a colorless oil (42.1 mg, 0.155 mmol, yield: 77%, R_f = 0.5, EtOAc/n-hexane = 1:10). Enantiomeric excess established by HPLC analysis using a Chiralcel OJ-H column, ee = 99.6% (HPLC: OJ-H, 210 nm, hexane/isopropanol = 95:5, flow rate 1.0 mL/min, 25 °C, t_r (major) = 5.3 min, t_r (minor) = 10.7 min). $[\alpha]_D^{25}$ = –20.8° (c 1.0, CH_2Cl_2).

^{1}H NMR (300 MHz, CDCl$_3$) δ 7.76–7.72 (m, 2H), 7.49–7.36 (m, 3H), 2.96 (s, 1H), 0.25 (s, 9H).

^{13}C NMR (75 MHz, CDCl$_3$) δ 135.2, 129.6, 128.3, 127.3, 123.3 (q, J = 283.5 Hz)100.3, 94.5, 73.2 (q, J = 32.3 Hz), –0.36.

^{19}F NMR (282 MHz, CDCl$_3$) δ –80.39.

IR (film): v (cm^{-1}) 3471, 2963, 1492, 1452, 1347, 1253, 1175, 1129, 1068, 1015, 933, 906, 845, 761, 697, 627, 498, 451.

(*S*)-1,1,1-Trifluoro-4-phenyl-2-(p-tolyl)but-3-yn-2-ol (26n)
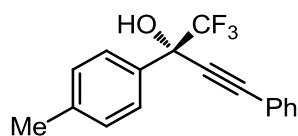
Starting from 2,2,2-trifluoro-1-(p-tolyl)ethanone (37.6 mg, 0.20 mmol) and phenylacetylene (61.3 mg, 0.60 mmol) according to the general procedure to give **26n** as a colorless oil (53.8 mg, 0.185 mmol, yield: 93%, R_f = 0.4, EtOAc/n-hexane = 1:10). Enantiomeric excess established by HPLC analysis using a Chiralcel OJ-H column, ee = 98.0% (HPLC: OJ-H, 254 nm, hexane/isopropanol = 85:15, flow rate 1.0 mL/min, 25 °C, t_r (minor) = 8.4 min, t_r (major) = 17.1 min). $[\alpha]_D^{25}$ = –29.0° (c 1.0, CH_2Cl_2).

^{1}H NMR (300 MHz, CDCl$_3$) δ 7.73 (d, J = 8.1 Hz, 2H), 7.58–7.54 (m, 2H), 7.46–7.33 (m, 3H), 7.32–7.22 (m, 2H), 3.10 (s, 1H), 2.41 (s, 3H).

^{13}C NMR (75 MHz, CDCl$_3$) δ 139.7, 132.6, 132.2, 129.3, 129.1, 128.6, 127.2, 123.6 (q, J = 283.8 Hz), 121.2, 88.1, 84.8, 73.5 (q, J = 32.3 Hz), 21.3.

^{19}F NMR (282 MHz, CDCl$_3$) δ –80.35.

HRMS (EI, m/z) calcd for C$_{17}$H$_{13}$F$_3$O [M]$^+$: 290.0918, found: 290.0925.

All spectroscopic data are in agreement with the literature.[20]

(S)-1,1,1-Trifluoro-4-phenyl-2-(m-tolyl)but-3-yn-2-ol (26o)
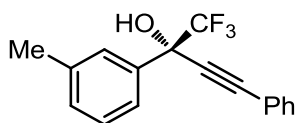
Starting from 2,2,2-trifluoro-1-(m-tolyl)ethanone (37.6 mg, 0.20 mmol) and phenylacetylene (61.3 mg, 0.60 mmol) according to the general procedure to give **26o** as a colorless oil (55.9 mg, 0.193 mmol, yield: 96%, R_f = 0.4, EtOAc/n-hexane = 1:10). Enantiomeric excess established by HPLC analysis using a Chiralcel OJ-H column, *ee* = 99.4% (HPLC: OJ-H, 254 nm, hexane/isopropanol = 85:15, flow rate 1.0 mL/min, 25 °C, t_r (minor) = 7.0 min, t_r (major) = 26.4 min). $[\alpha]_D^{25}$ = −14.8° (*c* 1.0, CH$_2$Cl$_2$).

^{1}H NMR (300 MHz, CDCl$_3$) δ 7.71–7.59 (m, 2H), 7.61–7.52 (m, 2H), 7.47–7.30 (m, 4H), 7.29–7.22 (m, 1H), 3.11 (s, 1H), 2.43 (s, 3H).

^{13}C NMR (75 MHz, CDCl$_3$) δ 138.2, 135.4, 132.2, 130.4, 129.7, 128.6, 128.3, 127.8, 123.6 (q, *J* = 283.8 Hz), 124.5, 121.2, 88.1, 84.8, 73.5 (q, *J* = 32.3 Hz), 21.7.

^{19}F NMR (282 MHz, CDCl$_3$) δ −80.74.

IR (film): *v* (cm^{-1}) 3543, 3470, 2923, 2861, 2232, 1603, 1488, 1445, 1351, 1242, 1181, 1150, 1110, 1079, 1023, 950, 913, 835, 783, 756, 727, 691, 629, 587, 557, 527, 438.

HRMS (FD, *m/z*) calcd for C$_{17}$H$_{13}$F$_3$O [M]$^+$: 290.0918, found: 290.0912.

All spectroscopic data are in agreement with the literature.[24]

(R)-1,1,1-Trifluoro-4-phenyl-2-(o-tolyl)but-3-yn-2-ol (26p)
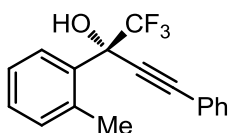
Starting from 2,2,2-trifluoro-1-(o-tolyl)ethanone (37.6 mg, 0.20 mmol) and phenylacetylene (61.3 mg, 0.60 mmol) according to the general procedure to give **26p** as a colorless oil (15.8 mg, 0.054 mmol, yield: 27%, R_f = 0.5, EtOAc/n-hexane = 1:10). Enantiomeric excess established by HPLC analysis using a Chiralcel OJ-H column, *ee* = 90.6% (HPLC: OJ-H, 254 nm, hexane/isopropanol = 85:15, flow rate 1.0 mL/min, 25 °C, t_r (minor) = 7.7 min, t_r (major) = 9.1 min). $[\alpha]_D^{25}$ = −33.6° (*c* 1.0, CH$_2$Cl$_2$).

^{1}H NMR (300 MHz, CDCl$_3$) δ 7.86 (d, *J* = 7.6 Hz, 1H), 7.58–7.48 (m, 2H), 7.45–7.20 (m, 6H), 3.05 (s,

1H), 2.70 (s, 3H).

^{13}C NMR (75 MHz, CDCl$_3$) δ 138.0, 132.9, 132.7, 132.0, 129.7, 129.5, 128.8, 128.6, 125.9, 124.2 (q, J = 285.0 Hz), 121.3, 88.8, 85.2, 74.2 (q, J = 32.8 Hz), 21.9 (q, J = 2.5 Hz).

^{19}F NMR (282 MHz, CDCl$_3$) δ –79.03.

IR (film): v (cm^{-1}) 3544, 3063, 2931, 2229, 1599, 1488, 1448, 1350, 1242, 1174, 1124, 1083, 1051, 1002, 916, 757, 730, 690, 657, 629, 585, 555, 524, 456.

HRMS (ESI, m/z) calcd for C$_{17}$H$_{13}$F$_3$O [M]$^+$: 290.0918, found: 290.0901.

All spectroscopic data are in agreement with the literature.[24]

(*S*)-1,1,1-Trifluoro-2-(4-methoxyphenyl)-4-phenylbut-3-yn-2-ol (26q).
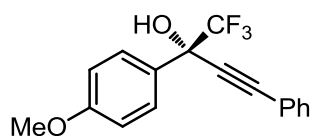
Starting from 2,2,2-trifluoro-1-(4-methoxyphenyl)ethanone (40.8 mg, 0.20 mmol) and phenylacetylene (61.3 mg, 0.60 mmol) according to the general procedure to give **26q** as a colorless oil (55.1 mg, 0.180 mmol, yield: 90%, R$_f$ = 0.3, EtOAc/n-hexane = 1:10). Enantiomeric excess established by HPLC analysis using a Chiralcel OJ-H column, ee = 98.8% (HPLC: OJ-H, 254 nm, hexane/isopropanol = 85:15, flow rate 1.0 mL/min, 25 °C, t$_r$ (minor) = 13.3 min, t$_r$ (major) = 34.5 min). [α]$_D^{25}$ = –24.6° (c 1.0, CH$_2$Cl$_2$).

^{1}H NMR (300 MHz, CDCl$_3$) δ 7.74 (d, J = 8.6 Hz, 2H), 7.59–7.49 (m, 2H), 7.46–7.31 (m, 3H), 7.03–6.91 (m, 2H), 3.84 (s, 3H), 3.14 (s, 1H).

^{13}C NMR (75 MHz, CDCl$_3$) δ 160.7, 132.2, 129.6, 128.7, 128.6, 127.6, 123.6 (q, J = 283.5 Hz), 121.2, 113.8, 88.1, 84.8, 73.3 (q, J = 32.3 Hz), 55.5.

^{19}F NMR (282 MHz, CDCl$_3$) δ –80.47.

HRMS (FD, m/z) calcd for C$_{17}$H$_{13}$F$_3$O$_2$ [M]$^+$: 306.0868, found: 306.0883.

All spectroscopic data are in agreement with the literature.[20]

(*S*)-2-(4-Bromophenyl)-1,1,1-Trifluoro-4-phenylbut-3-yn-2-ol (26r)
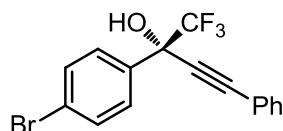
Starting from 1-(4-bromophenyl)-2,2,2-trifluoroethanone (50.6 mg, 0.20 mmol) and phenyl-acetylene (61.3 mg, 0.60 mmol) according to the general procedure to give **26r** as a colorless oil (70.2 mg, 0.198 mmol, yield: 99%, R_f = 0.3, EtOAc/*n*-hexane = 1:10). Enantiomeric excess established by HPLC analysis using a Chiralcel OJ-H column, *ee* = 99.0% (HPLC: OJ-H, 254 nm, hexane/isopropanol = 85:15, flow rate 1.0 mL/min, 25 °C, t_r (minor) = 6.6 min, t_r (major) = 8.1 min). $[\alpha]_D^{25}$ = −15.2° (*c* 1.0, CH$_2$Cl$_2$).

^{1}H NMR (300 MHz, CDCl$_3$) δ 7.69 (d, *J* = 8.4 Hz, 2H), 7.62–7.50 (m, 4H), 7.47–7.33 (m, 3H), 3.14 (s, 1H).

^{13}C NMR (75 MHz, CDCl$_3$) δ 134.5, 132.2, 131.6, 129.9, 129.1, 128.7, 124.2, 123.3 (q, *J* = 284.0 Hz) 120.8, 88.6, 84.0, 73.2 (q, *J* = 32.5 Hz).

^{19}F NMR (282 MHz, CDCl$_3$) δ −80.39.

HRMS (FD, *m/z*) calcd for C$_{16}$H$_{10}$BrF$_3$O [M]$^+$: 353.9867, found: 353.9852.

All spectroscopic data are in agreement with the literature.[20]

(*S*)-2-(3-Bromophenyl)-1,1,1-Trifluoro-4-phenylbut-3-yn-2-ol (26s)
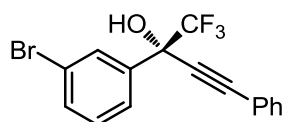
Starting from 1-(3-bromophenyl)-2,2,2-trifluoroethanone (50.6 mg, 0.20 mmol) and phenylacetylene (61.3 mg, 0.60 mmol) according to the general procedure to give **26s** as a colorless oil (70.1 mg, 0.198 mmol, yield: 99%, R_f = 0.3, EtOAc/*n*-hexane = 1:10). Enantiomeric excess established by HPLC analysis using a Chiralcel OJ-H column, *ee* = 98.8% (HPLC: OJ-H, 254 nm, hexane/isopropanol = 85:15, flow rate 1.0 mL/min, 25 °C, t_r (minor) = 5.9 min, t_r (major) = 8.1 min). $[\alpha]_D^{25}$ = −53.2° (*c* 1.0, CH$_2$Cl$_2$).

^{1}H NMR (300 MHz, CDCl$_3$) δ 7.98 (s, 1H), 7.85–7.71 (m, 1H), 7.62–7.50 (m, 3H), 7.49–7.27 (m, 4H), 3.13 (s, 1H).

^{13}C NMR (75 MHz, CDCl$_3$) δ 137.6, 132.8, 132.3, 130.5, 130.5, 129.9, 128.7, 126.1, 123.3 (q, *J* = 284.0 Hz), 122.5, 120.8, 88.8, 83.9, 73.0 (q, *J* = 32.5 Hz).

^{19}F NMR (282 MHz, CDCl$_3$) δ −80.22.

HRMS (FD, *m/z*) calcd for C$_{16}$H$_{10}$BrF$_3$O [M]$^+$: 353.9867, found: 353.9848.

All spectroscopic data are in agreement with the literature.[20]

(*S*)-1,1,1-Trifluoro-4-phenyl-2-(4-(trifluoromethyl)phenyl)but-3-yn-2-ol (26t)
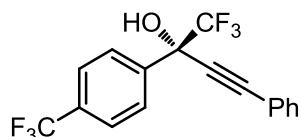
Starting from 2,2,2-trifluoro-1-(4-(trifluoromethyl)phenyl)ethanone (48.4 mg, 0.20 mmol) and phenylacetylene (61.3 mg, 0.60 mmol) according to the general procedure to give **26t** as a colorless oil (68.5 mg, 0.199 mmol, yield: 99%, R$_f$ = 0.3, EtOAc/*n*-hexane = 1:10). Enantiomeric excess established by HPLC analysis using a Chiralpak IG column, *ee* = 98.8% (HPLC: IG, 254 nm, hexane/isopropanol = 99:1, flow rate 1.0 mL/min, 25 °C, t$_r$ (minor) = 7.7 min, t$_r$ (major) = 12.4 min). [α]$_D$^{25} = −10.8° (*c* 1.0, CH$_2$Cl$_2$).

^{1}H NMR (300 MHz, CDCl$_3$) δ 7.96 (d, *J* = 8.3 Hz, 2H), 7.71 (d, *J* = 8.3 Hz, 2H), 7.63–7.50 (m, 2H), 7.48–7.33 (m, 3H), 3.21 (s, 1H).

^{13}C NMR (75 MHz, CDCl$_3$) δ 139.3, 132.3, 131.9 (q, *J* = 32.5 Hz), 130.0, 128.7, 128.0, 127.9, 125.4 (q, *J* = 3.8 Hz), 124.0 (q, *J* = 270.5 Hz), 123.0 (q, *J* = 284.0 Hz), 121.4, 88.9, 83.8, 73.2 (q, *J* = 32.5 Hz).

^{19}F NMR (282 MHz, CD$_3$OD) δ −80.24, −62.85.

IR (film): *v* (cm^{-1}) 3601, 3064, 2233, 1619, 1490, 1414, 1323, 1245, 1167, 1128, 1071, 1010, 921, 840, 800, 756, 721, 688, 631, 595, 529, 457, 408.

HRMS (FD, *m/z*) calcd for C$_{17}$H$_{10}$F$_6$O [M]$^+$: 344.0636, found: 344.0622.

(*S*)-1,1,1-Trifluoro-2-(naphthalen-2-yl)-4-phenylbut-3-yn-2-ol (26u)
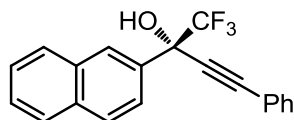
Starting from 2,2,2-trifluoro-1-(naphthalen-1-yl)ethanone (44.8 mg, 0.20 mmol) and phenylacetylene (61.3 mg, 0.60 mmol) according to the general procedure to give **26u** as a white solid (62.5 mg, 0.192 mmol, yield: 96%, R$_f$ = 0.2, EtOAc/*n*-hexane = 1:10). MP: 59 °C. Enantiomeric excess established by

HPLC analysis using a Chiralcel OJ-H column, *ee* = 98.8% (HPLC: OJ-H, 254 nm, hexane/isopropanol = 85:15, flow rate 1.0 mL/min, 25 °C, t_r (minor) = 11.0 min, t_r (major) = 22.5 min). $[\alpha]_D^{25}$ = −19.2° (*c* 1.0, CH_2Cl_2).

^{1}H NMR (300 MHz, CDCl$_3$) δ 8.35 (s, 1H), 8.06–7.80 (m, 4H), 7.72–7.49 (m, 4H), 7.48–7.31 (m, 3H), 3.25 (s, 1H).

^{13}C NMR (75 MHz, CDCl$_3$) δ 133.8, 132.9, 132.8, 132.3, 129.8, 128.8, 128.7, 128.2, 127.8, 127.21, 127.16, 126.6, 124.4, 123.7 (q, *J* =283.8 Hz), 121.1, 88.5, 84.7, 73.7 (q, *J* =32.3 Hz). ^{19}F NMR (282 MHz, CDCl$_3$) δ −79.90.

HRMS (FD, *m/z*) calcd for $C_{20}H_{13}F_3O$ [M]$^+$: 326.0918, found: 326.0915.

All spectroscopic data are in agreement with the literature.[21]

(*S*)-1,5-Diphenyl-3-(trifluoromethyl)pent-1-yn-3-ol (26v)
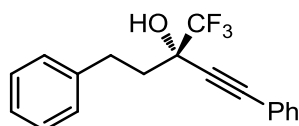
Starting from 1,1,1-trifluoro-4-phenylbutan-2-one (40.4 mg, 0.20 mmol) and phenylacetylene (61.3 mg, 0.60 mmol) according to the general procedure to give **26v** as a colorless oil (26.8 mg, 0.088 mmol, yield: 44%, R_f = 0.3, EtOAc/*n*-hexane = 1:10). Enantiomeric excess established by HPLC analysis using a Chiralcel OJ-H column, *ee* = 62.4% (HPLC: OJ-H, 254 nm, hexane/isopropanol = 85:15, flow rate 1.0 mL/min, 25 °C, t_r (minor) = 8.2 min, t_r (major) = 9.1 min). $[\alpha]_D^{25}$ = 26.6° (*c* 1.0, CH_2Cl_2).

^{1}H NMR (300 MHz, CDCl$_3$) δ 7.56–7.47 (m, 2H), 7.43–7.19 (m, 8H), 3.11–2.96 (m, 2H), 2.65 (s, 1H), 2.33–2.14 (m, 2H).

^{13}C NMR (75 MHz, CDCl$_3$) δ 141.0, 132.2, 129.6, 128.7, 128.63, 128.61, 126.4, 124.2 (q, *J* =283.5 Hz), 121.2, 88.1, 83.5, 72.4 (q, *J* =31.5 Hz), 36.8, 30.0.

^{19}F NMR (282 MHz, CDCl$_3$) δ −81.53.

HRMS (FD, *m/z*) calcd for $C_{18}H_{15}F_3O$ [M]$^+$:304.1075, found: 304.1070.

All spectroscopic data were in agreement with the literature.[24]

(*R*)-Ethyl 2-hydroxy-4-phenyl-2-(trifluoromethyl)but-3-ynoate (26w)
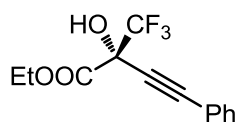
Starting from ethyl trifluoropyruvate (34.0 mg, 0.20 mmol) and phenylacetylene (61.3 mg, 0.60 mmol) according to the general procedure to give **26w** as a colorless oil (37.9 mg, 0.139 mmol, yield: 70%, R_f = 0.3, EtOAc/*n*-hexane = 1:10). Enantiomeric excess established by HPLC analysis using a Chiralcel OJ-H column, *ee* = 6.8% (HPLC: OJ-H, 254 nm, hexane/isopropanol = 90:10, flow rate 1.0 mL/min, 25 °C, t_r (minor) = 8.1 min, t_r (major) = 9.5 min).

^{1}H NMR (300 MHz, CDCl$_3$) δ 7.60–7.46 (m, 2H), 7.47–7.27 (m, 3H), 4.58–4.37 (m, 2H), 4.28 (s, 1H), 1.40 (t, J = 7.1 Hz, 3H).

^{13}C NMR (75 MHz, CDCl$_3$) δ 166.7, 132.3, 129.8, 128.5, 121.9 (q, J =284.5 Hz), 120.8, 87.4, 79.9, 71.9 (q, J =34.0 Hz), 65.2, 14.0.

^{19}F NMR (282 MHz, CDCl$_3$) δ −78.19.

All spectroscopic data are in agreement with the literature.[25]

(*S*)-1-Chloro-1,1-difluoro-2,4-diphenylbut-3-yn-2-ol (26x)
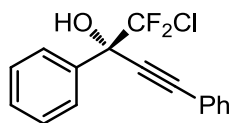
Starting from 2-chloro-2,2-difluoro-1-phenylethanone (38.1 mg, 0.20 mmol) and phenylacetylene (61.3 mg, 0.60 mmol) according to the general procedure to give **26x** as a colorless oil (57.7 mg, 0.176 mmol, yield: 99%, R_f = 0.4, EtOAc/*n*-hexane = 1:10). Enantiomeric excess established by HPLC analysis using a Chiralcel OJ-H column, *ee* = 99.4% (HPLC: OJ-H, 254 nm, hexane/isopropanol = 60:40, flow rate 1.0 mL/min, 25 °C, t_r (minor) = 6.9 min, t_r (major) = 16.0 min). $[\alpha]_D^{25}$ = −26.8° (*c* 1.0, CH$_2$Cl$_2$).

^{1}H NMR (300 MHz, CDCl$_3$) δ 7.88–7.85 (m, 2H), 7.61–7.52 (m, 2H), 7.51–7.33 (m, 6H), 3.30 (s, 1H).

^{13}C NMR (75 MHz, CDCl$_3$) δ 135.6, 132.2, 129.7, 129.6 (t, J = 300.0 Hz), 129.2, 128.6, 128.2, 127.9, 121.2, 88.5, 85.6, 77.4(t, J = 27.7 Hz).

^{19}F NMR (282 MHz, CDCl$_3$) δ −63.85, −64.41, −65.52, −66.08.

HRMS (FD, *m/z*) calcd for C$_{16}$H$_{11}$ClF$_2$O [M]$^+$: 292.0466, found: 292.0450.

All spectroscopic data are in agreement with the literature.[20]

Procedure for the synthesis of (*S*)-28a
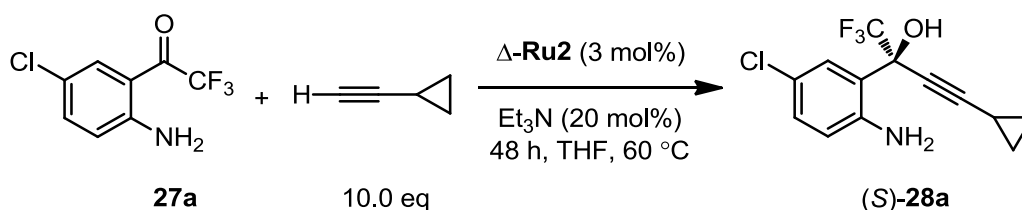
A dried 10 mL Schlenk tube was charged with the catalyst Δ-**Ru2** (3.0 mg, 3 mol%) and 1-(2-amino-5-chlorophenyl)-2,2,2-trifluoroethanone **27a** (22.4 mg, 0.20 mmol). The tube was purged with nitrogen, THF (0.2 mL) and Et$_3$N (2.8 μL, 0.2 eq) were added via syringe, and followed by cyclopropylacetylene (84.7 μL, 10.0 eq). The vial was sealed and the reaction was stirred at 60 °C for 48 hours under nitrogen atmosphere. The solvent was removed and the residue was purified by flash chromatography on silica gel (EtOAc/hexane = 1:50) to afford 7.1 mg (25% yield, R$_f$ = 0.2, EtOAc/*n*-hexane = 1:5) of **27a** as a light yellow solid. Racemic sample was obtained by using *rac*-**Ru2**. The (*S*)-configuration of the product (*S*)-**28a** was obtained by using Δ-**Ru2** as catalyst. The (*S*)-configuration of the product **28a** was assigned by comparison with published chiral HPLC retention time data. Chiral HPLC with (*S*)-**28a:** (Daicel Chiralpak AD-H column, 254 nm, hexane/isopropanol = 85:15, flow rate 1.0 mL/min, 25 °C) t$_r$ (major) = 7.3 min, t$_r$ (minor) = 11.9 min. Lit.[26]: t$_r$ (major) = 6.8 min, t$_r$ (minor) = 11.1 min. Optical rotation of (*S*)-**28a:** [α]$_D^{22}$ = −53.6° (*c* 0.5, CH$_2$Cl$_2$, 99.0% *ee*).

^{1}H NMR (300 MHz, CDCl$_3$) δ 7.54 (d, *J* = 2.4 Hz, 1H), 7.12 (dd, *J* = 8.6, 2.5 Hz, 1H), 6.62 (d, *J* = 8.6 Hz, 1H), 4.44 (s, 3H), 1.43–1.34 (m, 1H), 0.99–0.76 (m, 4H).

^{13}C NMR (75 MHz, CDCl$_3$) δ 143.8, 130.5, 130.3, 124.2 (q, *J* =285.0 Hz), 123.7, 120.8, 120.7, 93.9, 74.9 (q, *J* =33.0 Hz), 70.6, 8.7, 8.6, –0.5.

^{19}F NMR (282 MHz, CDCl$_3$) δ −80.82.

All other spectroscopic data are in agreement with the literature.[26]

Procedure for the synthesis of (*S*)-28b
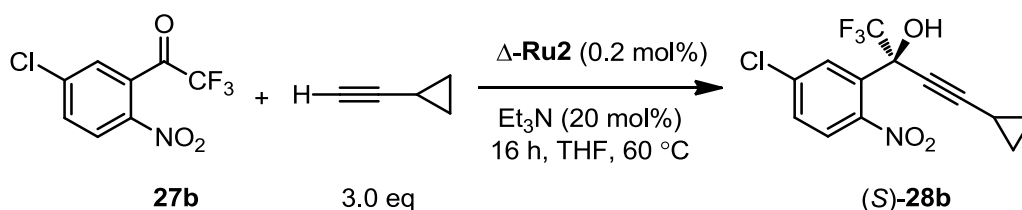
A dried 10 mL Schlenk tube was charged with 1-(5-chloro-2-nitrophenyl)-2,2,2-trifluoroethanone **27b** (50.6 mg, 0.20 mmol). The tube was purged with nitrogen, 0.4 mL of Δ-**Ru2** in THF (1.0 mg/mL) and Et₃N (5.6 μL, 0.2 eq) were added via syringe, and followed by cyclopropylacetylene (50.9 μL, 3.0 eq). The vial was sealed and the reaction was stirred at 60 °C for 16 hours under nitrogen atmosphere. The solvent was removed and the residue was purified by flash chromatography on silica gel (EtOAc/hexane = 1:50) to afford 60.6 mg (95% yield, R_f = 0.3, EtOAc/*n*-hexane = 1:5) of (*S*)-**28b** as a light-yellow oil. Racemic sample was obtained by using *rac*-**Ru2**. The (*S*)-configuration of the product (*S*)-**28b** was obtained by using Δ-**Ru2** as catalyst. The (*S*)-configuration of the product (*S*)-**28b** was assigned by comparison with published rotation data. $[\alpha]_D^{22}$ = −26.0° (*c* 1.0, CH₂Cl₂, 99.4% *ee*). Lit.[27]: $[\alpha]_D^{25}$ = −22.0° (*c* 0.38, CHCl₃, 93% *ee* for *S*-configuration).Enantiomeric excess established by HPLC analysis using a Chiralpak OD-H column, *ee* = 99.4% (HPLC: OD-H, 220 nm, hexane/isopropanol = 95:5, flow rate 1.0 mL/min, 25 °C, t_r (minor) = 7.9 min, t_r (major) = 8.8 min).

¹H NMR (300 MHz, CDCl₃) δ 7.80 (s, 1H), 7.53–7.41 (m, 2H), 3.63 (s, 1H), 1.40–1.14 (m, 1H), 0.95–0.75 (m, 4H).

¹³C NMR (75 MHz, CDCl₃) δ 148.7, 137.1, 130.5, 130.1 (q, *J* = 2.2 Hz), 129.8, 125.6, 122.7 (q, *J* = 284.8 Hz), 94.5, 71.8 (q, *J* = 33.8 Hz), 68.6, 8.4, –0.8.

¹⁹F NMR (282 MHz, CDCl₃) δ −78.28.

All other spectroscopic data are in agreement with the literature. [27]

Large-scale reaction for (*S*)-28b: A dried 25 mL Schlenk tube was charged with the catalyst Δ-**Ru2** (10 mg, 0.2 mol%) and 1-(5-chloro-2-nitrophenyl)-2,2,2-trifluoroethanone **27b** (1.268 g, 5.0 mmol). The tube was purged with nitrogen, 10 mL THF and Et₃N (138.6 μL, 0.2 eq) were added via syringe, and followed by cyclopropylacetylene (1.27 mL, 3.0 eq). The vial was sealed and the reaction was stirred at 60 °C for 16 hours under nitrogen atmosphere. The solvent was removed and the residue was purified by flash chromatography on silica gel (EtOAc/hexane = 1:50) to afford 1.555 g (97% yield) of

(*S*)-**28b** as a light-yellow oil.

Procedure for the synthesis of (*S*)-28c
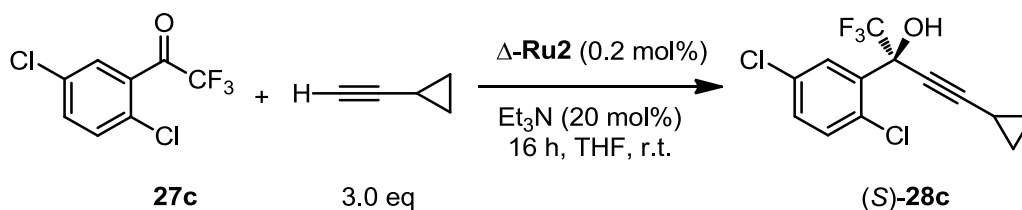
A dried 10 mL Schlenk tube was charged with 1-(2,5-dichlorophenyl)-2,2,2-trifluoroethanone **27c** (48.6 mg, 0.20 mmol). The tube was purged with nitrogen, 0.4 mL of Δ-**Ru2** in THF (1.0 mg/mL) and Et₃N (5.6 μL, 0.2 eq) were added via syringe, and followed by cyclopropylacetylene (50.9 μL, 3.0 eq). The vial was sealed and the reaction was stirred at room temperature for 16 hours under nitrogen atmosphere. The solvent was removed and the residue was purified by flash chromatography on silica gel (EtOAc/hexane = 1:50) to afford 58.5 mg (95% yield, R_f = 0.5, EtOAc/*n*-hexane = 1:10) of (*S*)-**28c** as a colourless oil. Racemic sample was obtained by using *rac*-**Ru2**. The (*S*)-configuration of the product (*S*)-**28c** was obtained by using Δ-**Ru2** as catalyst. The (*S*)-configuration of the product **28c** was assigned by comparison with published rotation data. $[\alpha]_D^{22}$ = +1.4° (*c* 1.0, CH₂Cl₂, 95.0% *ee*). Lit.[27]: $[\alpha]_D^{25}$ = +4.87° (*c* 1.39, CHCl₃, 91% ee for *S*-configuration). Enantiomeric excess established by HPLC analysis using a Chiralpak AD-H column, *ee* = 95.0% (HPLC: AD-H, 220 nm, hexane/isopropanol = 98:2, flow rate 1.0 mL/min, 25 °C, t_r (major) = 11.2 min, t_r (minor) = 14.0 min).

¹H NMR (300 MHz, CDCl₃) *δ* 7.88 (d, *J* = 2.4 Hz, 1H), 7.39–7.26 (m, 2H), 3.42 (s, 1H), 1.40–1.31 (m, 1H), 0.98–0.70 (m, 4H).

¹³C NMR (75 MHz, CDCl₃) *δ* 134.0, 132.87, 132.85, 131.3, 130.4, 130.1, 123.3 (q, *J* = 285.0 Hz), 94.1, 71.9 (q, *J* = 33.5 Hz), 69.3, 8.2 (d, *J* = 5.3 Hz), –0.54.

¹⁹F NMR (282 MHz, CDCl₃) *δ* –78.60.

All other spectroscopic data are in agreement with the literature.[27]

Large-scale reaction for (*S*)-28c: A dried 25 mL Schlenk tube was charged with the catalyst Δ-**Ru2** (8.0 mg, 0.2 mol%) and 1-(2,5-dichlorophenyl)-2,2,2-trifluoroethanone **27c** (972.0 mg, 4.0 mmol). The tube was purged with nitrogen, 8 mL THF and Et₃N (110.9 μL, 0.2 eq) were added via syringe, and followed by cyclopropylacetylene (1.02 mL, 3.0 eq). The vial was sealed and the reaction was

stirred at room temperature for 16 hours under nitrogen atmosphere. The solvent was removed and the residue was purified by flash chromatography on silica gel (EtOAc/hexane = 1:50) to afford 1.224 g (99% yield) of (*S*)-**28c** as a colorless oil.

Reference

1   SADABS. *Bruker AXS area detector scaling and absorption correction*, Bruker AXS Inc., Madison, Wisconsin, USA, **2014**.

2   G. M. Sheldrick, *Acta Cryst. A*, **2015**, *71*, 3–8.

3   SHELXL-2013, G. M. Sheldrick, University of Göttingen, Germany, 2013.

4   G. M. Sheldrick, *Acta Cryst. C*, **2015**, *71*, 3–8.

5   S. Parsons, H. Flack, T. Wagner, *Acta Cryst. B*, **2013**, *69*, 249–259.

6   E. A. Krasnokutskaya, N. I. Semenischeva, V. D. Filimonov, P.Knochel, *Synthesis* **2007**, *1*, 81–84.

7   M. W. Khan, A. Akther, M. S. Alam, *Synlett* **2014**, *25*, 0831–0834.

8   T. Su, S. Xie, B. Li, J. Yan, L. Huang, X. Li, *Synlett* **2015**, *26*, 215–220.

9   X. Shen, H. Huo, C. Wang, B. Zhang, K. Harms, E. Meggers, *Chem. Eur. J.* **2015**, *21*, 9720–9726.

10   J. Ma, X. Shen, K. Harms, E. Meggers, *Dalton Trans.* **2016**, *45*, 8320–8323.

11   E. Mihelich, D. Eickhoff, *J. Org. Chem.* **1983**, *48*, 4135–4137.

12   Y. Chen, R. Lin, C. Chen, *Tetrahedron: Asymmetry* **2004**, *15*, 3561–3571.

13   A. Malkov, M. Bell, M. Vassieu, V. Bugatti, P. Kočovský, *Journal of Molecular Catalysis A:Chemical* **2003**, *196*, 179–186.

14   L. Yang, A. Zelewsky, H. Nguyen, G. Muller, G. Labat, H. Evans, *Inorg. Chim. Acta.* **2009**, *362*, 3853–3856.

15   C. Wang, J. Qin, X. Shen, R. Riedel, K. Harms, E. Meggers, *Angew. Chem. Int. Ed.* **2016**, *55*, 685–688.

16   P. Khodakovskiy, D. Volochnyuk, D. Panov, I. Pervak, E. Zarudnitskii, O. Shishkin, A. Yurchenko,   A. Shivanyuk, A. Tolmachev, *Synthesis* **2008**, 948–956.

17   S. Ladouceur, D. Fortin, E. Zysman-Colman, *Inorg. Chem.* **2010**, *49*, 5625–5641.

18   L. Paloque, C. Hemmert, A. Valentin, H. Gornitzka, *Eur. J. Med. Chem.* **2015**, *94*, 22–29.

19 G. Stephan, A. Martin, K. Anes, W. F. Jack, H. C. Robert, *Dalton Trans*. **2002**, 2163. *J. Chem. Soc., Dalton Trans.* **2002**, 2163–2167.

20 J. Ito, S. Ubukata, S. Muraoka, H. Nishiyama, *Chem. Eur. J.* **2016**, *22*, 16801–16804.

21 G.-W. Zhang, W. Meng, H. Ma, J. Nie, W.-Q. Zhang, J.-A. Ma, *Angew. Chem. Int. Ed.* **2011**, *50*, 3538–3542.

22 H. Wang, K. -F. Yang L, Li, Y. Bai, Z. -J. Zheng, W. -Q. Zhang, Z. -W. Gao, L. -W. Xu, *ChemCatChem*, **2014**, *6*, 580–591.

23 C. A. Correia, D. T. McQuade, P. T. Seeberger, *Adv. Synth. Catal.* **2013**, *355*, 3517–3521.

24 R. Motoki, M. Kanai, M. Shibasaki, *Org. Lett.* **2007**, *9*, 2997–3000.

25 K. Aikawa, Y. Hioki, K. Mikami, *Org. Lett.* **2010**, *12*, 5716–5719.

26 N.Chinkov, A. Warm, E. M. Carreira, *Angew. Chem., Int. Ed*. **2011**, *50*, 2957–2961.

27 S. Okusu, K. Hirano, Y. Yasuda, J. Tanaka, E. Tokunaga, H. Fukaya, N. Shibata, *Org. Lett.* **2016**, *18*, 5568–5571.

Chapter 6: Appendices

6.1 List of Abbreviations

^{1}H NMR	proton nuclear magnetic resonance spectroscopy
^{13}C NMR	carbon nuclear magnetic resonance spectroscopy
^{19}F NMR	fluorine nuclear magnetic resonance spectroscopy
δ	chemical shift
J	coupling constant
br	broad
s	singlet
d	doublet
t	triplet
q	quartet
m	multiplet
ppm	parts per million
AcOH	acetic acid
aq	aqueous
Ar	argon
bpy	2,2´-bipyridine
CD	circular dichroism
CH_2Cl_2	dichloromethane
CD_2Cl_2	dideuteromethylenechloride
$CHCl_3$	chloroform
$CDCl_3$	deuterochloroform
CH_3CN/ MeCN	acetonitrile
conc	concentrated
DMAP	4-dimethylaminopyridine
DMF	dimethylformamide
DMSO	dimethyl sulfoxide
ee	enantiomeric excesses
e.g.	exempli gratia (lat.: for example)
et al.	et alii (lat.: and others)
ESI	electrospray ionization

EtOH	ethanol
Et$_2$O	diethyl ether
Et$_3$N	triethyl amine
EtOAc	ethyl acetate
EWG	electron withdrawing group
h	hour(s)
HPLC	high performance liquid chromatography
HRMS	high resolution mass spectrometry
Hz	Hertz
IR spectra	infrared spectra
Ir	iridium
L	liter(s)
M	mol/liter
m	meta-
min	minute(s)
mL	milliliter(s)
mmol	millimole
MS	mass spectroscopy
N$_2$	nitrogen
Nu	nucleophile
Ph	phenyl
ppy	2-phenylpyridine
rac	racemic
Rh	rhodium
rt	room temperature
TFA	trifluoroacetic acid
THF	tetrahydrofuran
TLC	thin layer chromatography
TPP	tetraphenylporphine
UV	ultraviolet

6.2 List of Schemes

6.3 List of Figures

6.4 List of Tables

6.5 List of Synthesized Compounds

6. 5.1 List of metal complexes

rac-, Λ- and Δ-**Ir(O)**   *rac*-, Λ- and Δ-**Rh(O)**   *rac*-, Λ- and Δ-**Ir(S)**
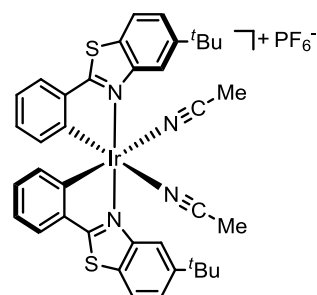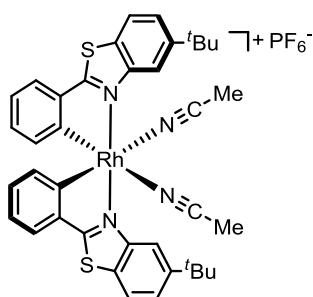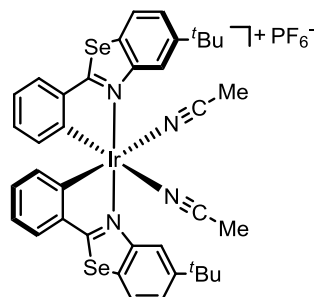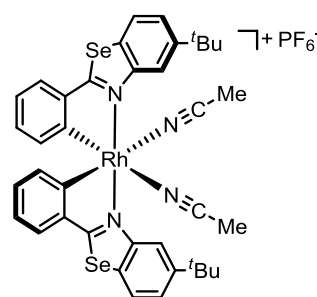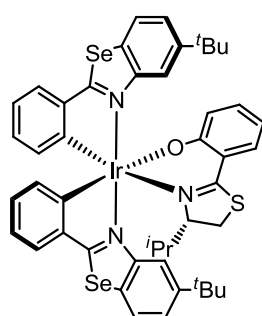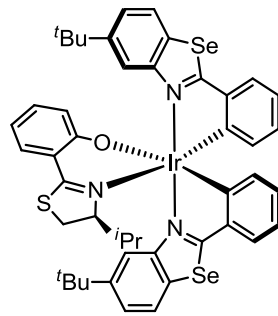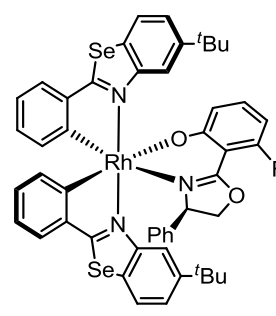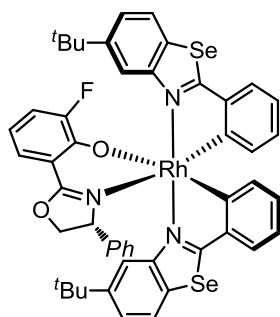
rac-, Λ- and Δ-**Rh(S)**   *rac*-, Λ- and Δ-**Ir(Se)**   *rac*-, Λ- and Δ-**Rh(Se)**

Λ-(*S*)-**3**   Δ-(*S*)-**3**   Λ-(*R*)-**4**

Δ-(*R*)-**4**   Δ-**Ru2-DPPE**

ΛΛ-**2Rh**   ΔΔ-**2Rh**   ΛΛ-**2Ir**   ΔΔ-**2Ir**

Λ-**RhPP**   Δ-**RhPP**   Λ-**IrPP**   Δ-**IrPP**

R = 3,5-Me₂Ph

rac-, Λ- and Δ-**Ru1**

rac-, Λ- and Δ-**Ru2**
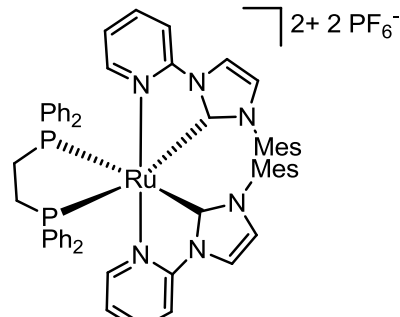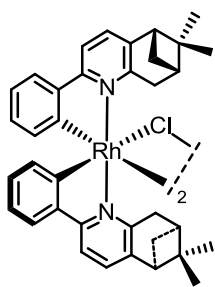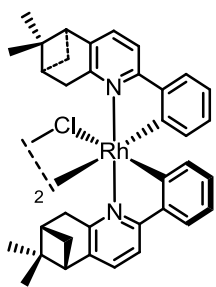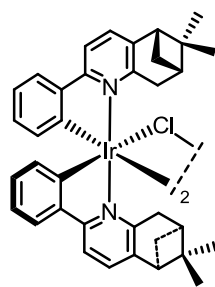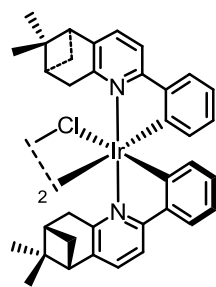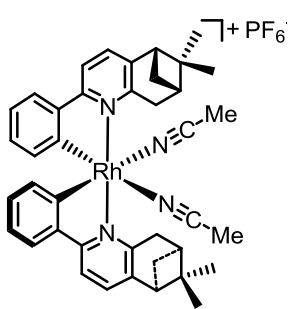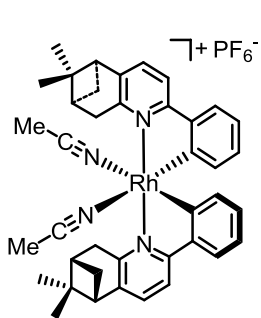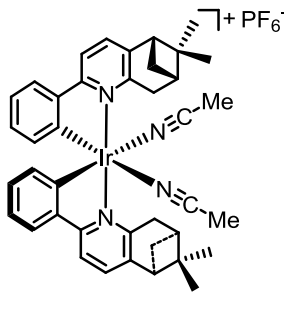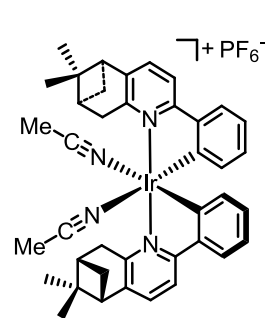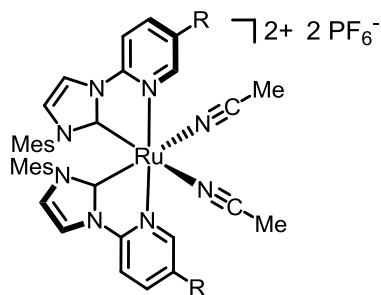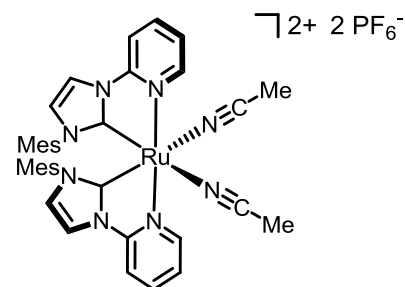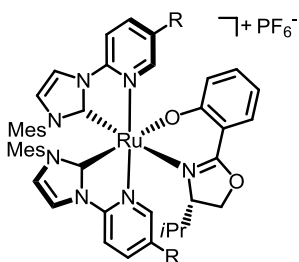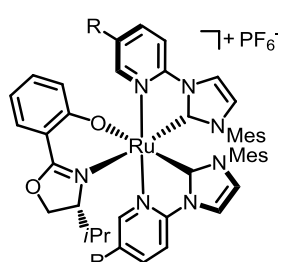
R = 3,5-Me₂Ph

R = 3,5-Me₂Ph

Λ-(*S*)-**Ru1**   Δ-(*R*)-**Ru1**   Λ-(*S*)-**Ru2**   Δ-(*R*)-**Ru2**

6.5.2 List of organic compounds
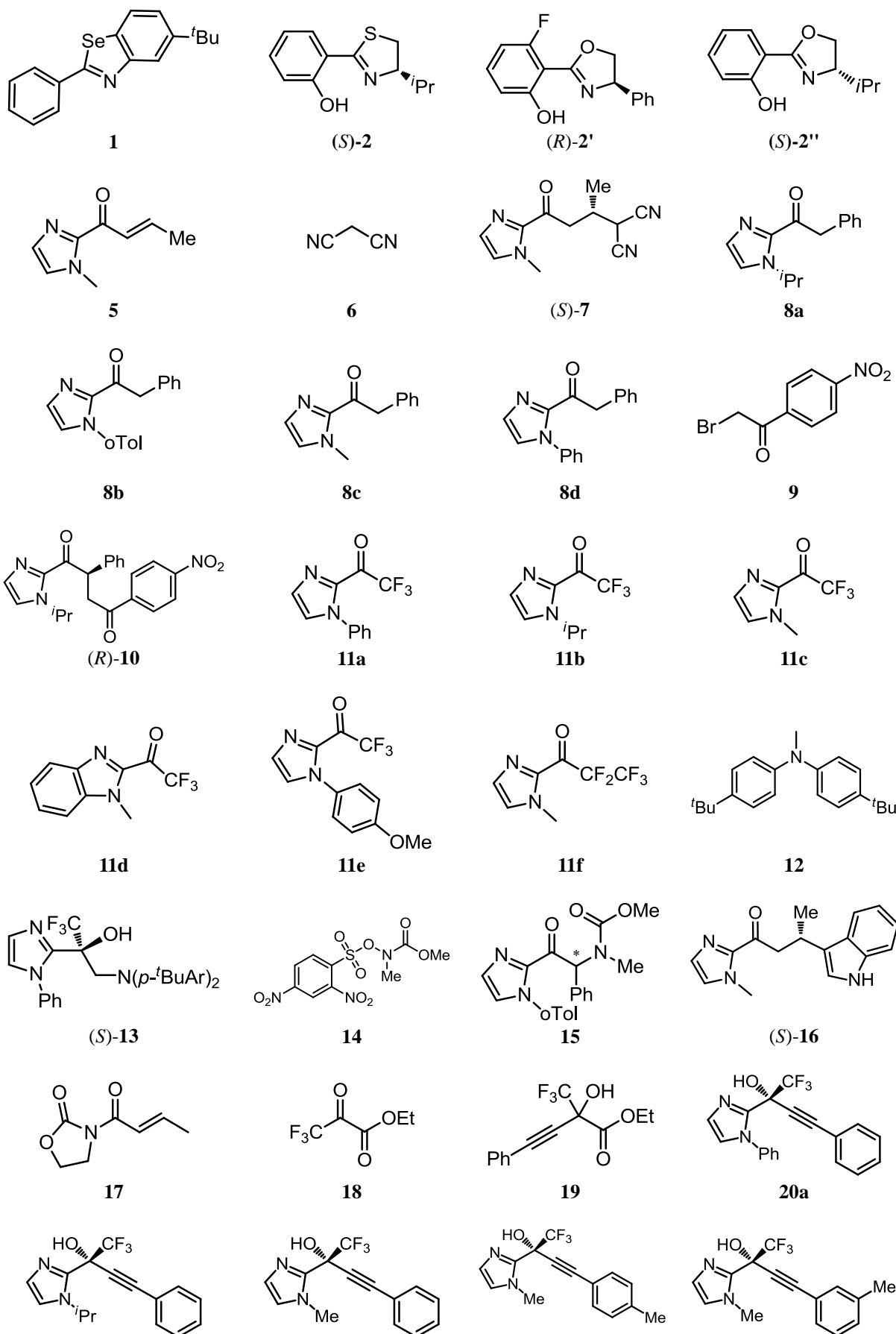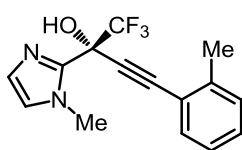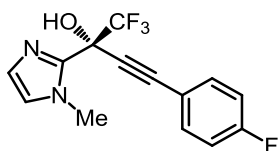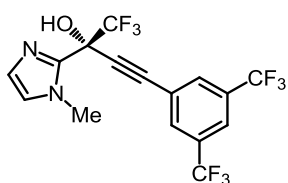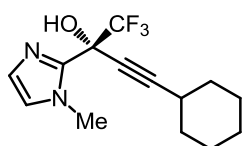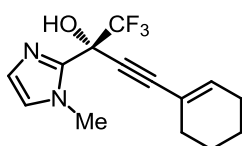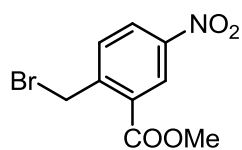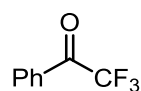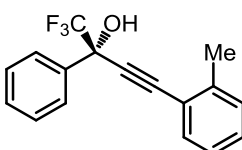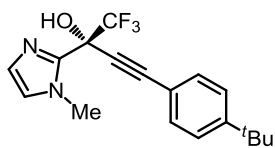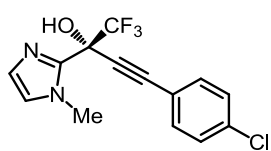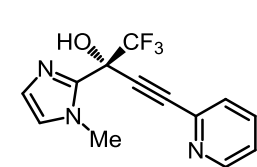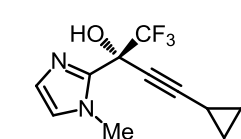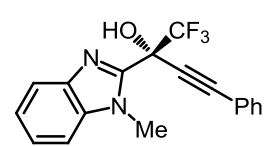
1

(*S*)-**2**

(*R*)-**2'**

(*S*)-**2''**

5

6

(*S*)-**7**

8a

8b

8c

8d

9

(*R*)-**10**

11a

11b

11c

11d

11e

11f

12

(*S*)-**13**

14

15

(*S*)-**16**

17

18

19

20a

20b

HO CF₃ / N / Me / Me

20c

HO CF₃ / N / Me / ᵗBu

20d

HO CF₃ / N / Me / Ph

20e

HO CF₃ / N / Me / OMe

20f

HO CF₃ / N / Me / F

20g

HO CF₃ / N / Me / Cl

20h

HO CF₃ / N / Me / Br

20i

HO CF₃ / N / Me / F

20j

HO CF₃ / N / Me / CF₃ / CF₃

20k

HO CF₃ / N / Me / N

20l

HO CF₃ / N / Me / S

20m

HO CF₃ / N / Me / nPent

20n

HO CF₃ / N / Me

20o

HO CF₃ / N / Me

20p

HO CF₃ / N / Me / Bn

20q

HO CF₃ / N / Me / SiMe₃

20r

HO CF₃ / N / Me

20s

HO CF₃ / N / Me / Ph

20t

HO CF₃ / N / Ph

20u

HO CF₂CF₃ / N / Ph / Ph

20v

Br / NO₂ / COOMe

20w

O / COOMe / * / N / Me / Ph / NO₂

20x

NPh₂ SiMe₃

20y

O / N / Ph / Ph / NPh₂

21

(R)-22

23

(R)-24

O / Ph CF₃

25a

F₃C OH / Ph / Ph

(S)-26a

F₃C OH / Me

(S)-26b

F₃C OH / Me

(S)-26c

F₃C OH / Me

(S)-26d

F₃C OH / OMe

(S)-26e

F₃C OH / Br

(S)-26f

F₃C OH / F
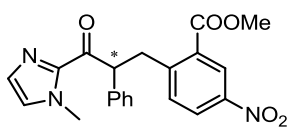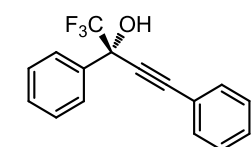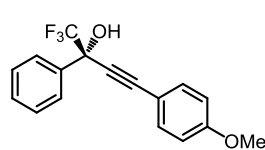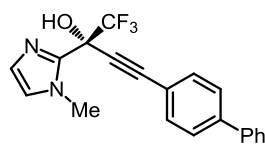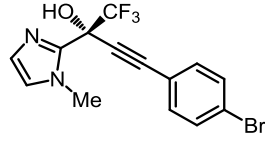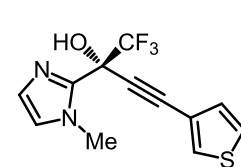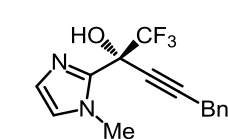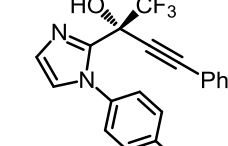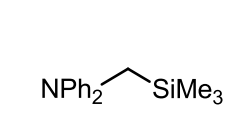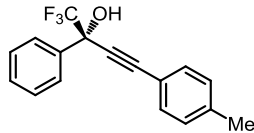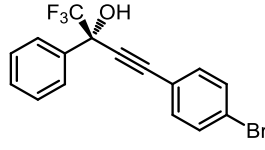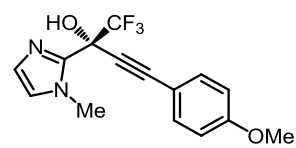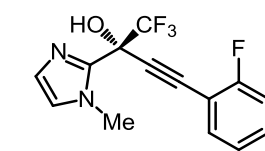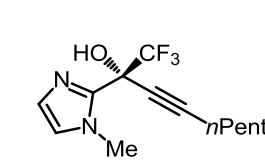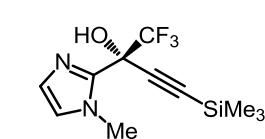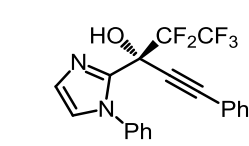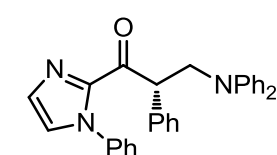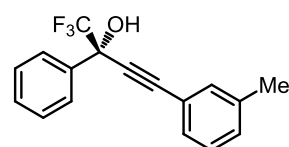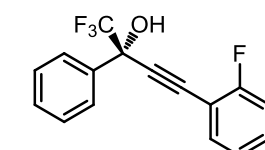
(S)-26g
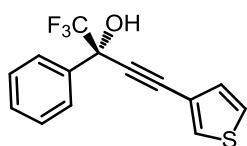
(*S*)-**26h**
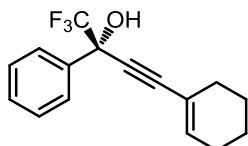
(*S*)-**26i**
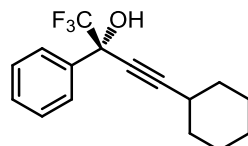
(*S*)-**26j**
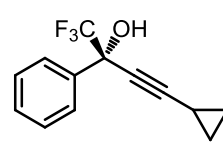
(*S*)-**26k**
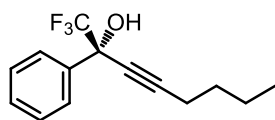
(*S*)-**26l**
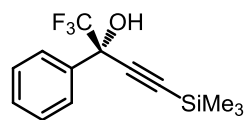
(*S*)-**26m**
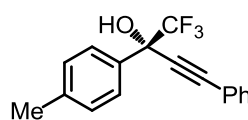
(*S*)-**26n**
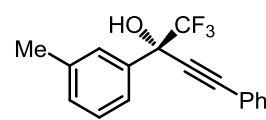
(*S*)-**26o**
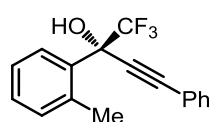
(*R*)-**26p**
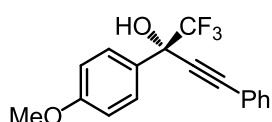
(*S*)-**26q**
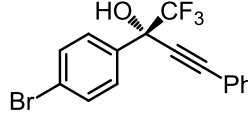
(*S*)-**26r**
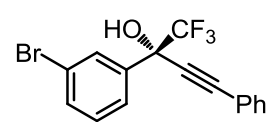
(*S*)-**26s**
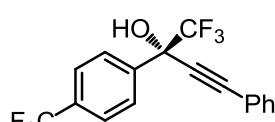
(*S*)-**26t**
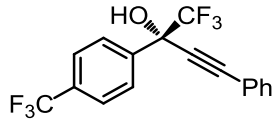
(*S*)-**26u**
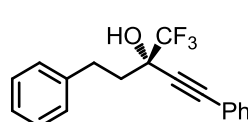
(*S*)-**26v**
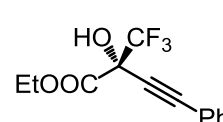
(*R*)-**26w**
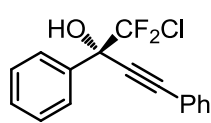
(*S*)-**26x**
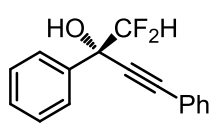
(*S*)-**26y**
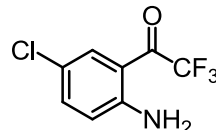
27a
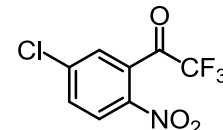
27b
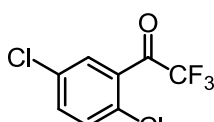
27c
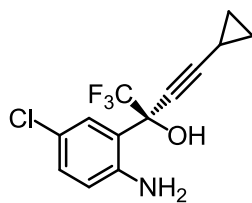
(*S*)-**28a**
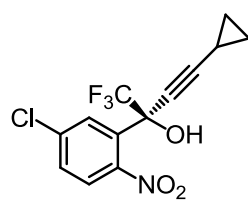
(*S*)-**28b**
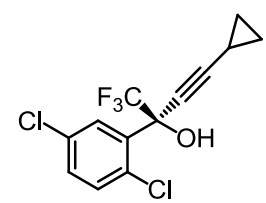
(*S*)-**28c**
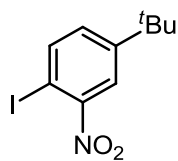
S1
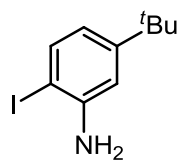
S2
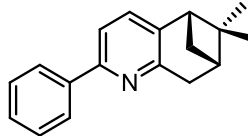
(*S*,*S*)-**PP**
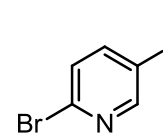
S1′
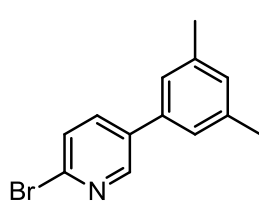
S3′
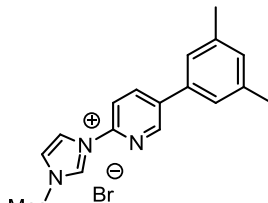
L1
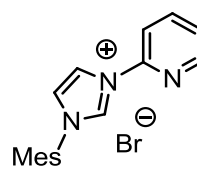
L2

6.6 List of Spectra of Complexes

6.6.1 NMR spectra of enantiopure metal complexes
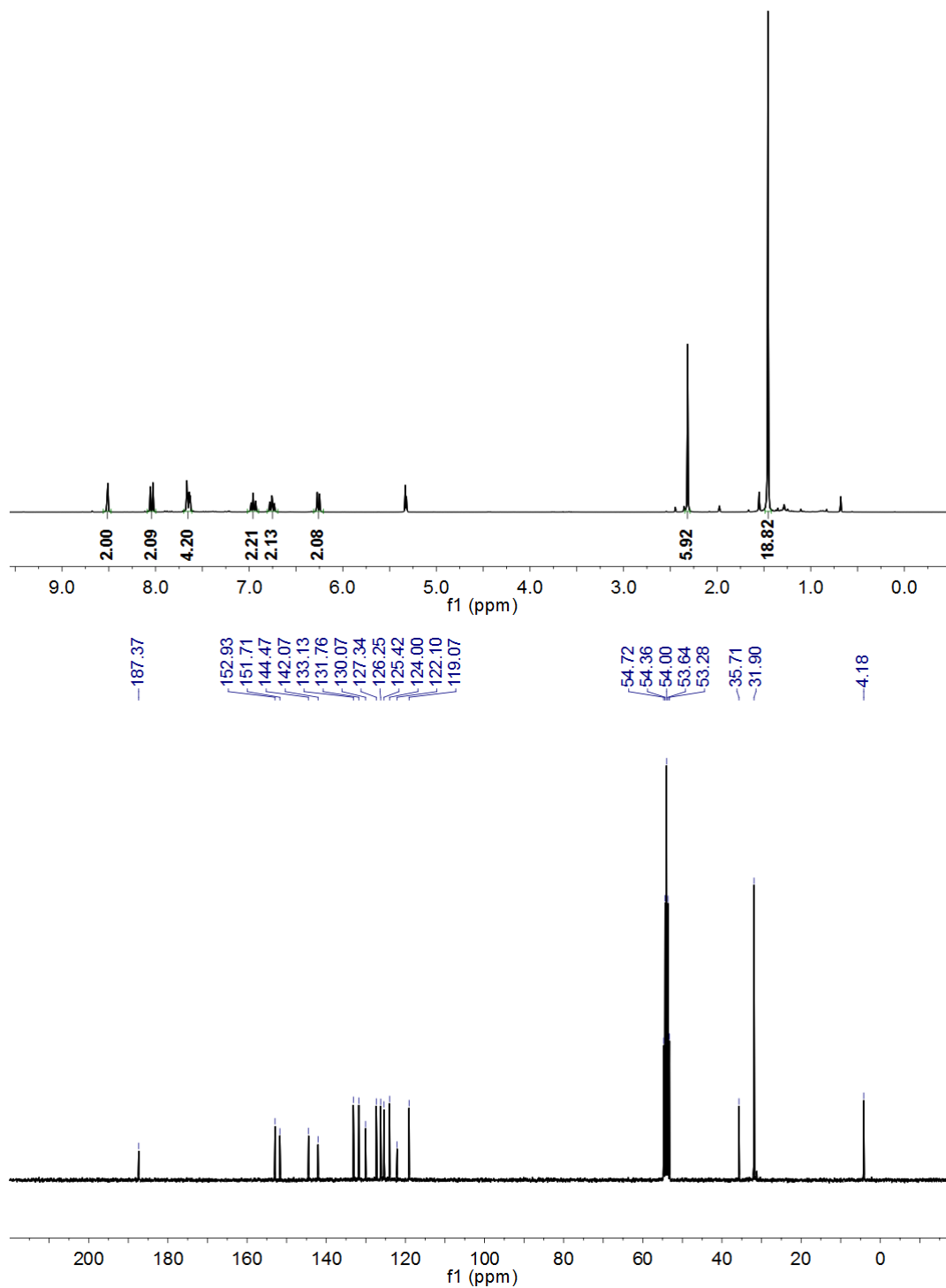
Figure 59 ^{1}H NMR and ^{13}C NMR spectra of *rac*-**Ir(Se)**.
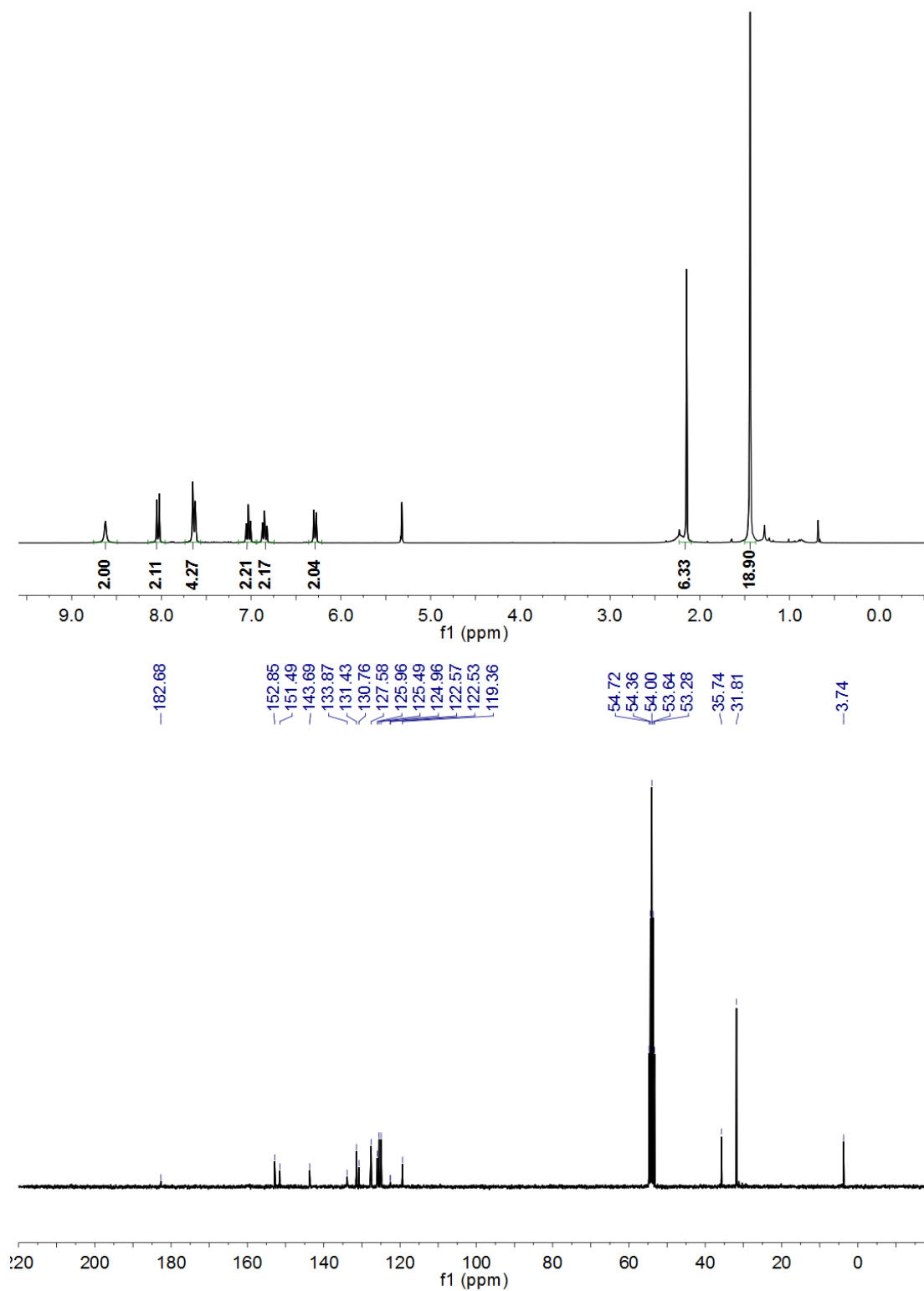
Figure 60 ^{1}H NMR and ^{13}C NMR spectra of *rac*-**Rh(Se)**.
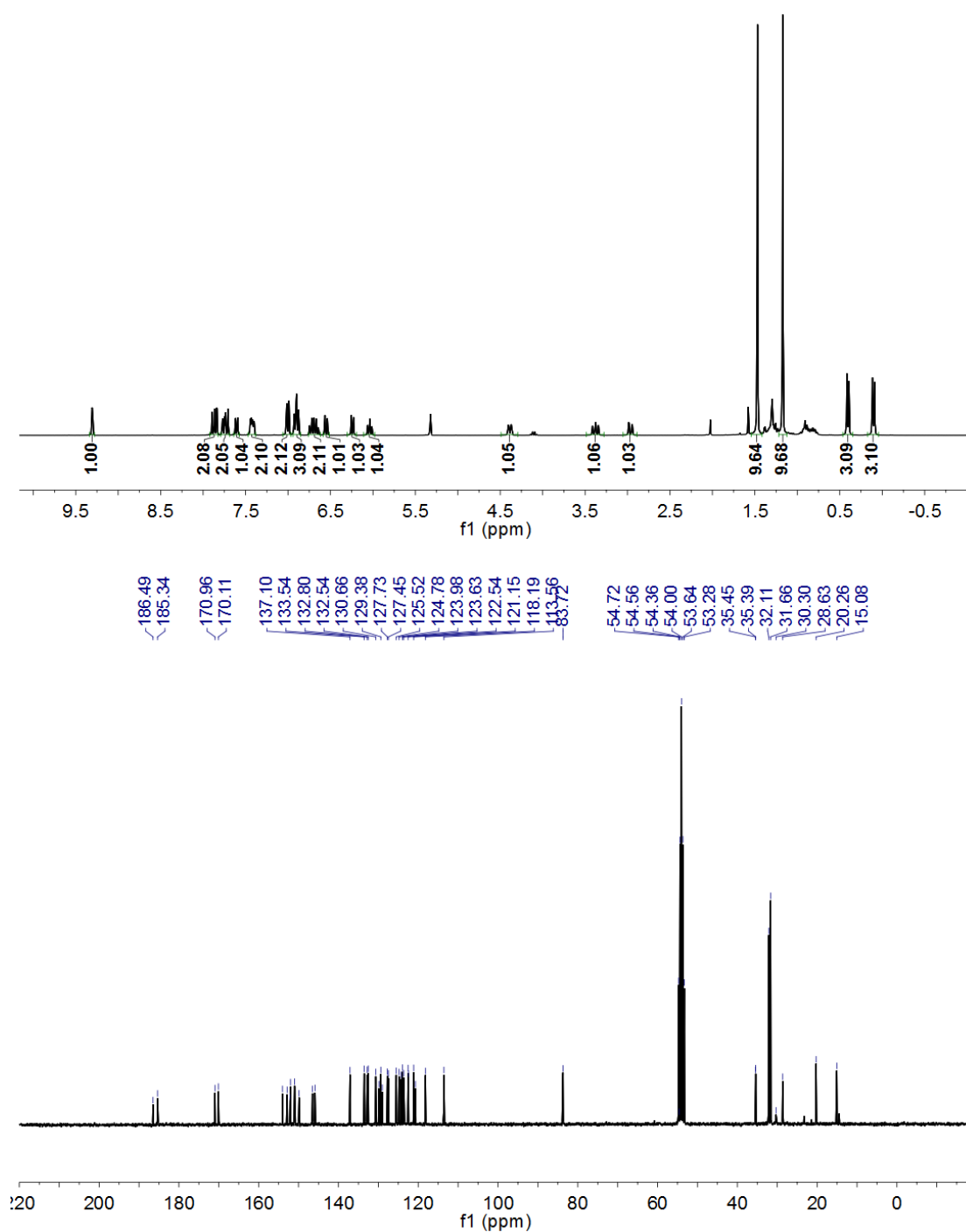
Figure 61 ¹H NMR and ¹³C NMR spectra of iridium auxiliary complex Λ-(*S*)-**3**.
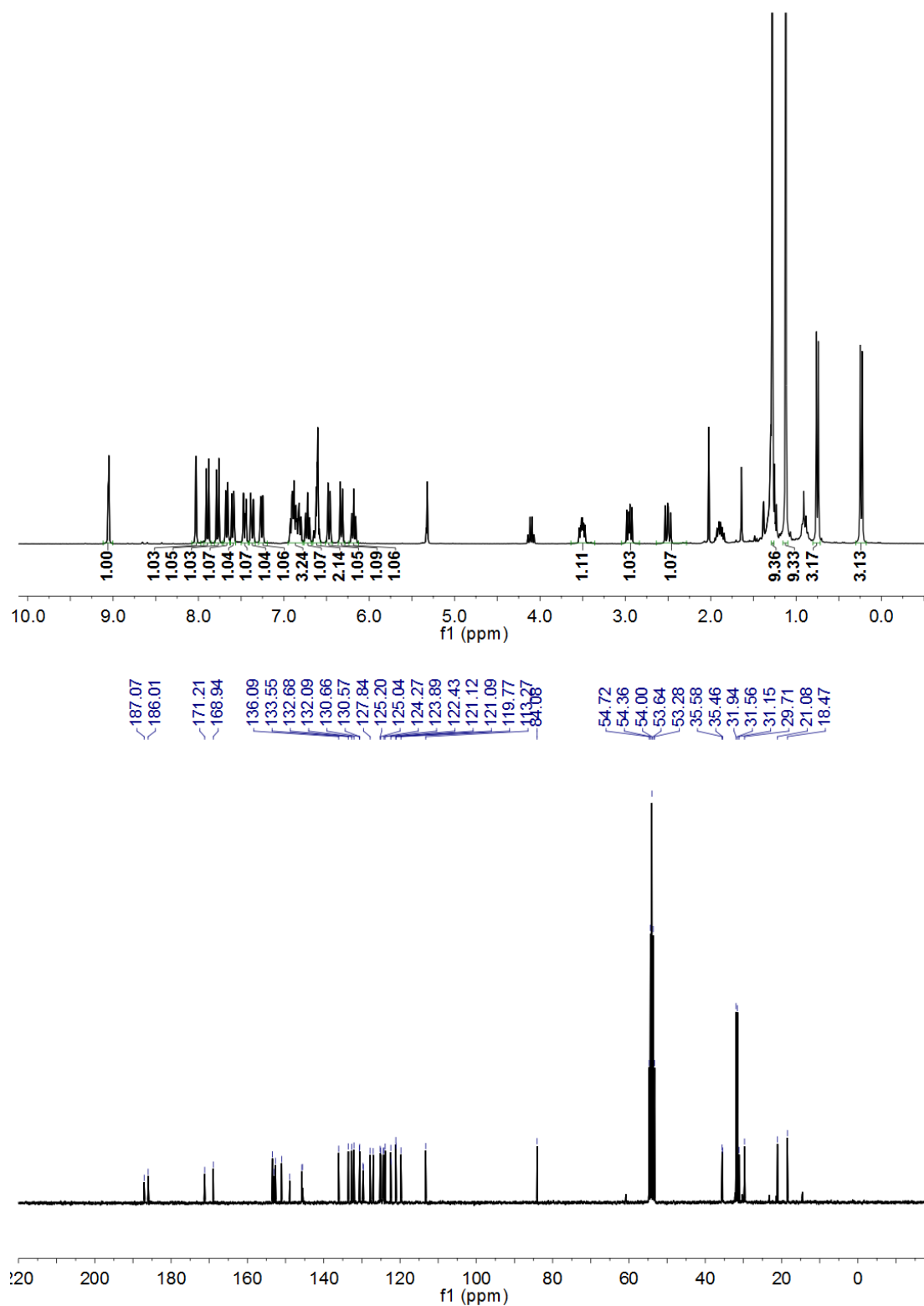
Figure 62 ^{1}H NMR and ^{13}C NMR spectra of iridium auxiliary complex Δ-(*S*)-**3**.
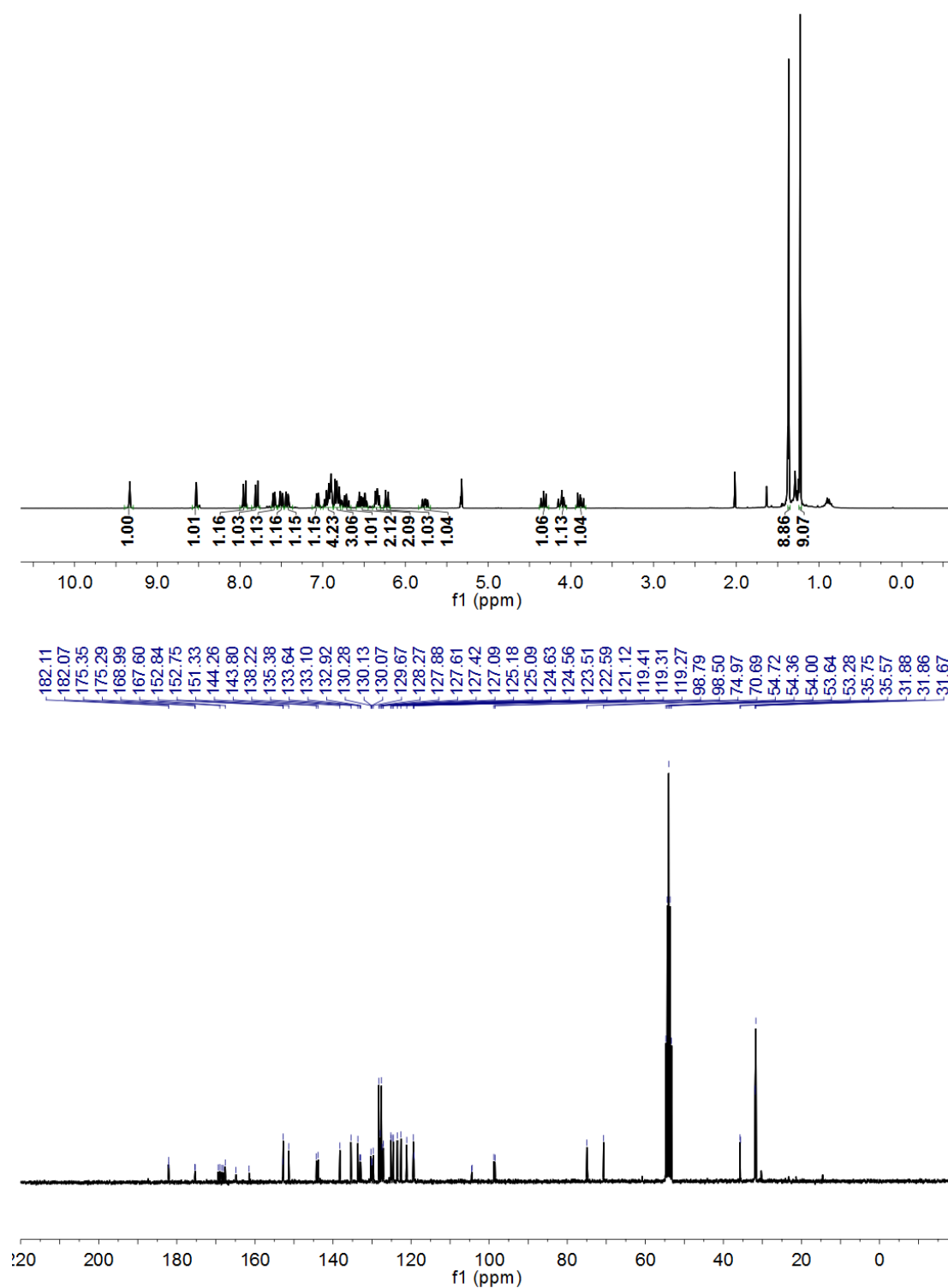
Figure 63 ^{1}H NMR and ^{13}C NMR spectra of rhodium auxiliary complex Λ-(*R*)-**4**.
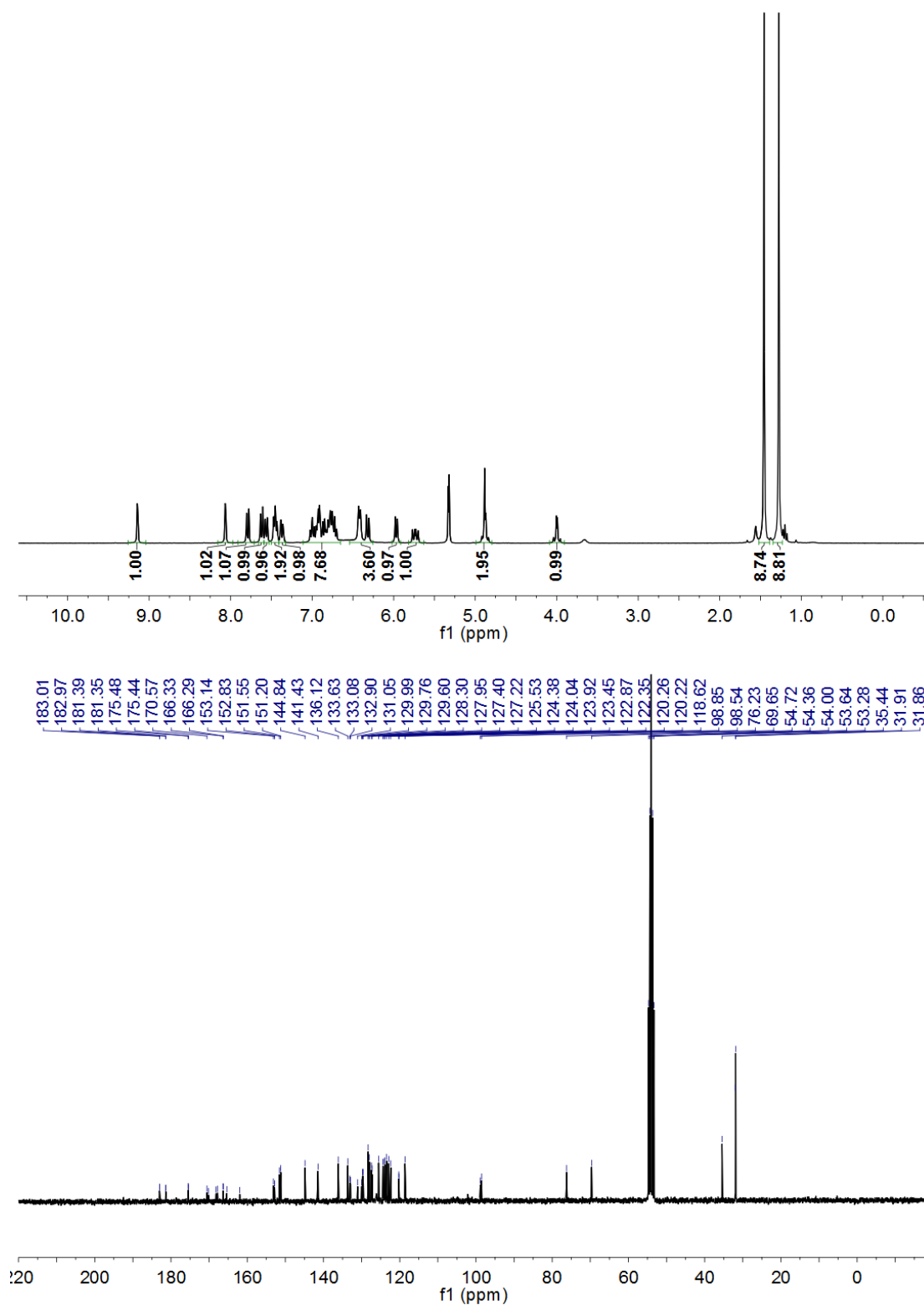
Figure 64 ^{1}H NMR and ^{13}C NMR spectrum of rhodium auxiliary complex Δ-(*R*)-**4**.
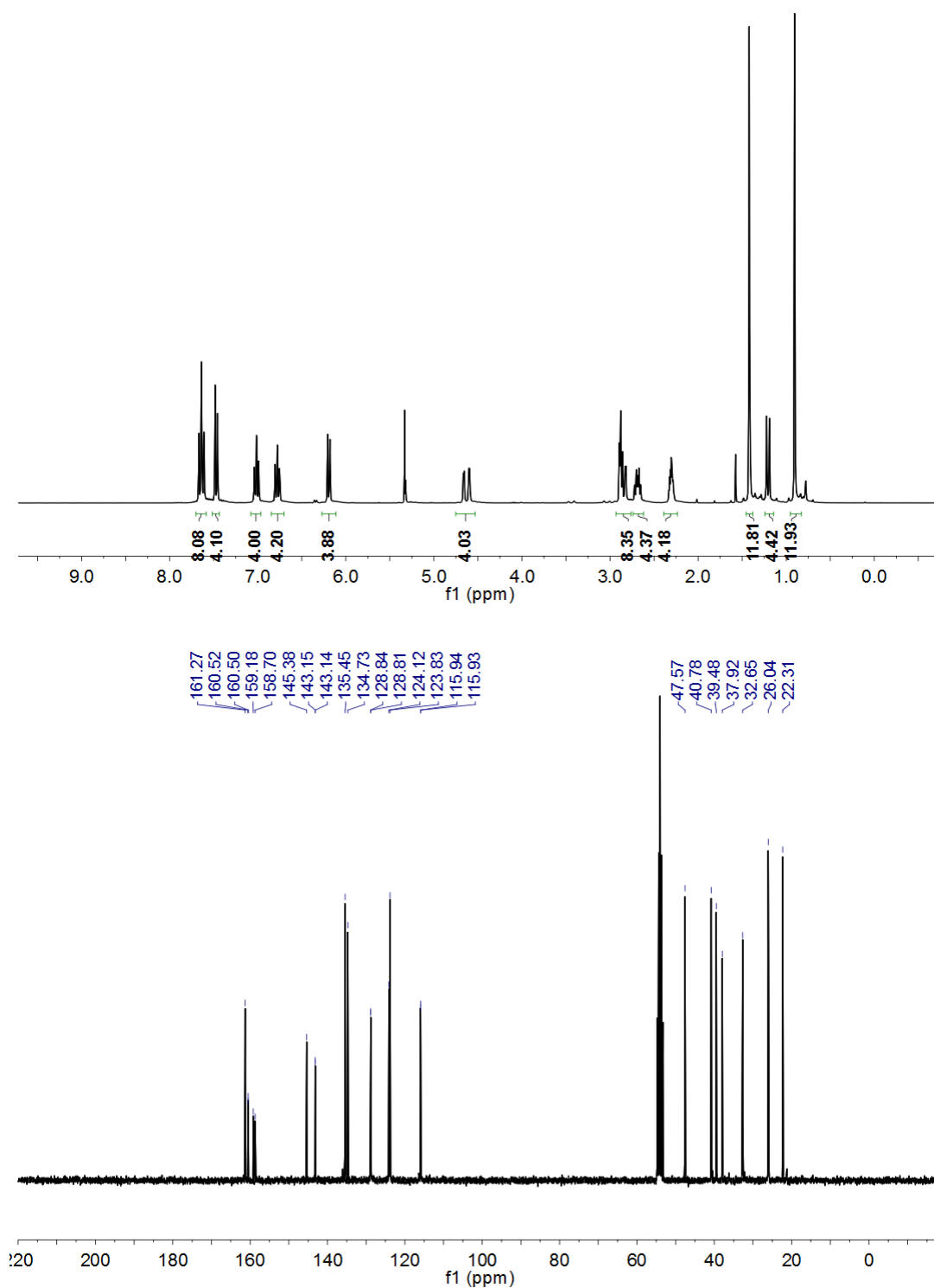
Figure 65 ^{1}H NMR and ^{13}C NMR spectra of ΛΛ-**2**$_{Rh}$.
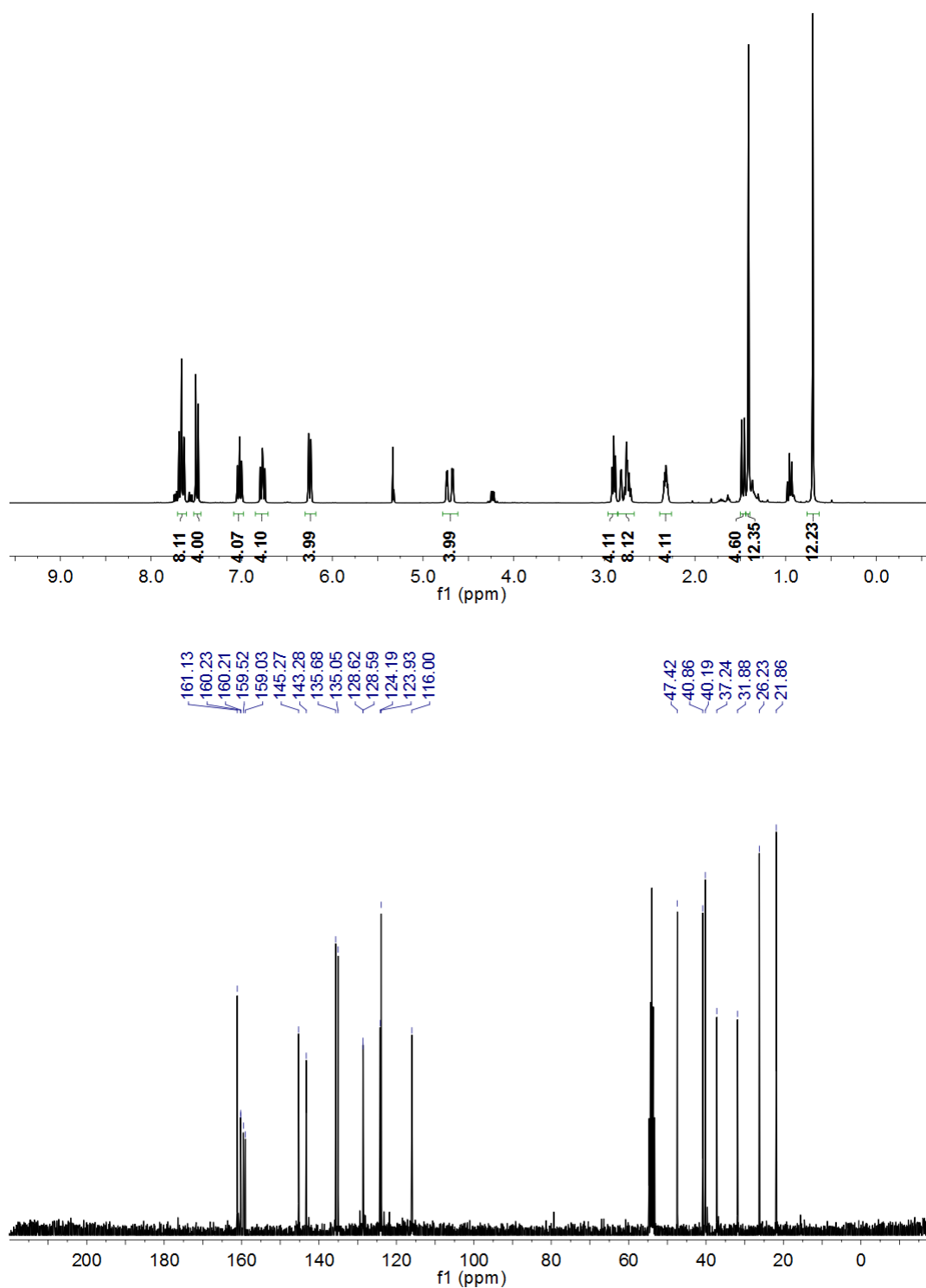
Figure 66 ^{1}H NMR and ^{13}C NMR spectra of ΔΔ-**2$_{Rh}$**.
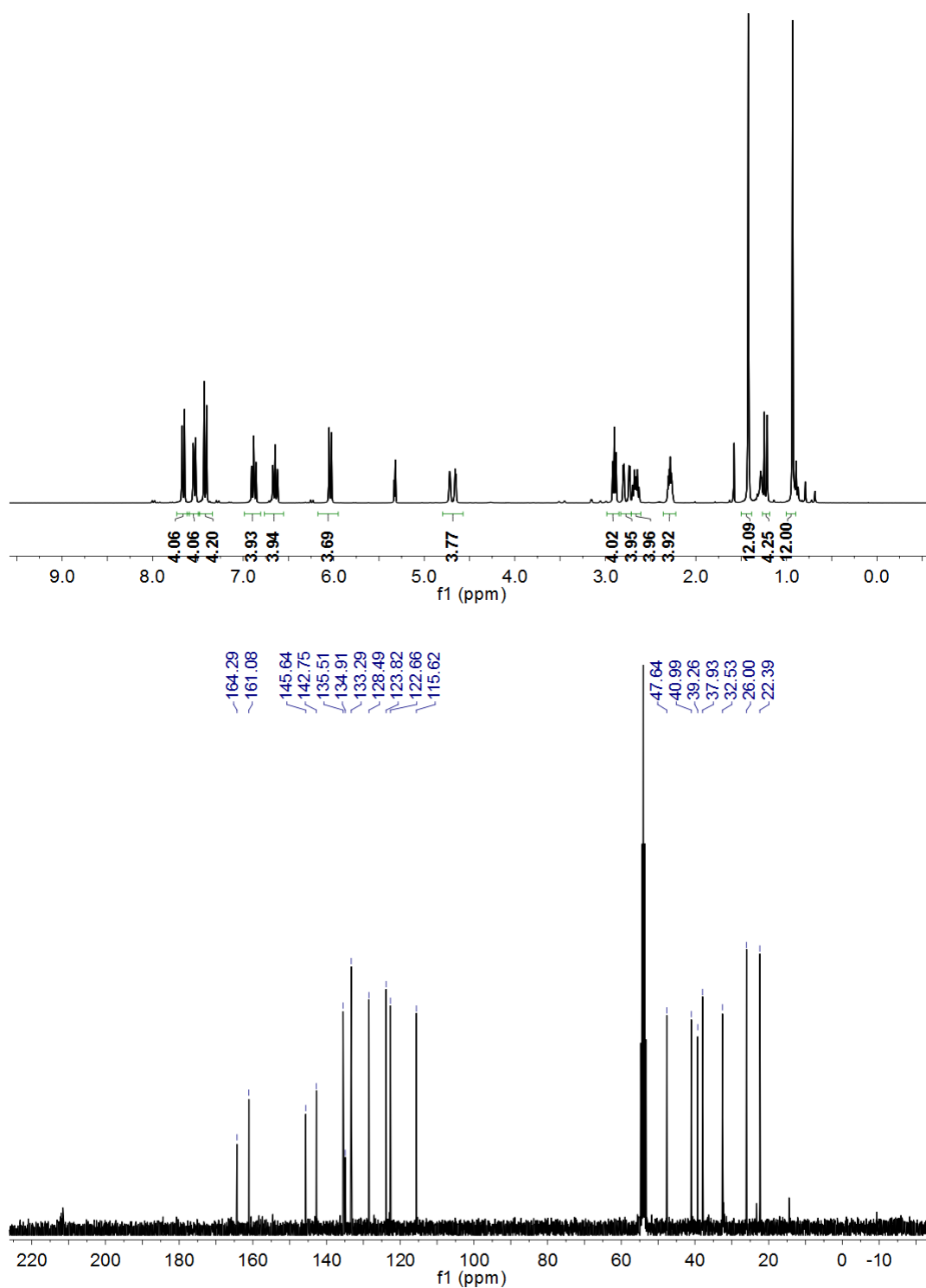
Figure 67 ^{1}H NMR and ^{13}C NMR spectra of ΛΛ-**2$_{Ir}$**.
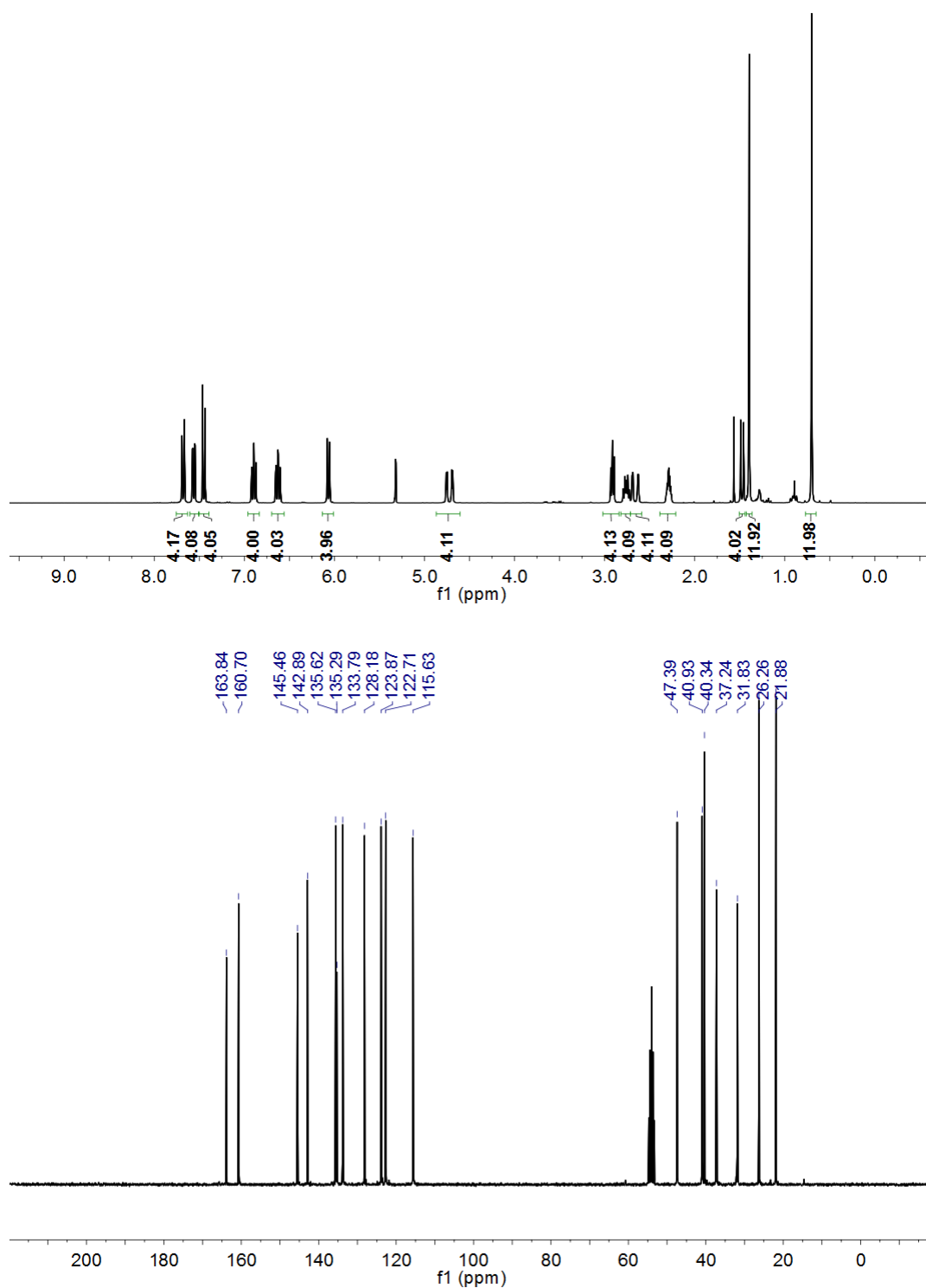
Figure 68 ^{1}H NMR and ^{13}C NMR spectra of ΔΔ-**2**$_{\text{Ir}}$.
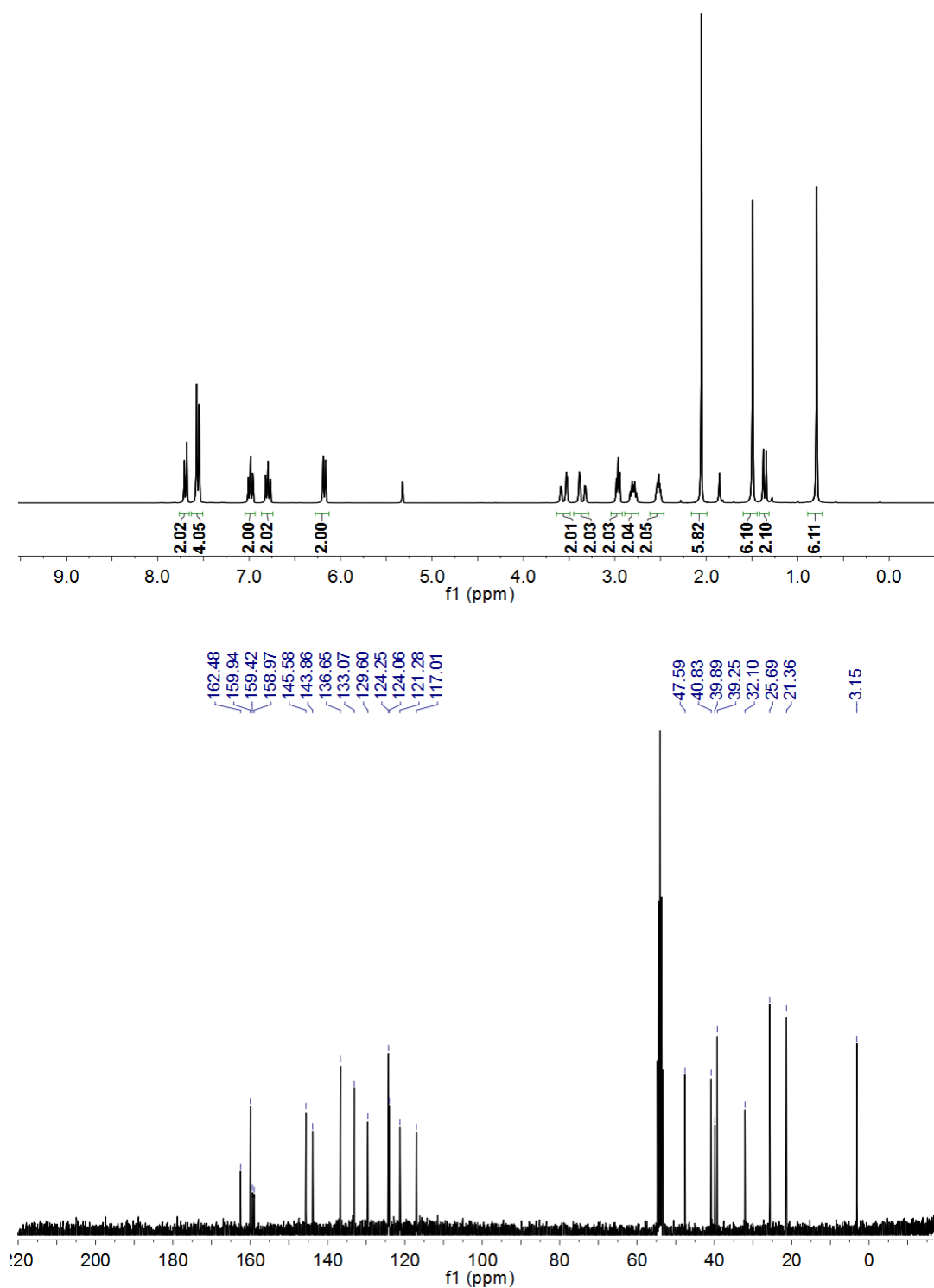
Figure 69 ^{1}H NMR and ^{13}C NMR spectra of Λ-**RhPP**.
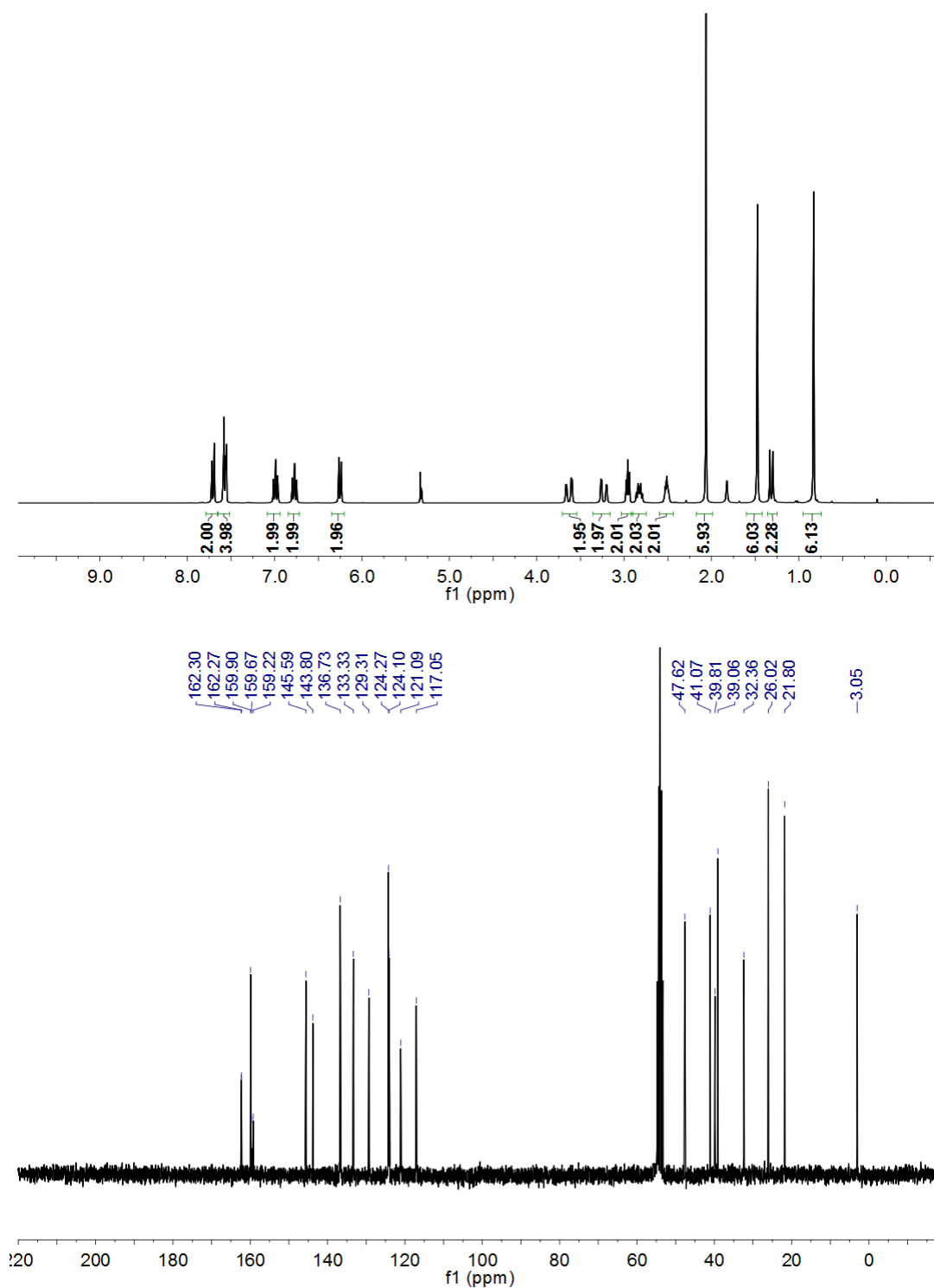
Figure 70 ^{1}H NMR and ^{13}C NMR spectra of Δ-**RhPP**.
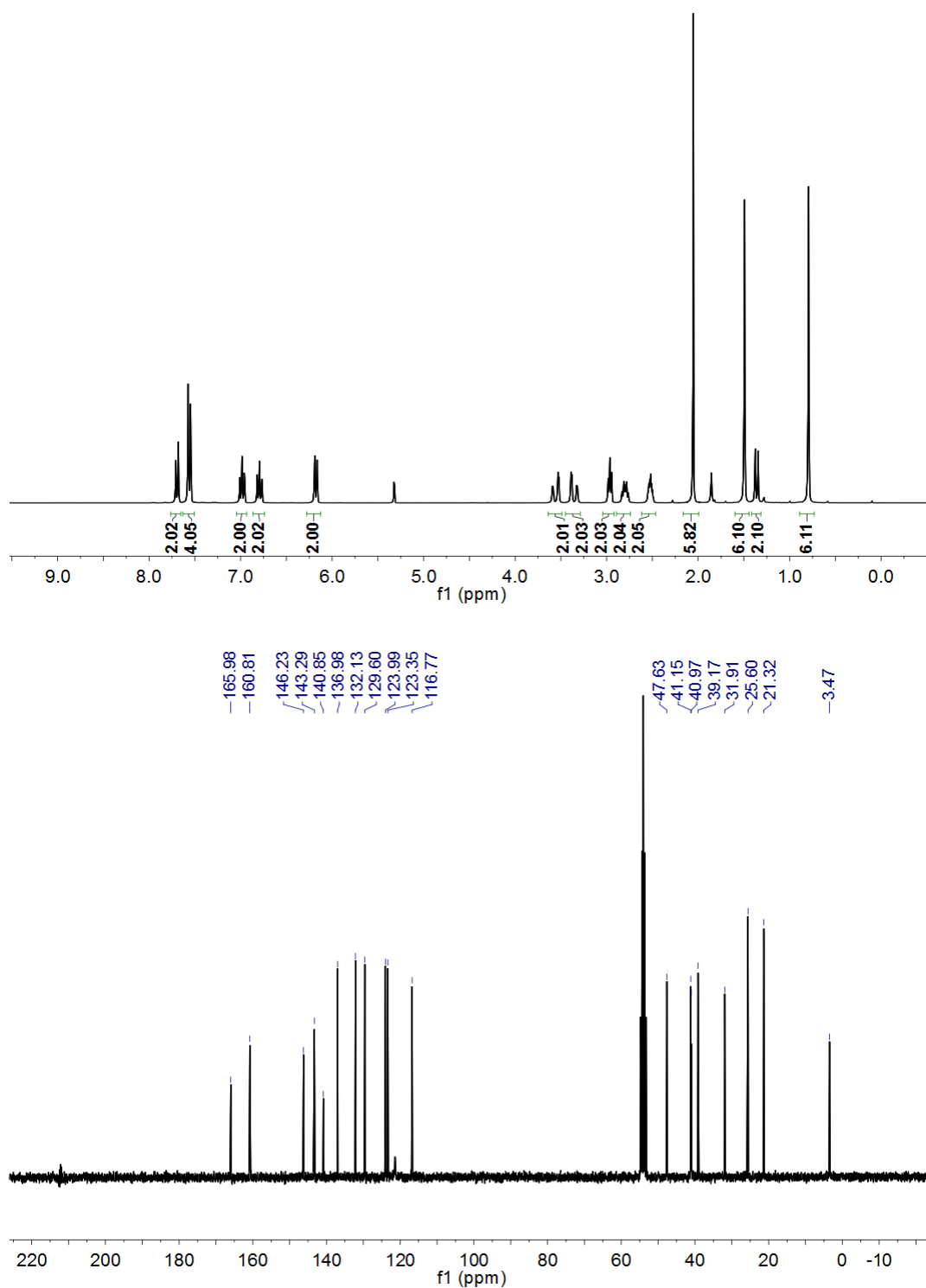
Figure 71 ^{1}H NMR and ^{13}C NMR spectra of Λ-**IrPP**.
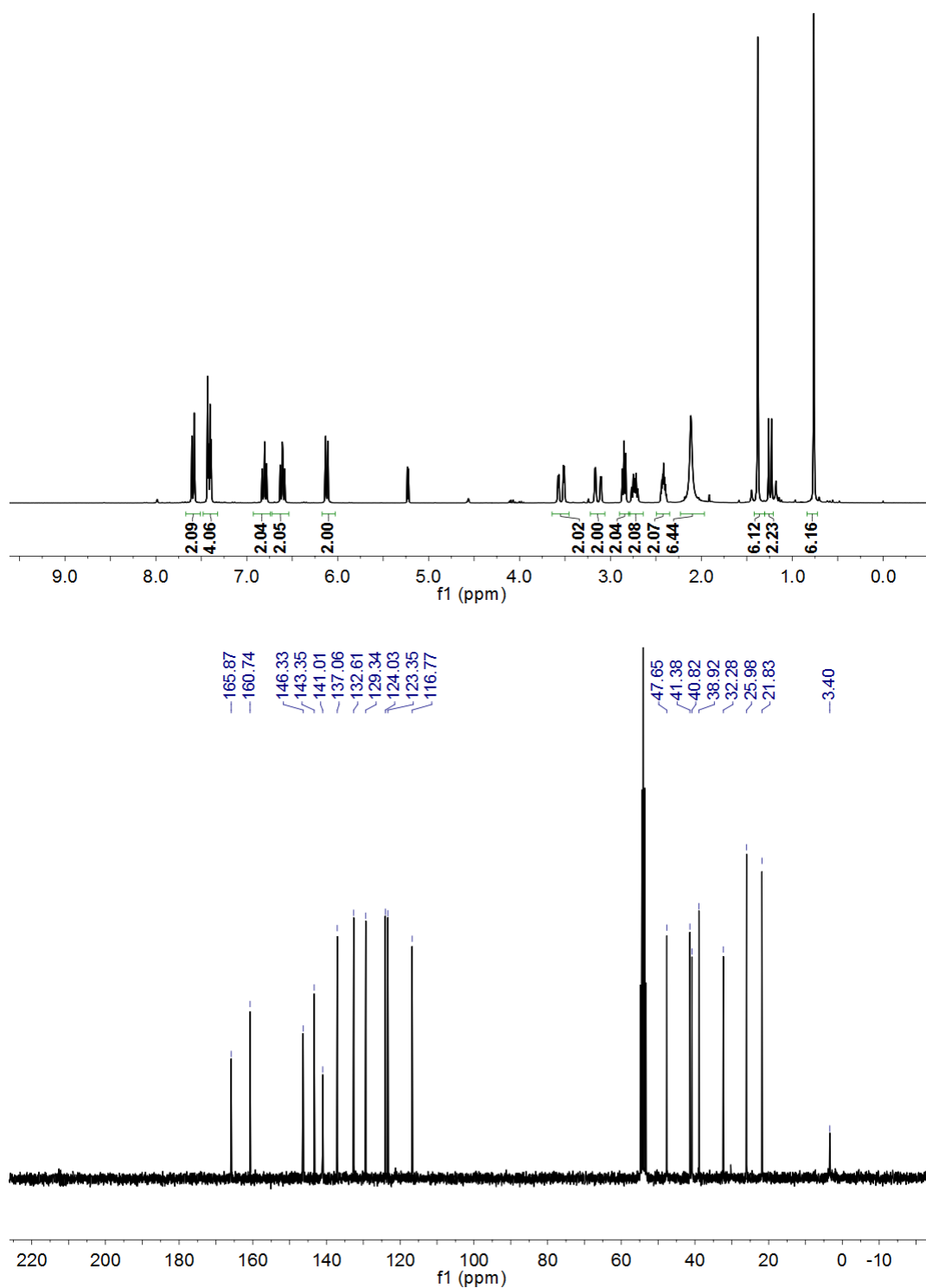
Figure 72 ^{1}H NMR and ^{13}C NMR spectra of Δ-**IrPP**.
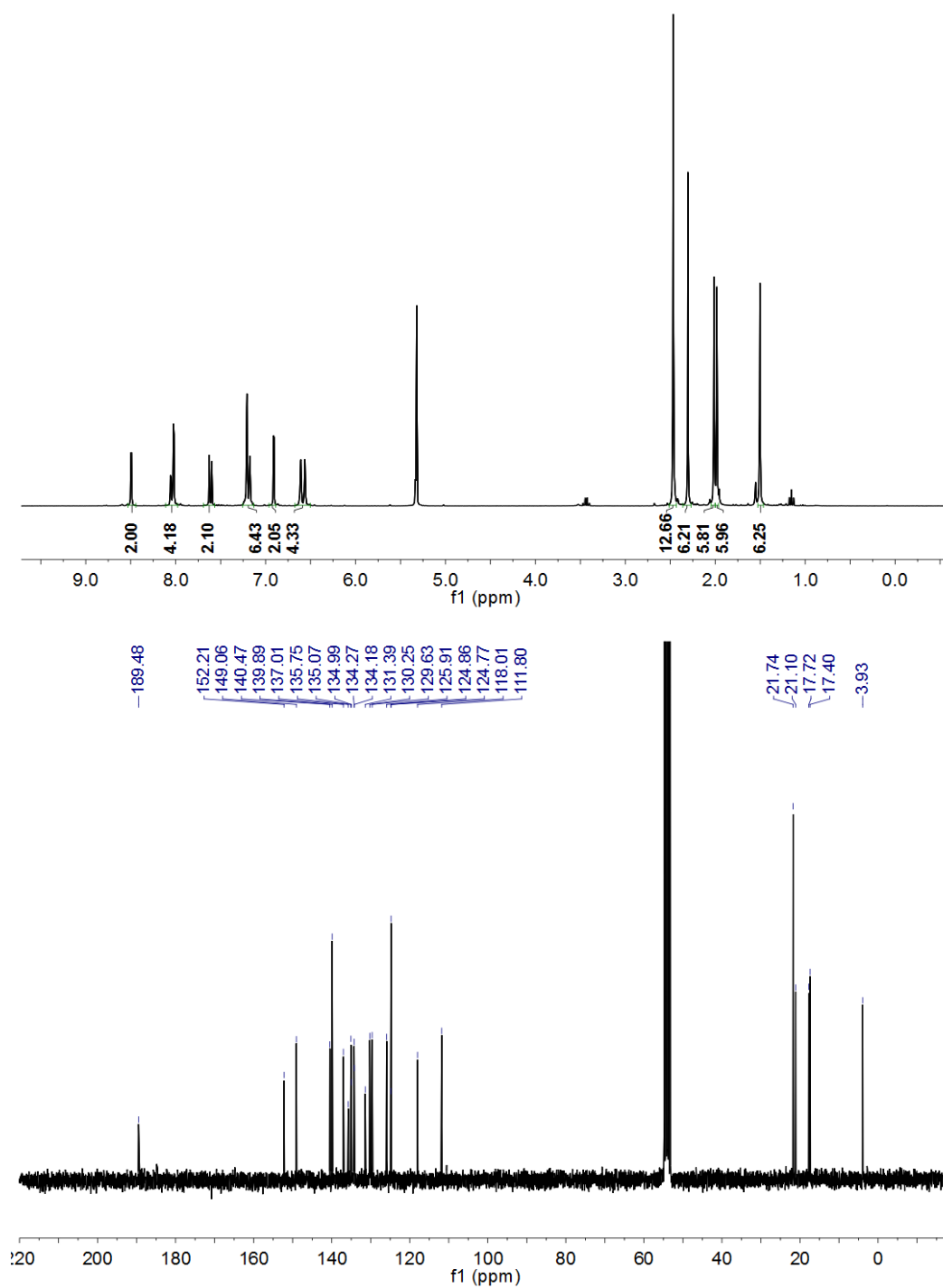
Figure 73 ^{1}H NMR and ^{13}C NMR spectra of *rac*-**Ru1**.
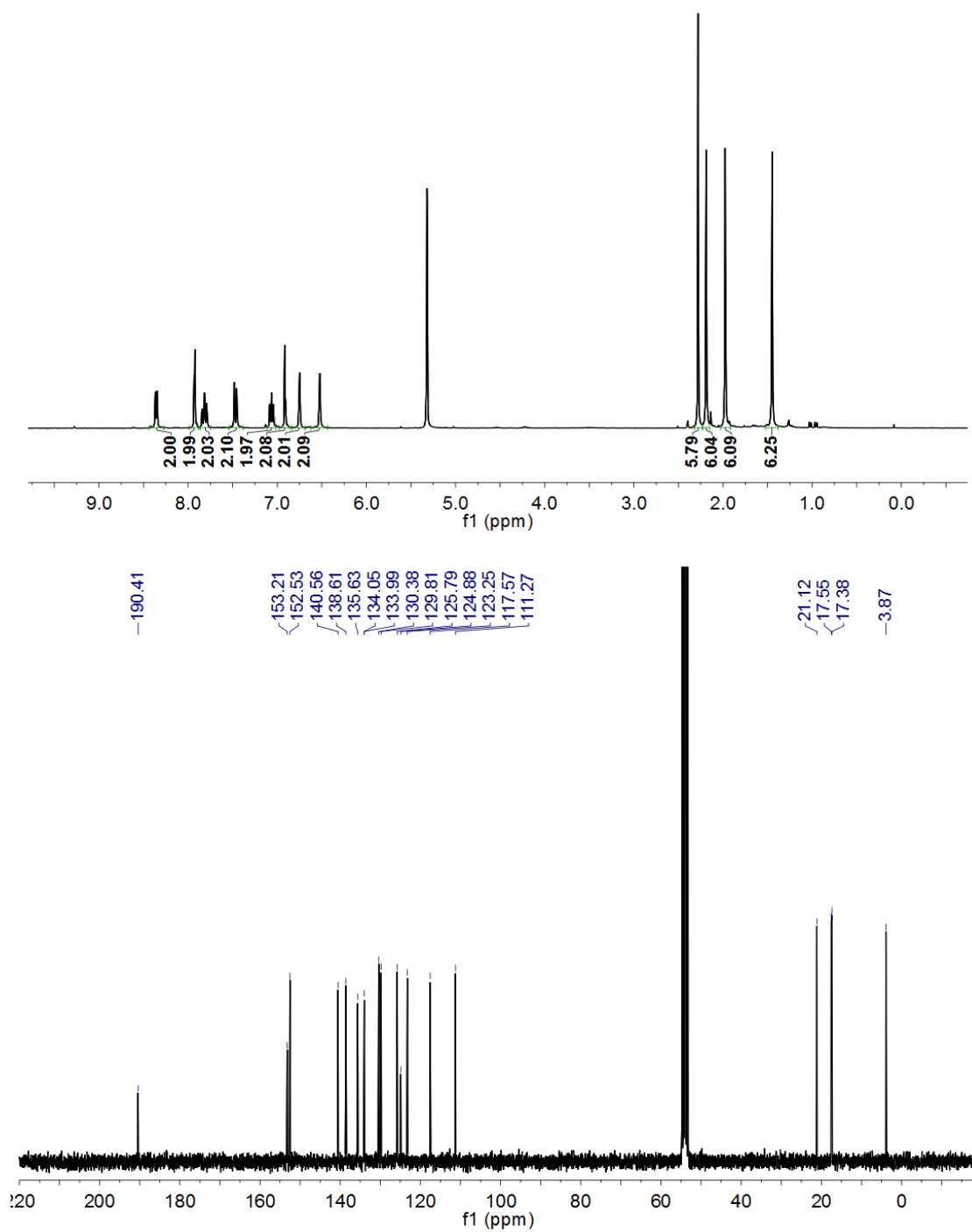
Figure 74 ^{1}H NMR and ^{13}C NMR spectra of *rac*-**Ru2**.
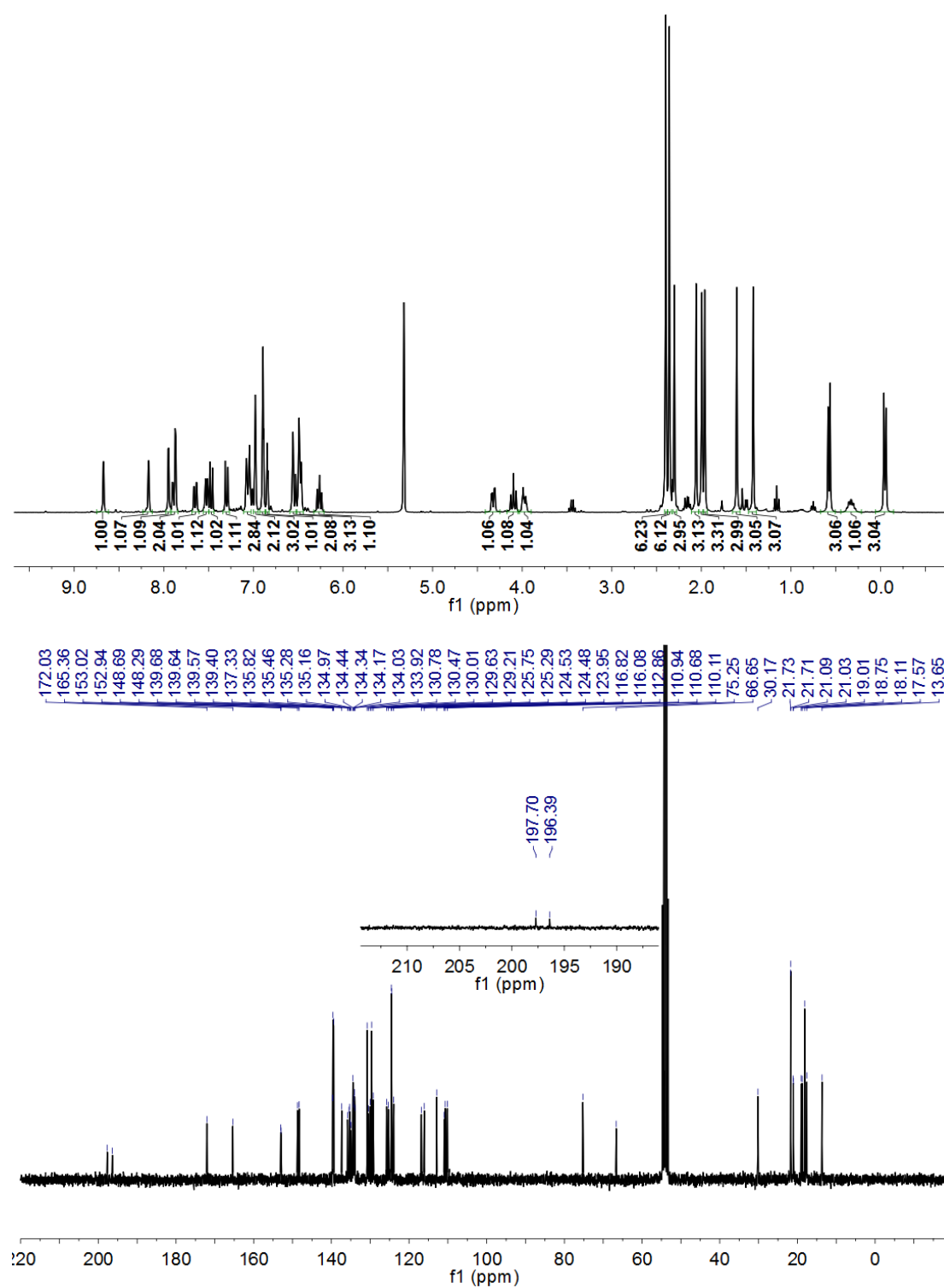
Figure 75 ^{1}H NMR and ^{13}C NMR spectra of Λ-(*S*)-**Ru1**.
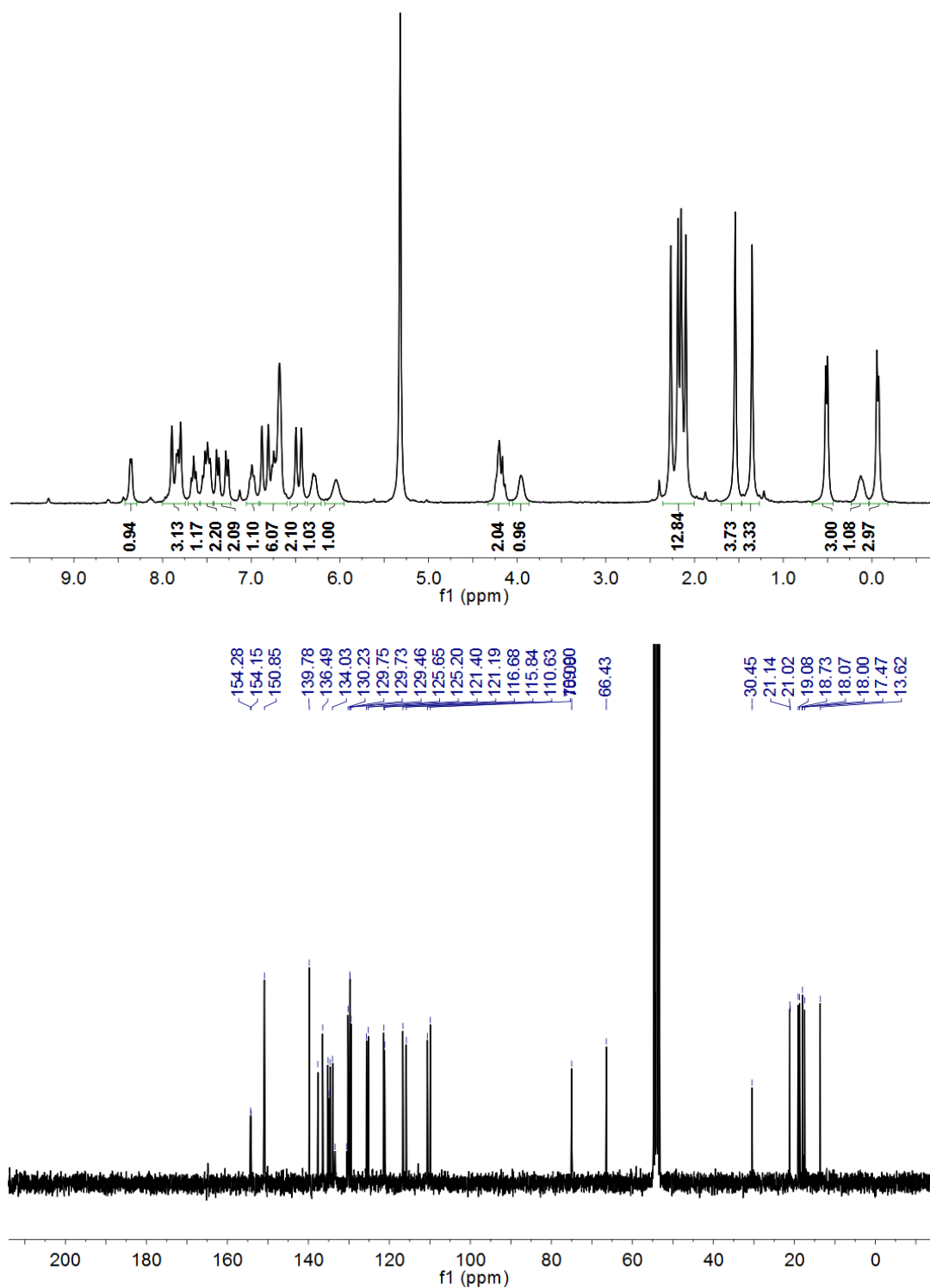
Figure 76 ^{1}H NMR and ^{13}C NMR spectra of Λ-(*S*)-**Ru2**.
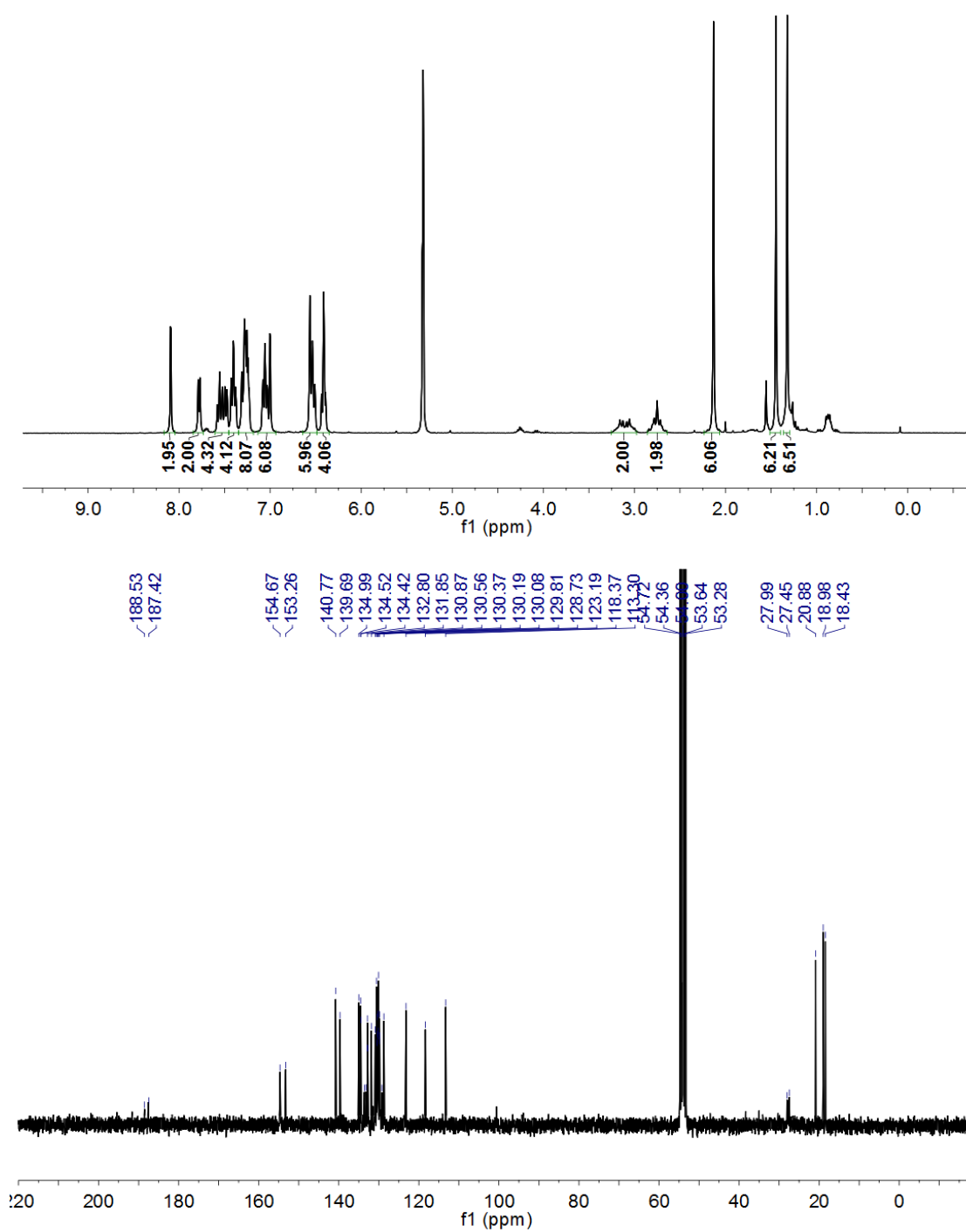
Figure 77 [superscript]1H NMR and [superscript]13C NMR spectra of Δ-**Ru2-DPPE**.

6.6.2 CD spectra of enantiopure metal complexes
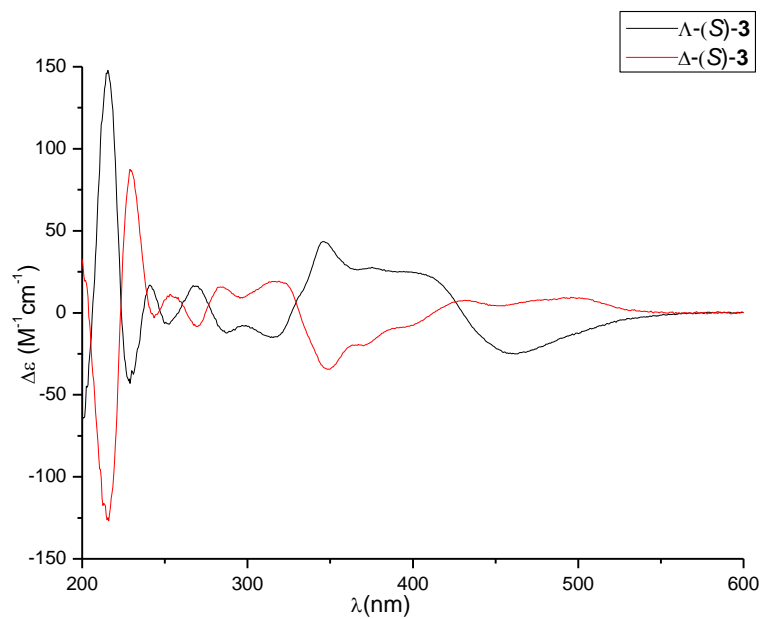
Figure 78 CD spectra of complexes Λ-(*S*)-**3** and Δ-(*S*)-**3** recorded in CH$_3$OH (0.2 mM).
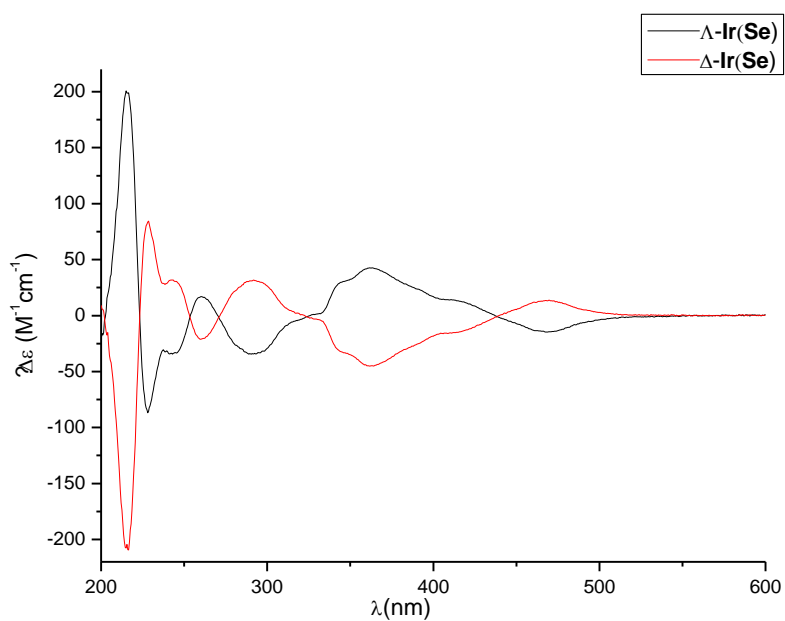
Figure 79 CD spectra of complexes Λ-**Ir**(**Se**) and Δ-**Ir**(**Se**) recorded in CH$_3$OH (0.2 mM).
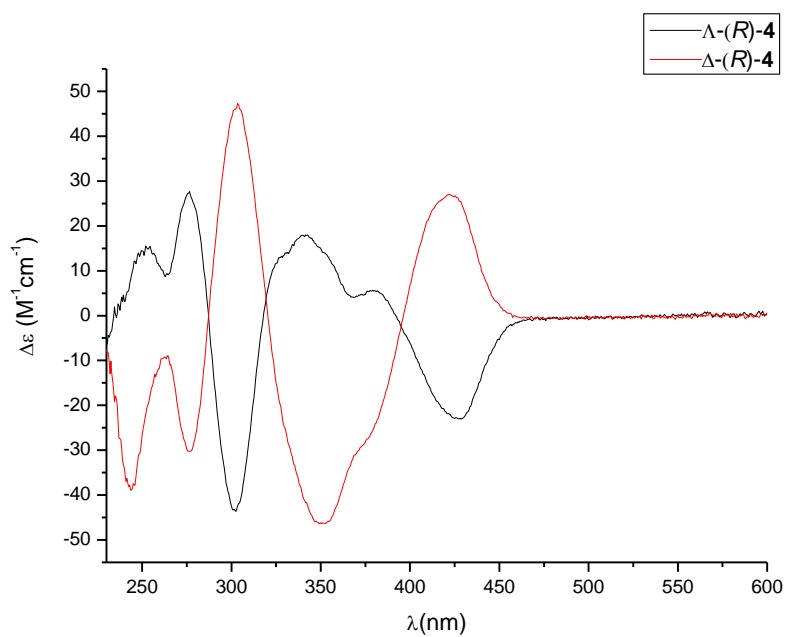
Figure 80 CD spectra of complexes Λ-(R)-**4** and Δ-(R)-**4** recorded in CH_3OH/CH_2Cl_2 = 4:1 (0.2 mM).
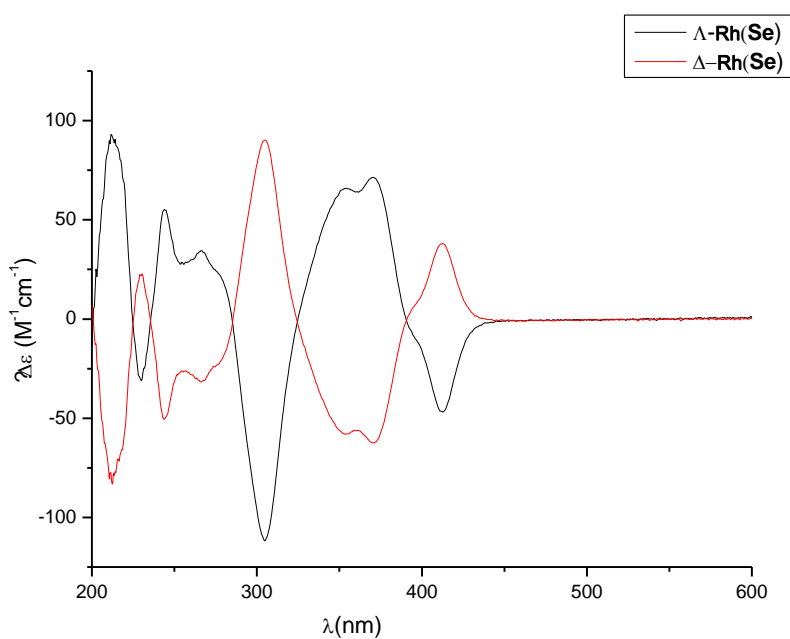
Figure 81 CD spectra of complexes Λ-**Rh**(**Se**) and Δ-**Rh**(**Se**) recorded in CH_3OH (0.2 mM).
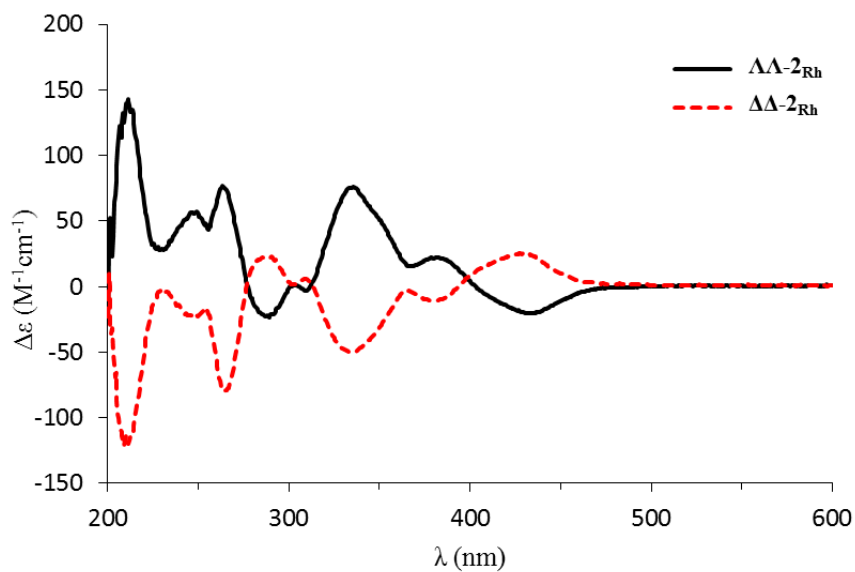
Figure 82 CD spectra of complexes $\Lambda\Lambda$-2_{Rh} and $\Delta\Delta$-2_{Rh} recorded in CH_3OH (0.2 mM).
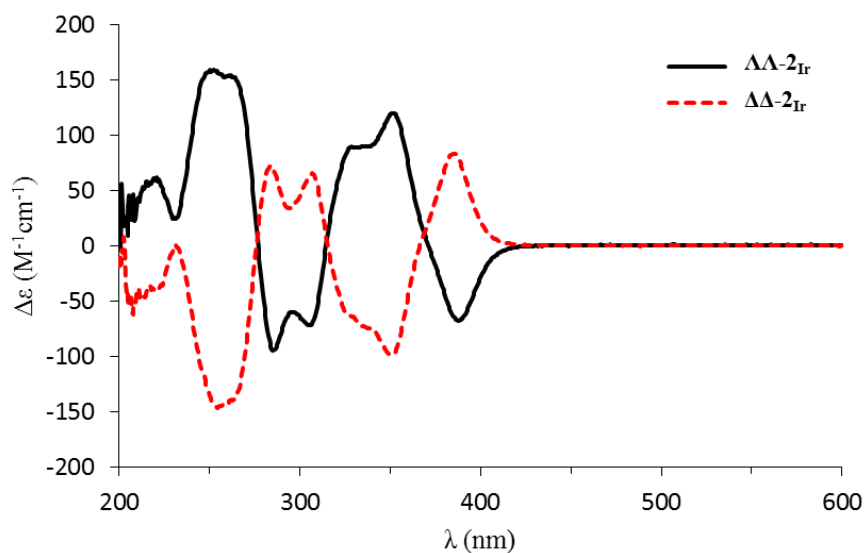
Figure 83 CD spectra of complexes $\Lambda\Lambda$-2_{Ir} and $\Delta\Delta$-2_{Ir} recorded in CH_3OH (0.2 mM).
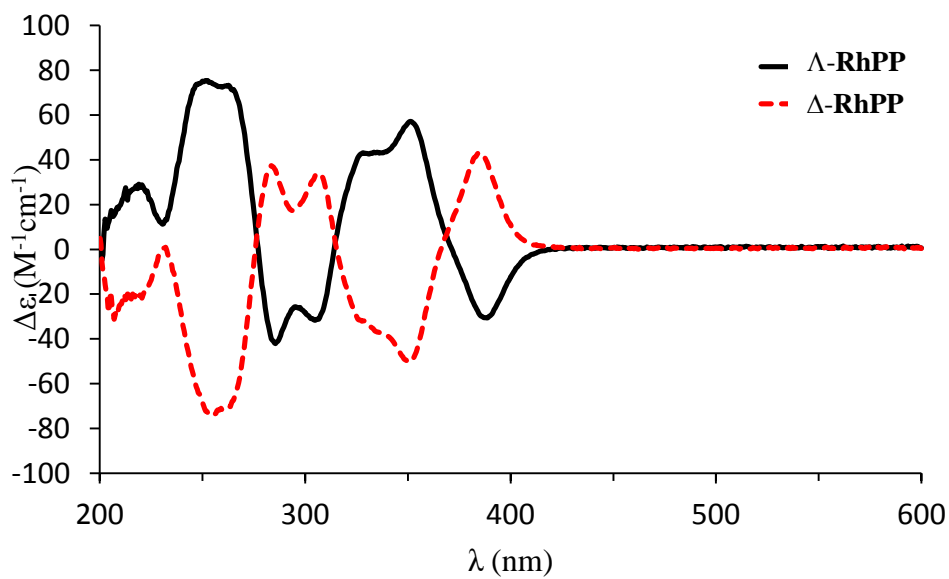
Figure 84 CD spectra of complexes Λ-**RhPP** and Δ-**RhPP** recorded in CH_3OH (0.2 mM).
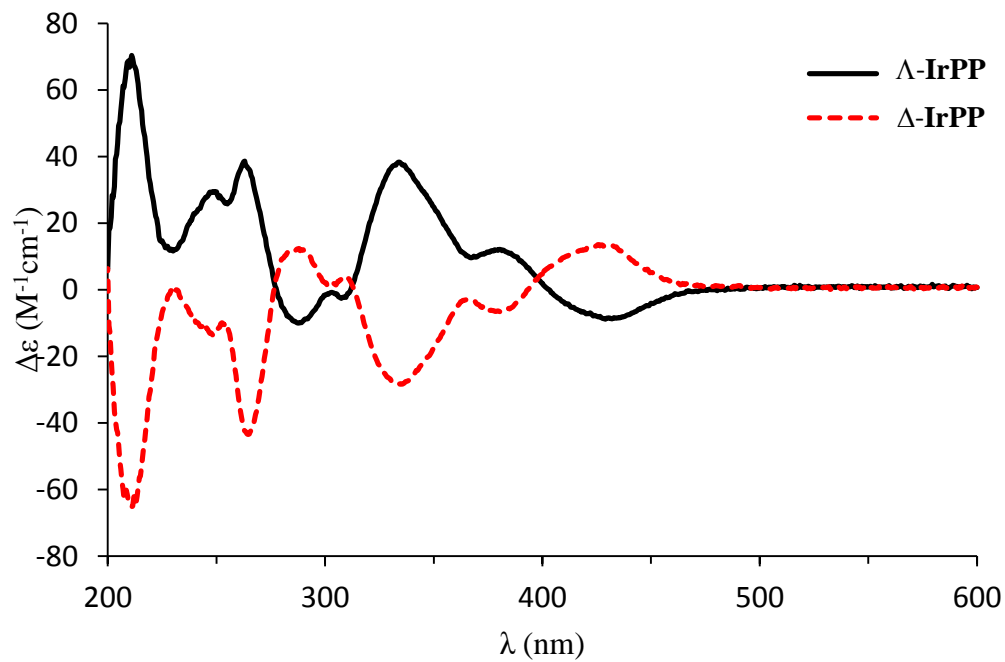
Figure 85 CD spectra of complexes Λ-**IrPP** and Δ-**IrPP** recorded in CH_3OH (0.2 mM).
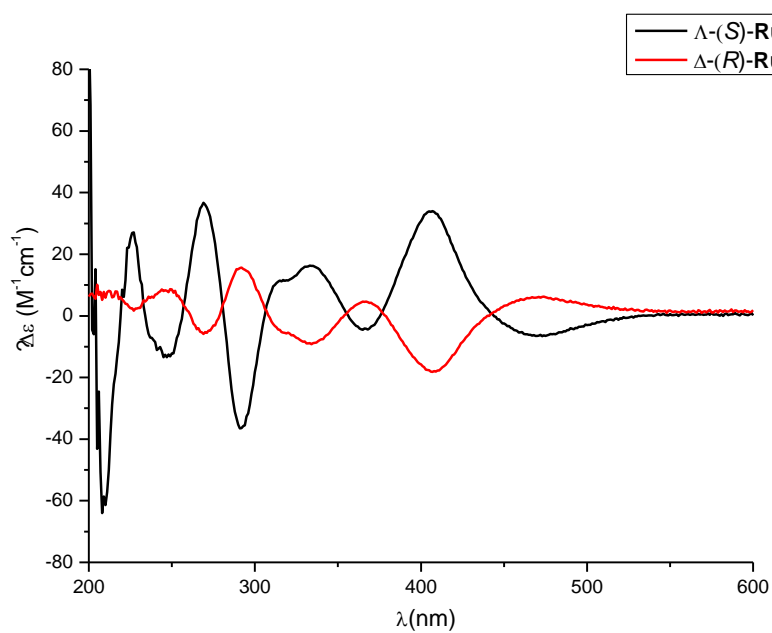
Figure 86 CD spectra of complexes Λ-(*S*)-**Ru1** and Δ-(*R*)-**Ru1** recorded in CH₃OH (0.2 mM).
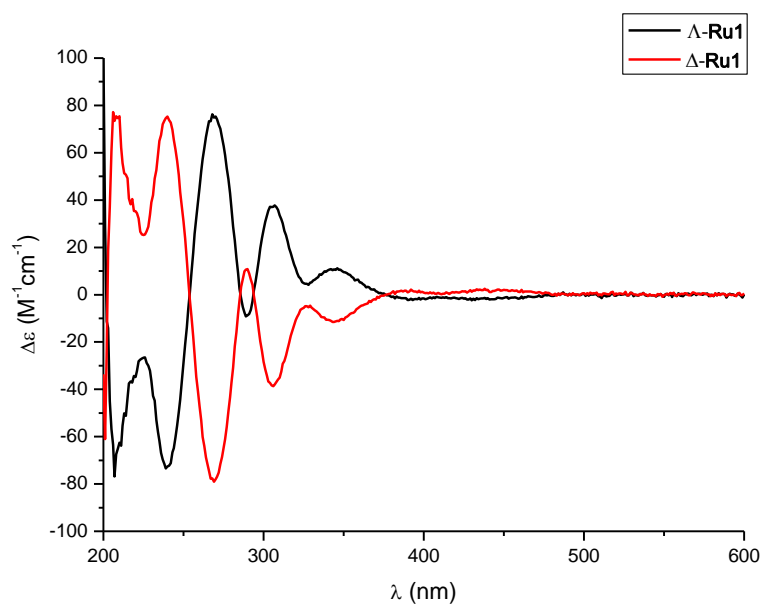
Figure 87 CD spectra of complexes Λ-**Ru1** and Δ-**Ru1** recorded in CH₃OH (0.2 mM).
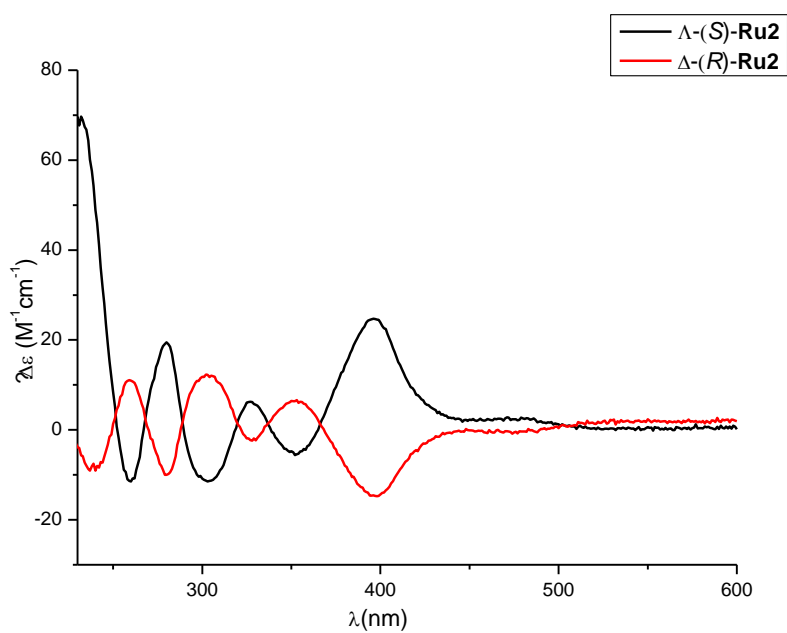
Figure 88 CD spectra of complexes Λ-(*S*)-**Ru2** and Δ-(*R*)-**Ru2** recorded in CH₃OH (0.2 mM).
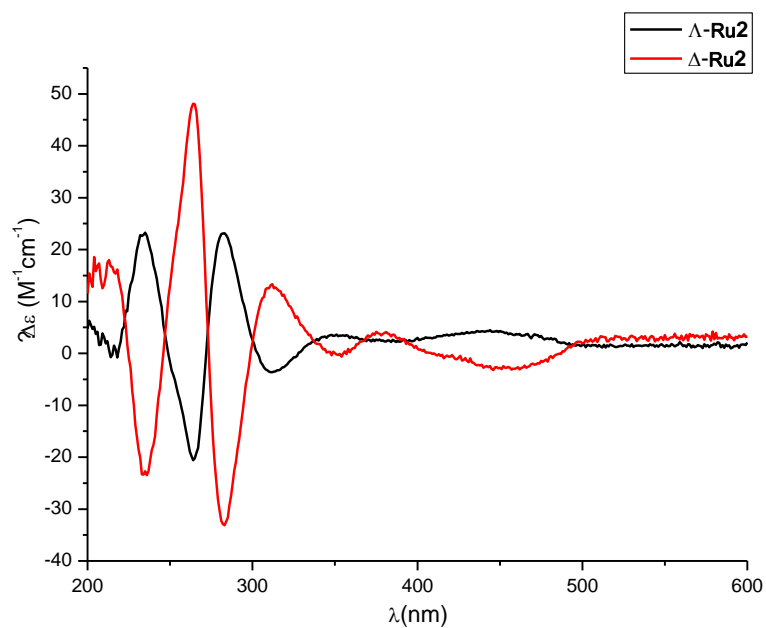
Figure 89 CD spectra of complexes Λ-**Ru2** and Δ-**Ru2** recorded in CH₃OH (0.2 mM).

6.6.3 HPLC spectra of compounds
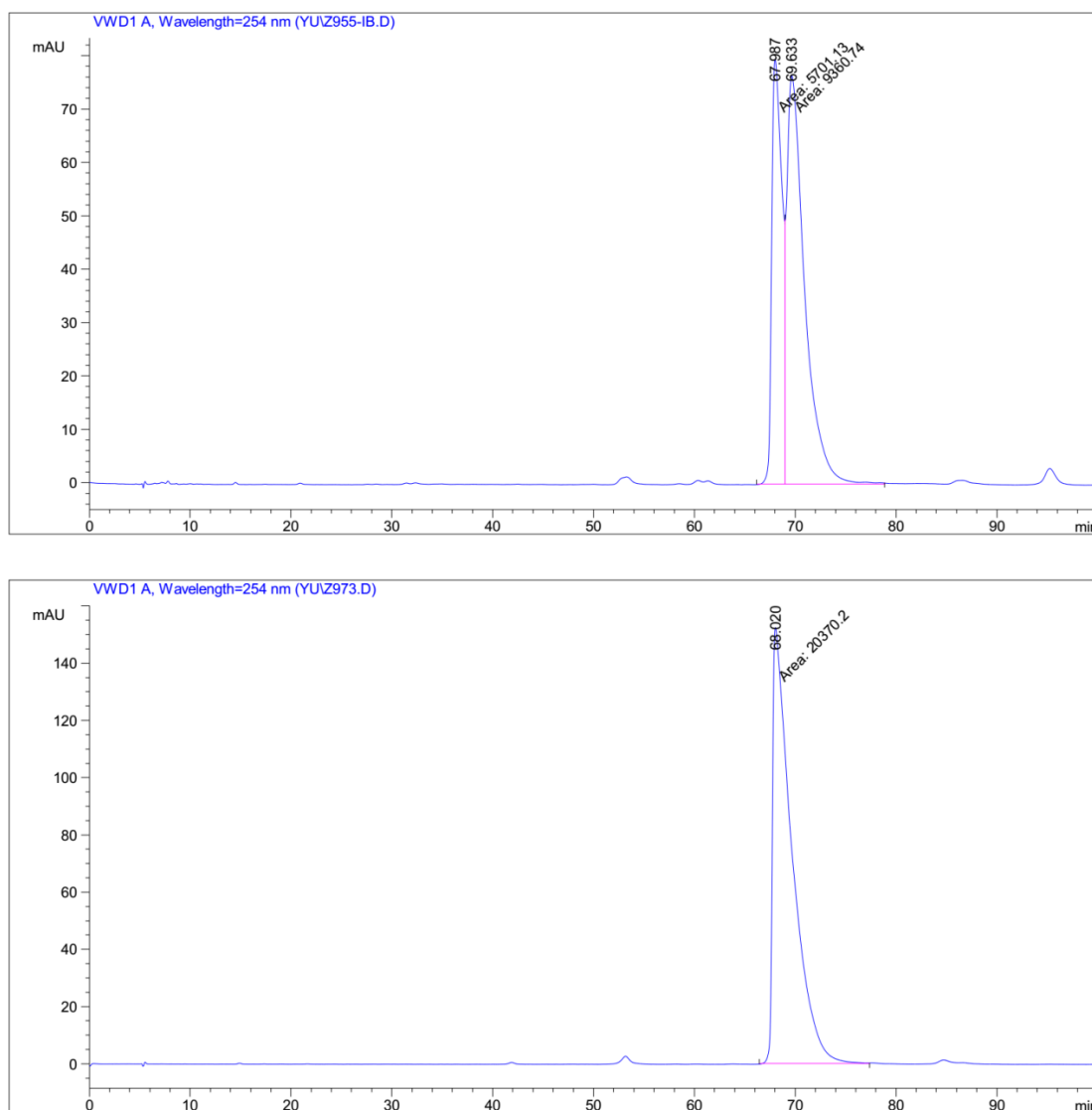
Figure 90 HPLC traces for the racemic reference complex Δ/Λ-**Ru1** and Λ-**Ru1**. HPLC conditions: HPLC column on an Agilent 1200 Series HPLC System. The column temperature was 25 ℃ and UV-absorption was measured at 254 nm. Solvent A = 0.1% TFA, solvent B = MeCN (Daicel Chiralpak IB (250 ×4.6 mm), with a linear gradient of 35% to 45% B in 180 min, flow rate = 0. 6 mL/min). HPLC trace for the complex Integration of peak areas > 100:1 e.r.
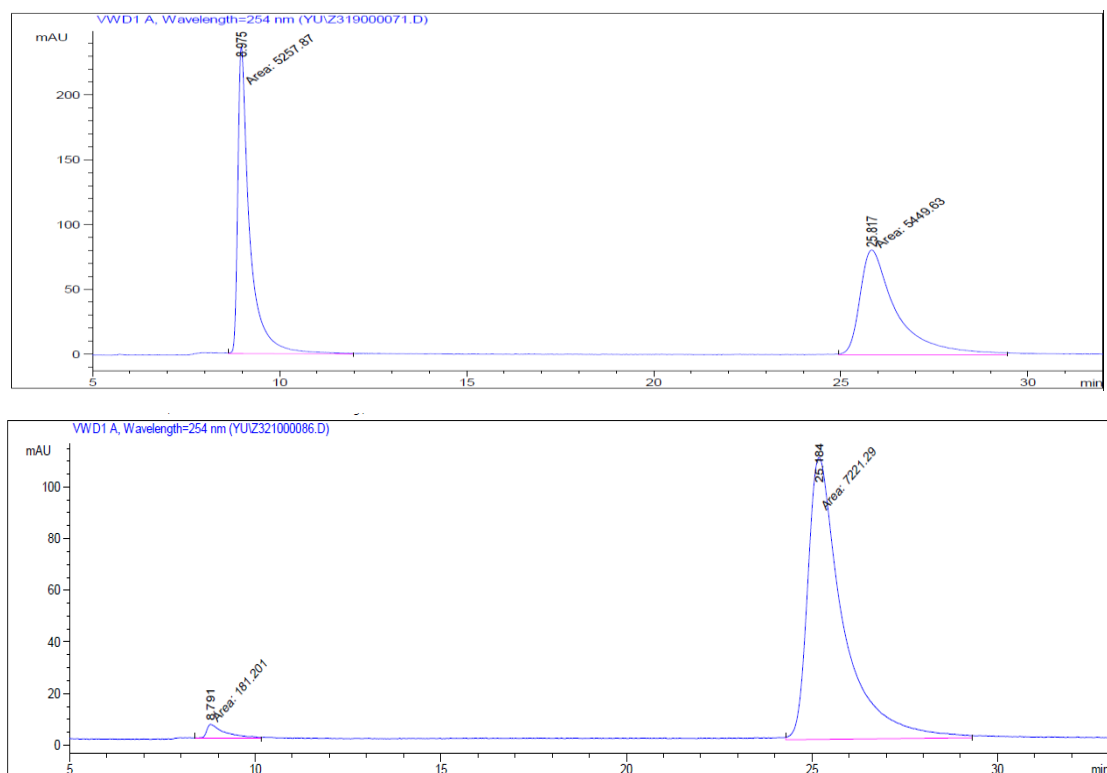
Peak #	RetTime [min]	Type	Width [min]	Area mAU *s	Height [mAU]	Area %
1	8.791	MM	0.5682	181.20065	5.31499	2.4478
2	25.184	MM	1.1008	7221.29150	109.33061	97.5522

Figure 91 HPLC traces (Daicel Chiralpak AD-H column) of *rac*-**20a** (reference) and (*R*)-**20a**. Area integration = 97.5:2.4 (95.1% *ee*).
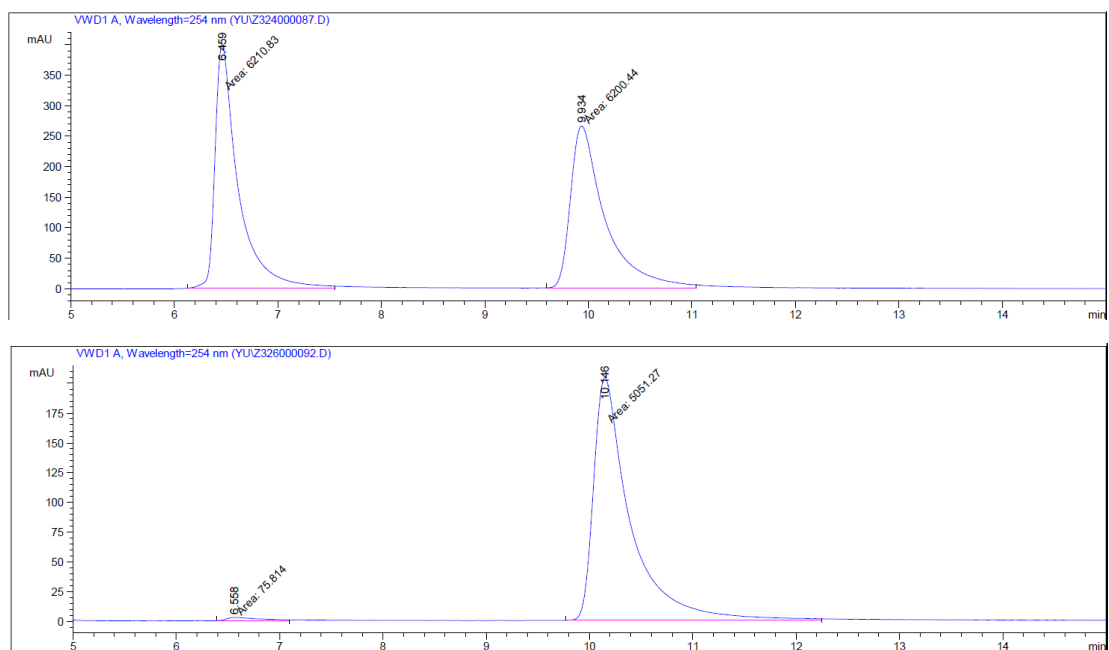
Peak	RetTime	Type	Width	Area	Height	Area
#	[min]		[min]	mAU *s	[mAU]	%
1	6.558	MM	0.4144	75.81399	3.04932	1.4787
2	10.146	MM	0.4133	5051.27393	203.70485	98.5213

Figure 92 HPLC traces (Daicel Chiralpak AD-H column) of *rac*-**20b** (reference) and (*R*)-**20b**. Area integration = 98.5:1.5 (97.0% *ee*).

```
Peak  RetTime Type   Width       Area        Height       Area
 #     [min]         [min]     [mAU*s]       [mAU]          %
----|-------|----|-------|----------|----------|--------|
   1   7.143 MM    0.3092     5.77289 3.11169e-1   0.1534
   2   9.150 BB    0.3510 3757.58447   148.60307  99.8466
```

Figure 93 HPLC traces (Daicel Chiralpak AD-H column) of *rac*-**20c** (reference) and (*R*)-**20c**. Area integration = 99.8:0.2 (99.6% *ee*).
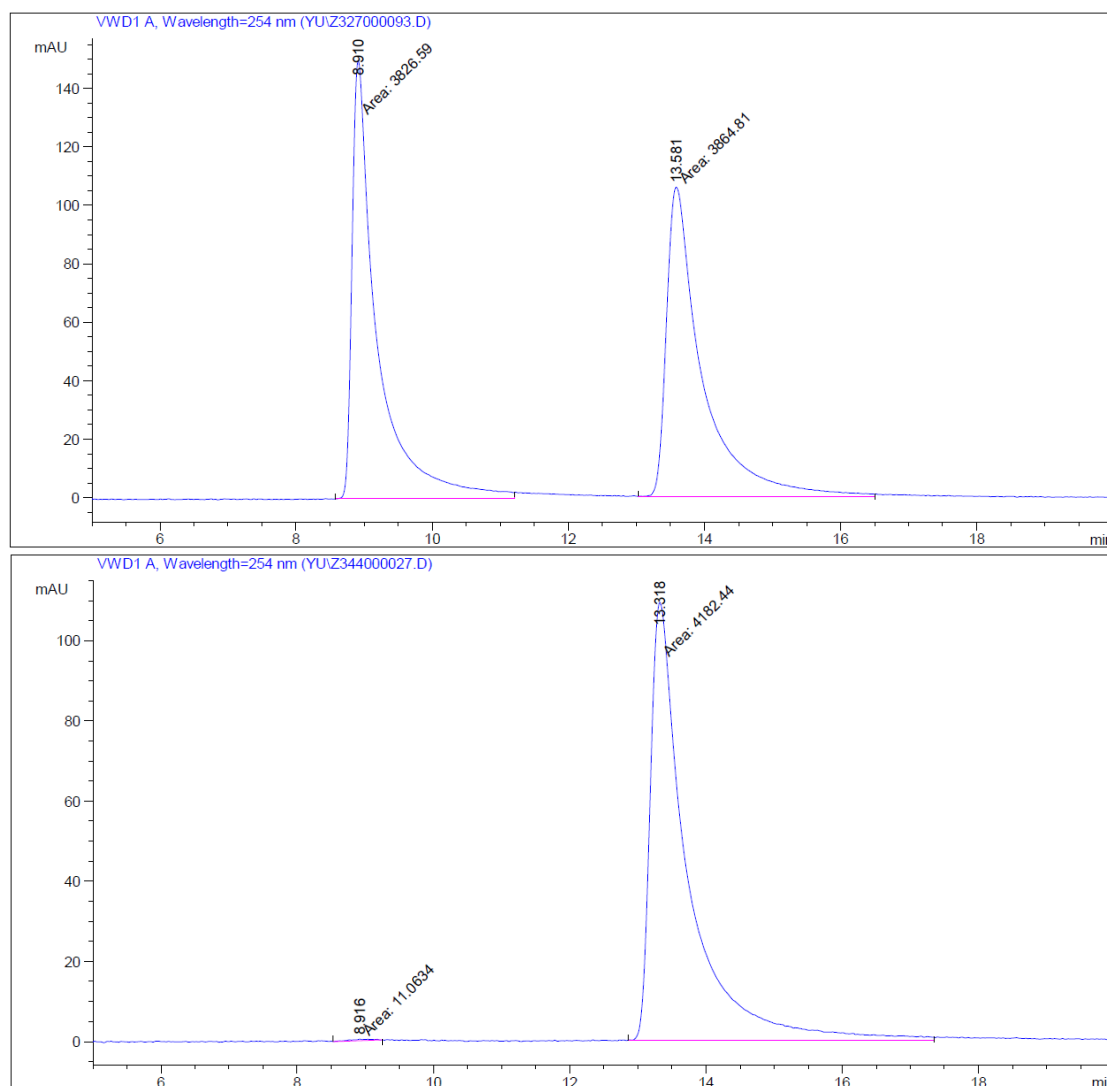
Peak	RetTime	Type	Width	Area	Height	Area
#	[min]		[min]	mAU *s	[mAU]	%
1	8.916	MM	0.4079	11.06345	4.52089e-1	0.2638
2	13.318	MM	0.6382	4182.44189	109.22511	99.7362

Figure 94 HPLC traces (Daicel Chiralpak AD-H column) of *rac*-**20d** (reference) and (*R*)-**20d**. Area integration = 99.7:0.3 (99.4% *ee*).

Peak #	RetTime [min]	Type	Width [min]	Area mAU *s	Height [mAU]	Area %
1	29.049	MM	1.4533	4472.37939	51.29166	100.0000

Figure 95 HPLC traces (Daicel Chiralpak AD-H column) of *rac*-**20e** (reference) and (*R*)-**20e**. Area integration > 99 (> 99% *ee*).

| Peak | RetTime | Type | Width | Area | Height | Area |
#	[min]		[min]	[mAU*s]	[mAU]	%
1	10.470	MM	0.2868	8.62185	5.00973e-1	0.3084
2	12.270	BB	0.2777	2787.45410	149.38736	99.6916

Figure 96 HPLC traces (Daicel Chiralpak AD-H column) of *rac*-**20f** (reference) and (*R*)-**20f**. Area integration = 99.7:0.3 (99.4% ee).

```
VWD1 A, Wavelength=254 nm (YU\Z330000103.D)
```

```
VWD1 A, Wavelength=254 nm (YU\Z340000006.D)
```

```
Peak  RetTime  Type   Width      Area          Height       Area
 #     [min]          [min]    mAU   *s      [mAU    ]       %
----|-------|----|-------|----------|----------|--------|
  1   12.439  MM    0.6038  4413.88232  121.82716  100.0000
```

Figure 97 HPLC traces (Daicel Chiralpak AD-H column) of *rac*-**20g** (reference) and (*R*)-**20g**. Area integration > 99 (> 99% *ee*).

```
Peak  RetTime Type   Width      Area       Height      Area
 #     [min]         [min]    mAU   *s    [mAU   ]       %
----|-------|----|-------|----------|----------|--------|
  1   13.287 MM    0.4286    33.99917     1.32199     0.6988
  2   22.621 MM    0.7504  4831.06250   107.29558    99.3012
```

Figure 98 HPLC traces (Daicel Chiralpak AD-H column) of *rac*-**20h** (reference) and (*R*)-**20h**. Area integration = 99.3:0.7 (98.6% *ee*).

```
Peak  RetTime Type   Width      Area        Height      Area
 #     [min]         [min]    [mAU*s]       [mAU]         %
----|-------|----|-------|----------|----------|--------|
  1   13.059 MM    0.6765   24.85729 6.12409e-1   0.2923
  2   18.629 BB    0.7642 8478.51953  133.81732  99.7077
```

Figure 99 HPLC traces (Daicel Chiralpak AD-H column) of *rac*-**20i** (reference) and (*R*)-**20i**. Area integration = 99.7:0.3 (99.4% *ee*).

Peak	RetTime	Type	Width	Area	Height	Area
#	[min]		[min]	mAU *s	[mAU]	%
1	11.430	MM	0.4903	4881.27100	165.91782	100.0000

Figure 100 HPLC traces (Daicel Chiralpak AD-H column) of *rac*-**20j** (reference) and (*R*)-**20j**. Area integration > 99 (>99% *ee*).
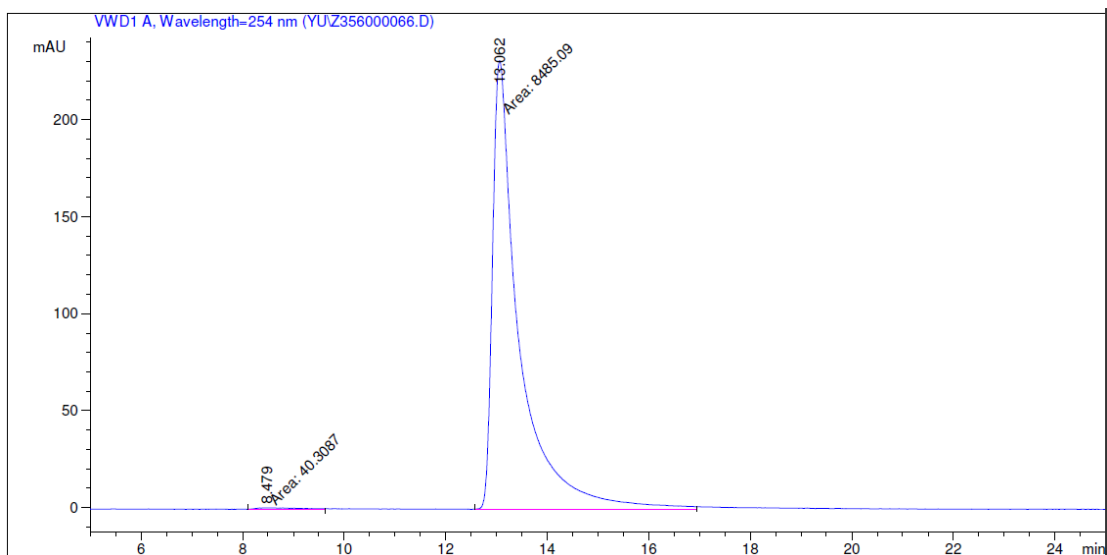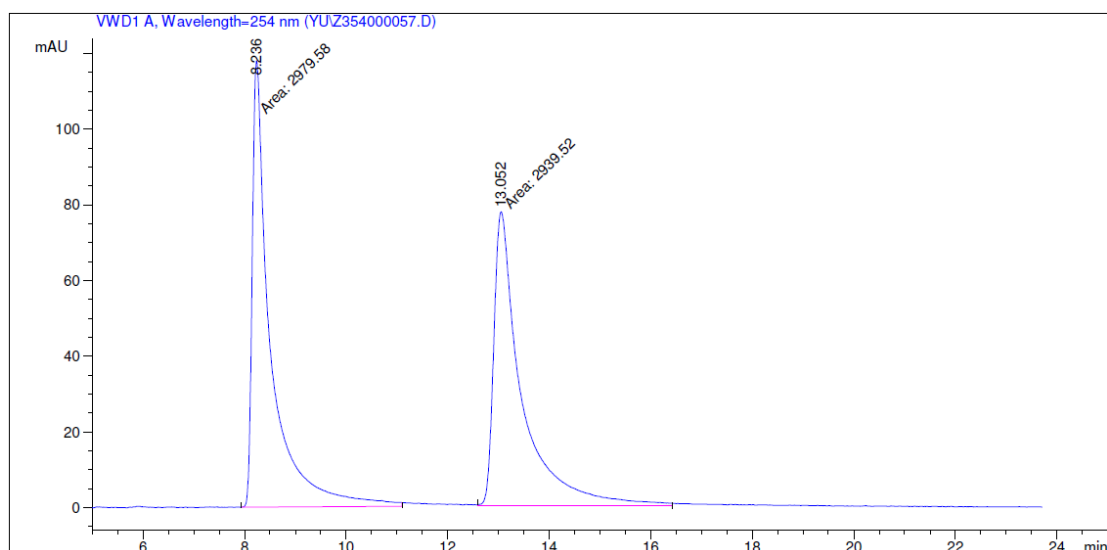
| Peak | RetTime | Type | Width | Area | Height | Area |
#	[min]		[min]	mAU *s	[mAU]	%
1	8.479	MM	0.9825	40.30870	6.83793e-1	0.4728
2	13.062	MM	0.6112	8485.09473	231.37567	99.5272

Figure 101 HPLC traces (Daicel Chiralpak AD-H column) of *rac*-**20k** (reference) and (*R*)-**20k**. Area integration = 99.5:0.5 (99.0% *ee*).

Peak	RetTime	Type	Width	Area	Height	Area
#	[min]		[min]	mAU *s	[mAU]	%
1	9.013	MM	0.5307	36.75679	1.15427	0.5950
2	14.988	MM	0.6489	6140.51953	157.72478	99.4050
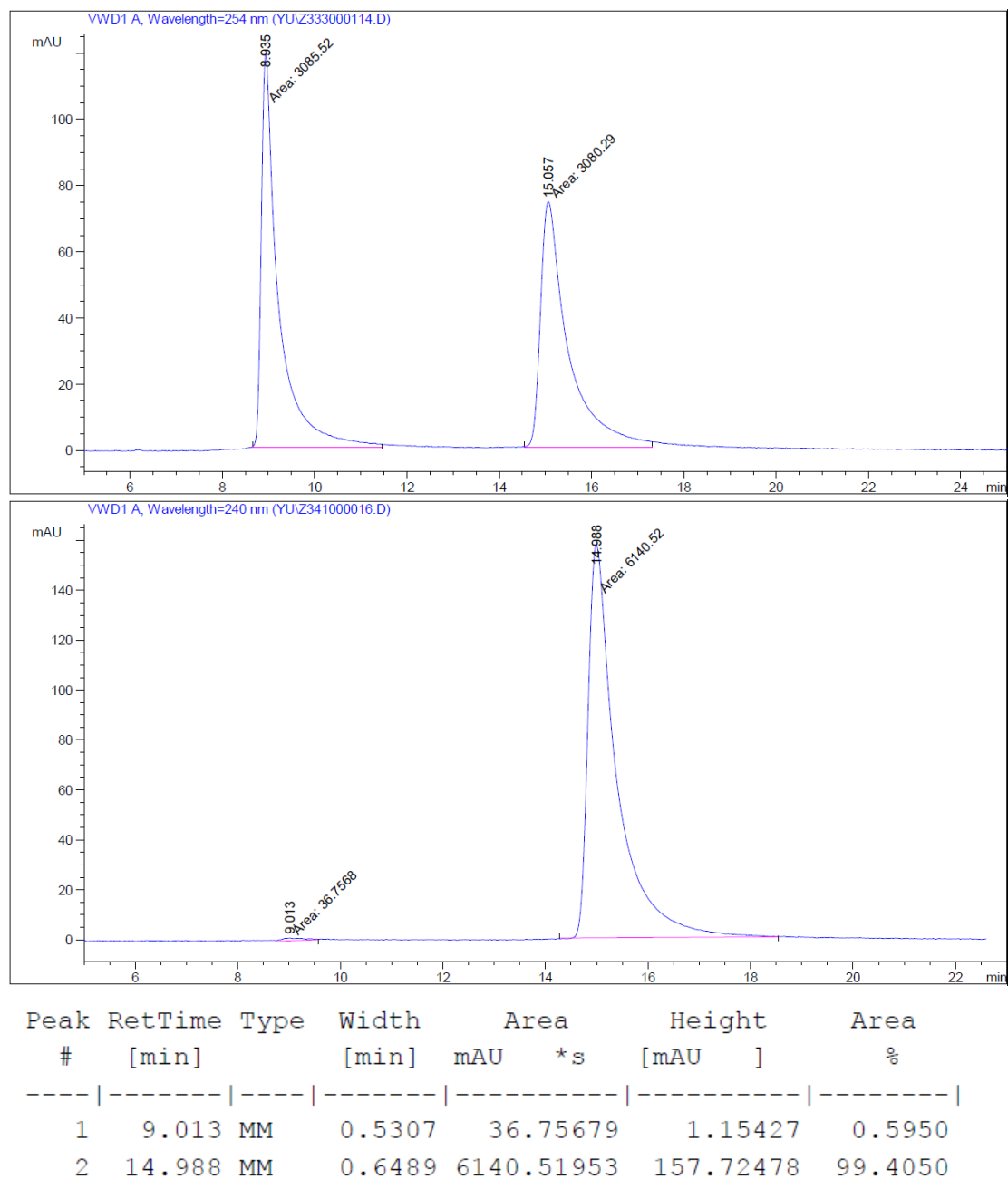
Figure 102 HPLC traces (Daicel Chiralpak AD-H column) of *rac*-**20l** (reference) and (*R*)-**20l**. Area integration = 99.4:0.6 (98.8% *ee*).

```
Peak RetTime Type  Width     Area      Height    Area
  #   [min]        [min]    [mAU*s]    [mAU]       %
----|-------|----|-------|----------|----------|--------|
  1   7.586 MM   0.3052    37.99678    2.07471   1.3045
  2   8.740 MM   0.4357  2874.81299  109.96486  98.6955
```

Figure 103 HPLC traces (Daicel Chiralpak AD-H column) of *rac*-**20m** (reference) and (*R*)-**20m**. Area integration = 98.7:1.3 (97.4% *ee*).

Peak	RetTime	Type	Width	Area	Height	Area
#	[min]		[min]	mAU *s	[mAU]	%
1	10.378	VB	0.4084	1.26752e4	440.68588	100.0000

Figure 104 HPLC traces (Daicel Chiralpak AD-H column) of *rac*-**20n** (reference) and (*R*)-**20n**. Area integration > 99 (>99% *ee*).
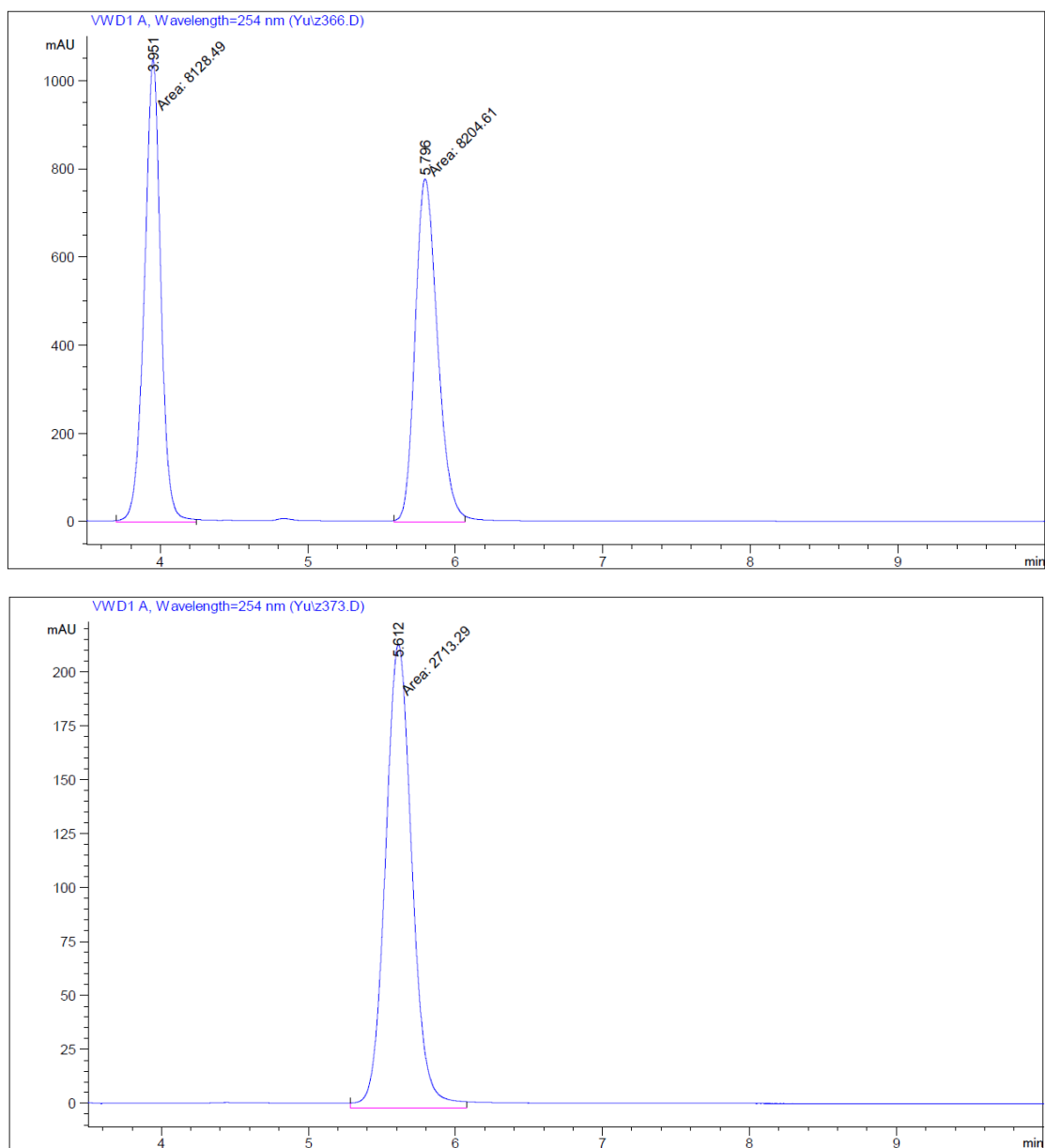
```
Peak  RetTime Type   Width      Area        Height     Area
  #    [min]         [min]    [mAU*s]      [mAU]        %
----|-------|----|-------|----------|-----------|--------|
  1   5.612 MM    0.2108 2713.28955  214.51393 100.0000
```

Figure 105 HPLC traces (Daicel Chiralpak AD-H column) of *rac*-**20o** (reference) and (*R*)-**20o**. Area integration > 99 (>99% *ee*).
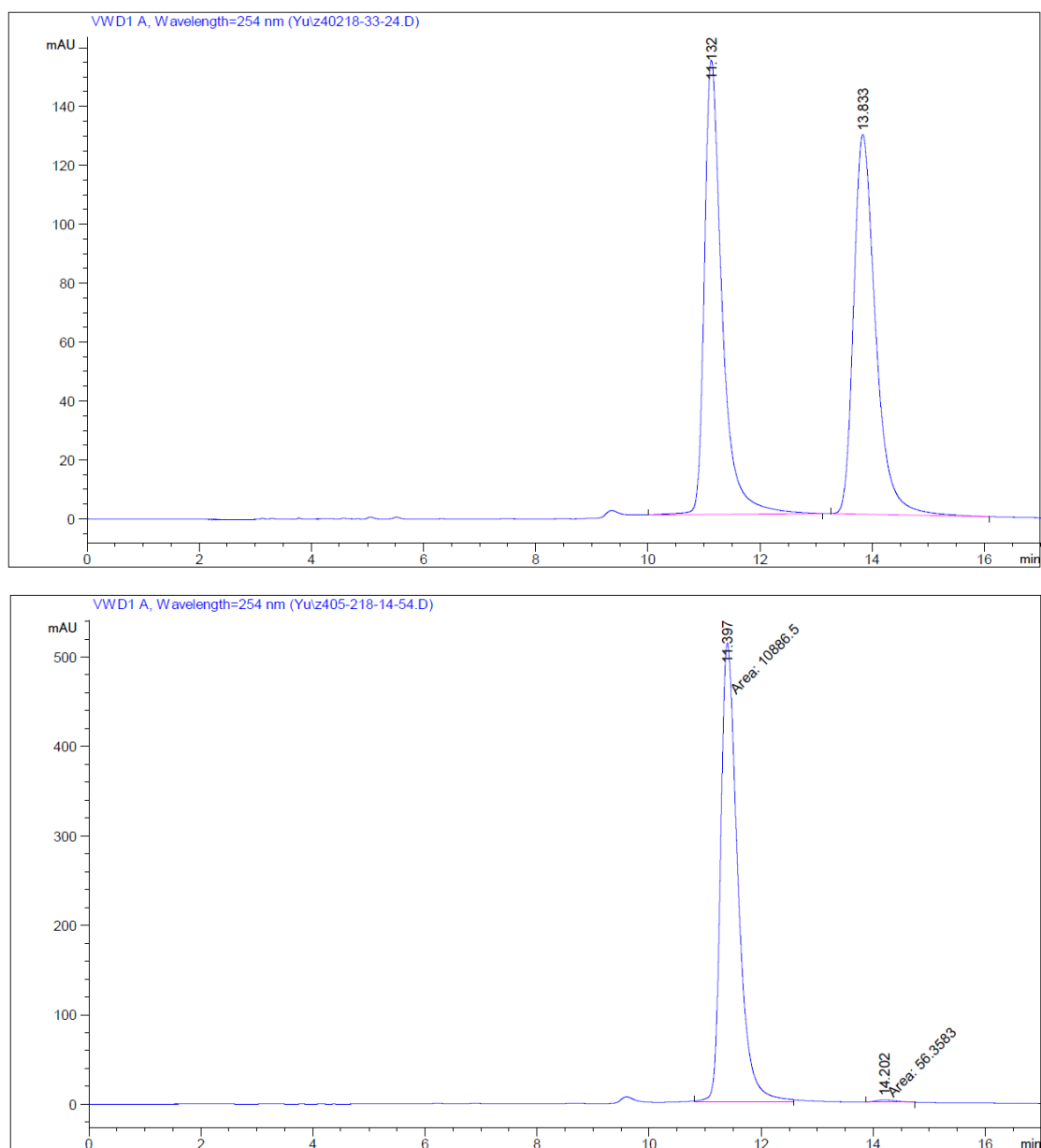
```
Peak RetTime Type  Width    Area      Height     Area
  #   [min]        [min]   [mAU*s]     [mAU]       %
----|-------|----|-------|----------|----------|--------|
  1  11.397 MM   0.3540 1.08865e4   512.62042  99.4850
  2  14.202 MM   0.3815   56.35826    2.46210   0.5150
```

Figure 106 HPLC traces (Daicel Chiralpak OJ-H column) of *rac*-**20p** (reference) and (*R*)-**20p**. Area integration = 99.5:0.5 (99.0% *ee*).
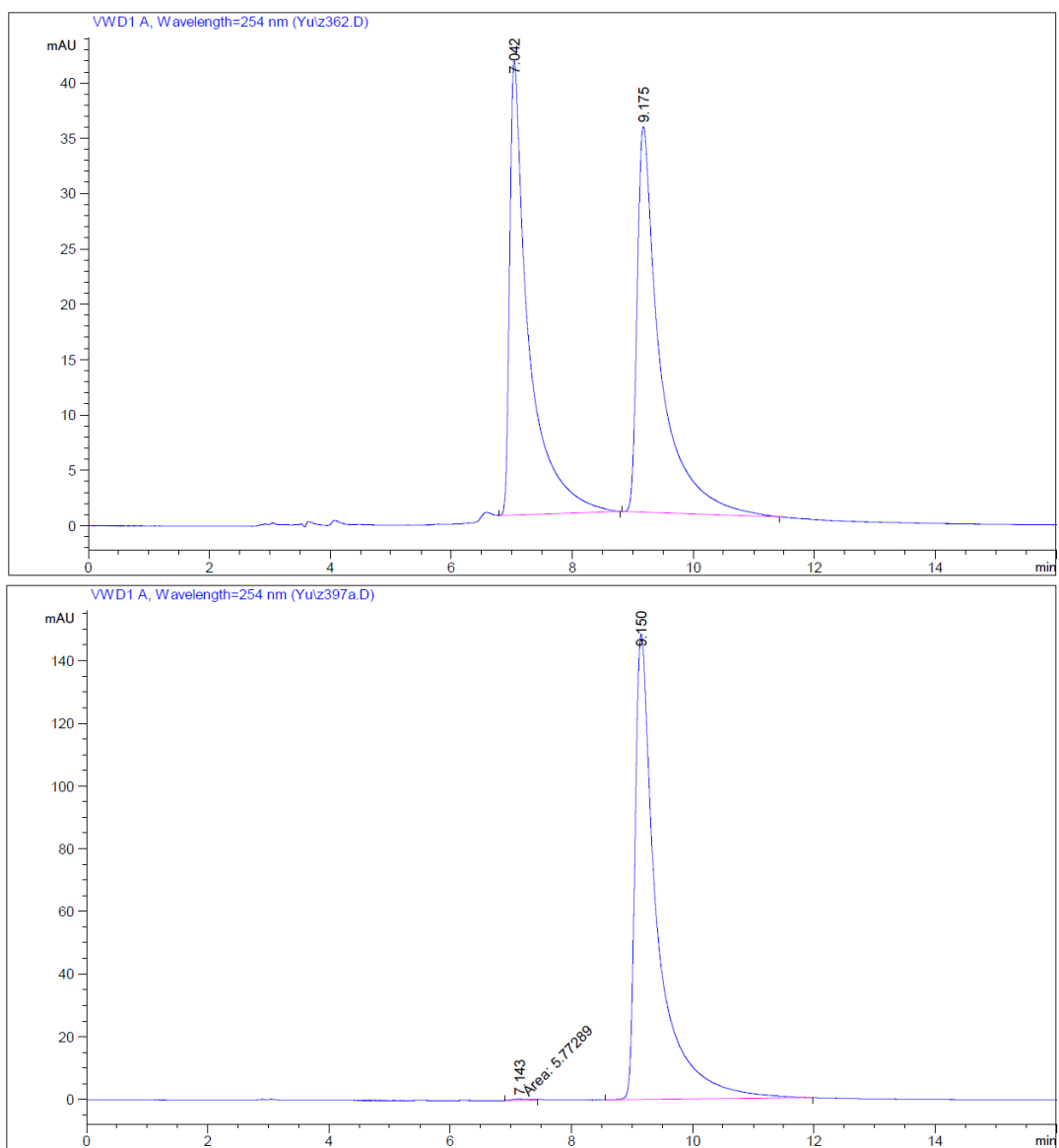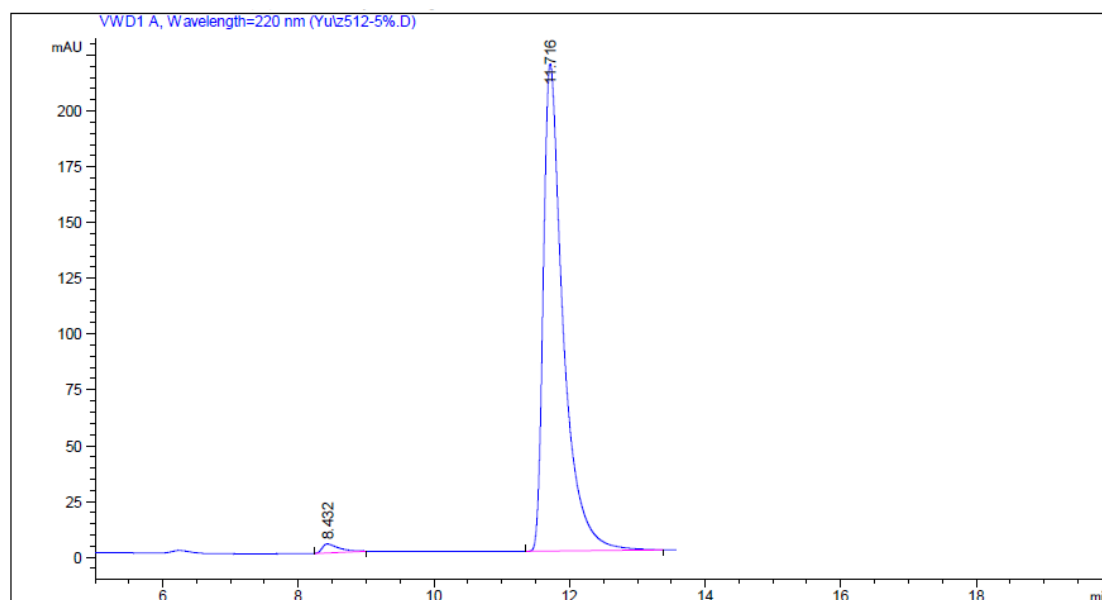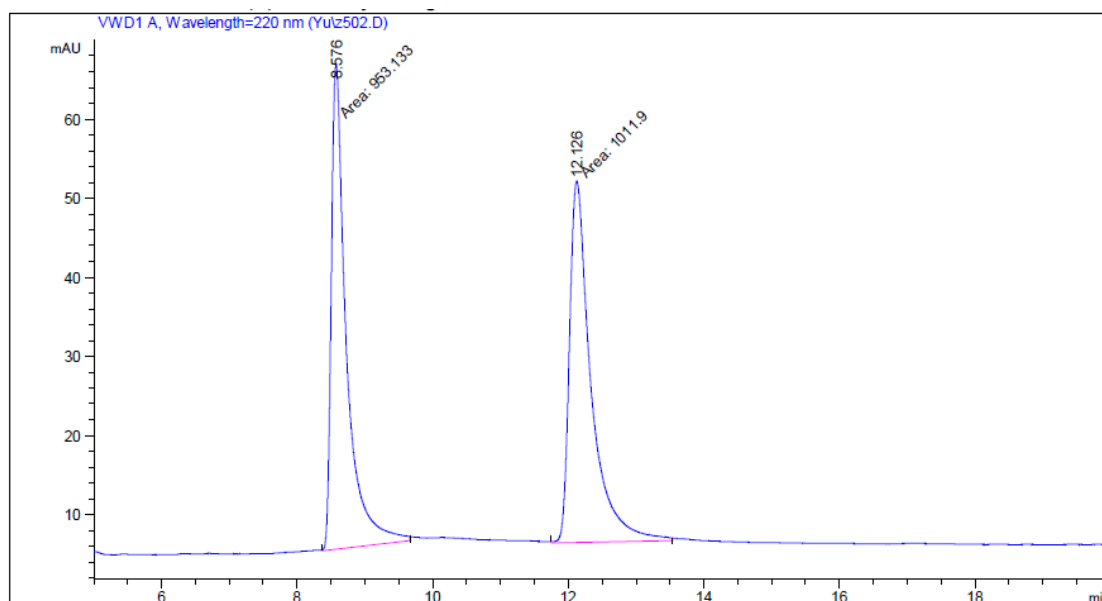
```
Peak RetTime Type  Width     Area     Height     Area
 #    [min]        [min]   [mAU*s]    [mAU]        %
----|-------|----|-------|----------|----------|--------|
  1   8.432 BB   0.1996    68.05143   4.00675   1.5121
  2  11.716 BB   0.2962  4432.49512 218.45798  98.4879
```

Figure 107 HPLC traces (Daicel Chiralpak AD-H column) of *rac*-**20q** (reference) and (*R*)-**20q**. Area integration = 98.5:1.5 (97.0% *ee*).
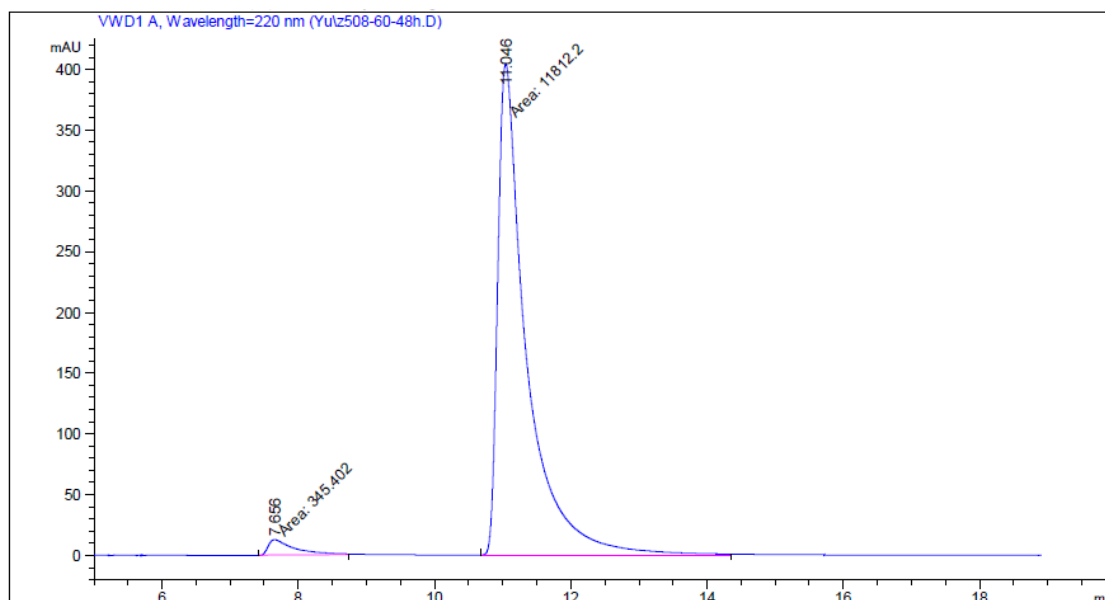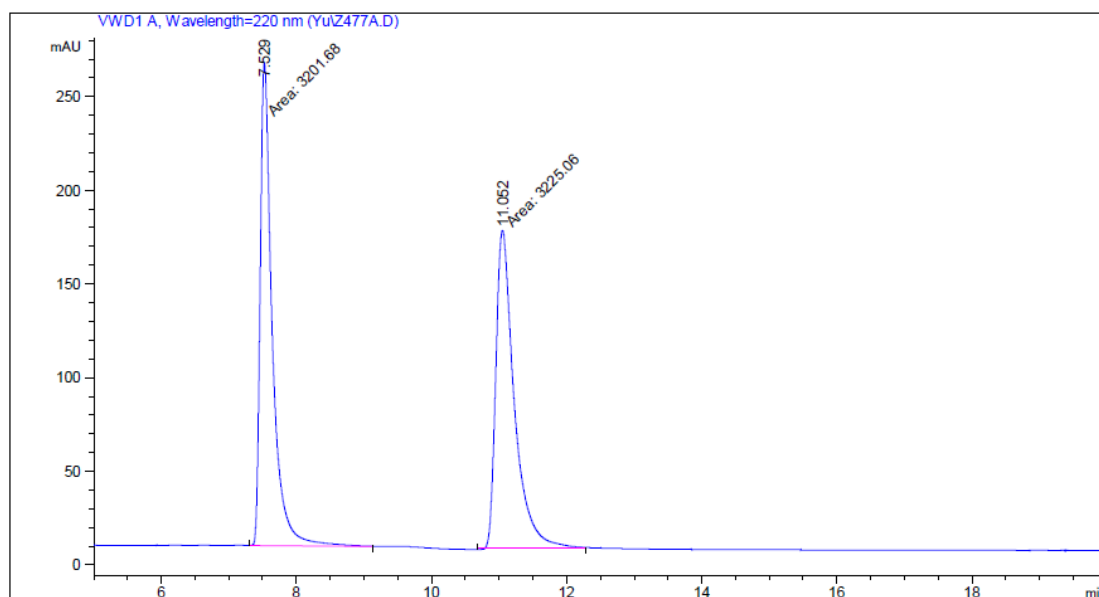
```
Peak  RetTime Type  Width      Area      Height      Area
  #    [min]         [min]    [mAU*s]     [mAU]        %
----|-------|----|-------|-----------|-----------|--------|
  1    7.656 MM    0.4537  345.40186   12.68941   2.8410
  2   11.046 MM    0.4870  1.18122e4   404.23776  97.1590
```

Figure 108 HPLC traces (Daicel Chiralpak AD-H column) of *rac*-**20r** (reference) and (*R*)-**20r**. Area integration = 97.2:2.8 (94.4% *ee*).
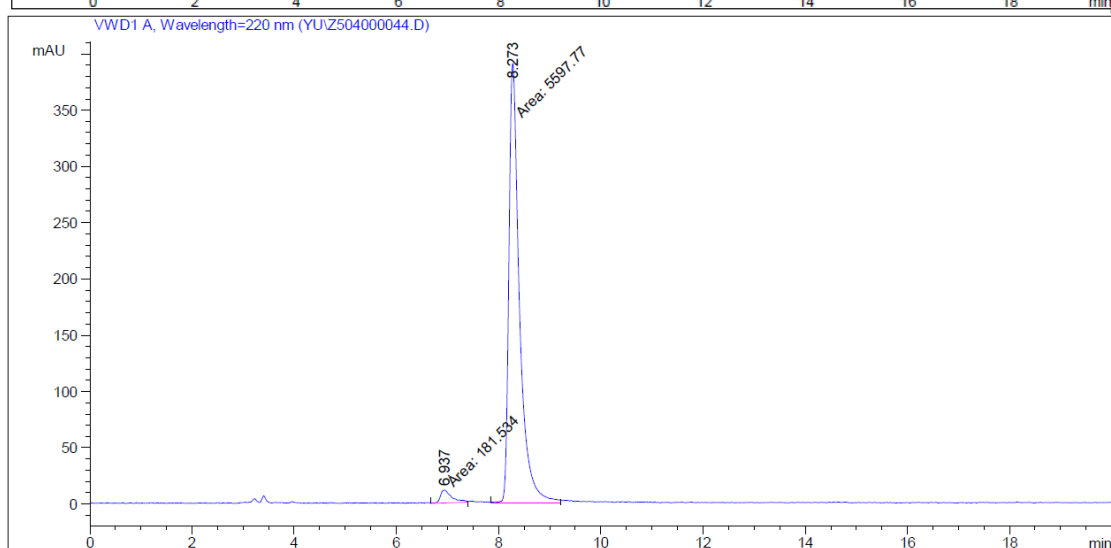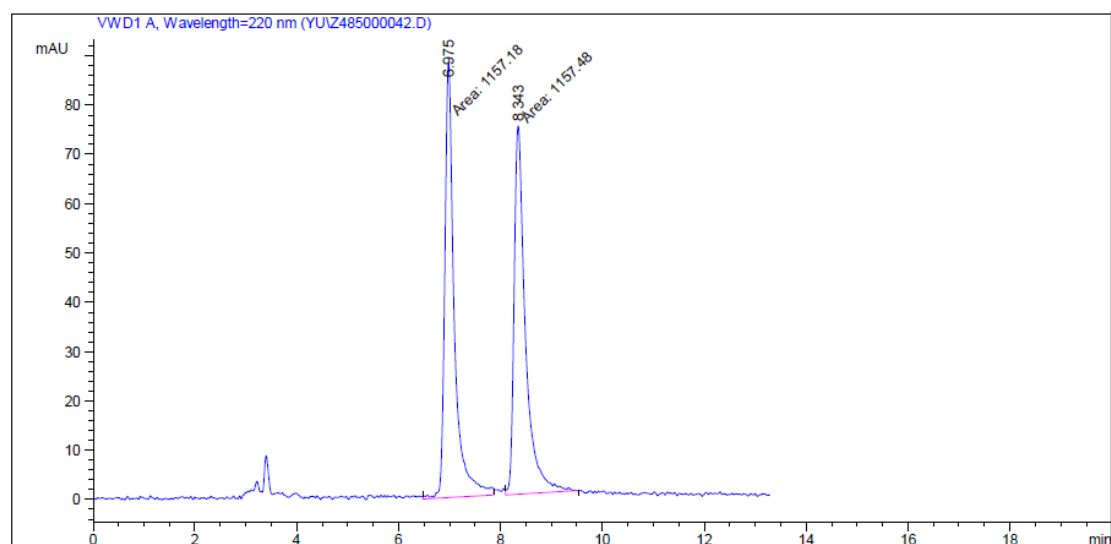
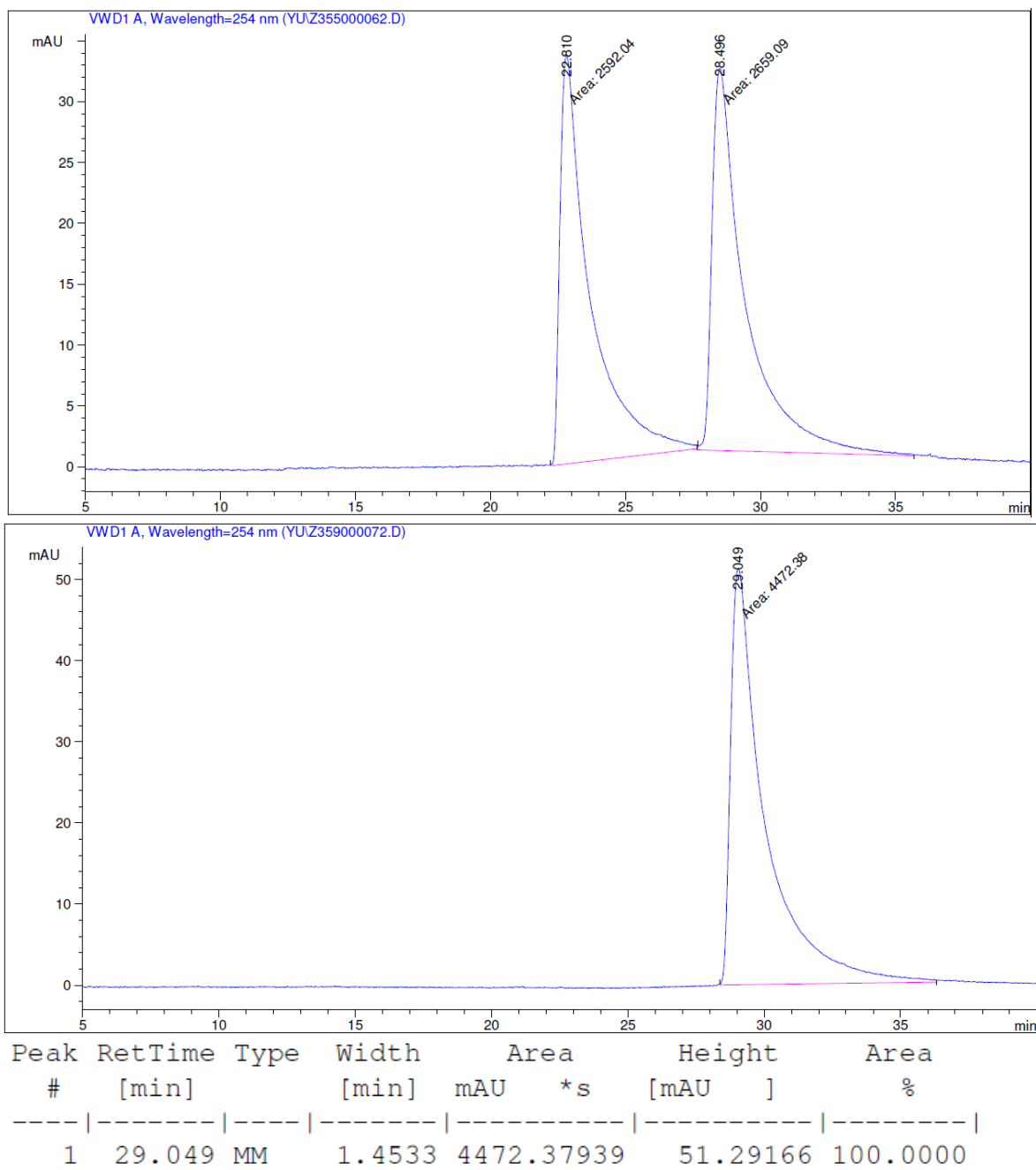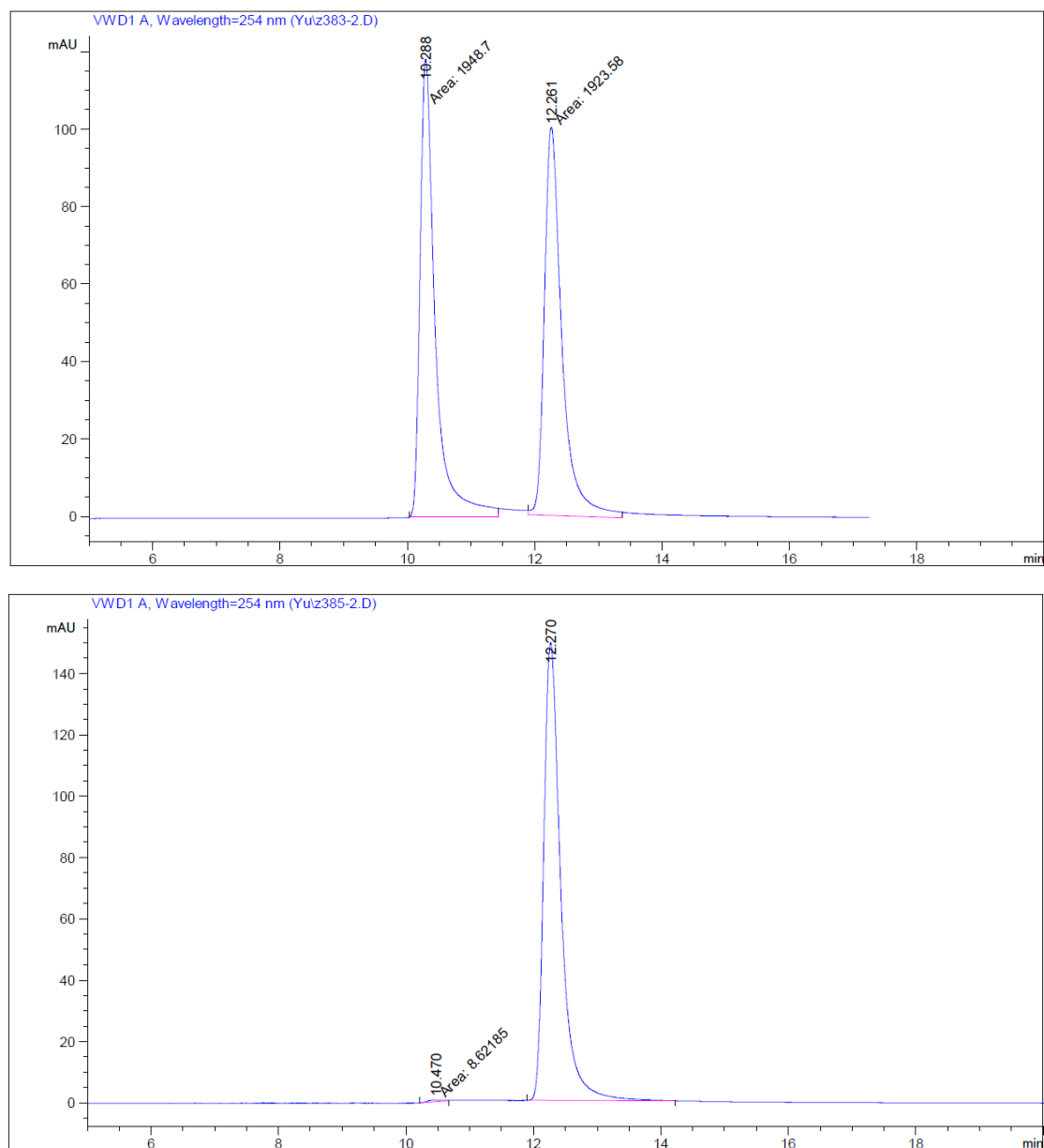| Peak	RetTime	Type	Width	Area	Height	Area
#	[min]		[min]	mAU *s	[mAU]	%
1	6.937	MM	0.2634	181.53435	11.48698	3.1411
2	8.273	MM	0.2391	5597.76562	390.21005	96.8589

Figure 109 HPLC traces (Daicel Chiralpak AD-H column) of *rac*-**20s** (reference) and (*R*)-**20s**. Area integration = 96.9:3.1 (93.8% *ee*).

| Peak | RetTime | Type | Width | Area | Height | Area |
#	[min]		[min]	[mAU*s]	[mAU]	%
1	8.638	MM	0.2955	20.47960	1.15490	0.6162
2	14.308	BV R	0.3816	3302.94287	124.05717	99.3838

Figure 110 HPLC traces (Daicel Chiralpak AD-H column) of *rac*-**20t** (reference) and (*R*)-**20t**. Area integration = 99.4:0.6 (98.8% *ee*).
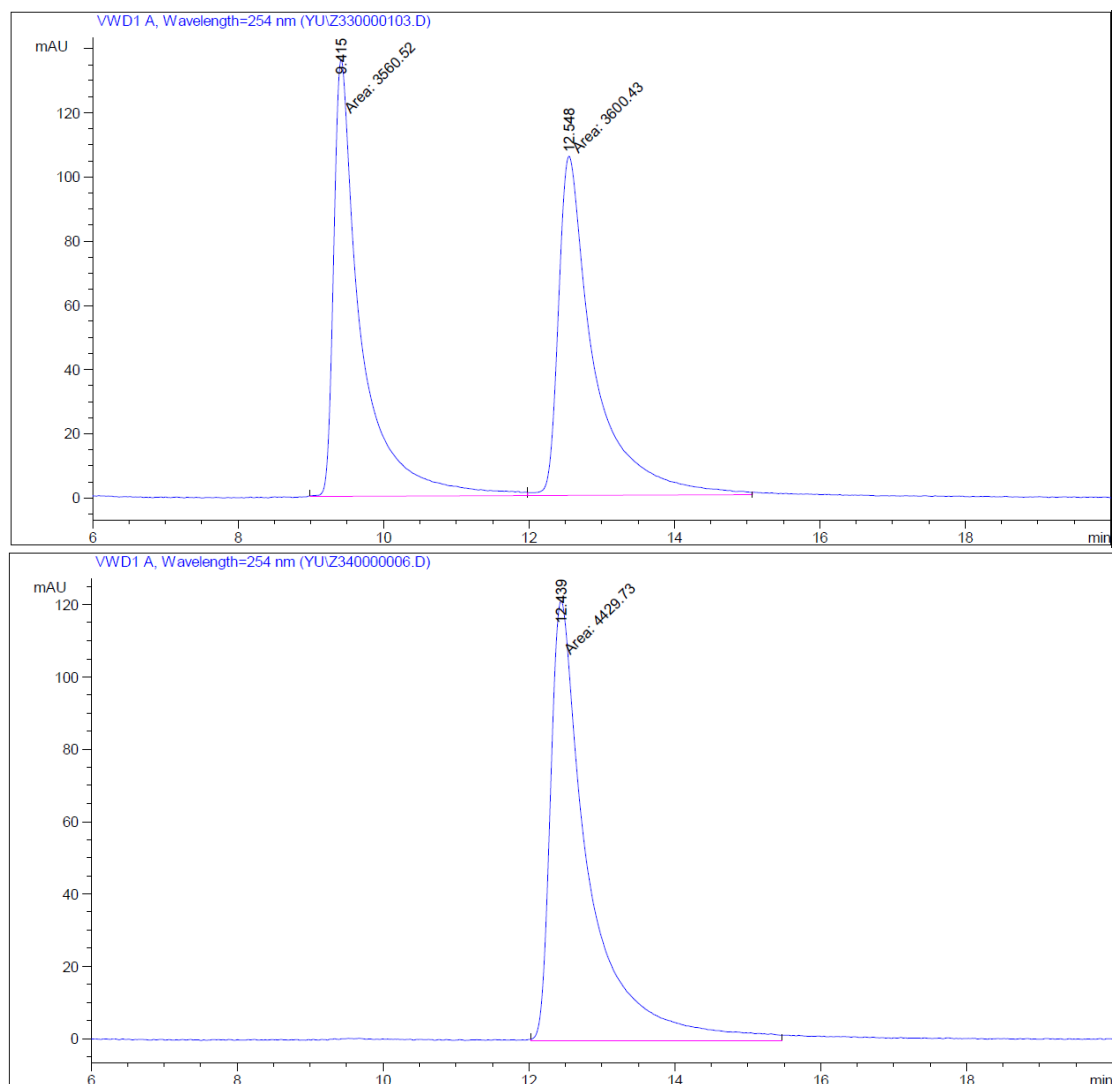
Peak	RetTime	Type	Width	Area	Height	Area
#	[min]		[min]	mAU *s	[mAU]	%
1	10.690	MM	0.5310	1.34408e4	421.88242	100.0000

Figure 111 HPLC traces (Daicel Chiralpak OD-H column) of *rac*-**20u** (reference) and (*R*)-**20u**. Area integration > 99 (>99% *ee*).

```
Peak RetTime Type  Width     Area     Height     Area
  #   [min]        [min]    [mAU*s]    [mAU]       %
----|-------|----|-------|----------|----------|--------|
   1  10.270 MM    0.4014  259.26907   10.76560   1.6519
   2  12.844 MM    0.3803 1.54357e4  676.42792  98.3481
```
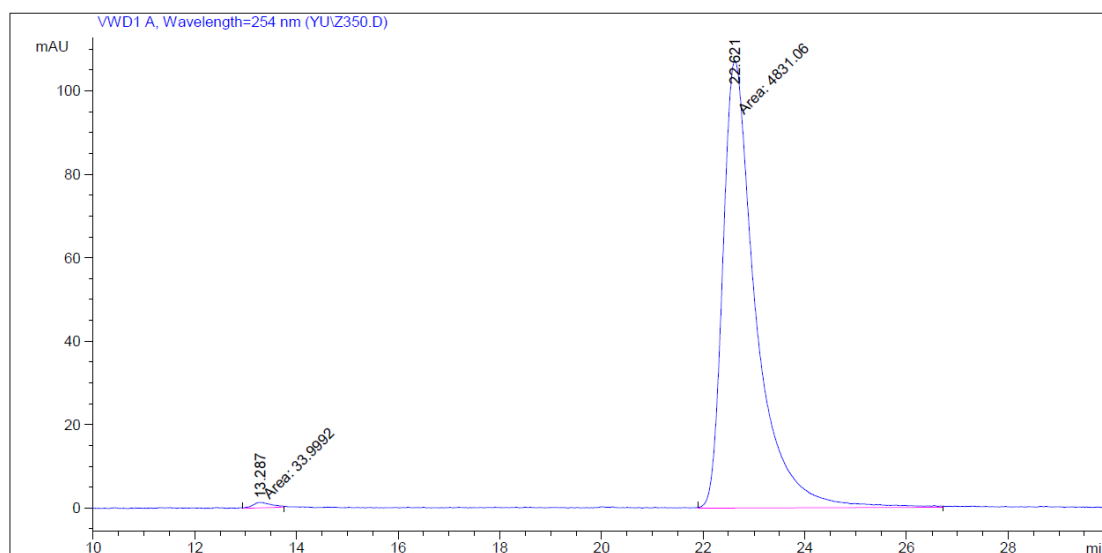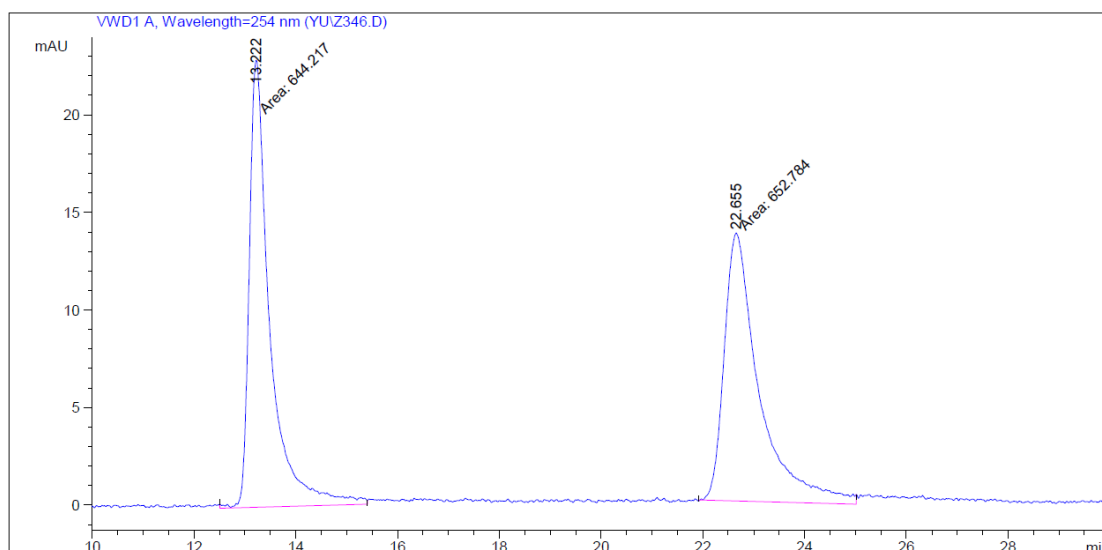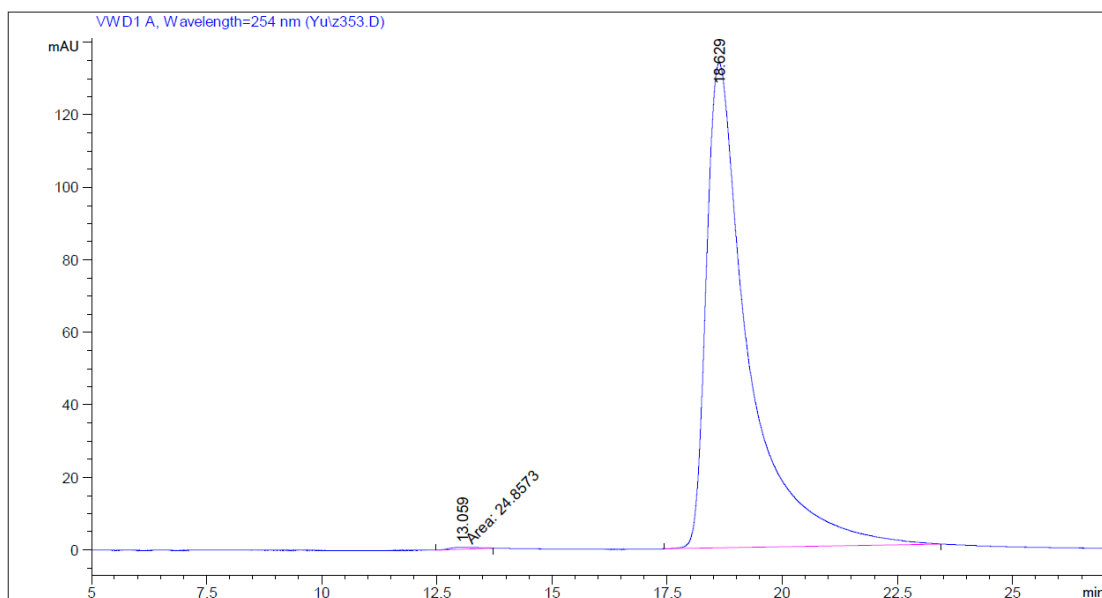
Figure 112 HPLC traces (Daicel Chiralpak AD-H column) of *rac*-**20v** (reference) and (*R*)-**20v**. Area integration = 98.3:1.7 (96.6% *ee*).
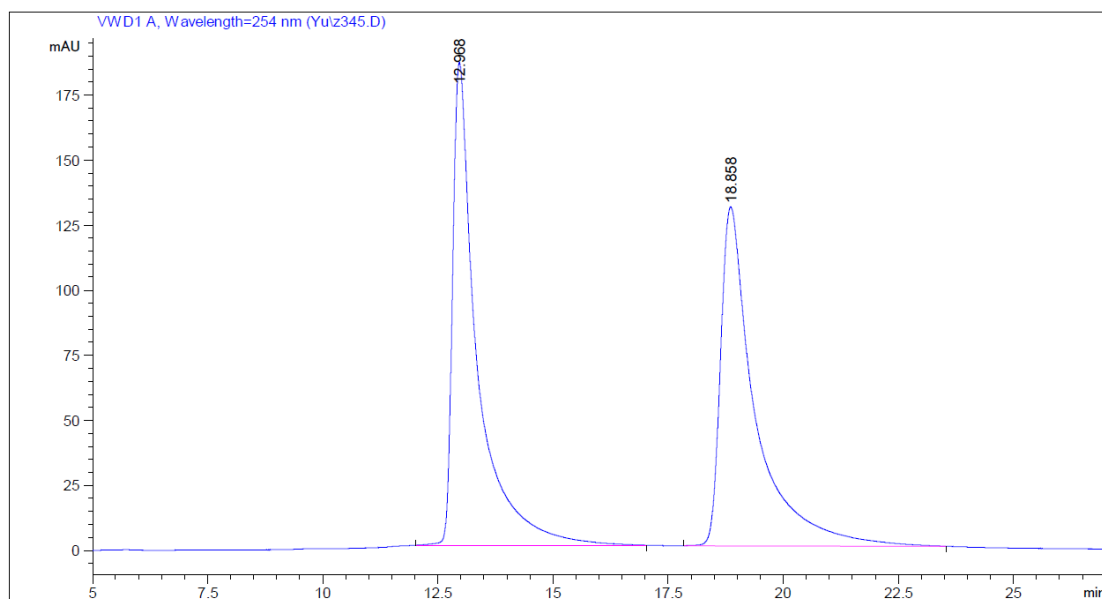
```
Peak  RetTime  Type  Width      Area        Height       Area
  #    [min]          [min]   mAU    *s    [mAU    ]       %
----|-------|----|-------|----------|-----------|--------|
   1  13.189  MM    0.5482 3795.86548  115.40844   99.4234
   2  16.228  MM    0.4653   22.01248 7.88535e-1    0.5766
```
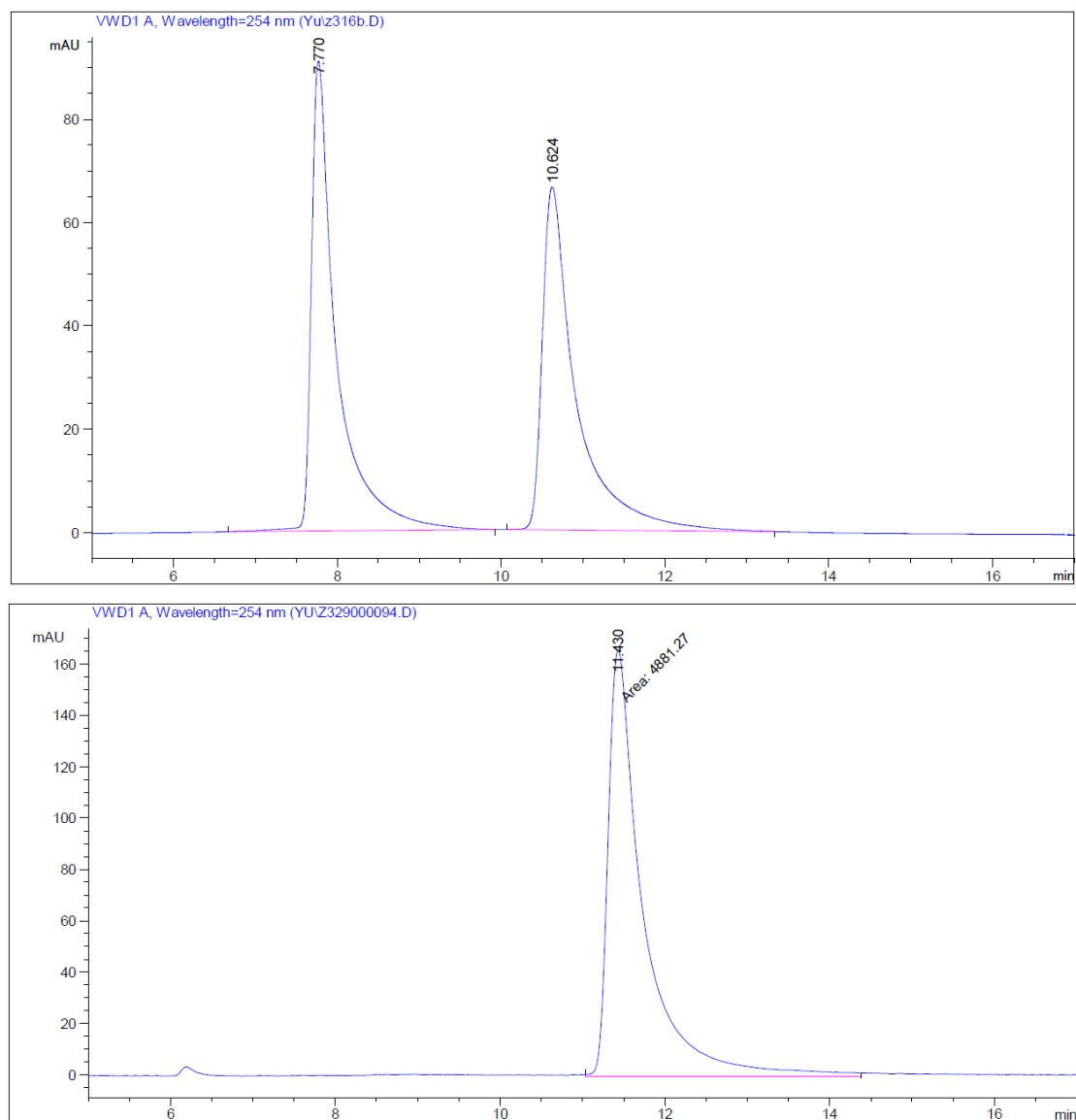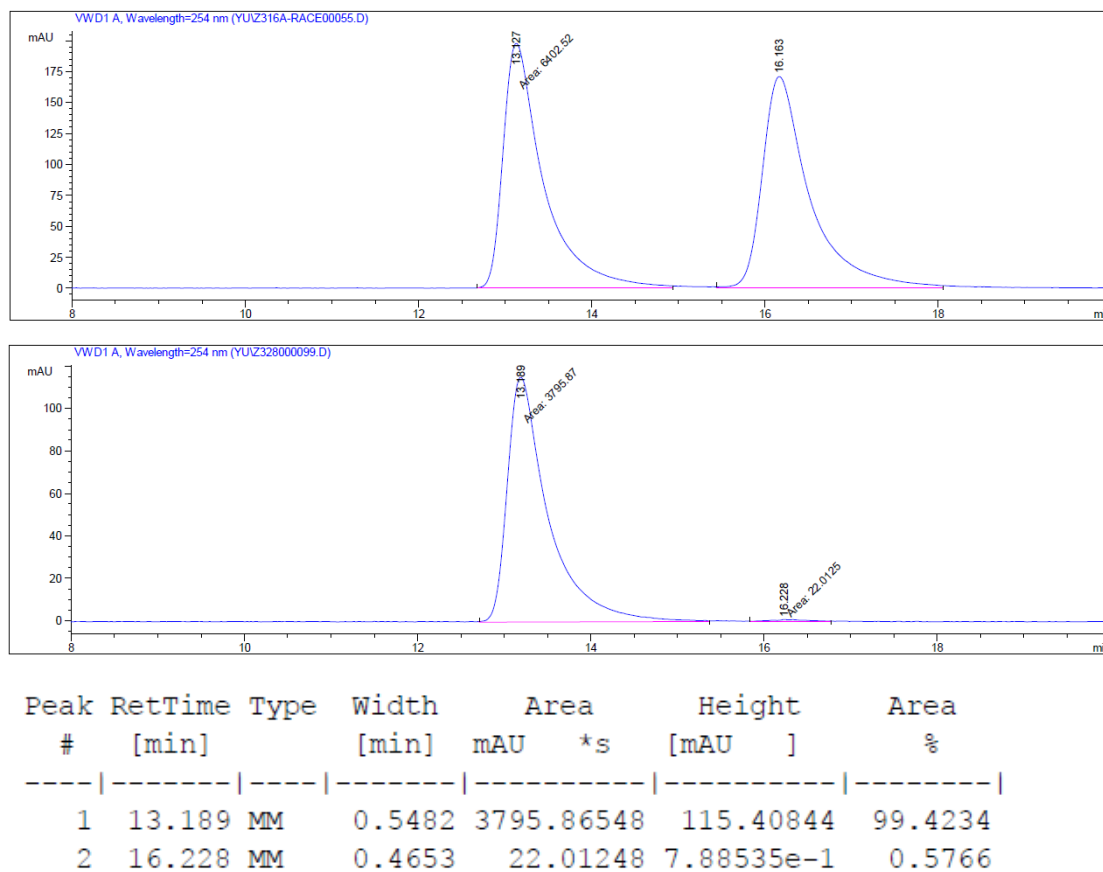
Figure 113 HPLC traces (Daicel Chiralpak AD-H column) of *rac*-**20w** (reference) and (*R*)-**20w**. Area integration = 99.4:0.6 (98.8% *ee*).

VWD1 A, Wavelength=254 nm (YU\Z389000021.D)

VWD1 A, Wavelength=254 nm (YU\Z391000013.D)

Peak	RetTime	Type	Width	Area	Height	Area
#	[min]		[min]	mAU *s	[mAU]	%
1	8.835	MM	0.4821	309.94058	10.71445	2.9348
2	13.071	MM	0.5601	1.02509e4	305.04431	97.0652
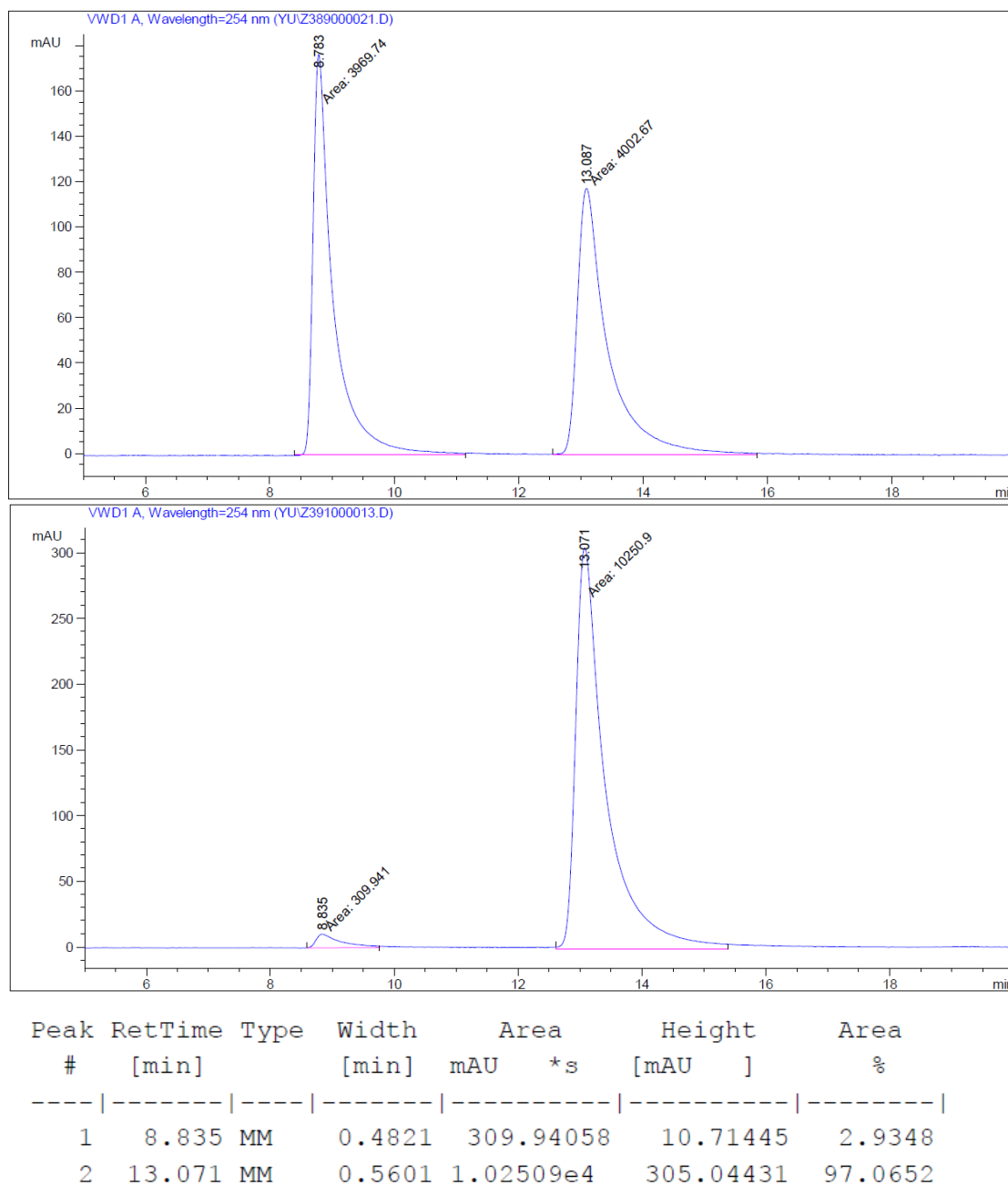
Figure 114 HPLC traces (Daicel Chiralpak AD-H column) of *rac*-**20x** (reference) and (*R*)-**20x**. Area integration= 97.1:2.9 (94.3% *ee*).
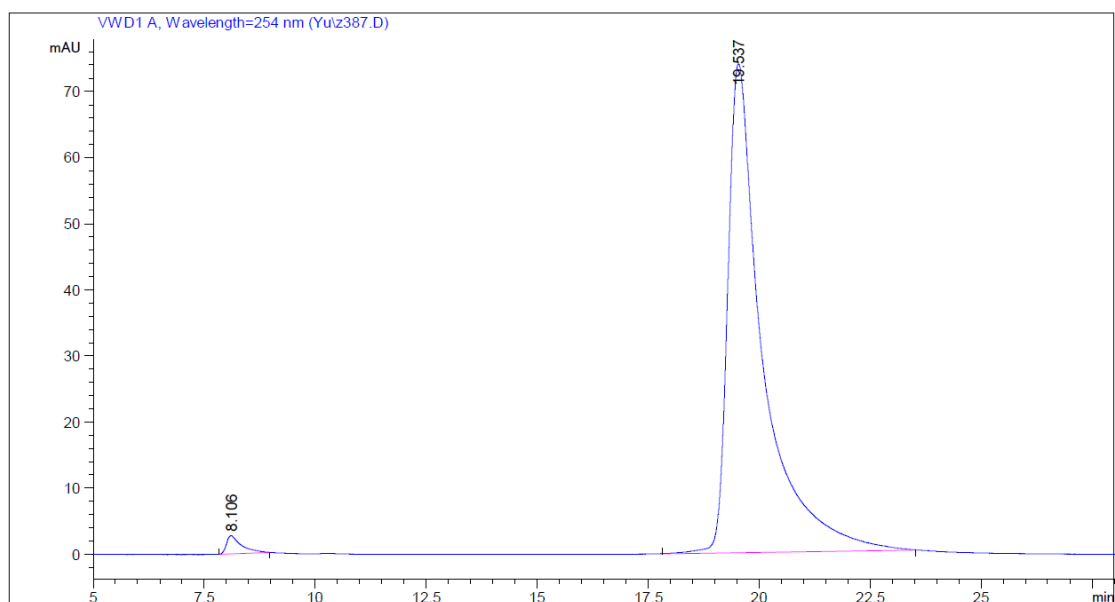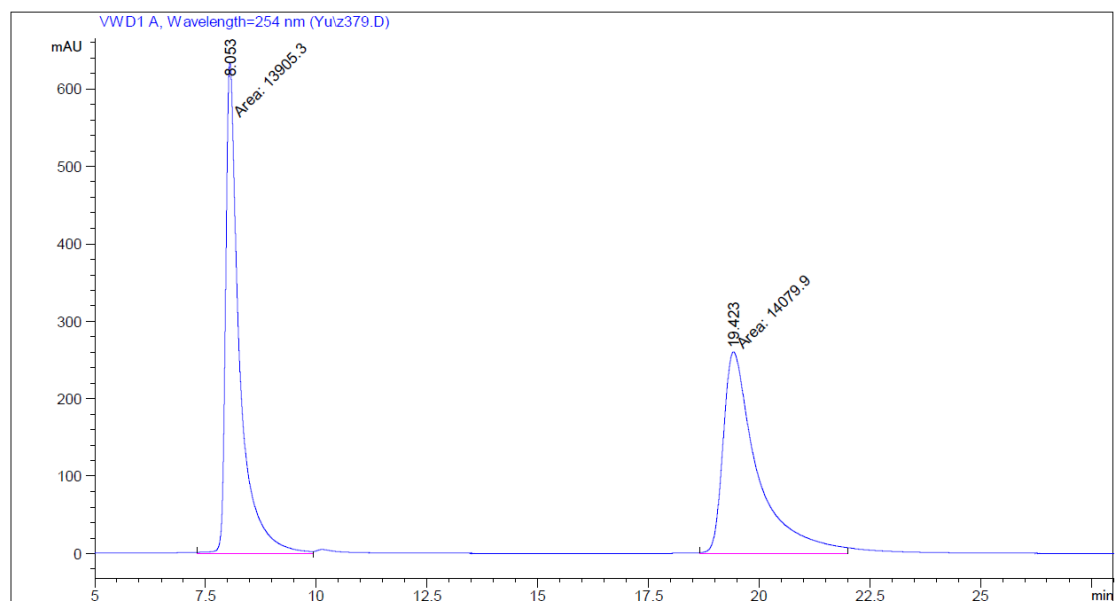
```
Peak  RetTime Type   Width     Area      Height     Area
  #    [min]         [min]    [mAU*s]     [mAU]       %
----|-------|----|-------|----------|----------|--------|
  1    8.106 BB    0.2737   63.75798    2.75290   1.5560
  2   19.537 VB R  0.6678 4033.90918   73.96357  98.4440
```

Figure 115 HPLC traces (Daicel Chiralpak AD-H column) of *rac*-**20y** (reference) and (*R*)-**20y**. Area integration = 98.4:1.6 (96.8% *ee*).

Peak	RetTime	Type	Width	Area	Height	Area
#	[min]		[min]	mAU *s	[mAU]	%
1	9.492	MM R	0.2524	14.43311	9.53005e-1	0.4431
2	25.244	BB	0.7864	3243.23242	63.82906	99.5569

Figure 116 HPLC traces (Daicel Chiralcel OJ-H column) of *rac*-**26a** (reference) and (*S*)-**26a**. Area integration = 99.6:0.4 (99.2% *ee*).
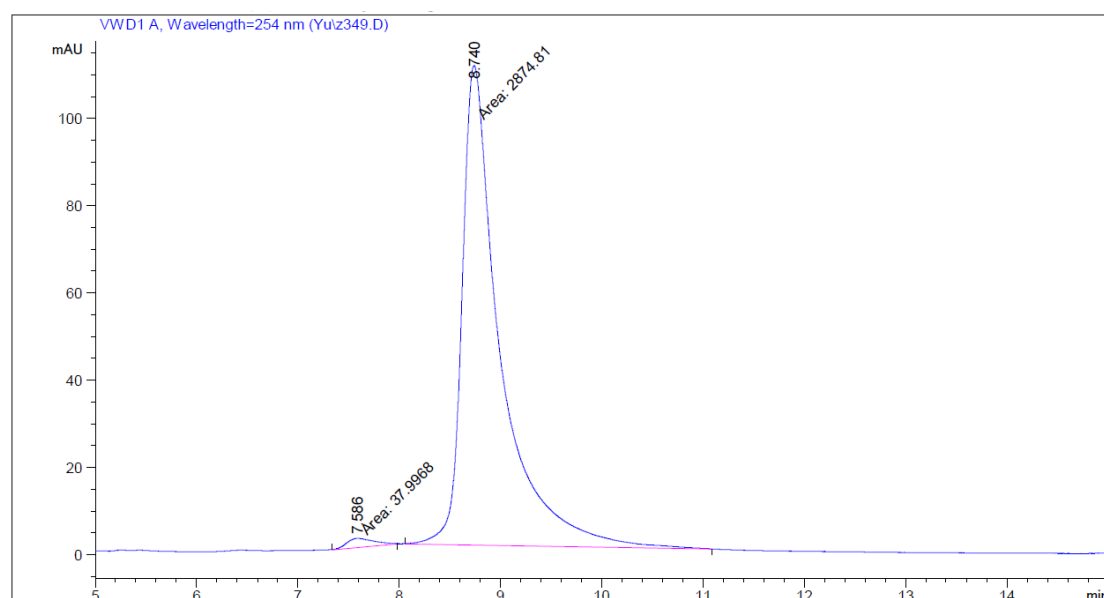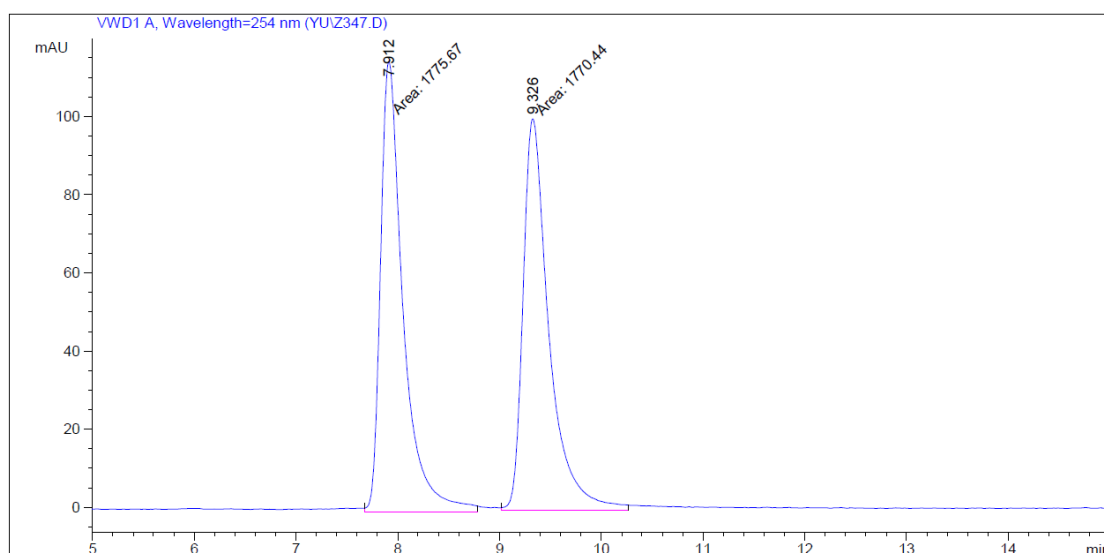
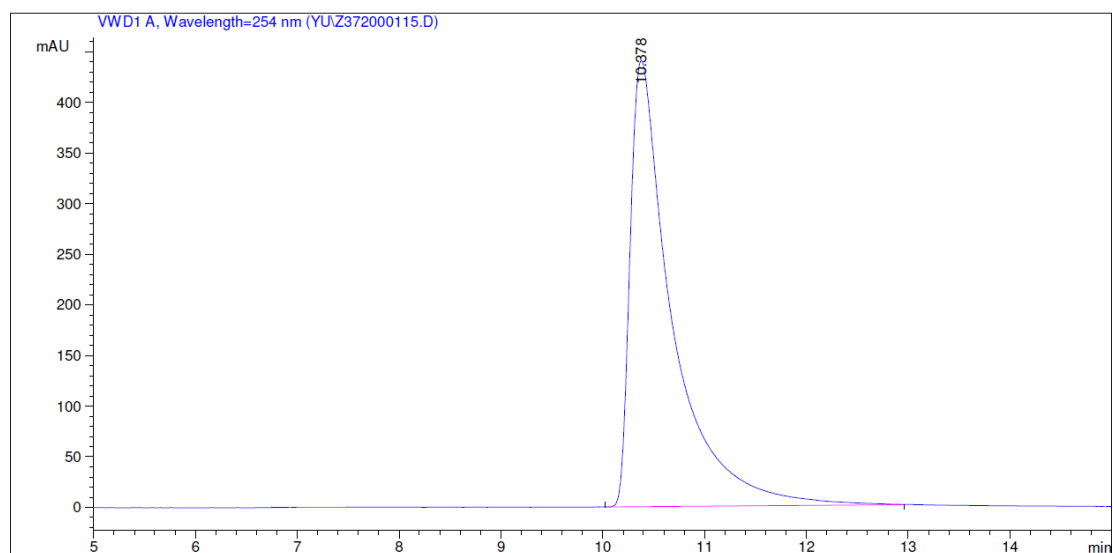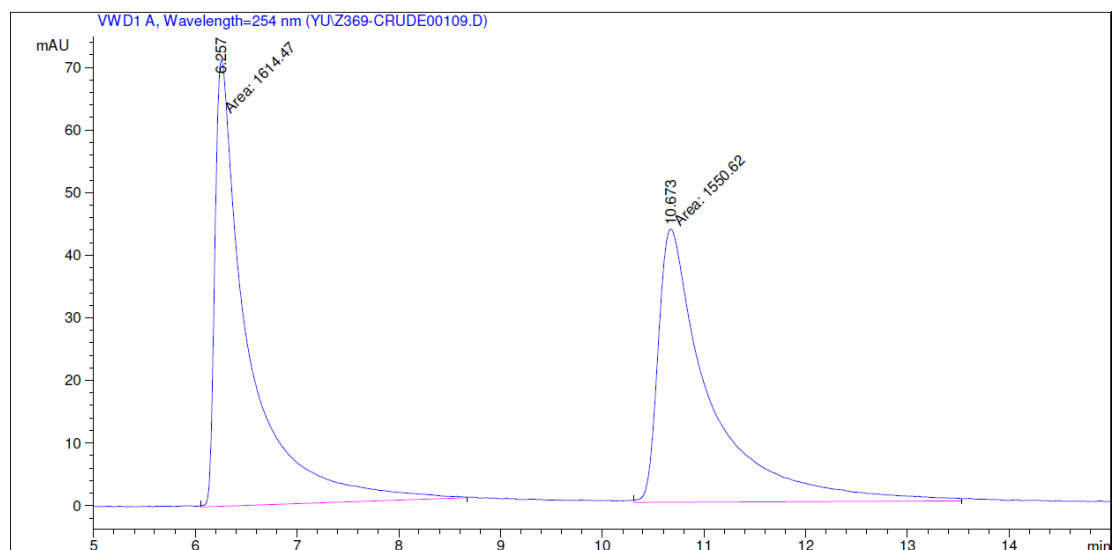| Peak #	RetTime [min]	Type	Width [min]	Area [mAU*s]	Height [mAU]	Area %
1	8.538	MM R	0.2815	21.44894	1.26990	0.3871
2	12.334	VB R	0.3811	5519.38184	219.69543	99.6129

Figure 117 HPLC traces (Daicel Chiralcel OJ-H column) of *rac*-**26b** (reference) and (*S*)-**26b**. Area integration = 99.6:0.4 (99.2% *ee*).

```
Peak RetTime Type  Width      Area      Height    Area
  #   [min]        [min]     [mAU*s]     [mAU]      %
----|-------|----|-------|-----------|----------|--------|
  1   6.915 FM R  0.1944    62.19359    5.33229   0.3971
  2  11.608 MF R  0.4219 1.55996e4    616.18958  99.6029
```

Figure 118 HPLC traces (Daicel Chiralcel OJ-H column) of *rac*-**26c** (reference) and (*S*)-**26c**. Area integration = 99.6:0.4 (99.2% *ee*).

VWD1 A, Wavelength=254 nm (TYQ\z993.D)

VWD1 A, Wavelength=254 nm (TYQ\TYQB22-1%.D)

Peak #	RetTime [min]	Type	Width [min]	Area [mAU*s]	Height [mAU]	Area %
1	6.534	MM R	0.1794	12.06940	1.12154	0.3744
2	8.868	BB	0.2530	3211.79810	195.16258	99.6256

Figure 119 HPLC traces (Daicel Chiralcel OJ-H column) of *rac*-**26d** (reference) and (*S*)-**26d**. Area integration = 99.6:0.4 (99.2% *ee*).

```
Peak  RetTime Type   Width      Area      Height      Area
  #    [min]         [min]    [mAU*s]     [mAU]        %
----|-------|----|-------|----------|----------|--------|
  1   20.062 MM R  0.6813    15.74068 3.85083e-1   0.5202
  2   22.094 MM R  0.7381  3010.23633   67.97128  99.4798
```

Figure 120 HPLC traces (Daicel Chiralcel OJ-H column) of *rac*-**26e** (reference) and (*S*)-**26e**. Area integration = 99.5:0.5 (99.0% *ee*).

```
Peak  RetTime Type   Width     Area      Height    Area
 #     [min]         [min]    [mAU*s]     [mAU]      %
----|-------|----|-------|----------|----------|--------|
  1  11.783 MM R  0.3970 8037.81641 337.46317  98.4998
  2  17.966 MM R  0.8016  122.41902   2.54524   1.5002
```

Figure 121 HPLC traces (Daicel Chiralcel OJ-H column) of *rac*-**26f** (reference) and (*S*)-**26f**. Area integration = 98.5:1.5 (97.0% *ee*).

VWD1 A, Wavelength=254 nm (TYQ\TYQ-z997.D)

VWD1 A, Wavelength=254 nm (TYQ\TYQB29.D)

```
Peak  RetTime Type   Width      Area        Height      Area
  #    [min]        [min]     [mAU*s]      [mAU]         %
----|-------|----|-------|----------|----------|--------|
  1    8.767 MM R  0.2488   14.22219  9.52706e-1    0.3165
  2   17.188 BB    0.5082 4479.72607  119.95274    99.6835
```

Figure 122 HPLC traces (Daicel Chiralcel OJ-H column) of *rac*-**26g** (reference) and (*S*)-**26g**. Area integration = 99.7:0.3 (99.4% *ee*).

```
Peak  RetTime Type  Width     Area      Height    Area
 #     [min]         [min]    [mAU*s]    [mAU]      %
----|-------|----|-------|----------|----------|--------|
   1   8.452  MM R  0.2729   47.66947   2.91115   1.8649
   2  18.403  BB    0.5252  2508.53540  56.15157  98.1351
```
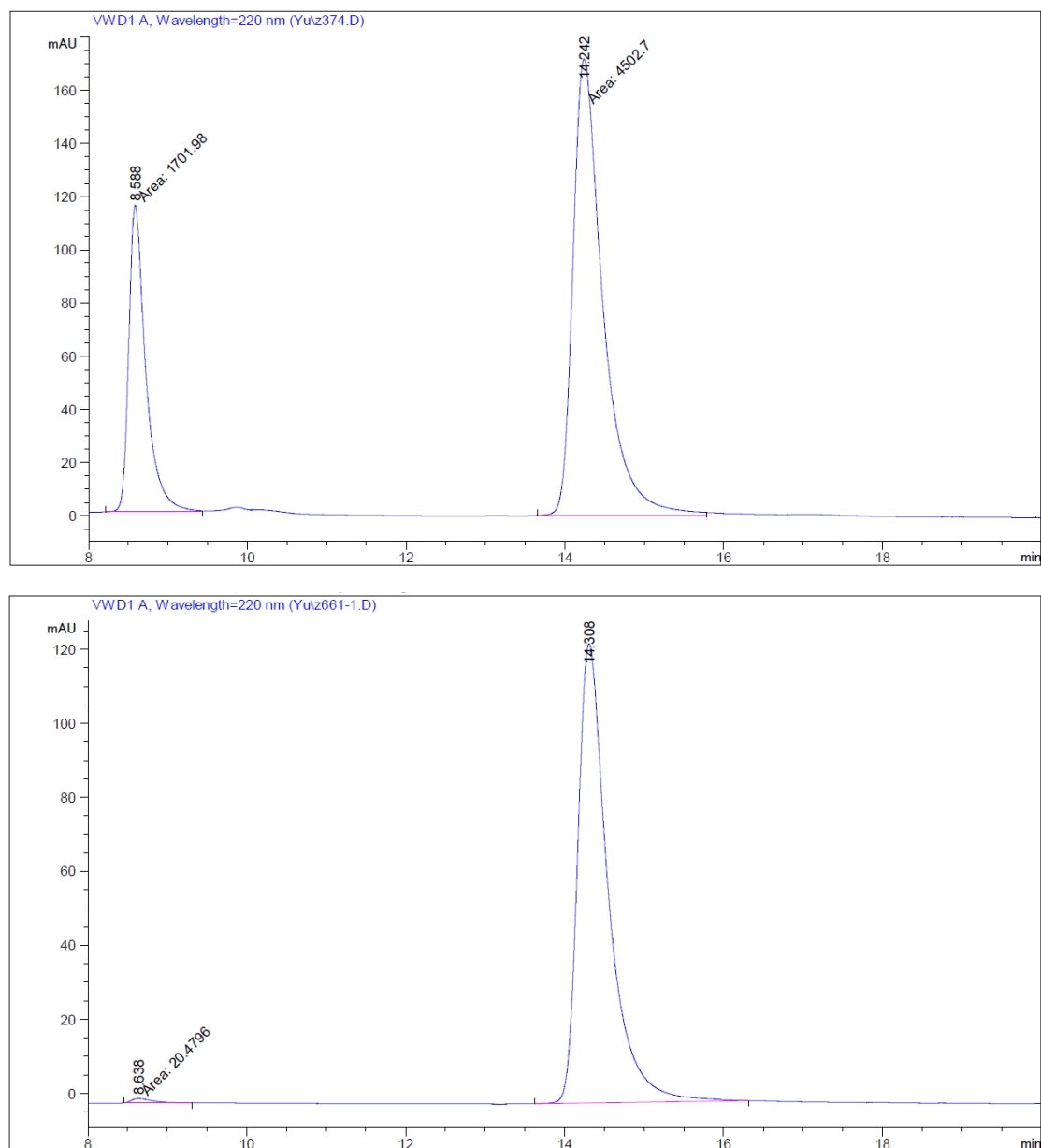
Figure 123 HPLC traces (Daicel Chiralcel OJ-H column) of *rac*-**26h** (reference) and (*S*)-**26h**. Area integration = 98.1:1.9 (96.2% *ee*).

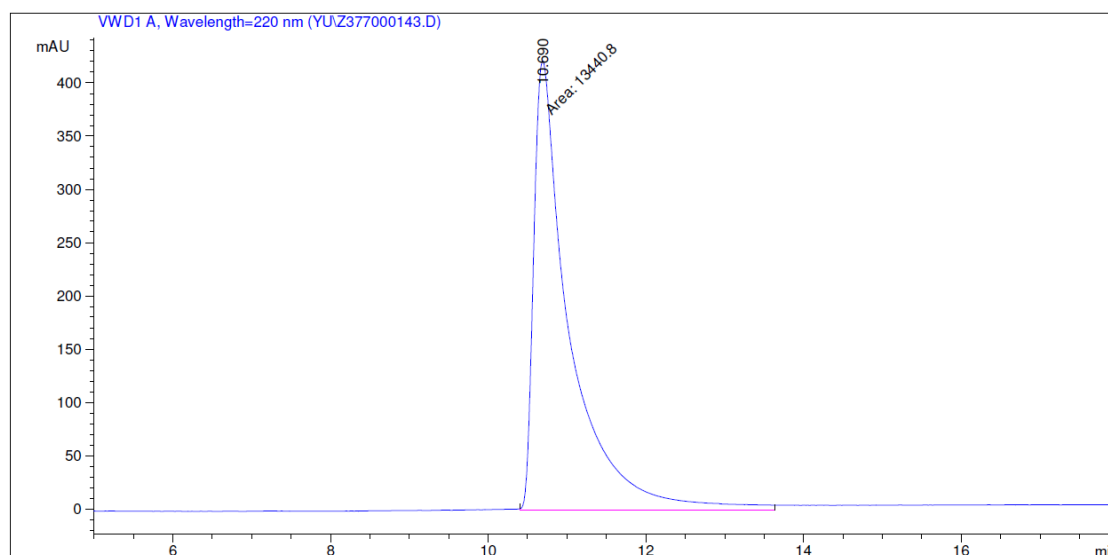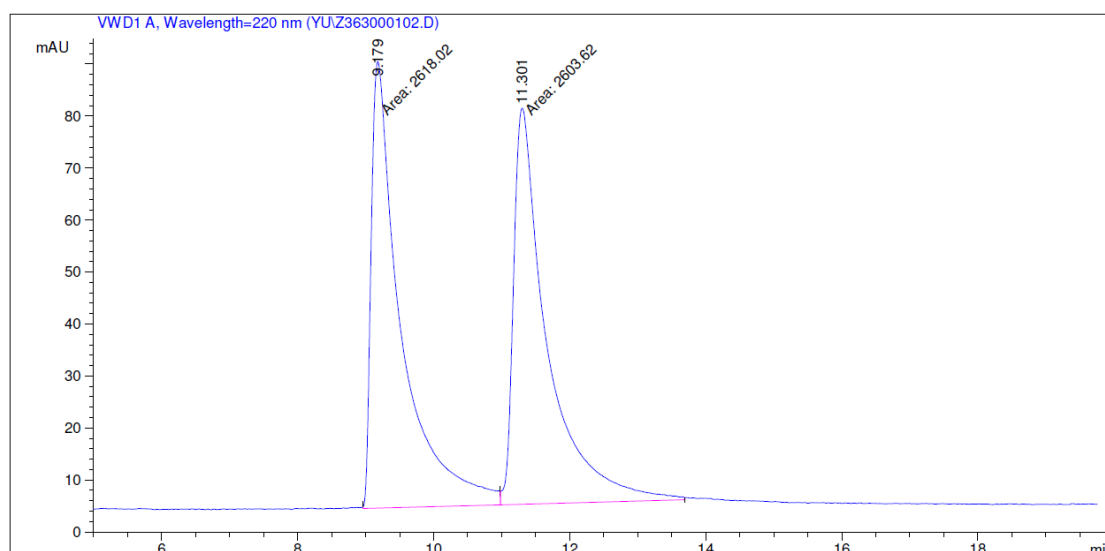| Peak	RetTime	Type	Width	Area	Height	Area
#	[min]		[min]	[mAU*s]	[mAU]	%
----	-------	----	-------	----------	----------	--------
1	14.466	MF R	0.4446	55.03230	2.06286	0.4316
2	15.356	FM R	0.4974	1.26948e4	425.33344	99.5684

Figure 124 HPLC traces (Daicel Chiralcel OJ-H column) of *rac*-**26i** (reference) and (*S*)-**26i**. Area integration = 99.6:0.4 (99.2% *ee*).

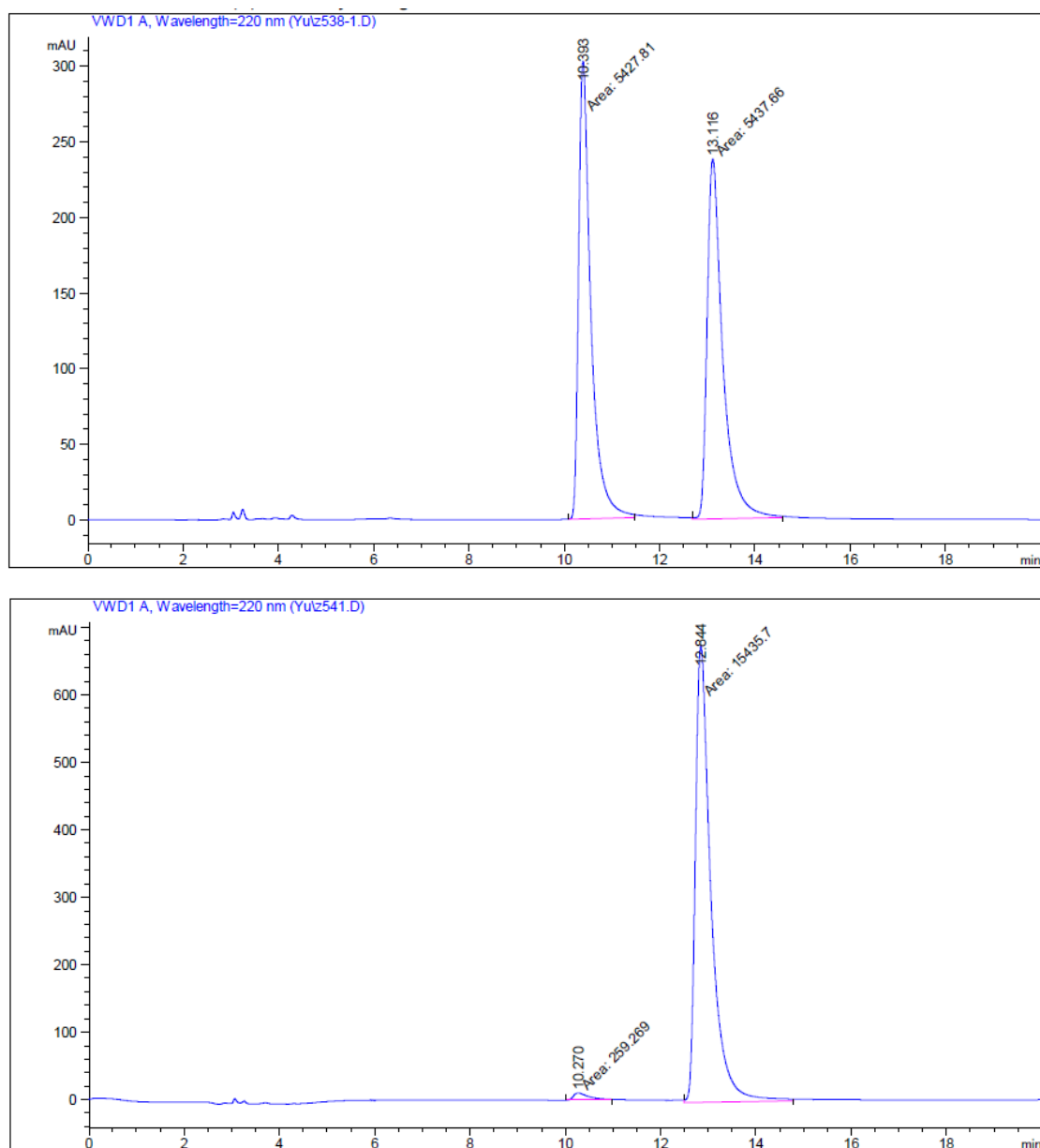| Peak #	RetTime [min]	Type	Width [min]	Area [mAU*s]	Height [mAU]	Area %
1	6.714	MM R	0.1790	7.61152	7.08536e-1	0.4085
2	9.450	BB	0.2340	1855.81030	116.07956	99.5915

Figure 125 HPLC traces (Daicel Chiralpak AD-H column) of *rac*-**26j** (reference) and (*S*)-**26j**. Area integration = 99.6:0.4 (99.2% *ee*).

Peak #	RetTime [min]	Type	Width [min]	Area mAU *s	Height [mAU]	Area %
1	15.704	MM R	0.4091	75.82781	3.08926	1.5418
2	18.076	BB	0.6896	4842.45947	99.59311	98.4582

Figure 126 HPLC traces (Daicel Chiralcel OJ-H column) of *rac*-**26k** (reference) and (*S*)-**26k**. Area integration = 98.5:1.5 (97.0% *ee*).

```
Peak  RetTime  Type   Width      Area           Height        Area
 #     [min]          [min]   mAU    *s     [mAU    ]         %
----|-------|----|-------|----------|----------|--------|
  1    7.598  MM R   0.1943     6.95182  5.96318e-1    0.4698
  2    9.338  BB     0.2831  1472.89966    80.59108   99.5302
```

Figure 127 HPLC traces (Daicel Chiralcel OJ-H column) of *rac*-**26l** (reference) and (*S*)-**26l**. Area integration = 99.5:0.5 (99.0% *ee*).
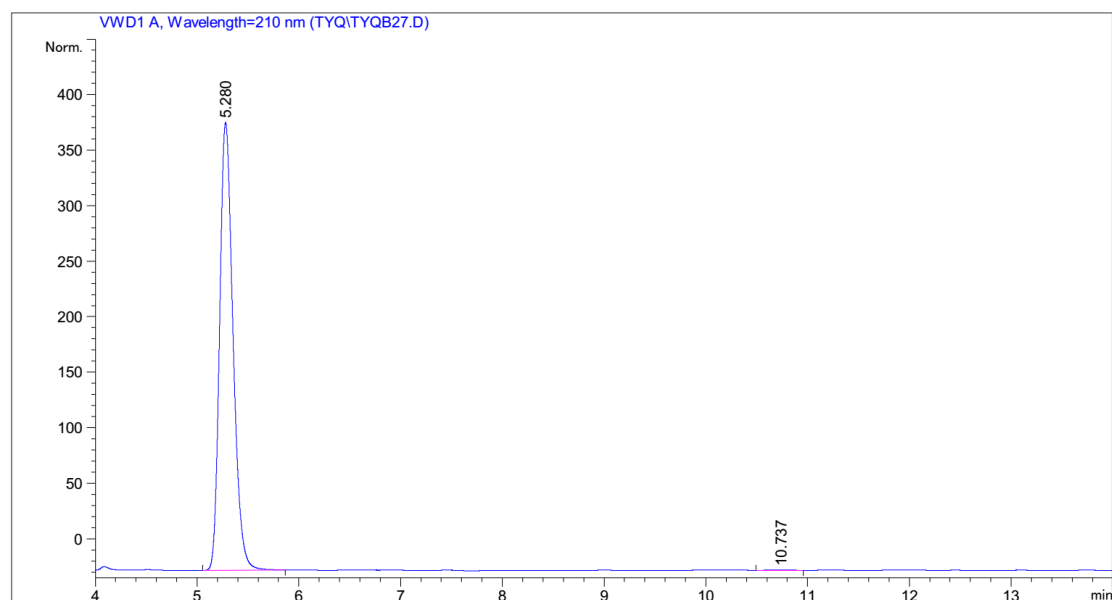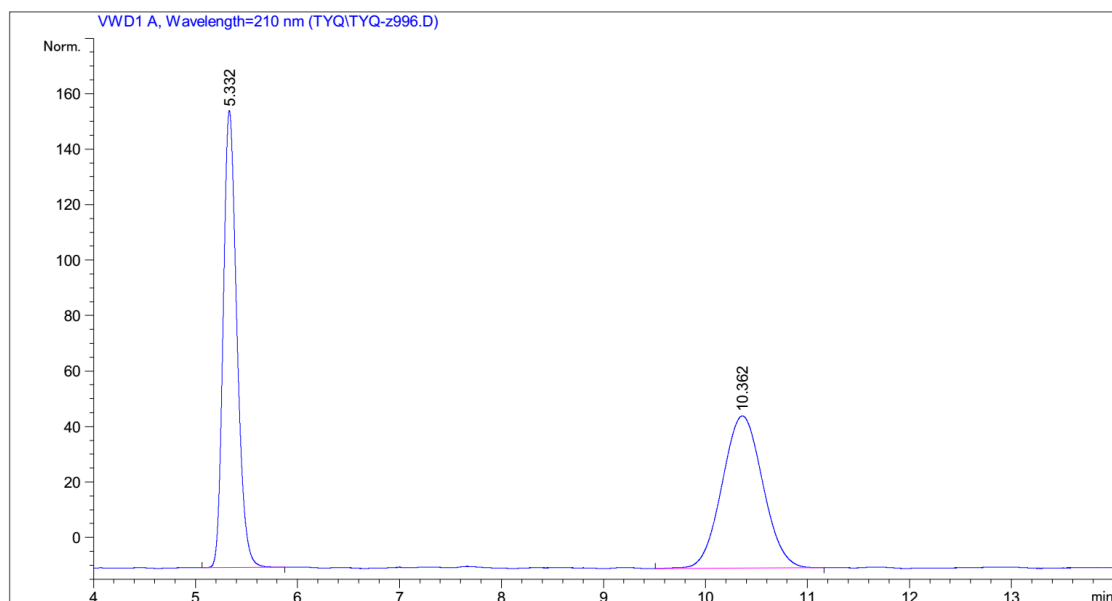
Peak #	RetTime [min]	Type	Width [min]	Area [mAU*s]	Height [mAU]	Area %
1	5.280	MM R	0.1519	3160.65942	346.74298	99.7981
2	10.737	MM R	0.2526	6.39458	4.21835e-1	0.2019

Figure 128 HPLC traces (Daicel Chiralcel OJ-H column) of *rac*-**26m** (reference) and (*S*)-**26m**. Area integration = 99.8:0.2 (99.6% *ee*).

VWD1 A, Wavelength=254 nm (TYQ\TYQB32.D)

VWD1 A, Wavelength=254 nm (TYQ\TYQB42.D)

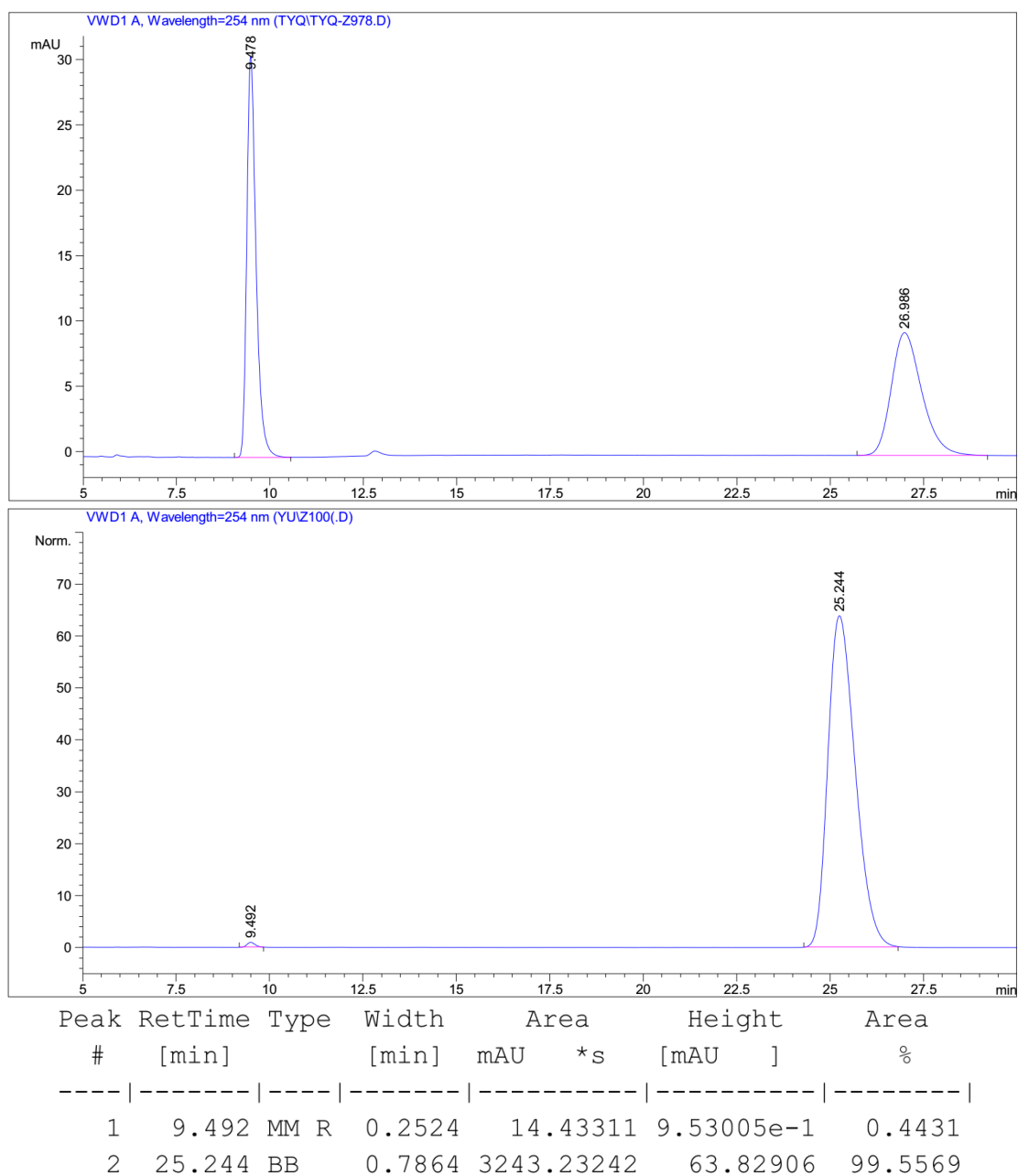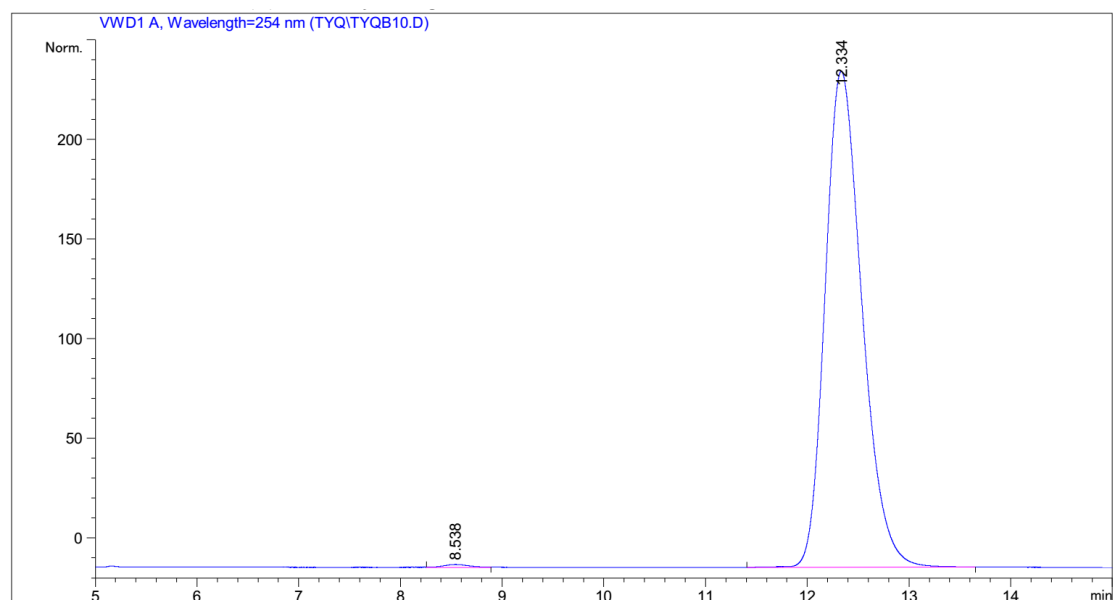| Peak #	RetTime [min]	Type	Width [min]	Area [mAU*s]	Height [mAU]	Area %
1	8.417	BV	0.1861	32.76804	2.14099	0.9363
2	17.147	MM R	0.6568	3466.96802	87.96998	99.0637

Figure 129 HPLC traces (Daicel Chiralcel OJ-H column) of *rac*-**26n** (reference) and (*S*)-**26n**. Area integration = 99.1:0.9 (98.2% *ee*).

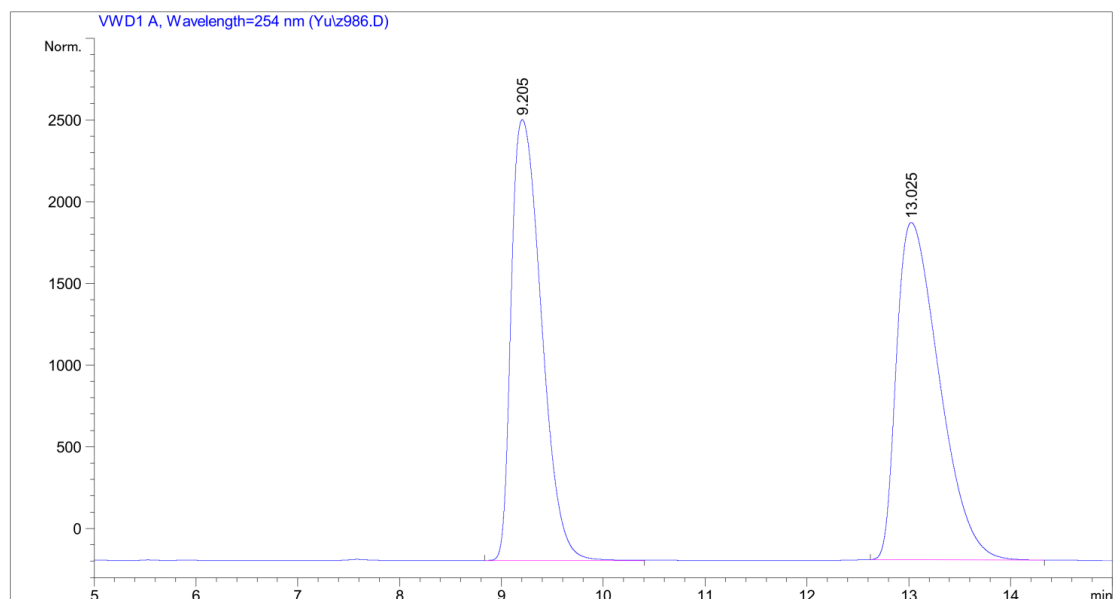| Peak #	RetTime [min]	Type	Width [min]	Area mAU *s	Height [mAU]	Area %
1	7.030	MM R	0.1953	8.06722	6.88325e-1	0.3008
2	26.368	BB	1.1024	2674.18872	36.61905	99.6992

Figure 130 HPLC traces (Daicel Chiralcel OJ-H column) of *rac*-**26o** (reference) and (*S*)-**26o**. Area integration = 99.7:0.3 (99.4% *ee*).
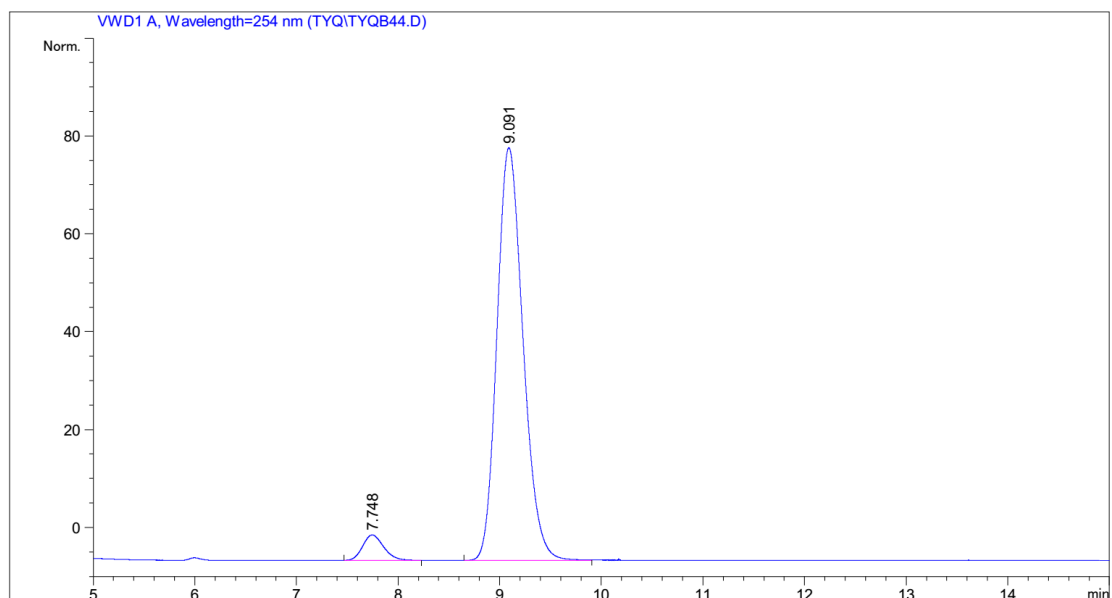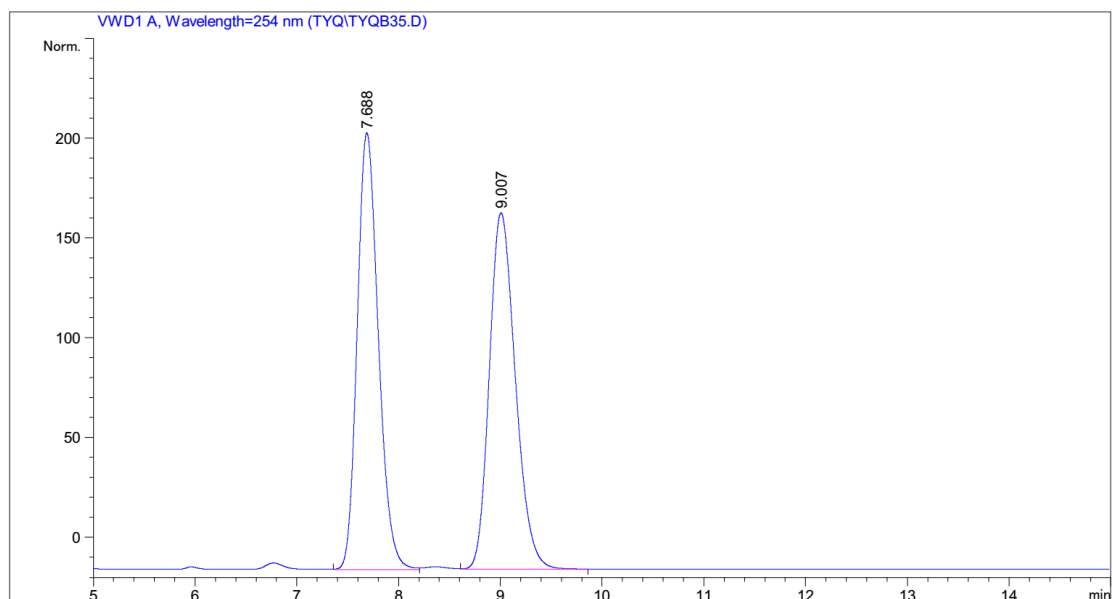
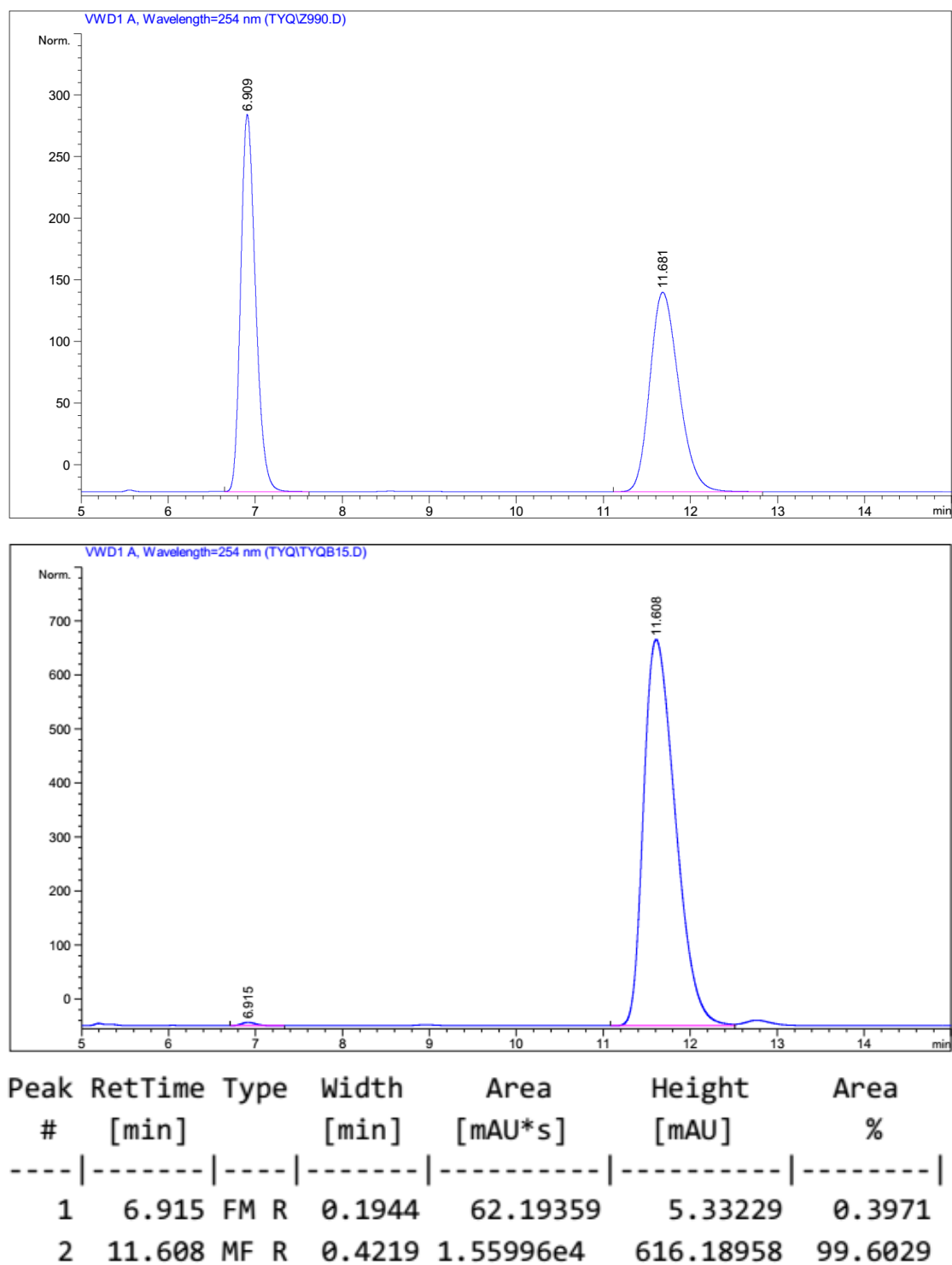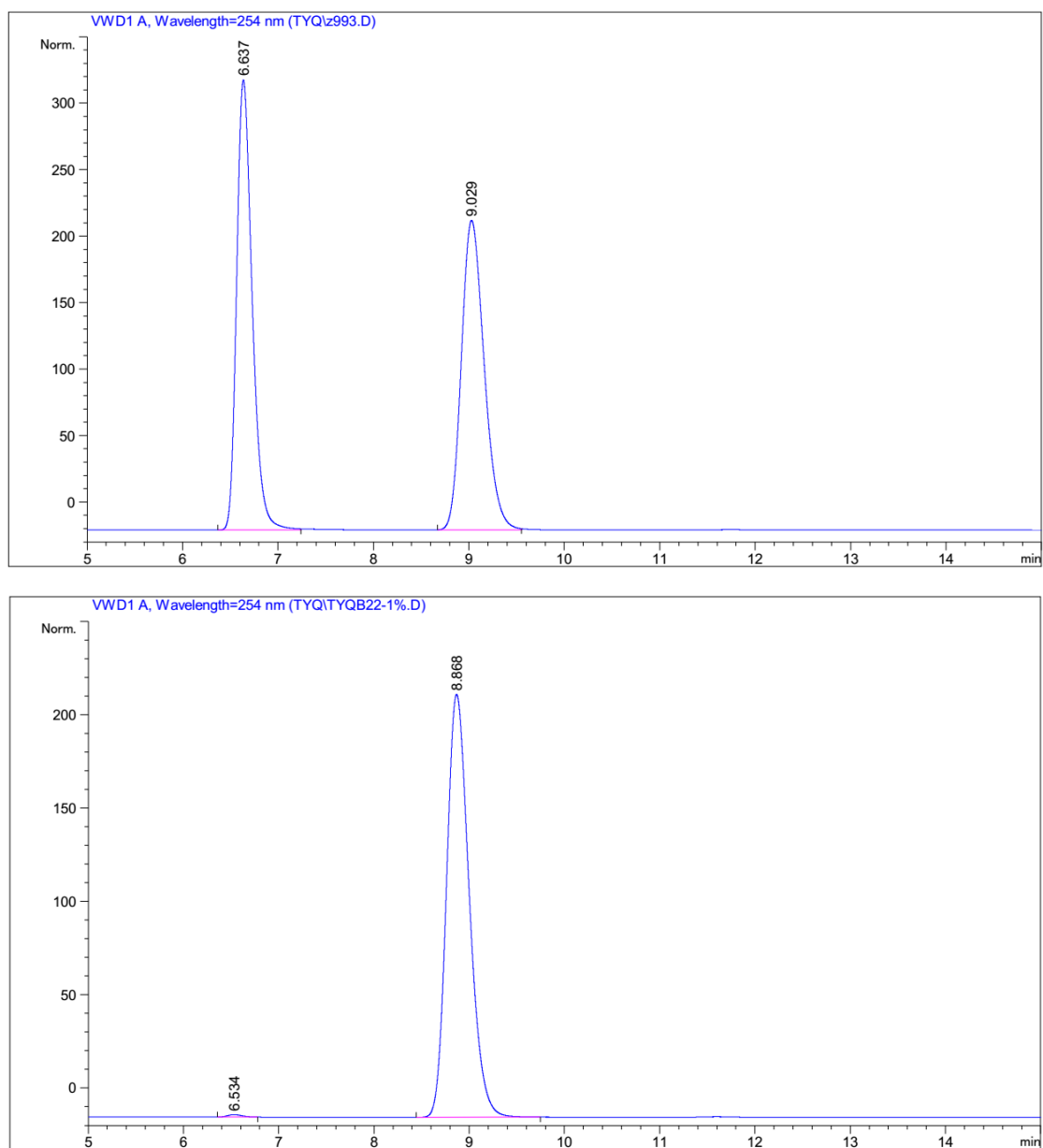| Peak #	RetTime [min]	Type	Width [min]	Area [mAU*s]	Height [mAU]	Area %
1	7.748	MM R	0.2384	62.38497	4.36123	4.7143
2	9.091	MM R	0.2968	1260.91943	70.79595	95.2857

Figure 131 HPLC traces (Daicel Chiralcel OJ-H column) of *rac*-**26p** (reference) and (*R*)-**26p**. Area integration = 95.3:4.7 (90.6% *ee*).
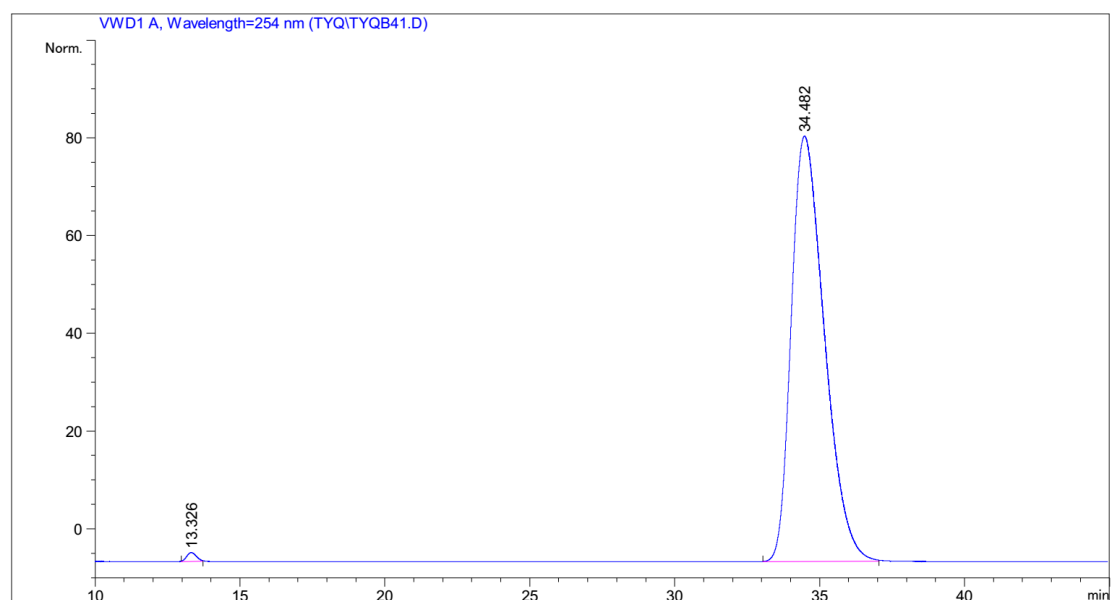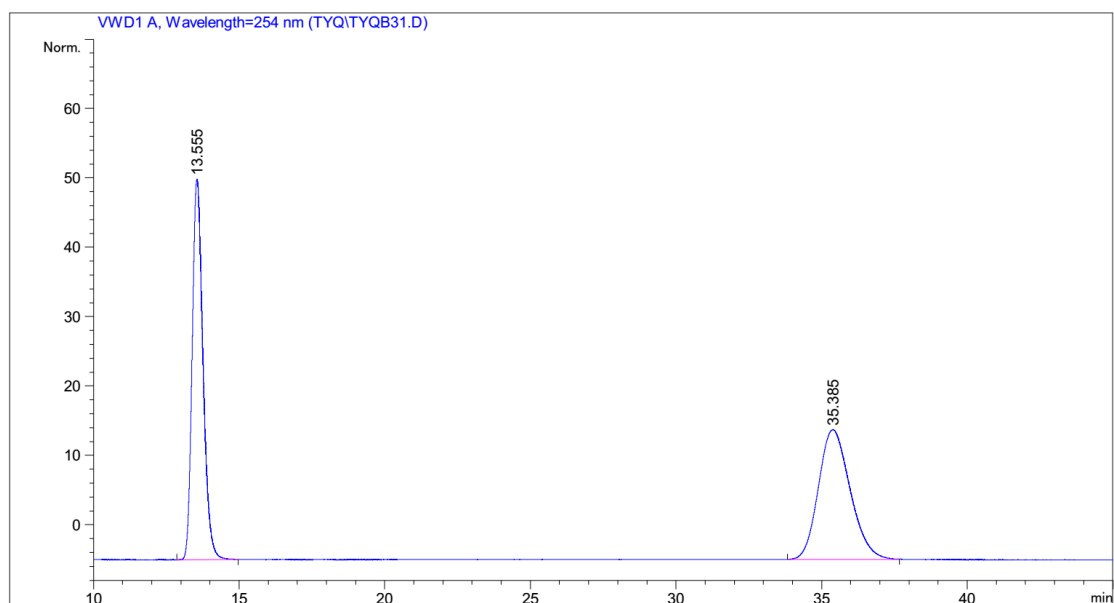
Peak #	RetTime [min]	Type	Width [min]	Area [mAU*s]	Height [mAU]	Area %
1	13.326	MM R	0.3862	36.07633	1.55675	0.6130
2	34.482	MM R	1.3214	5849.49658	73.77778	99.3870

Figure 132 HPLC traces (Daicel Chiralcel OJ-H column) of *rac*-**26q** (reference) and (*S*)-**26q**. Area integration = 99.4:0.6 (98.8% *ee*).
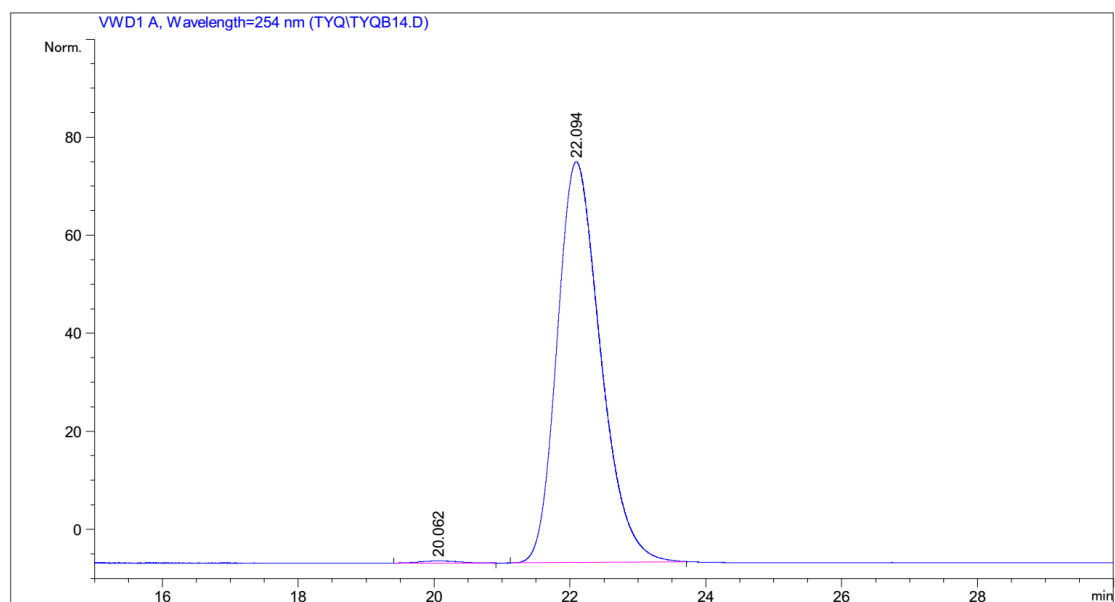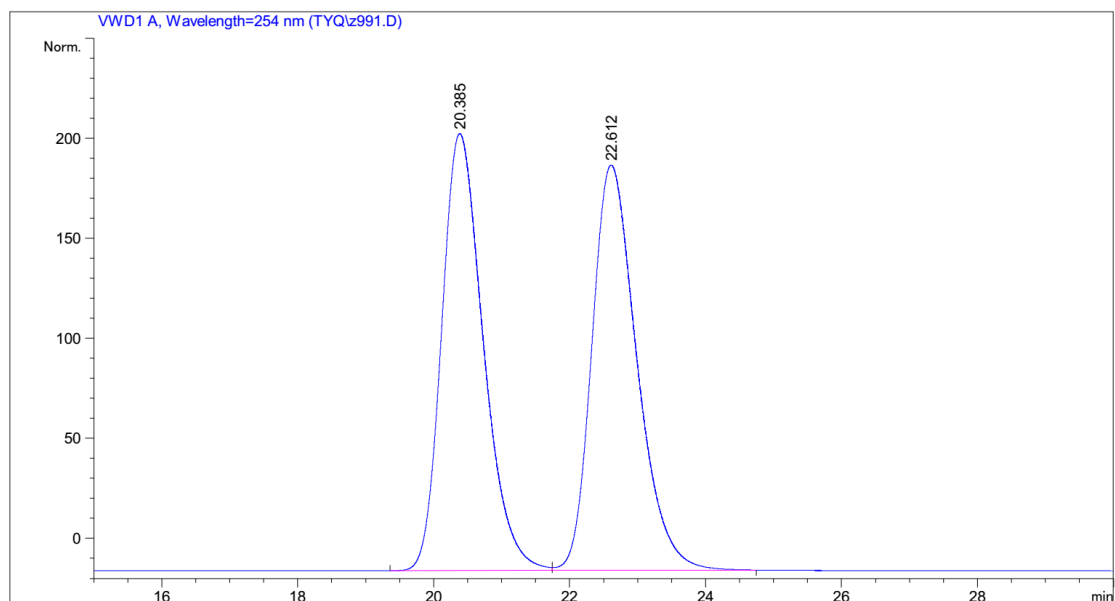
```
Peak RetTime Type  Width     Area      Height    Area
  #    [min]       [min]    [mAU*s]     [mAU]      %
----|-------|----|-------|----------|----------|--------|
  1   6.640 BB   0.1354   20.20992    1.80115   0.5063
  2   8.075 BB   0.2482 3971.10498  250.81017  99.4937
```
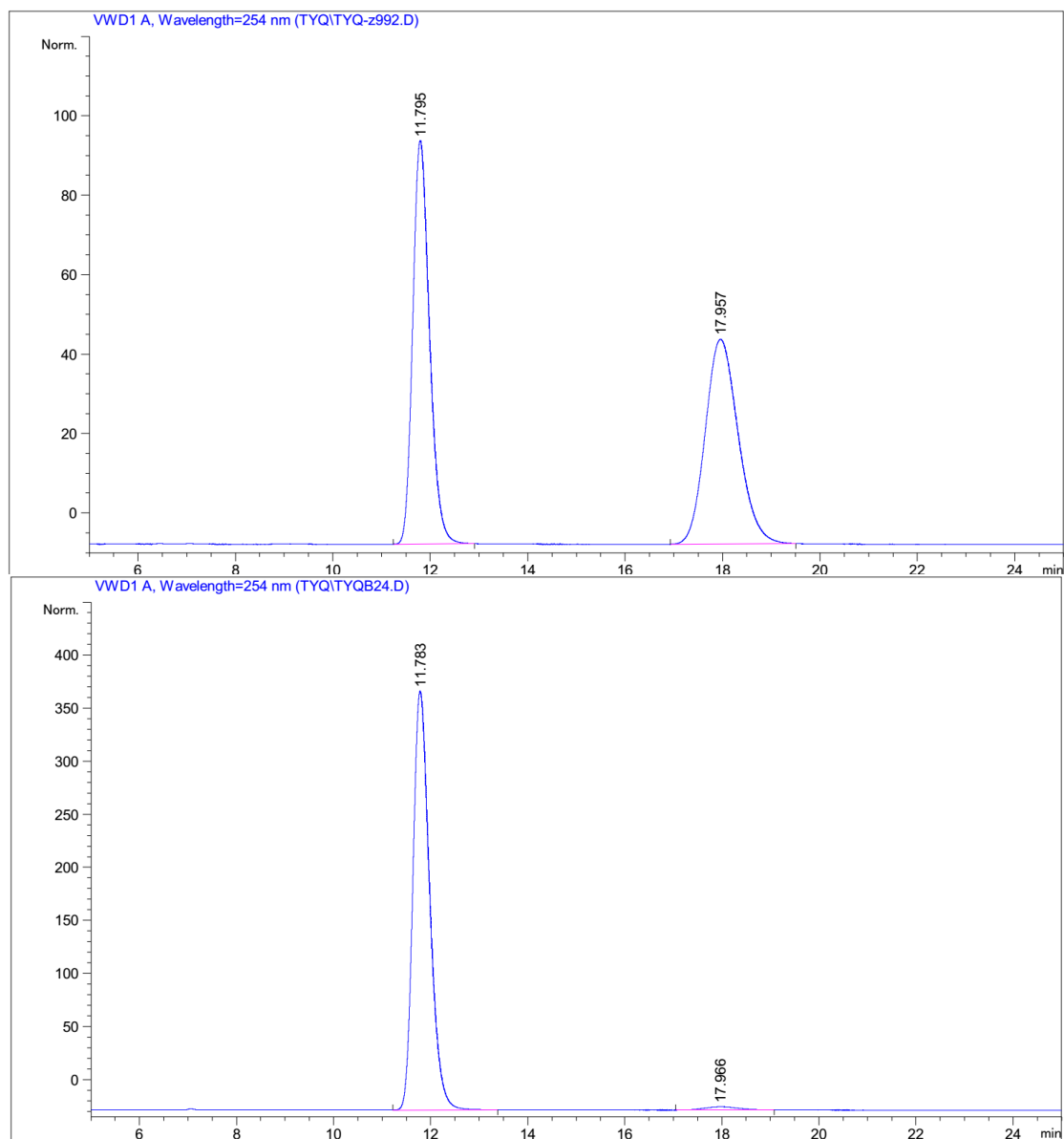
Figure 133 HPLC traces (Daicel Chiralcel OJ-H column) of *rac*-**26r** (reference) and (*S*)-**26r**. Area integration = 99.5:0.5 (99.0% *ee*).
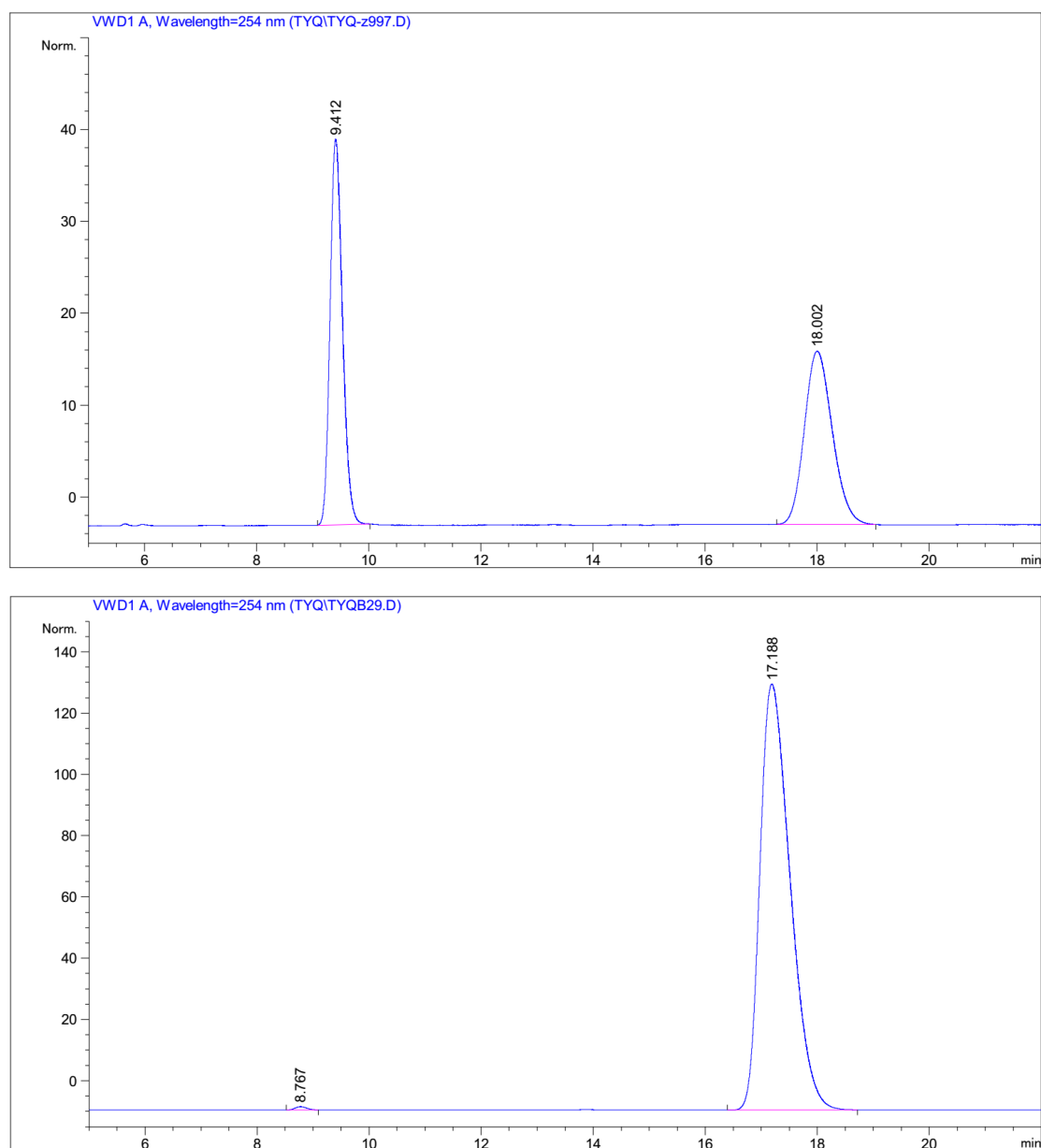
VWD1 A, Wavelength=254 nm (TYQ\TYQB33.D)

VWD1 A, Wavelength=254 nm (TYQ\TYQB43.D)

Peak #	RetTime [min]	Type	Width [min]	Area [mAU*s]	Height [mAU]	Area %
1	5.883	MM R	0.1706	22.24080	2.17339	0.6001
2	8.127	MM R	0.2753	3684.16943	223.07819	99.3999

Figure 134 HPLC traces (Daicel Chiralcel OJ-H column) of *rac*-**26s** (reference) and (*S*)-**26s**. Area integration = 99.4:0.6 (98.8% *ee*).
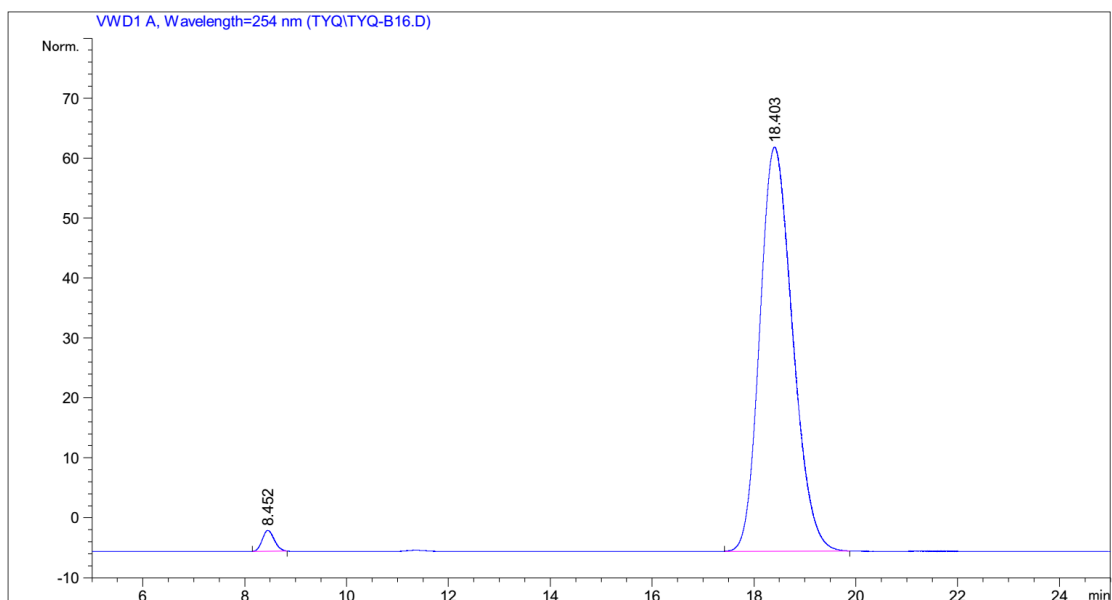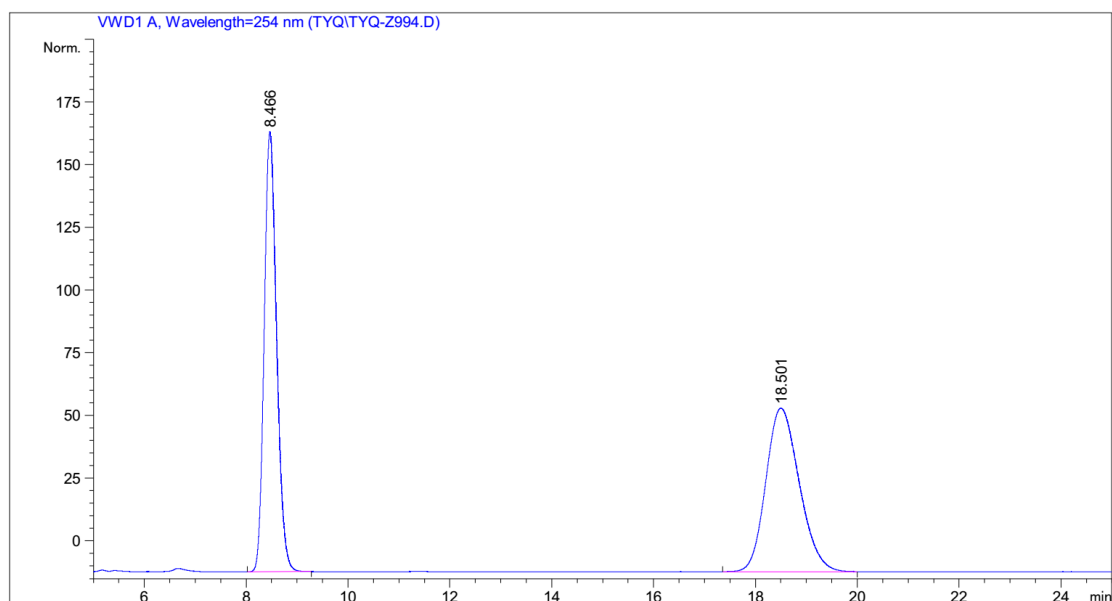
VWD1 A, Wavelength=254 nm (TYQ\TYQ38-3.D)

VWD1 A, Wavelength=254 nm (TYQ\TYQ46.D)
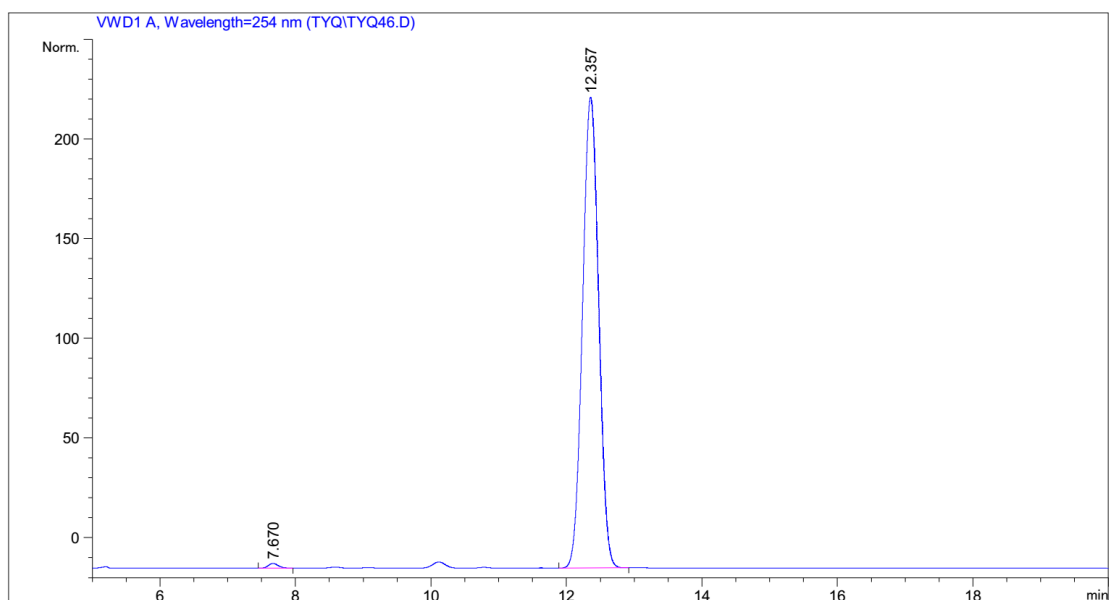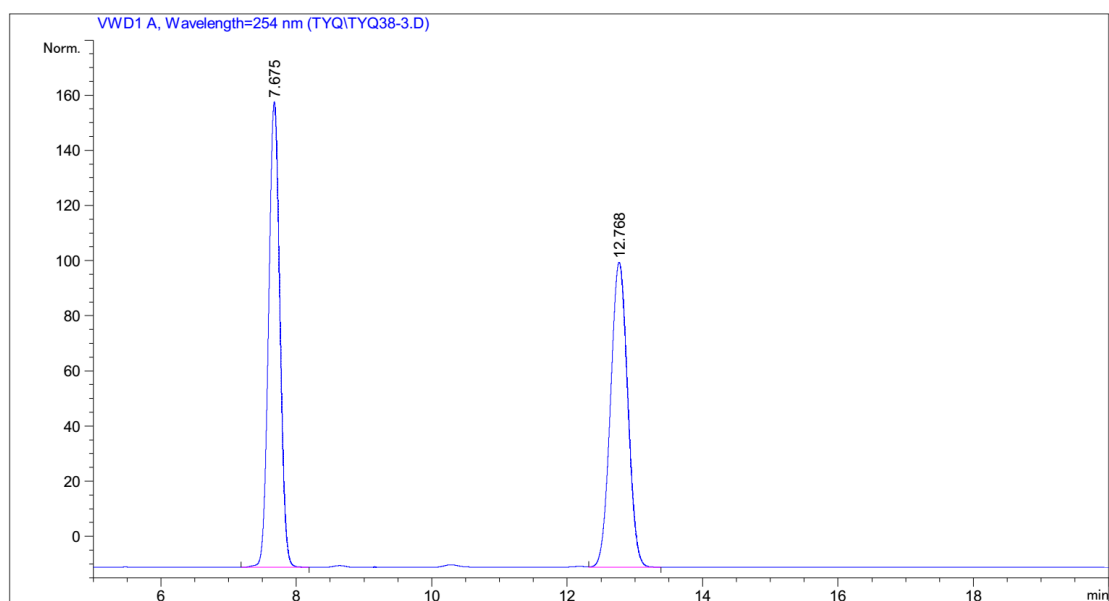
```
Peak RetTime Type  Width     Area      Height     Area
  #   [min]        [min]    [mAU*s]     [mAU]       %
----|-------|----|-------|----------|----------|--------|
  1   7.670 BB    0.1192    20.76823    2.06762   0.6066
  2  12.357 BB    0.2601  3402.83789  205.58575  99.3934
```

Figure 135 HPLC traces (Daicel Chiralpak IG column) of *rac*-**26t** (reference) and (*S*)-**26t**. Area integration = 99.4:0.6 (98.8% *ee*).
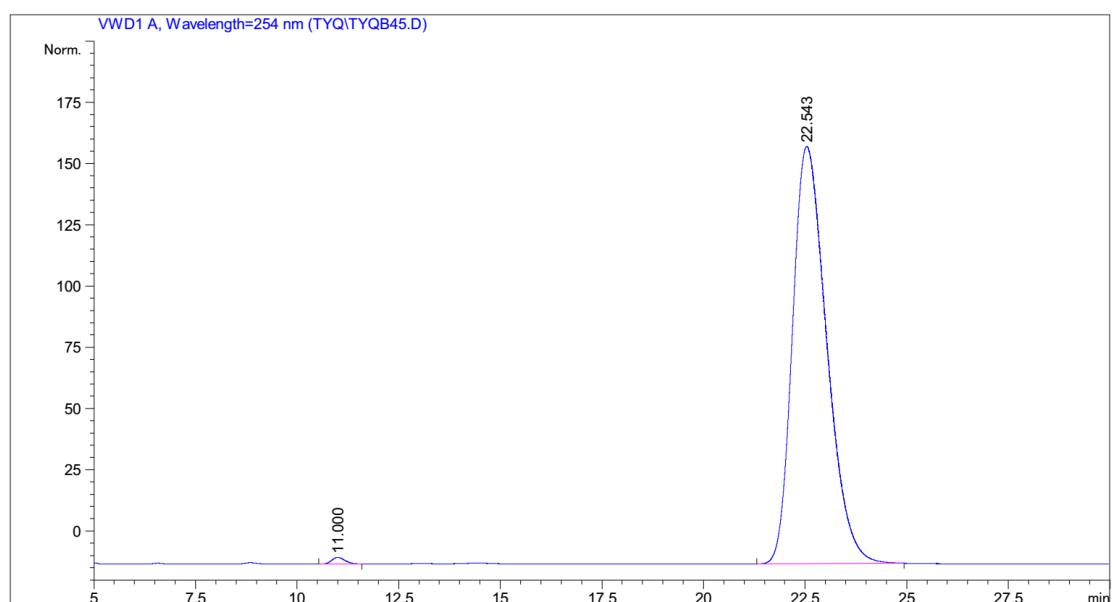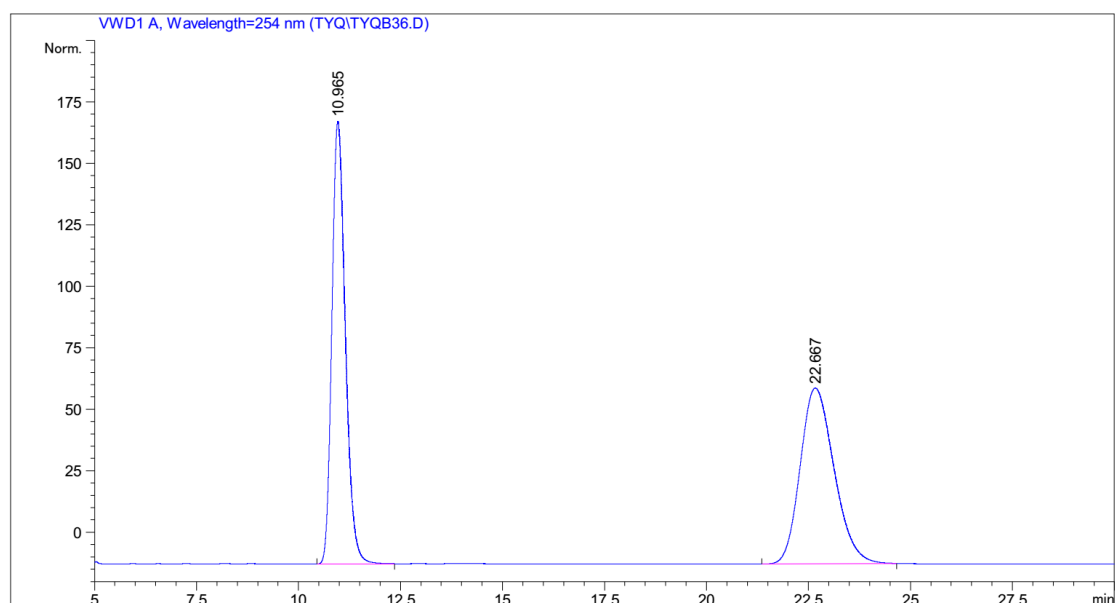
```
Peak RetTime Type  Width    Area      Height    Area
  #   [min]        [min]    [mAU*s]    [mAU]      %
----|-------|----|-------|----------|----------|--------|
   1  11.000 BB   0.2636   51.00896   2.26582   0.6064
   2  22.543 BB   0.6918 8361.14941 143.39133  99.3936
```
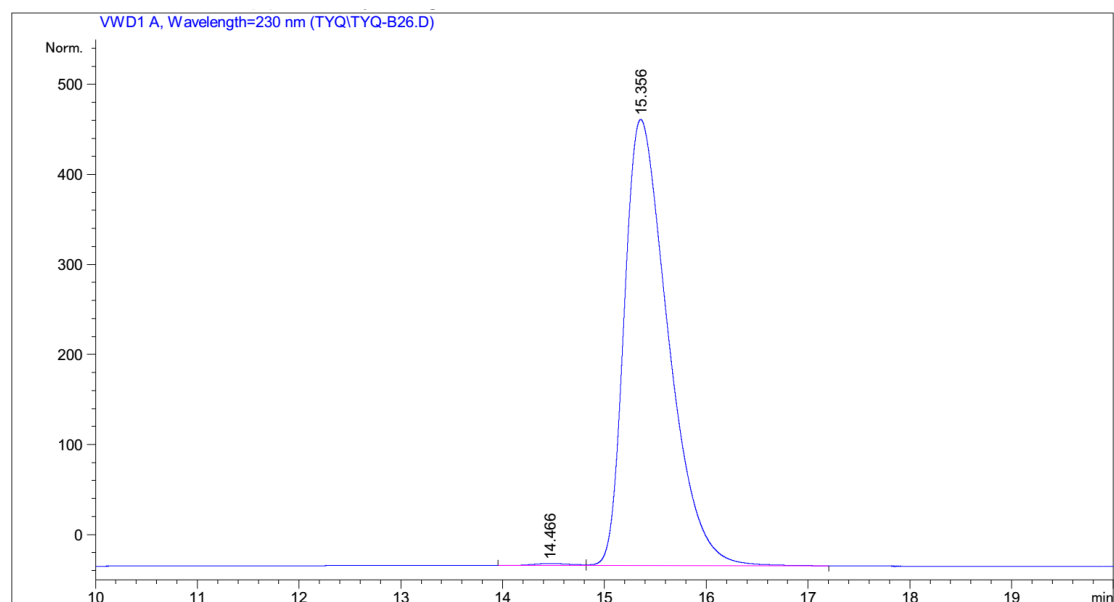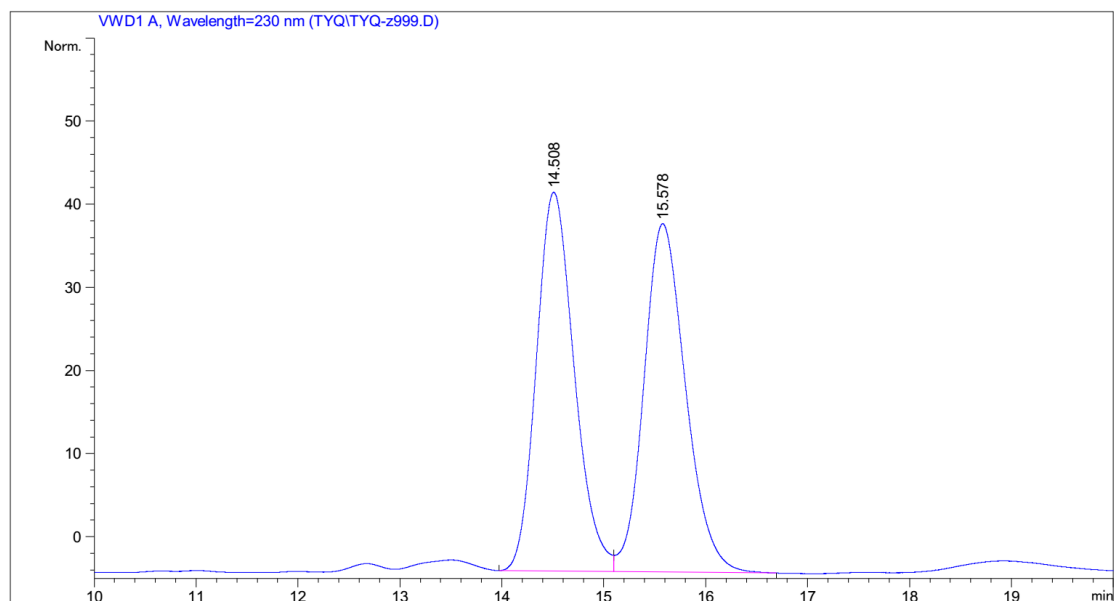
Figure 136 HPLC traces (Daicel Chiralcel OJ-H column) of *rac*-**26u** (reference) and (*S*)-**26u**. Area integration = 99.4:0.6 (98.8% *ee*).

```
Peak  RetTime  Type   Width      Area            Height        Area
  #    [min]          [min]    mAU    *s      [mAU    ]         %
----|-------|----|-------|----------|-----------|--------|
   1   8.200  BB    0.1834   282.63858     23.85525     18.7858
   2   9.101  BB    0.2130  1221.89209     89.57323     81.2142
```
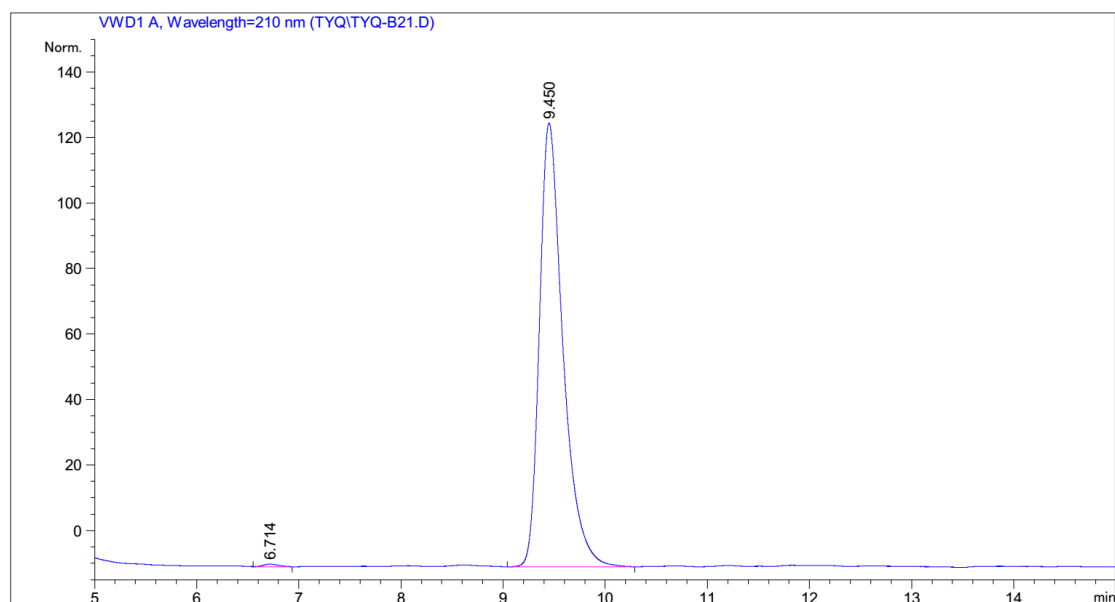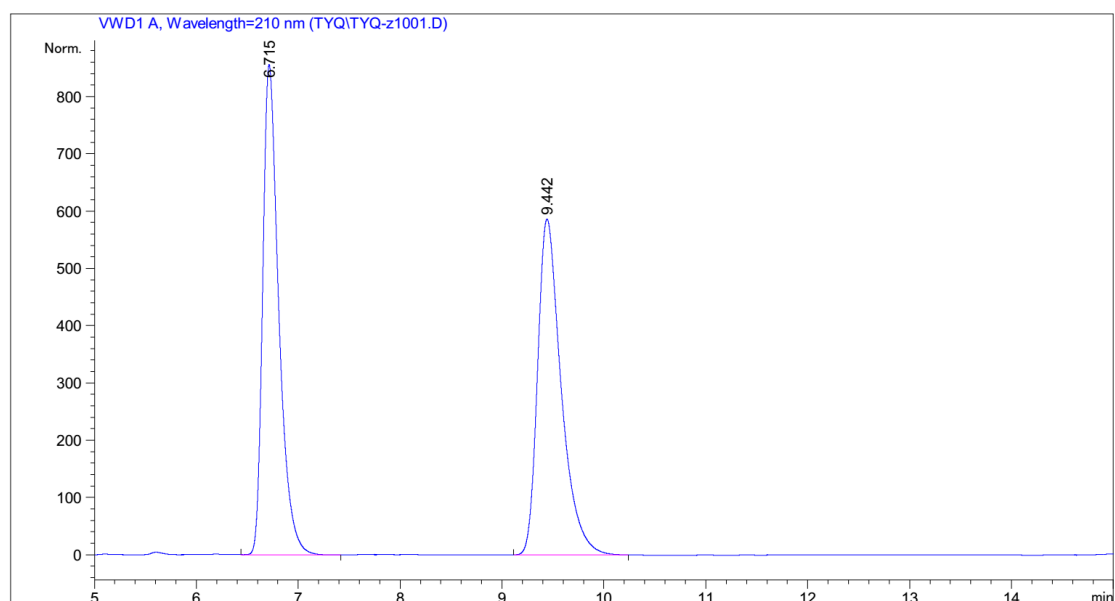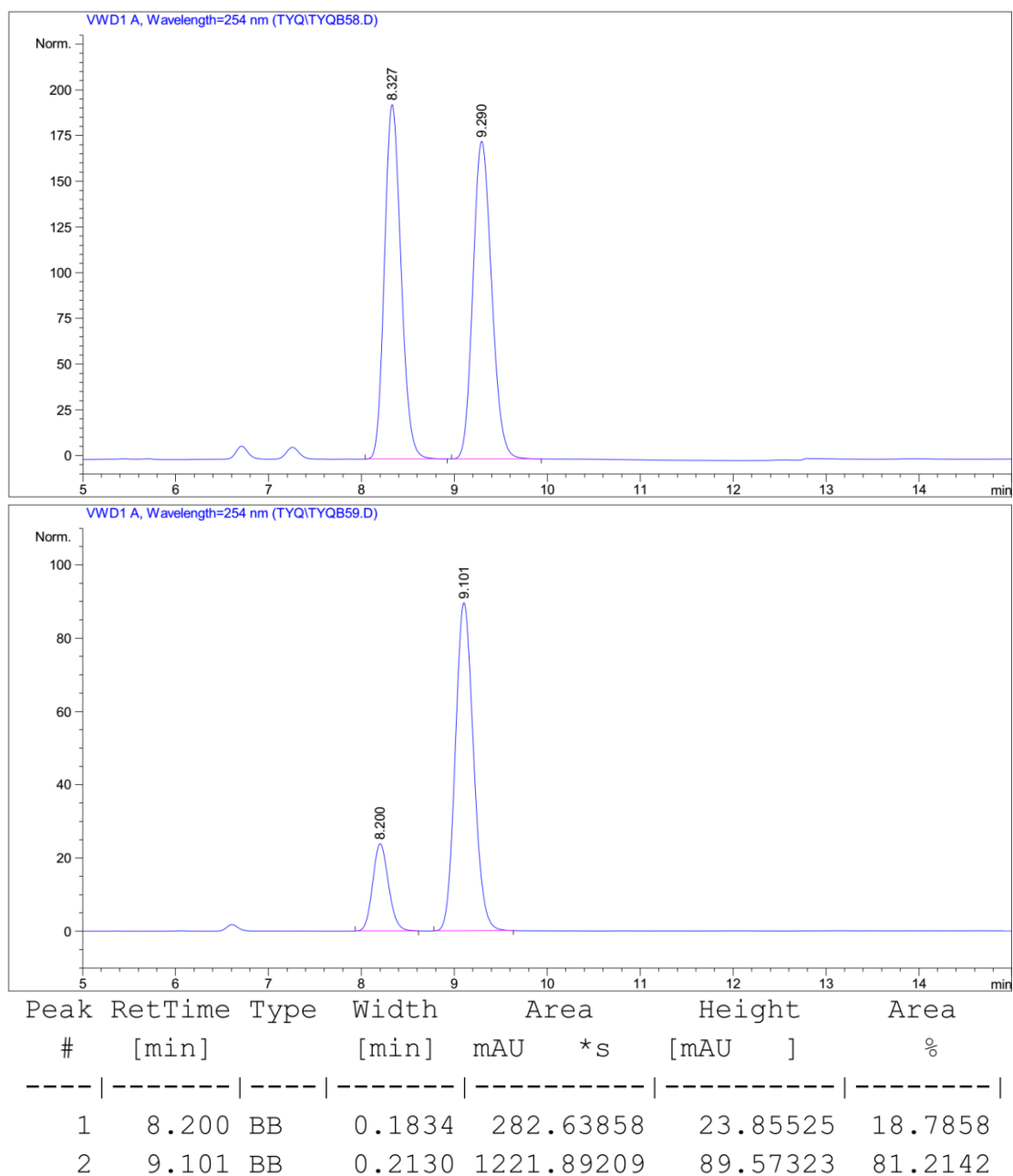
Figure 137 HPLC traces (Daicel Chiralcel OJ-H column) of *rac*-**26v** (reference) and (*S*)-**26v**. Area integration = 81.2:18.8 (62.4% *ee*).
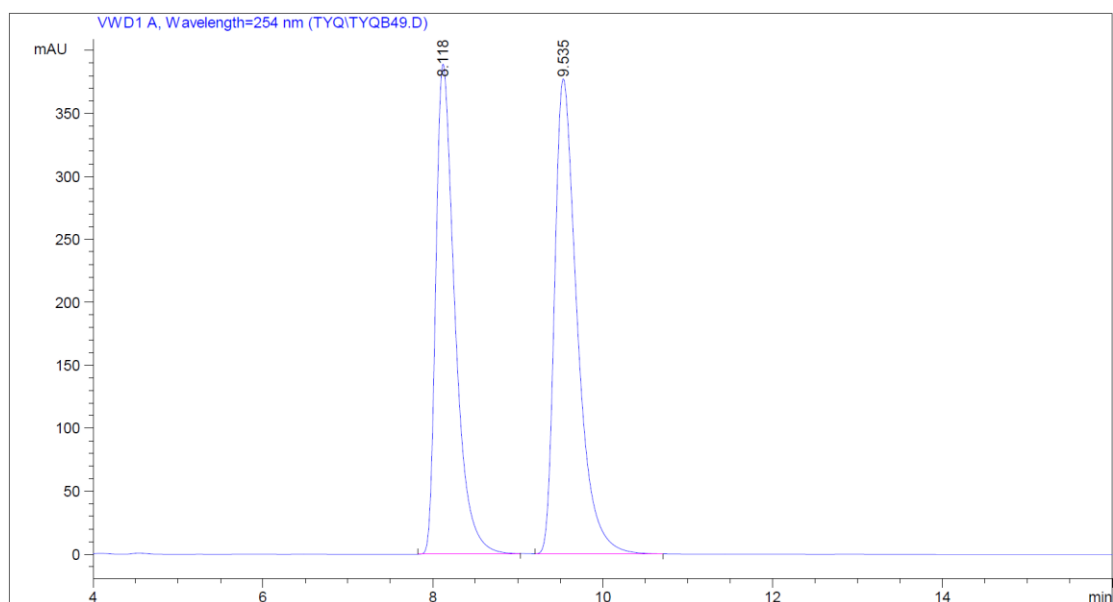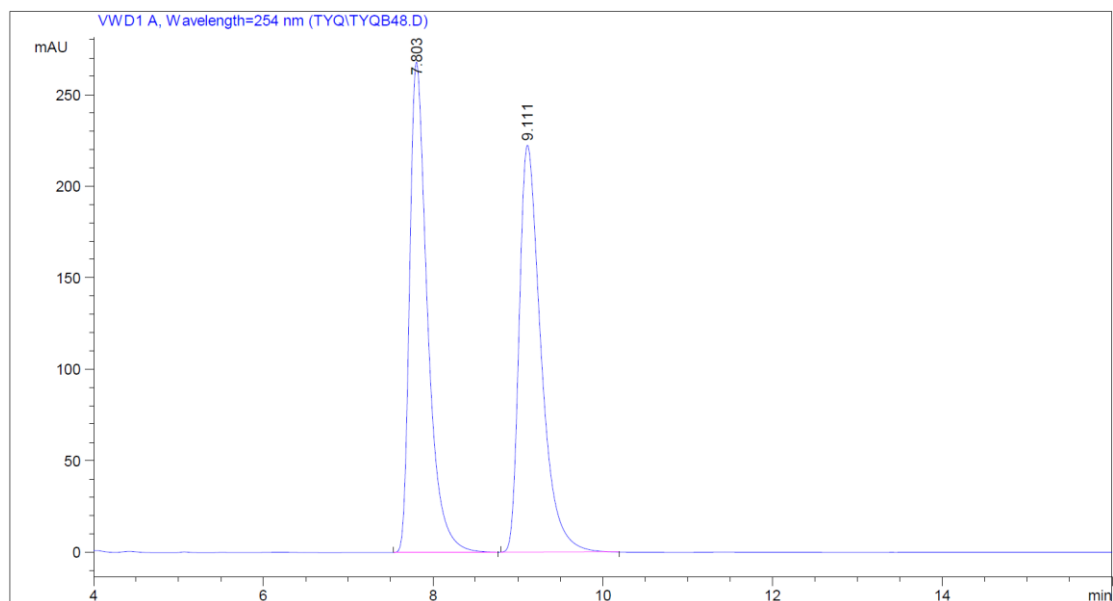
Peak #	RetTime [min]	Type	Width [min]	Area mAU *s	Height [mAU]	Area %
1	8.118	BB	0.2371	6063.54932	389.12308	46.5635
2	9.535	BB	0.2808	6958.55566	377.18008	53.4365

Figure 138 HPLC traces (Daicel Chiralcel OJ-H column) of *rac*-**26w** (reference) and (*R*)-**26w**. Area integration = 53.4:46.6 (6.8% *ee*).
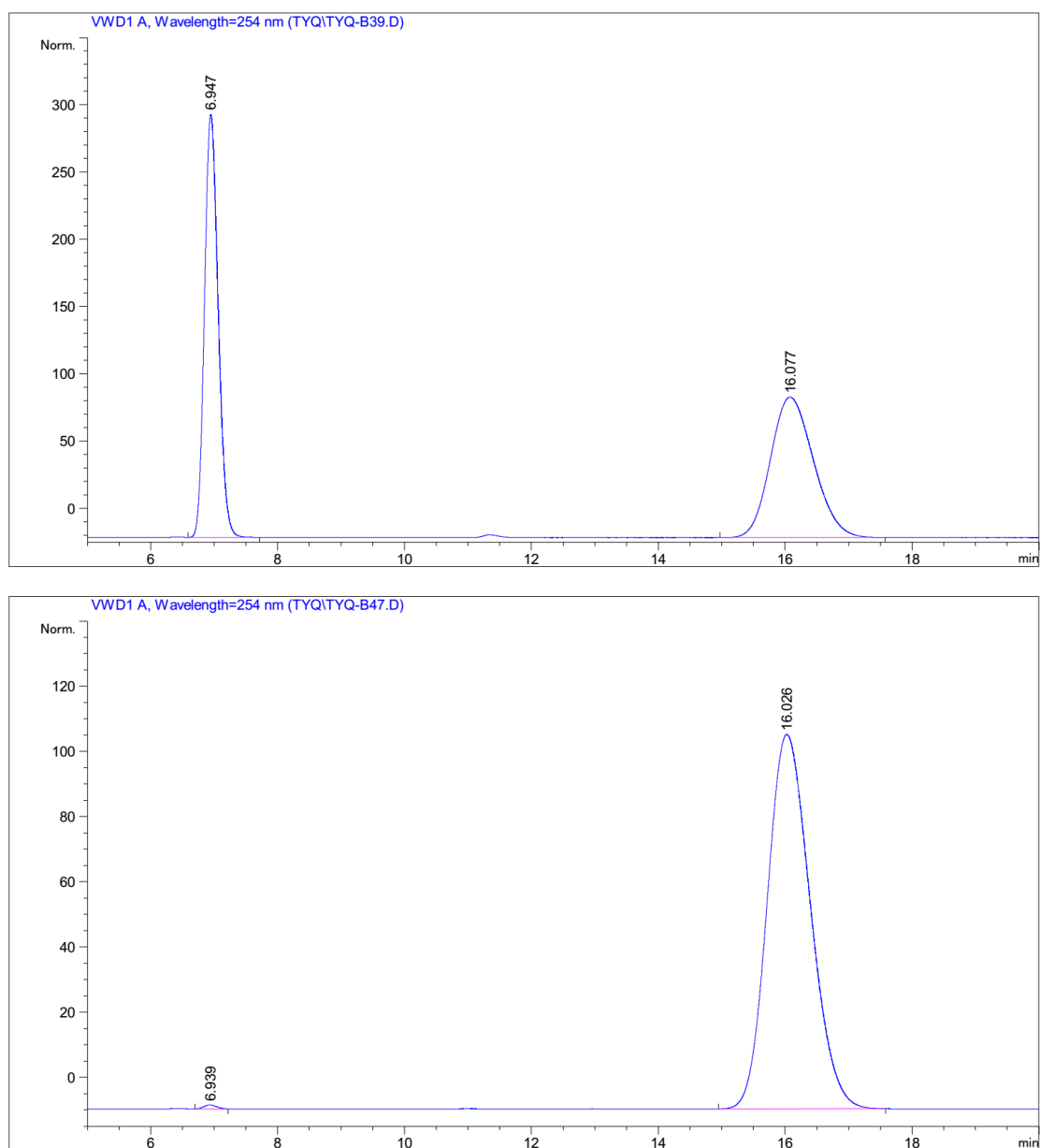
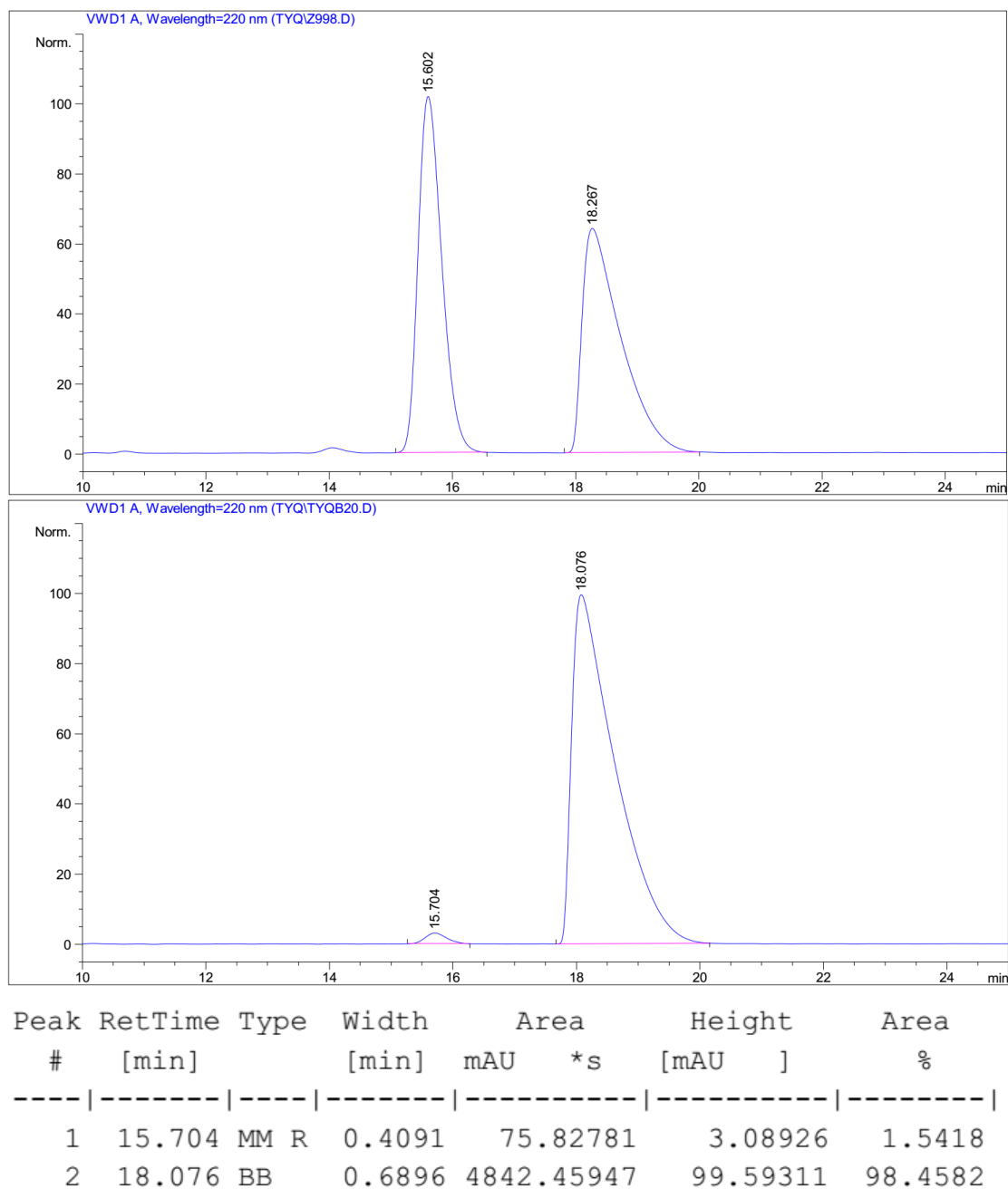| Peak | RetTime | Type | Width | Area | Height | Area |
#	[min]		[min]	[mAU*s]	[mAU]	%
1	6.939	MM R	0.2281	13.87741	1.01412	0.3091
2	16.026	BB	0.5558	4476.02588	95.41243	99.6909

Figure 139 HPLC traces (Daicel Chiralcel OJ-H column) of *rac*-**26x** (reference) and (*S*)-**26x**. Area integration = 99.7:0.3 (99.4% *ee*).
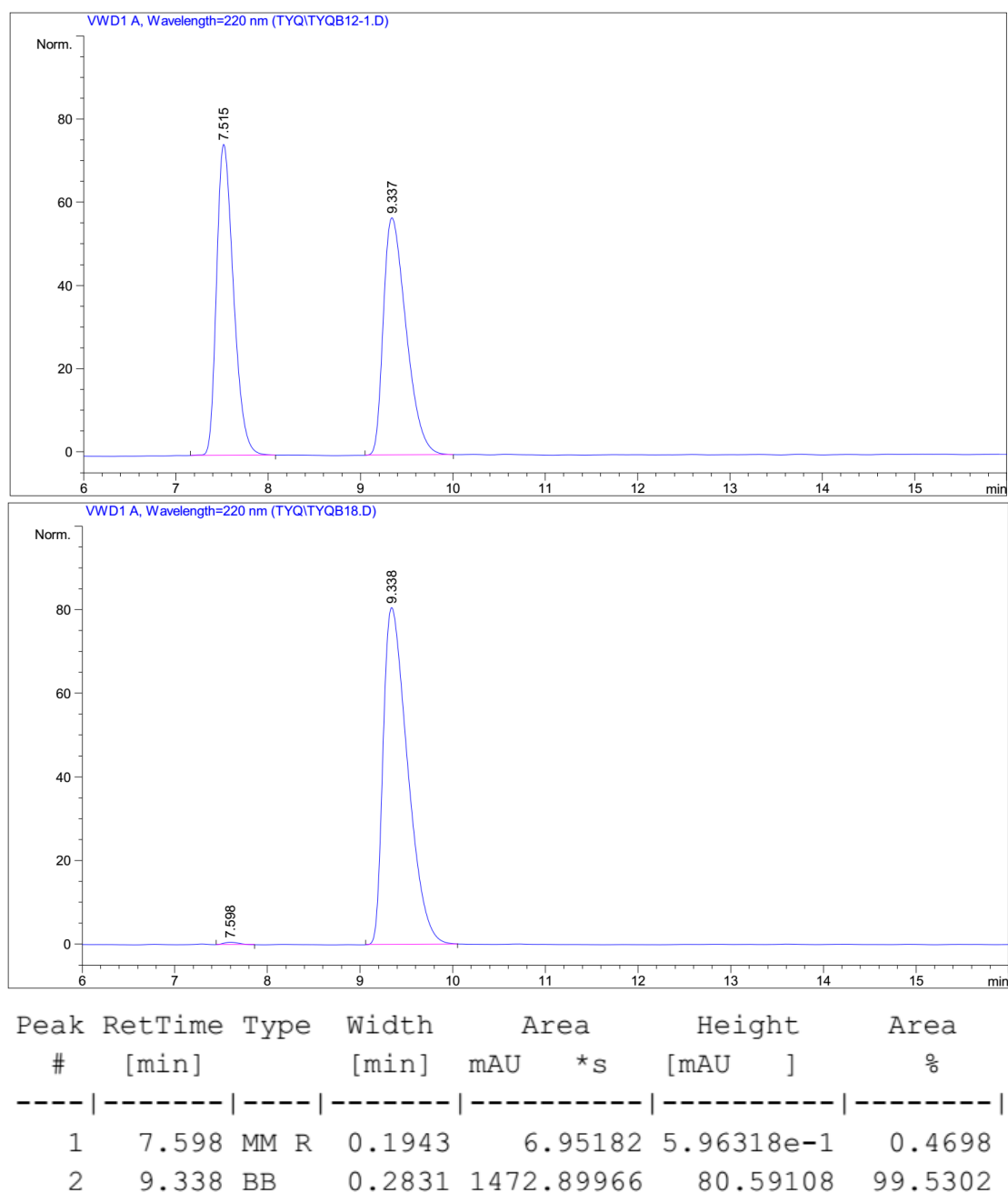
```
VWD1 A, Wavelength=254 nm (YU\Z1028.D)
```
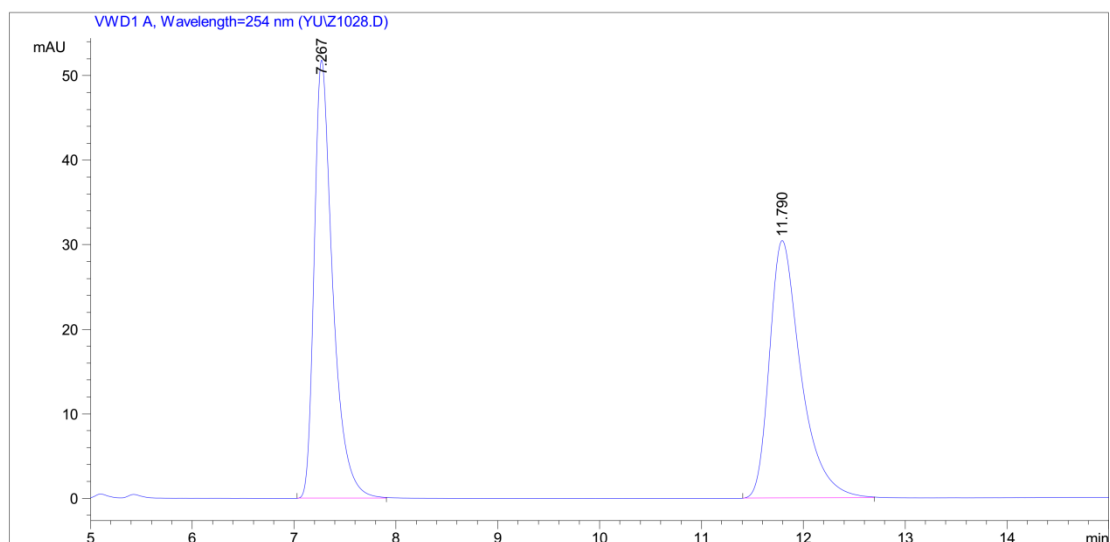
```
Peak  RetTime Type  Width     Area         Height      Area
  #    [min]         [min]   mAU    *s    [mAU    ]      %
----|-------|----|-------|----------|----------|--------|
  1    7.267 BB    0.1897   655.29541    51.85161   50.0360
  2   11.790 BB    0.3218   654.35321    30.47823   49.9640
```



```
VWD1 A, Wavelength=254 nm (YU\Z1084.D)
```
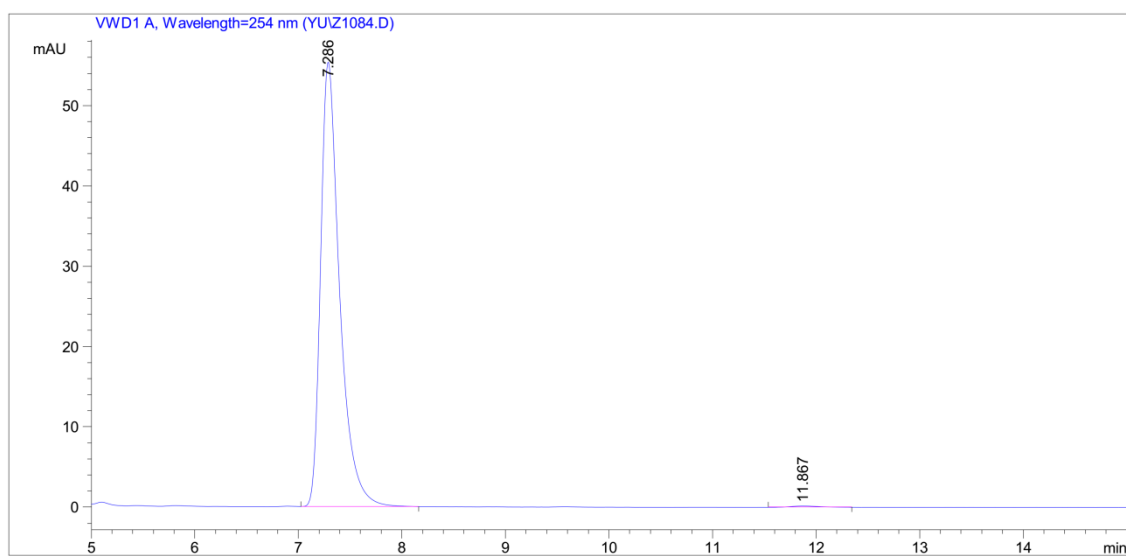
```
Peak  RetTime Type  Width     Area         Height      Area
  #    [min]         [min]   mAU    *s    [mAU    ]      %
----|-------|----|-------|----------|----------|--------|
  1    7.286 MM R  0.2131   708.06873    55.38374   99.4919
  2   11.867 MM R  0.3719     3.61591 1.62049e-1    0.5081
```

Figure 140 HPLC traces (Daicel Chiralpak AD-H column) of *rac*-**28a** (reference) and (*S*)-**28a**. Area integration = 99.5:0.5 (99.0% *ee*).
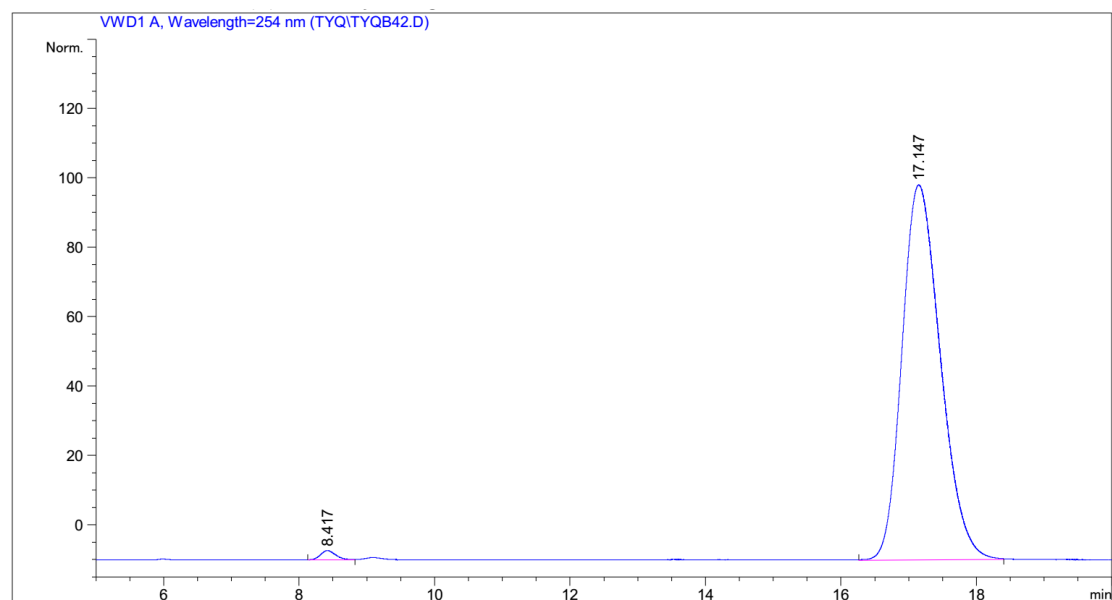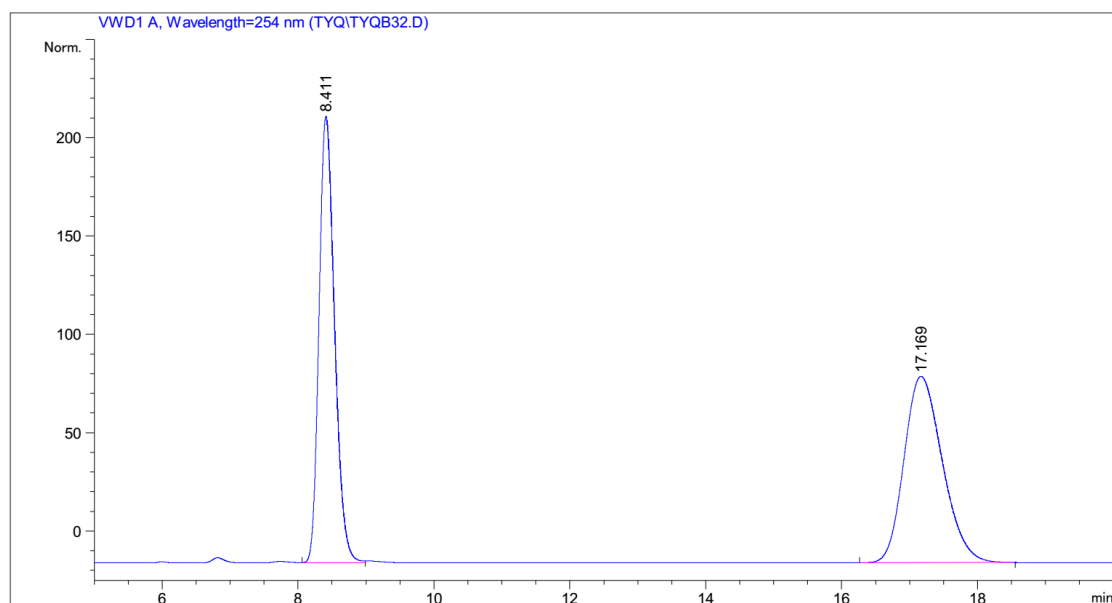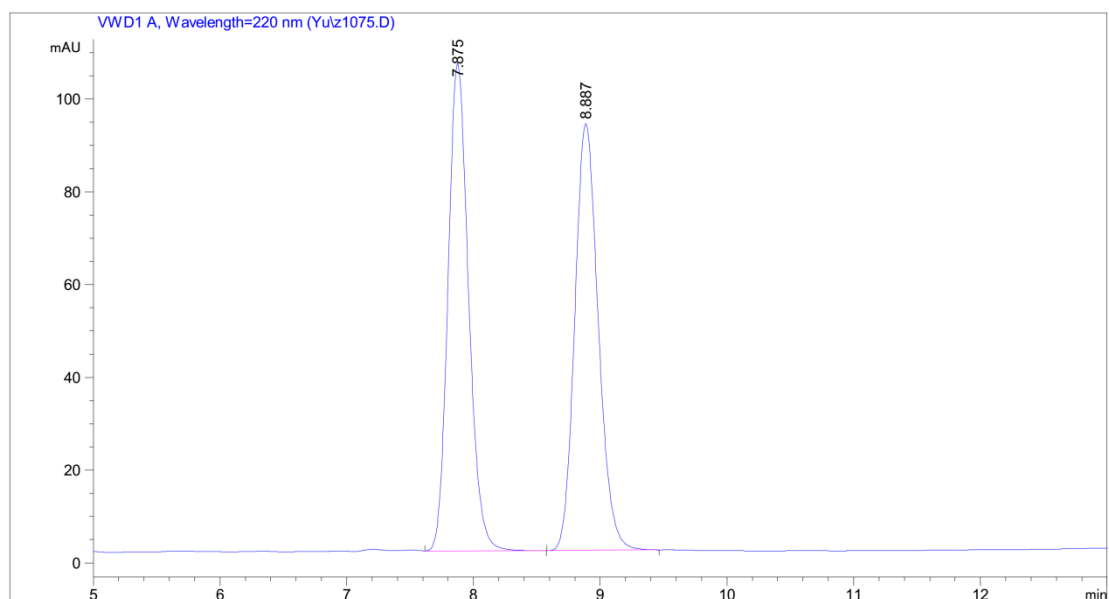
Peak	RetTime	Type	Width	Area	Height	Area
#	[min]		[min]	[mAU*s]	[mAU]	%
----	-------	----	-------	----------	----------	--------
1	7.875	BB	0.1731	1180.99463	105.07318	49.9676
2	8.887	BB	0.1989	1182.52405	92.03837	50.0324
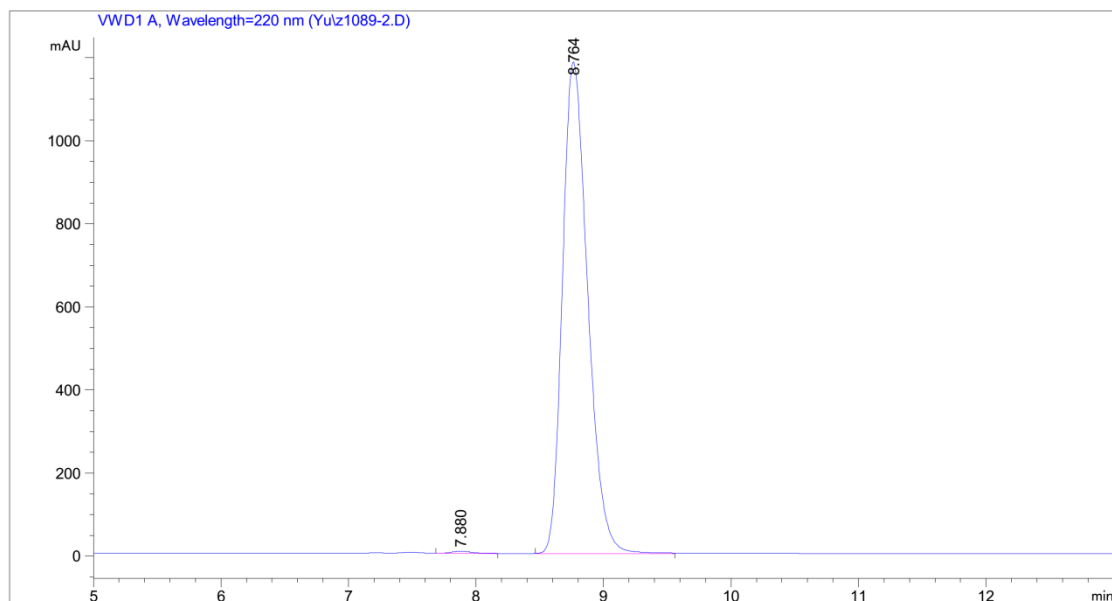
Peak	RetTime	Type	Width	Area	Height	Area
#	[min]		[min]	[mAU*s]	[mAU]	%
----	-------	------	-------	----------	----------	--------
1	7.880	MM R	0.1885	54.65084	4.83102	0.3345
2	8.764	MM R	0.2151	1.62838e4	1184.01367	99.6655

Figure 141 HPLC traces (Daicel Chiralpak OD-H column) of *rac*-**28b** (reference) and (*S*)-**28b**. Area integration = 99.7:0.3 (99.4% *ee*).
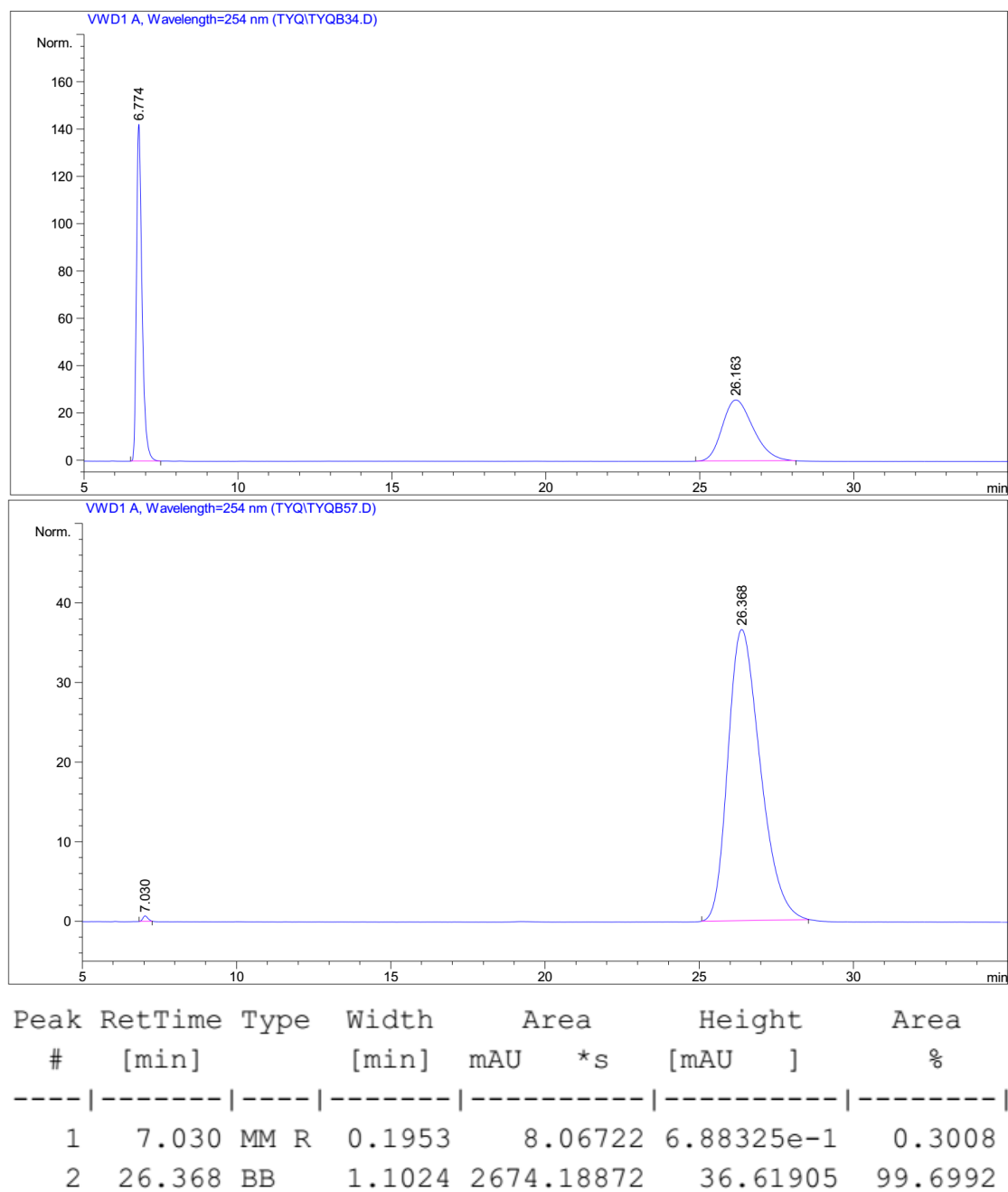
225
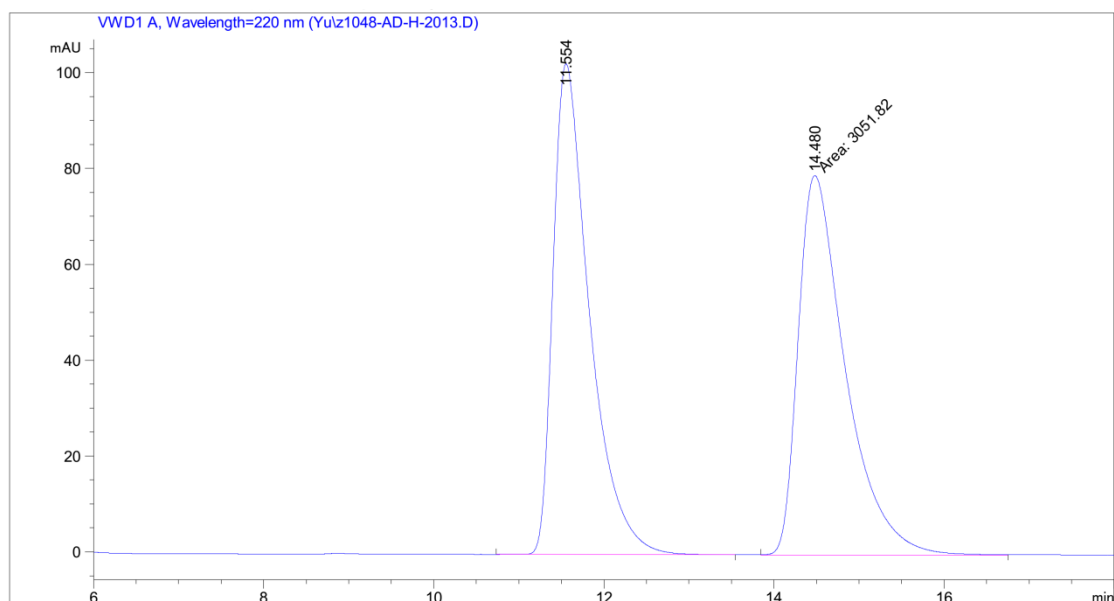
Peak #	RetTime [min]	Type	Width [min]	Area [mAU*s]	Height [mAU]	Area %
1	11.554	BB	0.4432	3046.60596	102.37451	49.9572
2	14.480	MM	0.6424	3051.82495	79.18198	50.0428

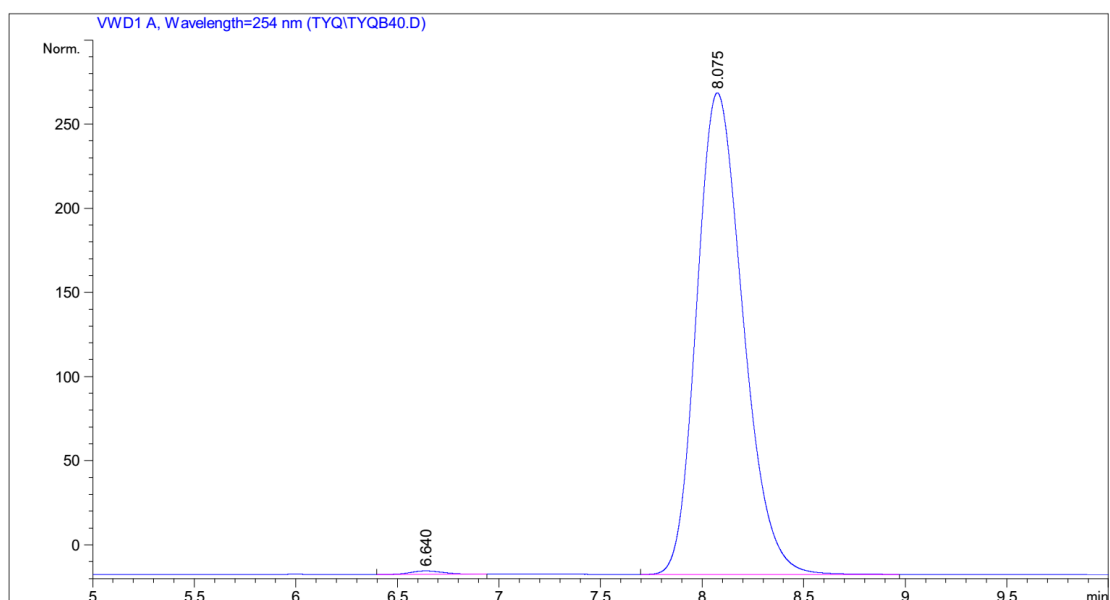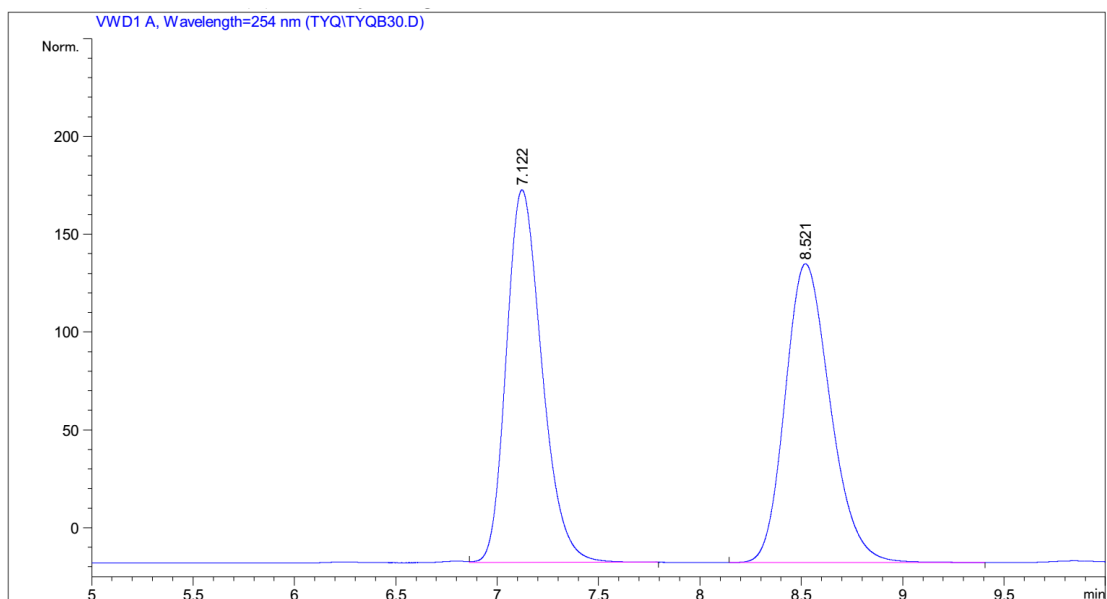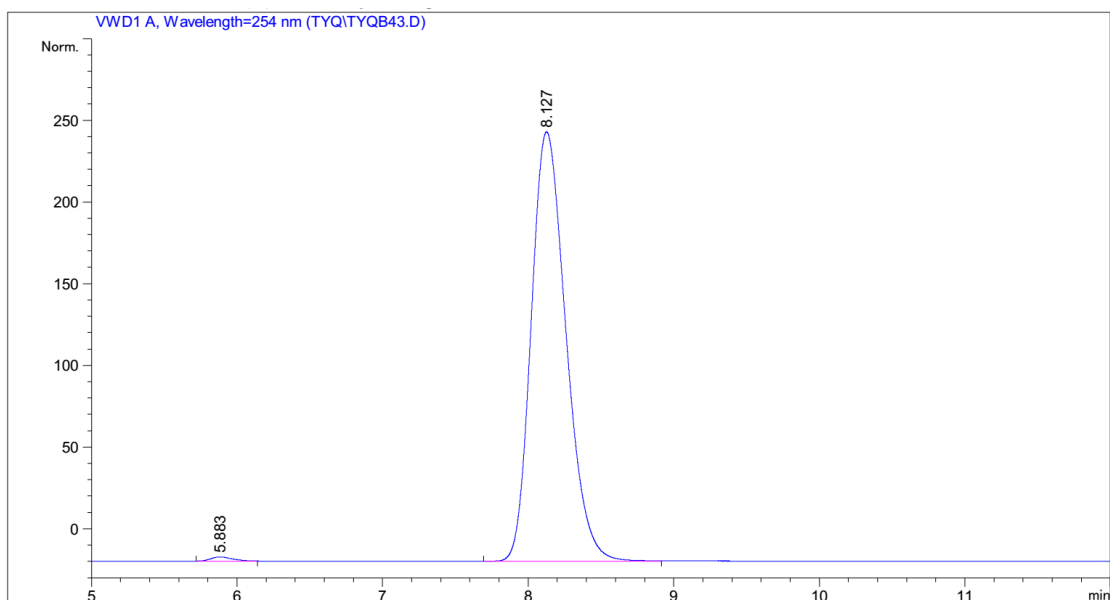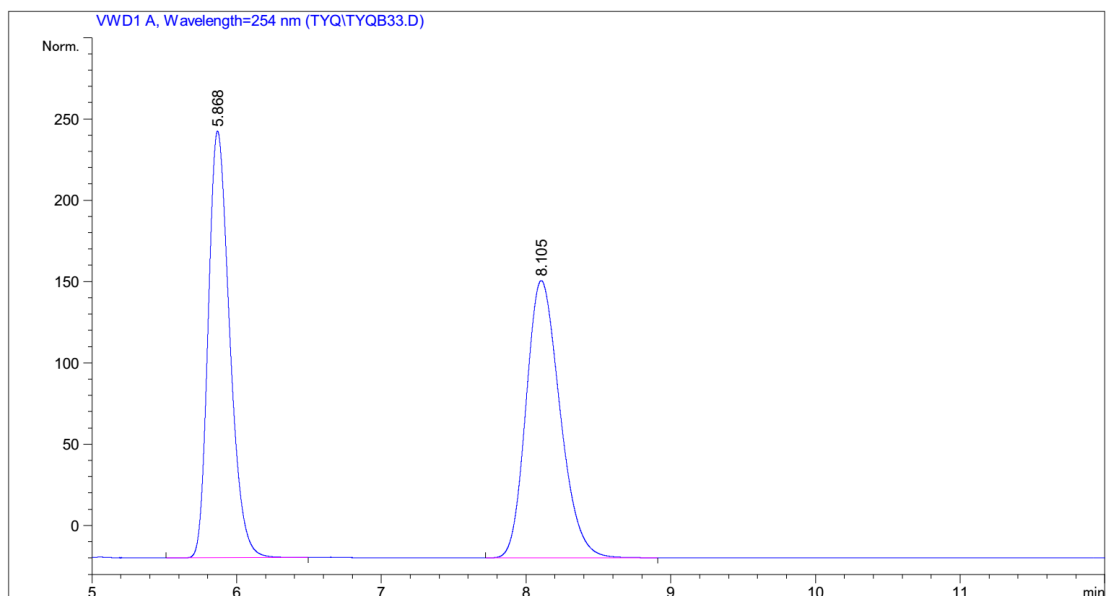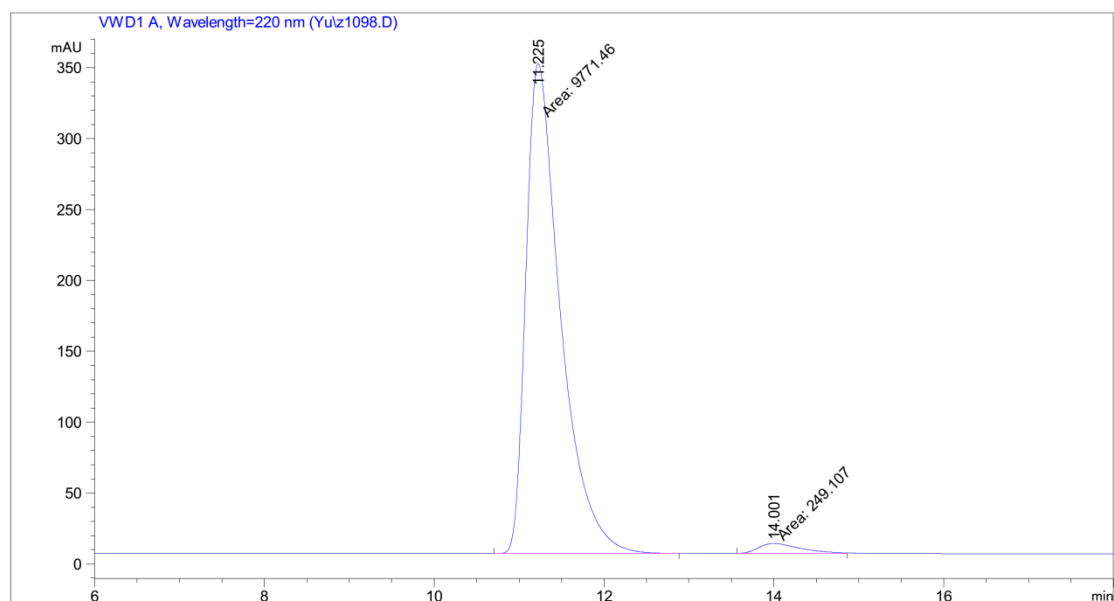| Peak #	RetTime [min]	Type	Width [min]	Area [mAU*s]	Height [mAU]	Area %
1	11.225	MM	0.4713	9771.46191	345.55936	97.5140
2	14.001	MM	0.5840	249.10698	7.10932	2.4860

Figure 142 HPLC traces (Daicel Chiralpak AD-H column) of *rac*-**28c** (reference) and (*S*)-**28c**. Area integration = 97.5:2.5 (95.0% *ee*).

6.7 List of Crystal Structure Data
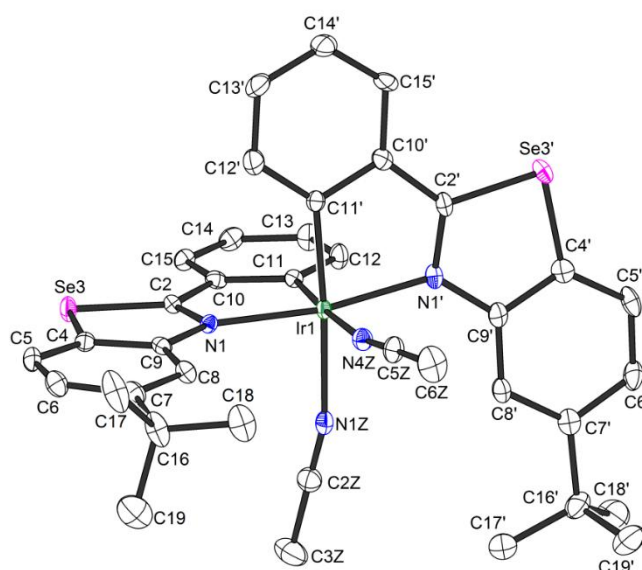
Figure 143 Crystal structure of *rac*-**Ir**(**Se**). ORTEP drawing with 50% probability thermal ellipsoids. The counteranion is omitted for clarity.

Table 7 Crystal Data and Structure Refinement for *rac*-**Ir**(**Se**).

Crystal data:

Identification code	z649_0m	
Habitus, colour	block, yellow	
Crystal size	0.37 x 0.30 x 0.16 mm^3	
Crystal system	Monoclinic	
Space group	P2$_1$	Z = 4
Unit cell dimensions	a = 17.0086(8) Å	α = 90 °.
	b = 16.2286(7) Å	β = 91.595(2) °.
	c = 17.2753(8) Å	γ = 90 °.
Volume	4766.6(4) Å^3	
Cell determination	9705 peaks with Theta 2.4 to 27.6 °.	
Empirical formula	$C_{41}H_{44}C_{16}F_6IrN_4PSe_2$	
Moiety formula	$C_{38}H_{38}IrN_4Se_2$, F_6P, 3(CH_2Cl_2)	
Formula weight	1300.59	
Density (calculated)	1.812 Mg/m^3	
Absorption coefficient	4.757 mm^{-1}	
F(000)	2536	

Data collection:

Diffractometer type	Bruker D8 QUEST area detector
Wavelength	0.71073 Å
Temperature	100(2) K
Theta range for data collection	2.116 to 27.600 °.
Index ranges	-22<=h<=22, -21<=k<=21, -22<=l<=22
Data collection software	APEX3 (Bruker AXS Inc., 2015)
Cell refinement software	SAINT V8.35A (Bruker AXS Inc., 2015)
Data reduction software	SAINT V8.35A (Bruker AXS Inc., 2015)

Solution and refinement:

Reflections collected	202475
Independent reflections	21990 [R(int) = 0.0366]
Completeness to theta = 25.242 °	99.9 %
Observed reflections	21415[I > 2(I)]
Reflections used for refinement	21990
Absorption correction	Numerical Mu From Formula
Max. and min. transmission	0.52 and 0.18
Flack parameter (absolute struct.)	-0.0038(13)
Largest diff. peak and hole	1.313 and -1.177 e.Å^{-3}
Solution	Direct methods
Refinement	Full-matrix least-squares on F^2
Treatment of hydrogen atoms	Calc. positions, constr. ref.
Programs used	XT V2014/1 (Bruker AXS Inc., 2014)
	SHELXL-2014/7 (Sheldrick, 2014)
	DIAMOND (Crystal Impact)
	ShelXle (Hübschle, Sheldrick, Dittrich, 2011)
Data / restraints / parameters	21990 / 37 / 1145
Goodness-of-fit on F^2	1.110
R index (all data)	wR2 = 0.0584
R index conventional [I>2sigma(I)]	R1 = 0.0250
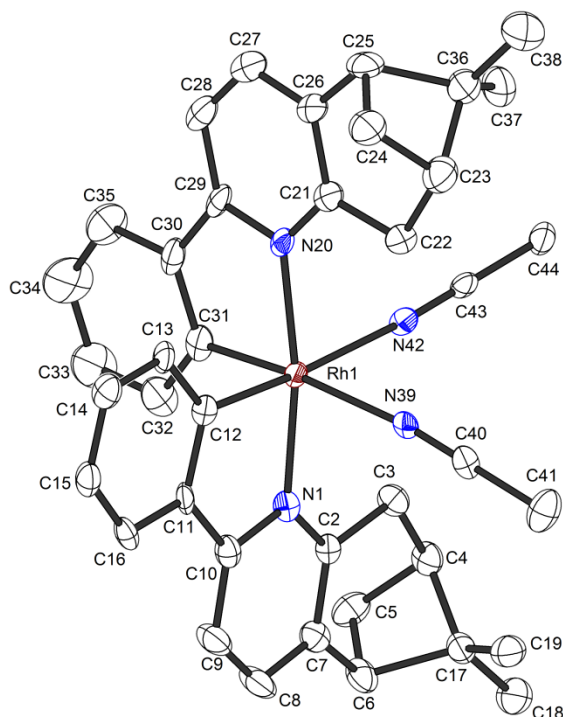
Figure 144 Crystal structure of Λ-**RhPP**. ORTEP drawing with 50% probability thermal ellipsoids. The hexafluorophosphate counteranion is omitted for clarity.

Table 8 Crystal Data and Structure Refinement for Λ-**RhPP**.

Crystal data:

Identification code	z244_0m	
Habitus, colour	needle, colourless	
Crystal size	0.46 x 0.18 x 0.09 mm^3	
Crystal system	Monoclinic	
Space group	P2$_1$	Z = 8
Unit cell dimensions	a = 16.3796(9) Å	α = 90 °.
	b = 18.1551(9) Å	β = 93.249(2) °.
	c = 27.7174(15) Å	γ = 90 °.
Volume	8229.2(8) Å^3	
Cell determination	9925 peaks with Theta 2.4 to 25.2 °.	
Empirical formula	C$_{40.80}$H$_{43.60}$Cl$_{1.60}$F$_6$N$_4$PRh	
Moiety formula	C$_{40}$H$_{42}$N$_4$ Rh, F$_6$P, 0.8(CH$_2$Cl$_2$)	
Formula weight	894.55	
Density (calculated)	1.444 Mg/m^3	
Absorption coefficient	0.619 mm^{-1}	
F(000)	3661	

Data collection:

Diffractometer type	Bruker D8 QUEST area detector
Wavelength	0.71073 Å
Temperature	110(2) K
Theta range for data collection	2.184 to 25.334 °.
Index ranges	-19<=h<=19, -21<=k<=21, -33<=l<=33
Data collection software	BRUKER APEX2 2014.9-0
Cell refinement software	BRUKER SAINT
Data reduction software	SAINT V8.34A (Bruker AXS Inc., 2013)

Solution and refinement:

Reflections collected	187023
Independent reflections	29991 [R(int) = 0.1334]
Completeness to theta = 25.242 °	99.9 %
Observed reflections	24833[I>2sigma(I)]
Reflections used for refinement	29991
Absorption correction	Semi-empirical from equivalents
Max. and min. transmission	0.95 and 0.84
Flack parameter (absolute struct.)	0.019(8)
Largest diff. peak and hole	1.392 and -1.061 e.Å^{-3}
Solution	Direct methods
Refinement	Full-matrix least-squares on F^2
Treatment of hydrogen atoms	Calculated positions, constr. ref
Programs used	XT V2014/1 (Bruker AXS Inc., 2014)
	SHELXL-2014/7 (Sheldrick, 2014)
	DIAMOND (Crystal Impact)
Data / restraints / parameters	29991 / 2029 / 2009
	Restraints for anisotropic thermal parameters ("RIGU")
Goodness-of-fit on F^2	1.065
R index (all data)	wR2 = 0.1222
R index conventional [I>2sigma(I)]	R1 = 0.0557
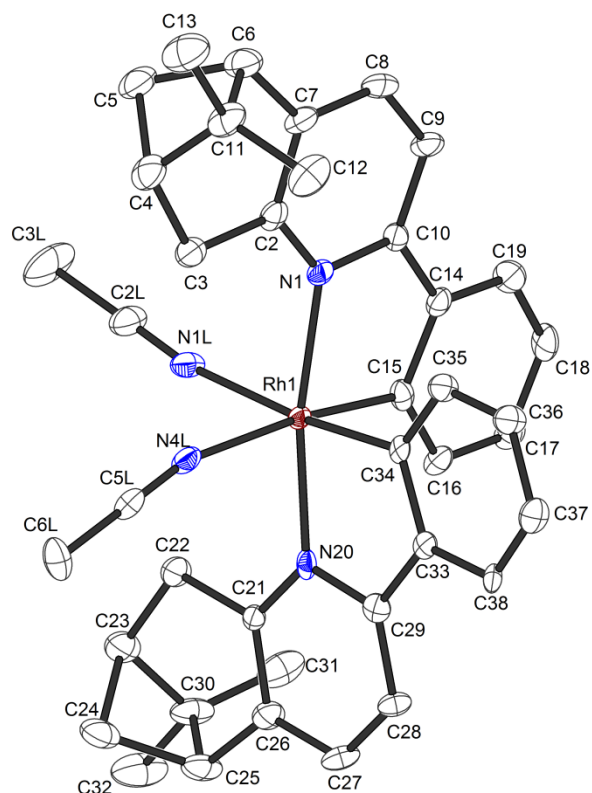
Figure 145 Crystal structure of Δ-**RhPP**. ORTEP drawing with 50% probability thermal ellipsoids. The hexafluorophosphate counteranion is omitted for clarity.

Table 9 Crystal Data and Structure Refinement for Δ-**RhPP**.

Crystal data:

Identification code	z339-zwei_0m
Habitus, colour	nugget, red
Crystal size	0.69 x 0.32 x 0.20 mm^3
Crystal system	Orthorhombic
Space group	P2$_1$2$_1$2$_1$ Z = 8
Unit cell dimensions	a = 15.3828(5) Å = 90°.
	b = 22.8555(9) Å = 90°.
	c = 25.3802(10) Å = 90°.
Volume	8923.2(6) Å^3
Cell determination	9665 peaks with Theta 2.2 to 25.3°.
Empirical formula	C$_{42}$H$_{46}$Cl$_4$F$_6$N$_4$PRh
Moiety formula	C$_{40}$H$_{42}$N$_4$Rh, F$_6$P, 2(CH$_2$Cl$_2$)
Formula weight	996.51
Density (calculated)	1.484 Mg/m^3
Absorption coefficient	0.718 mm^{-1}
F(000)	4064

Data collection:

Diffractometer type	Bruker D8 QUEST area detector
Wavelength	0.71073 Å
Temperature	100(2) K
Theta range for data collection	2.220 to 25.315 °.
Index ranges	-18<=h<=18, -26<=k<=27, -30<=l<=30
Data collection software	BRUKER APEX2 2014.9-0
Cell refinement software	BRUKER SAINT
Data reduction software	SAINT V8.34A (Bruker AXS Inc., 2013)

Solution and refinement:

|	
Reflections collected	66861
Independent reflections	16195 [R(int) = 0.0589]
Completeness to theta = 25.242 °	99.8 %
Observed reflections	14816[I>2sigma(I)]
Reflections used for refinement	16195
Absorption correction	Semi-empirical from equivalents
Max. and min. transmission	0.87 and 0.74
Flack parameter (absolute struct.)	0.005(9)
Largest diff. peak and hole	0.381 and -1.027 e.Å^{-3}
Solution	Direct methods
Refinement	Full-matrix least-squares on F^2
Treatment of hydrogen atoms	Calculated positions, constr. ref.
Programs used	XT V2014/1 (Bruker AXS Inc., 2014)
	SHELXL-2014/7 (Sheldrick, 2014)
	DIAMOND (Crystal Impact)
Data / restraints / parameters	16195 / 663 / 1121
Goodness-of-fit on F^2	1.110
R index (all data)	wR2 = 0.0807
R index conventional [I>2sigma(I)]	R1 = 0.0396
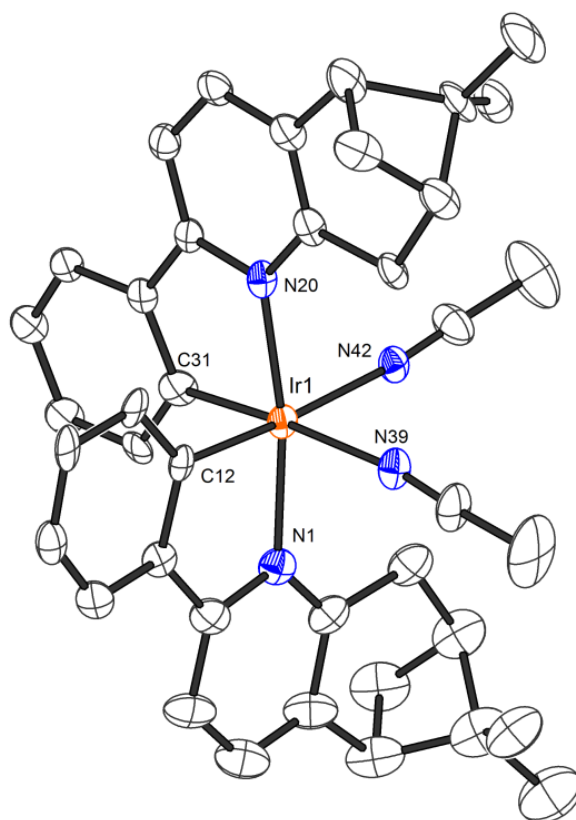
Figure 146 Crystal structure of Λ-**IrPP**. ORTEP drawing with 50% probability thermal ellipsoids. The hexafluorophosphate counteranion is omitted for clarity.

Table 10 Crystal Data and Structure Refinement for Λ-**IrPP**.

Crystal data:

Identification code	z97_0m	
Habitus, colour	plate, yellow	
Crystal size	0.20 x 0.14 x 0.06 mm^3	
Crystal system	Monoclinic	
Space group	P21	Z = 8
Unit cell dimensions	a = 16.3847(13) Å	= 90 °.
	b = 18.1929(15) Å	= 93.095(2) °.
	c = 27.453(2) Å	= 90 °.
Volume	8171.4(11) Å^3	
Cell determination	9347 peaks with Theta 2.3 to 25.2 °.	
Empirical formula	C$_{40.88}$H$_{43.75}$C$_{11.75}$F$_6$IrN$_4$P	
Moiety formula	C$_{40}$H$_{42}$IrN$_4$, F$_6$P, 0.88 (CH$_2$Cl$_2$)	
Formula weight	990.25	
Density (calculated)	1.610 Mg/m^3	

Absorption coefficient	3.483 mm^{-1}
F(000)	3942

Data collection:

Diffractometer type	Bruker D8 QUEST area detector
Wavelength	0.71073 Å
Temperature	100(2) K
Theta range for data collection	2.193 to 25.356 °.
Index ranges	-19<=h<=19, -21<=k<=21, -33<=l<=31
Data collection software	BRUKER APEX2 2014.9-0
Cell refinement software	BRUKER SAINT
Data reduction software	SAINT V8.34A (Bruker AXS Inc., 2013)

Solution and refinement:

|	
Reflections collected	112143
Independent reflections	29568 [R(int) = 0.0532]
Completeness to theta = 25.242 °	99.9 %
Observed reflections	27002[I>2sigma(I)]
Reflections used for refinement	29568
Absorption correction	Numerical
Max. and min. transmission	0.82 and 0.57
Flack parameter (absolute struct.)	0.055(8)
Largest diff. peak and hole	4.835 and -1.145 e.Å^{-3}
Solution	Direct methods
Refinement	Full-matrix least-squares on F^2
Treatment of hydrogen atoms	Calculated positions, constr. ref.
Programs used	XT V2014/1 (Bruker AXS Inc., 2014)
	SHELXL-2014/7 (Sheldrick, 2014)
	DIAMOND (Crystal Impact)
Data / restraints / parameters	29568 / 1774 / 2007
Goodness-of-fit on F^2	1.089
R index (all data)	wR2 = 0.1121
R index conventional [I>2sigma(I)]	R1 = 0.0484

Figure 147 Crystal structure of Δ-**IrPP**. ORTEP drawing with 50% probability thermal ellipsoids. The hexafluorophosphate counteranion is omitted for clarity.

Table 11 Crystal Data and Structure Refinement for Δ-**IrPP**.

Crystal data:

Identification code	z98b_0m	
Habitus, colour	plate, yellow	
Crystal size	0.25 x 0.12 x 0.05 mm^3	
Crystal system	Orthorhombic	
Space group	P21212	Z = 4
Unit cell dimensions	a = 15.3905(7) Å	= 90 °.
	b = 22.8141(13) Å	= 90 °.
	c = 12.6639(6) Å	= 90 °.
Volume	4446.6(4) Å^3	
Cell determination	9601 peaks with Theta 2.3 to 25.3 °.	
Empirical formula	C$_{42}$H$_{46}$Cl$_4$ F$_6$IrN$_4$P	
Moiety formula	C$_{40}$H$_{42}$IrN$_4$, F$_6$P, 2(CH$_2$Cl$_2$)	
Formula weight	1085.80	
Density (calculated)	1.622 Mg/m^3	
Absorption coefficient	3.339 mm^{-1}	
F(000)	2160	

Data collection:

Diffractometer type	Bruker D8 QUEST area detector
Wavelength	0.71073 Å
Temperature	100(2) K
Theta range for data collection	2.222 to 25.284 °.
Index ranges	-18<=h<=17, -14<=k<=27, -13<=l<=15
Data collection software	BRUKER APEX2 2014.9-0
Cell refinement software	BRUKER SAINT
Data reduction software	SAINT V8.34A (Bruker AXS Inc., 2013)

Solution and refinement:

Reflections collected	15571
Independent reflections	7935 [R(int) = 0.0296]
Completeness to theta = 25.242 °	99.6 %
Observed reflections	7212[I>2sigma(I)]
Reflections used for refinement	7935
Absorption correction	Numerical
Max. and min. transmission	0.85 and 0.53
Flack parameter (absolute struct.)	0.007(5)
Largest diff. peak and hole	1.257 and -0.575 e.Å^{-3}
Solution	Direct methods
Refinement	Full-matrix least-squares on F^2
Treatment of hydrogen atoms	Calculated positions, constr. ref.
Programs used	XT V2014/1 (Bruker AXS Inc., 2014)
	SHELXL-2014/7 (Sheldrick, 2014)
	DIAMOND (Crystal Impact)
Data / restraints / parameters	7935 / 0 / 530
Goodness-of-fit on F^2	0.966
R index (all data)	wR2 = 0.0608
R index conventional [I>2sigma(I)]	R1 = 0.0301
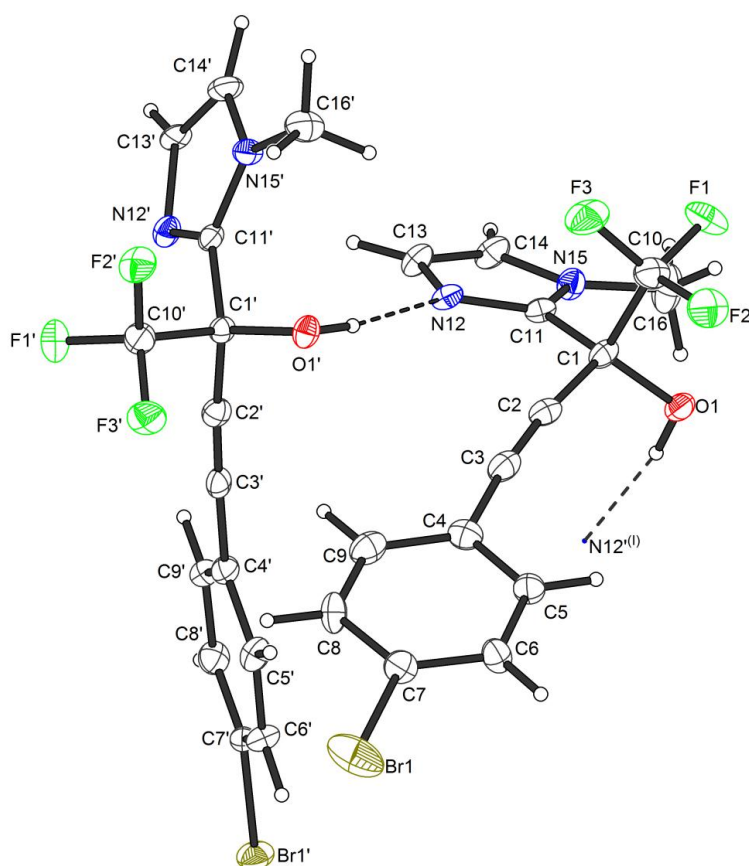
Figure 148 Crystal structure of **20l**. ORTEP drawing with 50% probability thermal ellipsoids.

Table 12 Crystal Data and Structure Refinement for **20l**.

Crystal data:

Identification code	z341_0m	
Habitus, colour	needle, colourless	
Crystal size	0.36 x 0.18 x 0.16 mm^3	
Crystal system	Orthorhombic	
Space group	P2$_1$2$_1$2$_1$	Z = 8
Unit cell dimensions	a = 10.9456(3) Å	= 90 °.
	b = 12.5890(4) Å	= 90 °.
	c = 21.7213(6) Å	= 90 °.
Volume	2993.07(15) Å^3	
Cell determination	9966 peaks with Theta 2.5 to 25.2 °.	
Empirical formula	C$_{14}$H$_{10}$BrF$_3$N$_2$O	
Moiety formula	C$_{14}$H$_{10}$BrF$_3$N$_2$O	
Formula weight	359.15	
Density (calculated)	1.594 Mg/m^3	

Absorption coefficient	2.778 mm^{-1}
F(000)	1424

Data collection:

Diffractometer type	Bruker D8 QUEST area detector
Wavelength	0.71073 Å
Temperature	100(2) K
Theta range for data collection	2.466 to 25.317 °.
Index ranges	-13<=h<=13, -15<=k<=15, -26<=l<=26
Data collection software	BRUKER APEX2 2014.9-0
Cell refinement software	BRUKER SAINT
Data reduction software	SAINT V8.34A (Bruker AXS Inc., 2013)

Solution and refinement:

Reflections collected	22310
Independent reflections	5384 [R(int) = 0.0530]
Completeness to theta = 25.242 °	99.9 %
Observed reflections	4902[I>2sigma(I)]
Reflections used for refinement	5384
Absorption correction	Numerical
Max. and min. transmission	0.67 and 0.35
Flack parameter (absolute struct.)	0.027(8)
Largest diff. peak and hole	0.235 and -0.270 e.Å^{-3}
Solution	Direct methods
Refinement	Full-matrix least-squares on F^2
Treatment of hydrogen atoms	CH calc. positions, constr., OH located, isotr. ref.
Programs used	XT V2014/1 (Bruker AXS Inc., 2014)
	SHELXL-2014/7 (Sheldrick, 2014)
	DIAMOND (Crystal Impact)
Data / restraints / parameters	5384 / 189 / 454
Goodness-of-fit on F^2	1.055
R index (all data)	wR2 = 0.0556
R index conventional [I>2sigma(I)]	R1 = 0.0290
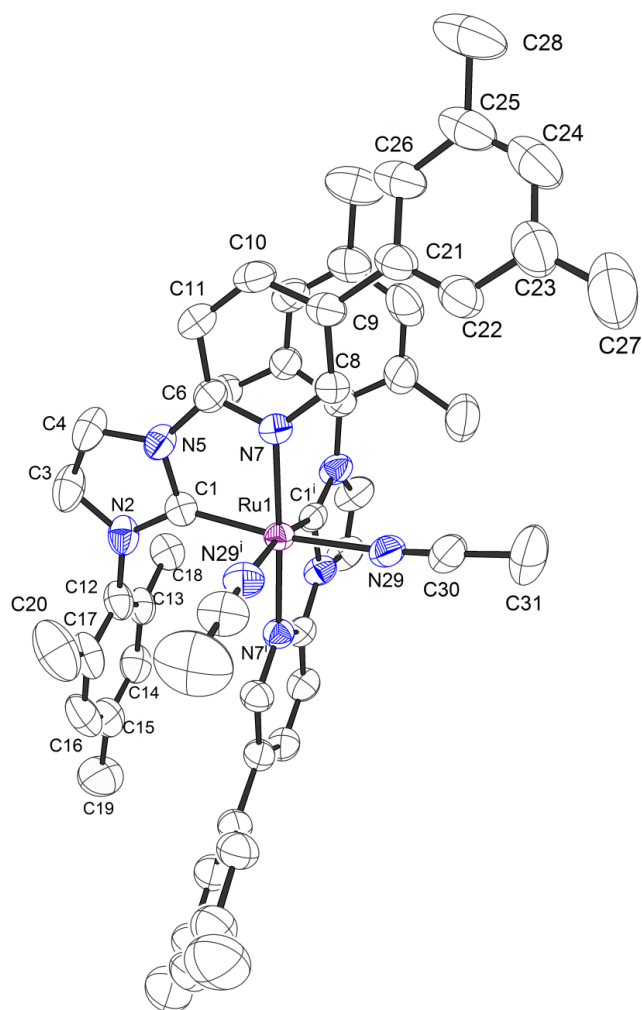
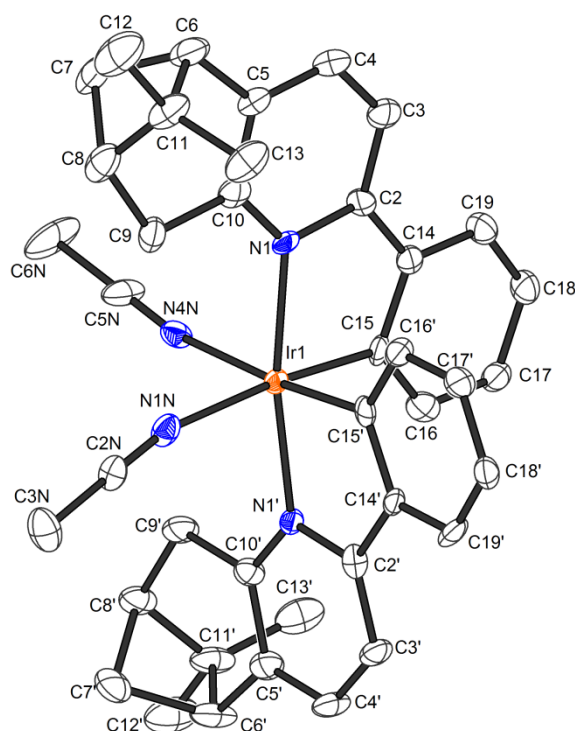**Figure 149** Crystal structure of *rac*-**Ru1**. ORTEP drawing with 50% probability thermal ellipsoids. The hexafluorophosphate counteranion is omitted for clarity.

Table 13 Crystal Data and Structure Refinement for *rac*-**Ru1**.

Crystal data:

Identification code	z1020c_0m	
Habitus, colour	needle, colourless	
Crystal size	0.62 x 0.13 x 0.11 mm^3	
Crystal system	Monoclinic	
Space group	C2/c	Z = 4
Unit cell dimensions	a = 19.8615(9) Å	= 90 °.
	b = 22.9601(10) Å	= 95.504(2) °.
	c = 13.8009(6) Å	= 90 °.
Volume	6264.5(5) Å^3	
Cell determination	9919 peaks with Theta 2.3 to 25.3 °.	
Empirical formula	C$_{56}$H$_{60}$C$_{l4}$F$_{12}$N$_8$P$_2$Ru	

Moiety formula	$C_{54}H_5N_8Ru$, $2(F_6P)$, $2(CH_2Cl_2)$
Formula weight	1377.93
Density (calculated)	1.461 Mg/m^3
Absorption coefficient	0.551 mm^{-1}
F(000)	2808

Data collection:

Diffractometer type	Bruker D8 QUEST area detector
Wavelength	0.71073 Å
Temperature	230(2) K
Theta range for data collection	2.312 to 25.297 °.
Index ranges	-23<=h<=23, -27<=k<=27, -16<=l<=16
Data collection software	APEX3 (Bruker AXS Inc., 2015)
Cell refinement software	SAINT V8.37A (Bruker AXS Inc., 2015)
Data reduction software	SAINT V8.37A (Bruker AXS Inc., 2015)

Solution and refinement:

|	
Reflections collected	47978
Independent reflections	5694 [R(int) = 0.0442]
Completeness to theta = 25.242 °	99.9 %
Observed reflections	4994[I > 2σ(I)]
Reflections used for refinement	5694
Absorption correction	Semi-empirical from equivalents
Max. and min. transmission	0.94 and 0.87
Largest diff. peak and hole	0.382 and -0.389 e.Å^{-3}
Solution	dual space algorithm
Refinement	Full-matrix least-squares on F^2
Treatment of hydrogen atoms	Calculated positions, constr. ref.
Programs used	XT V2014/1 (Bruker AXS Inc., 2014)
	SHELXL-2014/7 (Sheldrick, 2014)
	DIAMOND (Crystal Impact)
	ShelXle (Hübschle, Sheldrick, Dittrich, 2011)
Data / restraints / parameters	5694 / 191 / 473
Goodness-of-fit on F^2	1.065
R index (all data)	wR2 = 0.0951
R index conventional [I>2sigma(I)]	R1 = 0.0370
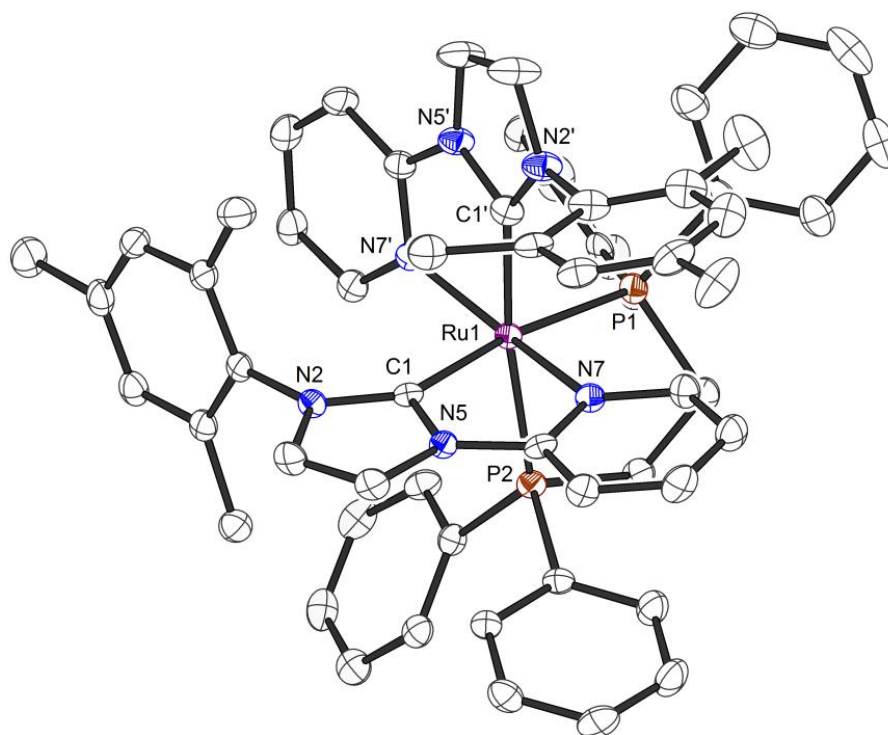
Figure 150 Crystal structure of Δ-**Ru2-DPPE**. ORTEP drawing with 50% probability thermal ellipsoids. The hexafluorophosphate counteranion is omitted for clarity.

Table 14 Crystal Data and Structure Refinement for Δ-**Ru2-DPPE**.

Crystal data:

Identification code	z1056_0m_sq	
Habitus, colour	plate, colourless	
Crystal size	0.31 x 0.30 x 0.14 mm^3	
Crystal system	Monoclinic	
Space group	P21	Z = 2
Unit cell dimensions	a = 14.2760(6) Å	= 90 °.
	b = 15.7178(7) Å	= 103.244(2) °.
	c = 14.3256(6) Å	= 90 °.
Volume	3129.0(2) Å^3	
Cell determination	9151 peaks with Theta 2.6 to 27.5 °.	
Empirical formula	$C_{60}H_{58}F_{12}N_6P_4Ru$ [+ solvent]	
Moiety formula	$C_{60}H_{58}N_6P_2Ru$, 2(F$_6$P) [+ solvent]	
	Disordered solvent has been "squeezed"	
Formula weight	1316.07	
Density (calculated)	1.397 Mg/m^3	

Absorption coefficient	0.431 mm^{-1}
F(000)	1344

Data collection:

Diffractometer type	Bruker D8 QUEST area detector
Wavelength	0.71073 Å
Temperature	110(2) K
Theta range for data collection	2.231 to 27.546 °.
Index ranges	-18<=h<=18, -20<=k<=20, -18<=l<=18
Data collection software	APEX3 (Bruker AXS Inc., 2015)
Cell refinement software	SAINT V8.37A (Bruker AXS Inc., 2015)
Data reduction software	SAINT V8.37A (Bruker AXS Inc., 2015)

Solution and refinement:

Reflections collected	71723
Independent reflections	14432 [R(int) = 0.0431]
Completeness to theta = 25.242 °	99.9 %
Observed reflections	13176[I > 2(I)]
Reflections used for refinement	14432
Extinction coefficient	X = 0.0009(2)
Absorption correction	Semi-empirical from equivalents
Max. and min. transmission	0.94 and 0.89
Flack parameter (absolute struct.)	-0.023(6)
Largest diff. peak and hole	0.343 and -0.343 e.Å^{-3}
Solution	Dual space algorithm
Refinement	Full-matrix least-squares on F^2
Treatment of hydrogen atoms	Calculated positions, constr. ref.
Programs used	XT V2014/1 (Bruker AXS Inc., 2014)
	SHELXL-2016/6 (Sheldrick, 2016)
	DIAMOND (Crystal Impact)
	ShelXle (Hübschle, Sheldrick, Dittrich, 2011)
Data / restraints / parameters	14432 / 280 / 810
Goodness-of-fit on F^2	1.023
R index (all data)	wR2 = 0.0563
R index conventional [I>2sigma(I)]	R1 = 0.0278

Statement

gemäß § 10, Abs. 1 der Promotionsordnung der mathematisch-naturwissenschaftlichen Fachbereiche und des Medizinischen Fachbereichs für seine mathematisch-naturwissenschaftlichen Fächer der Philipps-Universität Marburg vom 15.07.2009

Ich erkläre, dass eine Promotion noch an keiner anderen Hochschule als der Philipps-Universität Marburg, Fachbereich Chemie, versucht wurde und versichere, dass ich meine vorgelegte Dissertation

Design of Novel Octahedral Stereogenic-at-Metal Complexes for Applications in Asymmetric Catalysis

selbst und ohne fremde Hilfe verfasst, nicht andere als die in ihr angegebenen Quellen oder Hilfsmittl benutzt, alle vollständig oder sinngemäß übernommenen Zitate als solche gekennzeichnet sowie die Dissertation in der vorliegenden oder ähnlichen Form noch bei keiner anderen in- oder ausländischen Hochschule anlässlich eines Promotionsgesuchs oder zu anderen Prüfungszwecken eingereicht habe.

Yu Zheng
Marburg, den 3.1.2018

Curriculum Vitae

Yu Zheng

Born May 14, 1987 in Anhui, P. R. China

E-mail：zhengyu0609@163.com

Education

11/2014–present   *Ph.D.* Organic Chemistry, University of Marburg, Germany
Advisor: Prof. Eric Meggers

09/2011–06/2014   *M.S.* Organometallic Chemistry, Soochow University, China
Advisor: Prof. Mingqiang Xue

09/2007–06/2011   *B.S.* Chemistry, Hefei Normal University, China

Research Experiences

Ph.D. study: Design of Novel Octahedral Stereogenic-at-Metal Complexes for Applications in Asymmetric Catalysis

Publications:

1. Y. Zheng, Y. Tan, K. Harms, M. Marsch, R. Riedel, L. Zhang, E. Meggers, *J. Am. Chem. Soc.* **2017**, *139*, 4322−4325. (highlighted by *Synfacts* **2017**, 0625).

2. Y. Zheng, K. Harms, L. Zhang, E. Meggers, *Chem. Eur. J.* **2016**, *22*, 11977−11981. (highlighted by *Synfacts* **2016**, 1156).

3. Y. Zheng, L. Zhang, E. Meggers, *Org. Process Res. Dev.* **2018**, *22*, 103−107.

4. C. Wang, Y. Zheng, H. Huo, P. Röse, L. Zhang, K. Harms, E. Meggers, *Chem. Eur. J.* **2015**, *21*, 7355−7359.

5. S. Luo, X. Zhang, Y. Zheng, K. Harms, L. Zhang, E. Meggers, *J. Org. Chem.* **2017***, 82*, 8995−9005.

M.S. study: Bis-β-diketiminato rare-earth-metals amides and lanthanide(II) complexes: syntheses, structures, and their catalytic activity

Publications:

1. M. Xue, Yu Zheng, Y. Hong, Y. Yao, F. Xu, Y. Zhang, Q. Shen, *Dalton Trans.*, **2015**, *44*, 20075−20086.

2. Y. Zheng, R. Jiao, X. Shen, M. Xue, Y. Yao, Y. Zhang Q. Shen, *Appl. Organometal. Chem.* **2014**, *28*, 461−470.

3. Y. Hong, Y. Zheng, M. Xue, Y. Yao, Y. Zhang, Q. Shen, *Z. Anorg. Allg. Chem.* **2015**, *641*, 1230−1237.

4. Q. Liu, Y. Hong, Y. Zheng, M. Xue, *Chin. J. Org. Chem.* **2016**, *36*, 2168−2174.

5. S. Chen, Y. Hong, Y. Liu, M. Xue, Yu Zheng, Q. Shen, *Chin. J. Org. Chem.* **2017**, *37*, 1198−1204.